Chen, John C., 1934-

THE UNIVERSITY OF MICHIGAN

INDUSTRY PROGRAM OF THE COLLEGE OF ENGINEERING

RADIANT HEAT TRANSFER IN PACKED MEDIA

John Chun-Chien Chen

A dissertation submitted in partial fulfillment
of the requirements for the degree of
Doctor of Philosophy in The
University of Michigan
1960

February, 1961

IP-497

ensn

UMR1162

To my parents

ACKNOWLEDGEMENTS

The author wishes to express his appreciation to the members of his committee for their guidance during the course of this work. Special thanks are due to Professor Stuart W. Churchill, chairman of the committee, for his initial suggestion of the topic and for his continued encouragement and aid during all phases of the work.

The author is indebted to the Research Center of the Owens-Corning Corporation for generous loan of experimental equipment and to the Monsanto Chemical Company for financial aid through the granting of a fellowship. Thanks are also due to the Industry Program of the College of Engineering for reproduction of the final thesis.

The author wishes to thank his laboratory mates, Doctors J. A. Leacock, G. D. Towell, J. D. Hellums, and Mr. J. Hiestand for their many helpful suggestions. Finally, the author wishes to thank his wife for her constant encouragement throughout the period of the work and for her aid in preparation of the final manuscript.

TABLE OF CONTENTS

TABLE OF CONTENTS (cont'd)

TABLE OF CONTENTS (cont'd)

LIST OF TABLES

LIST OF FIGURES

LIST OF FIGURES (cont'd)

LIST OF FIGURES (cont'd)

ABSTRACT

This thesis presents the results of an experimental investigation of radiant heat transfer in packed media. Steady state, one dimensional, simultaneous, radiative and conductive heat transfer in quiescent packed beds was analyzed theoretically. If a two flux model is used to represent absorption and scattering, radiation and conduction can be represented by a set of nonlinear differential equations. In this model the radiant properties of the media are specified in terms of an absorption cross section and a back scattering cross section per unit volume. With this representation, a minimum of three dimensionless dependent variables, one dimensionless independent variable, and six dimensionless parameters are necessary to define the system.

The experimental program was designed to obtain measurements of the two attenuation cross sections for a number of typical packings. This was accomplished by making transmission measurements of modulated blackbody radiation and correlating with the two-flux model by least square regression.

Twelve packings were tested, covering four types of materials (glass, aluminum oxide, steel, and silicon carbide), three types of shapes (spheres, cylinders, and irregular grains), and a range of sizes (3 mm., 4mm., 5mm., 1/8 inch, 5/32 inch, 3/16 inch, mesh 4, and mesh 16). Measurements were made at several source temperatures in the range of 800°F to 2000°F.

Results showed that back scattering is the major mechanism of attenuation for packings of glass, aluminum oxide, and steel. The measured absorption cross sections for these packings are all less than seven percent

of the value of the corresponding back scattering cross sections. Absorption was found to be important only for packings of silicon carbide, for which the absorption cross sections may be as high as 60 percent of the value of the back scattering cross sections.

In general, it was found that back scattering cross sections decrease with increasing particle size and solid emmissivity. The absorption cross sections were found to decrease with decreasing solid emissivity and with increasing particle size. Aluminum oxide cylinders are exceptions in that the absorption cross sections were found to increase with increasing particle size. Two graphical correlations of absorption and back scattering parameters are presented to enable interpolation and extrapolation of the experimental data for first-order estimates of the parameters for other packings and other operating conditions.

Equivalent radiant conductivities calculated from the measured cross sections were found to be substantially different from a priori estimates calculated from various theoretical models which have been proposed previously. A possible explanation is that these models do not account correctly for scattering and solid-transmission effects.

The radiant conductivities were found to increase with temperature of radiation, solid transmissivity and emissivity, and particle size. The temperature dependence was found to be quite different from the third power dependence usually assumed. In the temperature range of 1600°F to 2000°F, the exponent of temperature ranged from a low of 1.6 to a high of 5.6 in the various packings tested.

Radiation was found to become important, relative to conduction, at temperatures of approximately 1000°F and to become predominant at temperatures of about 2000°F. For example, at 2000°F, radiation was found to

account for approximately 35 percent of the total heat transfer for packings of mesh 4 silicon carbide grains, 45 percent for 3/16 inch steel spheres, 60 percent for 3/16 inch aluminum oxide cylinders, and 85 percent for 5mm. glass spheres.

PART I

INTRODUCTION

PURPOSE AND SCOPE OF STUDY

Purpose

Particulate aggregates in the form of either packed beds or powders are important in a wide variety of applications such as catalytic reactors, pebble bed heaters, adsorbers, powder castings, solid propellents, and thermal insulations. In addition, many processes of technical interest, such as underground combustion for petroleum production or underground-contained nuclear explosion, deal with aggregate materials. In almost all these cases, the heat transfer characteristic of the packed aggregate is an important design and operational factor.

Some investigations on heat transfer in packed media, both theoretical and experimental, have been reported in the literature. Recent comprehensive reviews are presented by Gorring and Churchill[11] and by Hill and Wilhelm[15]. These previous investigations were mainly concerned with overall thermal conductivities and were generally limited to temperatures of less than 500°F. At such temperatures, conduction was found to be the dominant transfer mechanism[38,36] so that the concept of an "effective overall conductivity" could be practically utilized.

However, this approach of grouping all effects under one overall conductivity is proving to be inadequate for recent technological demands of high temperature, close tolerance operations. It is recognized that radiation becomes increasingly important at higher temperatures and could easily become the same order of magnitude as conduction at temperatures above 1000°F[15]. The heat transfer characteristics of the bed then become quite complex due to the coupling of conduction, a linear temperature function, with radiation, a fourth order temperature function. Moreover, at points

near walls, the radiant heat transfer becomes affected by the emission properties of the wall itself[20], so that any "effective conductivity" would be a function of the properties of the wall as well as of particle characteristics. The temperature distribution would no longer be linear as it is for the case of conduction controlling heat transfer.

In order to understand and adequately treat this more complex case of simultaneous conduction and radiation, it was felt that the mechanism of radiant transfer needed to be isolated and studied in detail by itself. A number of authors [1,3,6,31,33] have proposed equations to describe the radiation contribution to total heat transfer. However, direct experimental measurement of radiant transfer in packed beds has apparently never been carried out although several investigators[15,33] have estimated radiation rates from measured total heat transfer rates. Due to this lack of actual data, even the relative importance of radiation and conduction is not clearly known at the present time.

The objectives of this study were, therefore, to:

a) find an experimental means of isolating radiant transfer for individual examination,

b) obtain direct measurements of radiant heat transfer in a number of typical packings,

c) clarify the relative importance of radiative heat transfer as compared to conductive heat transfer,

d) check the validity of various methods of a priori estimations of radiant conductivity which have been proposed, by comparison to experimental measurements,

e) determine a practical means of characterizing radiant transfer properties of packed media, and

f) provide a start toward correlating the bulk transfer characteristics with physical properties of the packing particles.

Scope

The analysis of this study dealt with the case of steady state heat transfer from an infinite flat wall at temperature T_1 to a second infinite wall at temperature T_2, across a quiescent gas-solid bed of packed particles, as shown in Figure 1. This one dimensional case was chosen for study because it lends itself to analysis and because many applications dealing with packed media have sensibly uniform cross-section temperatures and can be treated as one dimensional cases. The experimentally measured parameters, however, are applicable to general problems of radiant transfer in any geometry.

The work of Rogers and Morrison[30] indicates that natural convection is negligible for the types of packings of interest and it was therefore not considered in this study. Only radiative and conductive heat transfer was taken into account.

A dimensional analysis, based on the two-flux transport model of Hamaker[13], was made to define the minimum number of variables and parametric groups necessary to specify the problem. Approximate solutions were obtained for the resulting dimensionless system of nonlinear differential equations. These solutions provide the local values of temperature, radiant energy flux, and conductive energy flux at every point of the packed bed.

An experimental method which was recently used by Larkin and Churchill[20] to study radiant heat transfer in fibrous insulations was found to be applicable also to close packed media. This method, utilizing transmission measurements of black body radiation, has the great advantage of isolating radiation effects for individual study, free from conduction and

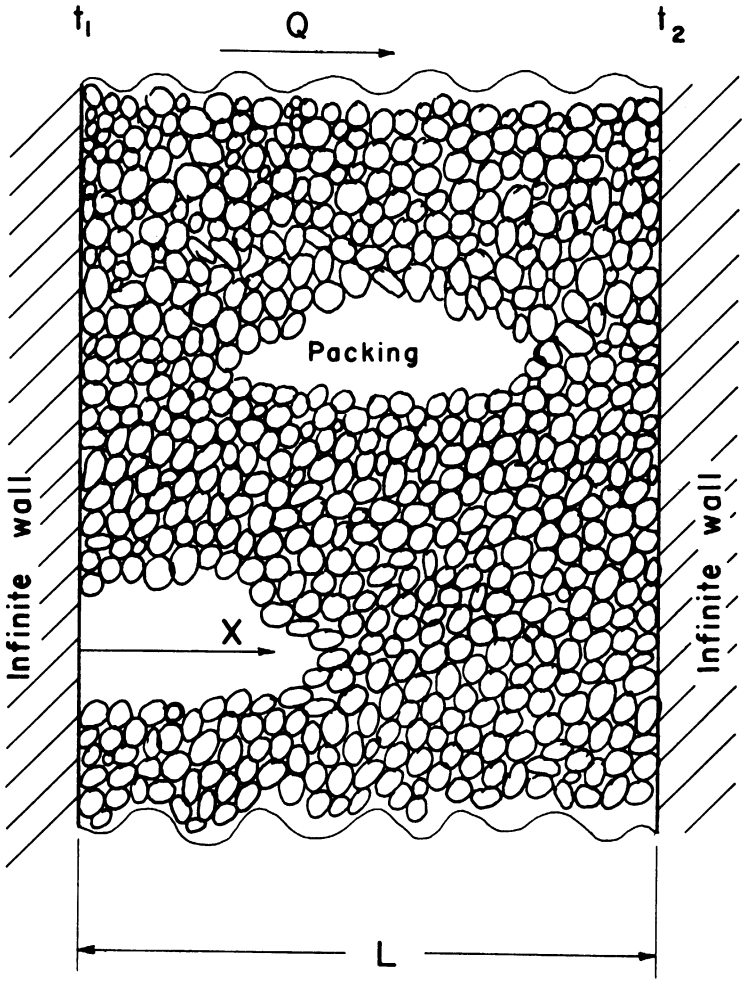

Figure 1. Geometry of Analysis Case

convection. Twelve types of packings were tested at temperatures ranging from 800°F to 2000°F. The particles were of four different materials, glass, aluminum oxide, steel, and silicon carbide. Three different shapes, spheres, cylinders, and irregular grains, were covered by the samples. Nominal particle diameters ranged from 1.7 mm to 5 mm.

An equivalent radiant conductivity, which is applicable at interior points of packed beds, was defined and calculated from the measured radiation parameters. This conductivity proved to be a useful means of characterizing radiant heat transfer properties of packed media, checking analytic estimates of radiant conductivities, and comparing the relative importance of radiative and conductive heat transfer.

An ultimate objective would be to define the effects of such variables as temperature of radiation, size of particle, shape of particle, and bulk void fraction on the radiation parameters determined from experimental measurements, so that predictions could be made for the behavior of any packing under any operating condition. A start toward such a general correlation is provided by this work.

LITERATURE REVIEW

Analytical Studies

It is generally recognized that a quiescent bed of packed particles in gas provides a highly complex system for heat transfer. There are five transfer processes that could occur: (a) conduction in solid, (b) conduction in gas, (c) convection in gas, (d) radiation between solid particles, and (e) radiation between solid particles and gaseous voids. Conceivably all five processes could contribute to the overall heat transfer and since each process is dependent on a number parameters (i.e., particle size and shape, pressure, volume of voids, emissivity of surfaces, temperature, conductivity of solid, conductivity of gas, particle arrangement, etc.), their interaction would be difficult to treat rigorously. All existing analyses have been based on simplifying assumptions of one type or another.

One assumption common to almost all treatments is that convective heat transfer is negligible[37,38,40]. A number of studies have been made on the conditions necessary to initiate natural convection, by such investigators as Horton and Rogers[17], Lapwood[19], and Rogers and Morrison[30]. However, no empirical or theoreticalequations to calculate the convective transfer in packed media has been proposed at the present time.

A second type of simplification common to a large number of analytical treatments is to approximate the heterogeneous random mixture of solid particles and gaseous voids by some regular geometrical arrangement of arbitrary solid and gaseous bodies. The first work along this line was by Rayleigh[29] near the beginning of the century, when he solved the general potential problem of conduction in a medium of conductivity k_1 through which are distributed spheres or cylinders of a different conductivity k_2. Maxwell[23]

also treated this same problem, but under the assumption that the spheres (or cylinders) were small in diameter relative to the distances between them so that there were no interactions. This assumption invalidates the results for packed beds where the particles are actually in contact. Eucken[9] was the first to suggest the possible application of this potential solution to thermal conduction in porous media.

The next major contribution along this line was by Schumann and Voss[34] in 1934. They represented the heterogeneous bed by a square, divided into two parts by a hyperbolic curve running between two diagonally opposite corners, as shown in Figure 2-a. One part was taken to represent the solid phase of the actual bed and the other part to represent the gas phase. Conduction was thus calculated as occurring in series through the two phases. Wilhelm et al.[38], have proposed slight modifications to Schumann and Voss' equations to account for conduction at contact points.

Russell[32], in 1935, presented a model where the solid particles were in the form of cubes located at the centers of cubic lattices, as shown in Figure 2-b. The conductivity for this assembly was determined and taken to approximate the conductivity of the real media. Deissler[7] and Woodside[39], in 1958, also worked with cubically packed models, though they both considered the particles to be spheres rather than cubes.

The above studies all were concerned mainly with conductive transfer. Nusselt[27], in 1913, was the first to present a geometric model for estimating radiant transfer of heterogeneous media. He considered alternating layers of solid and gas where the relative thicknesses were dependent on the porosity of the medium (see Figure 2-c). The equation he obtained

for an equivalent radiant conductivity was,

$$K_r = 4L\sigma T^3 \qquad (1)$$

where L = thickness of gas layer.

All later geometric analyses for radiant transfer were based on this or some modified form of this model. Damköhler[6], in 1937, introduced several correction factors into Nusselt's equation to obtain,

$$K_r = 4\sigma a \tau' D_p T^3 \qquad (2a)$$

where a = absorptivity of solid surfaces

D_p = particle diameter

τ' = "fraction free area for radiation".

Argo and Smith[1] gives the following as Damköhler's simplified expression,

$$K_r = 4\sigma \left(\frac{\epsilon}{2-\epsilon}\right) D_p T^3 \qquad (2b)$$

where ϵ = particle emissivity.

More recently, Laubitz[21] used Russell's cubical model to estimate radiant transfer. This may be considered as another modification of Nusselt laminar model, with the solid layers being cut into cubes. The expression obtained by Laubitz was,

$$K_r = 4\sigma \epsilon \frac{a}{p} (1 - p^{\frac{1}{3}} + p^{\frac{4}{3}}) T^3 \qquad (3)$$

where a = length of solid cubes

p = fractional volume of solids

ϵ = emissivity of solids.

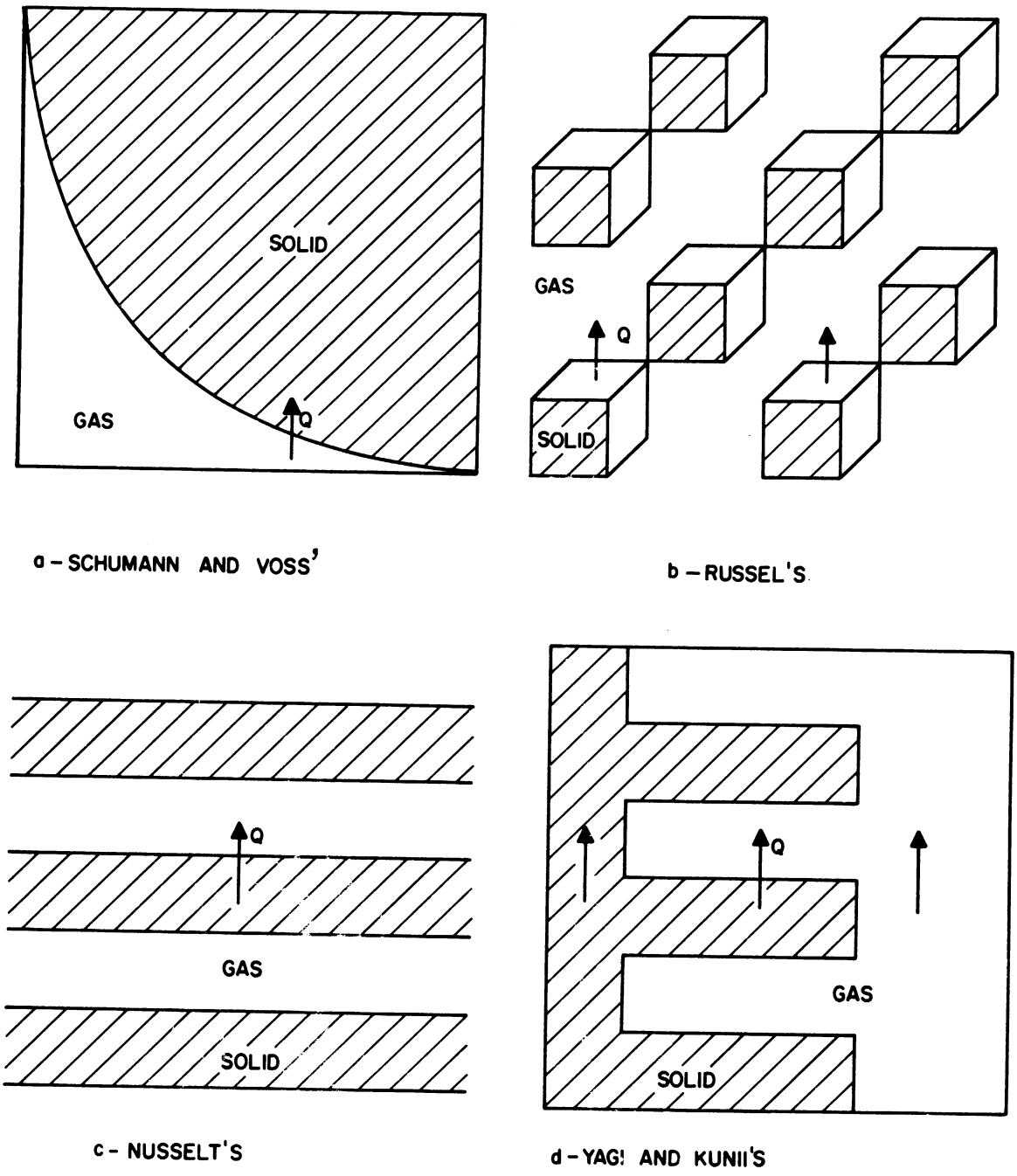

Figure 2. Analysis Models

Yagi and Kunii[40] used a composite laminar representation as shown in Figure 2-d to account for five transfer processes. Their result for quiescent beds was presented as a ratio of equivalent bed conductivity to gas conductivity,

$$\frac{K_e}{K_g} = \frac{\beta(1-\epsilon)}{\gamma\left(\frac{K_g}{K_s}\right) + \left[\frac{1}{\phi} + \frac{D_p h_{rs}}{K_g}\right]} + \epsilon\beta\,\frac{D_p h_{rv}}{K_g} \qquad (4)$$

where k_e = equivalent bed conductivity

k_g = gas conductivity

h_{rs} = heat transfer coefficient for radiation solid to solid

$$= 0.195\,\frac{p}{2-p}\left(\frac{t+273}{100}\right)^3, \quad \frac{\text{Kcal.}}{m^2.\text{hr.}^\circ\text{C}}$$

h_{rv} = heat transfer coefficient for radiation void to void

$$= 0.195\left[1 + \frac{\epsilon}{2(1-\epsilon)}\cdot\frac{(1-p)}{p}\right]^{-1}\cdot\left[\frac{t+273}{100}\right]^3, \quad \frac{\text{Kcal.}}{m^2.\text{hr.}^\circ\text{C}}$$

$p, \beta, \gamma, \epsilon, \phi, D_p$ = properties of the bed.

Schotte[33] also treated coupled conduction and radiation from the geometric point of view. He considered the energy transfered from a plane located on one side of a particle to a second plane on the far side of the particle. Conduction in the particle, parallel radiation across the voids, and conduction-radiation in series were all taken into account. The following expression was obtained by Schotte for equivalent radiant conductivity,

$$K_r = \frac{1-\delta_p}{\frac{1}{K_s} + \frac{1}{K_r^\circ}} + \delta_p K_r^\circ \qquad (5)$$

where k_s = conductivity of solid

k_r° = radiant conductivity between particles

$$= 0.692\,\epsilon\,D_p\,T^3 \times 10^{-8} \quad \frac{\text{Btu}}{\text{hr ft.}^\circ\text{F}}$$

δ_p = void fraction

ϵ = emissivity

D_p = particle diameter

As an alternate to the geometric approach of the above works, some authors have proposed a kinetic or diffusion type of treatment. Rosseland[31] considered radiant transfer as a diffusion of photons through the media and obtain the following expression for equivalent conductivity,

$$K_r = \frac{4}{3} l T^3 \qquad (6)$$

where l = mean free path for the photons.

Bosworth[3] has proposed that for a packed bed, l may be set equal to the particle diameter, D_p.

A third approach is to represent the heterogeneous media by an equivalent homogeneous media, making it possible to treat the particulate problem as a continuous one and to define the heat transfer processes by differential or integro-differential equations with suitable boundary conditions. This approach has a distinct advantage in that it is not necessary to assume any specific geometric model or to arbitrary specify the paths of the various transfer processes. While continuous representation of what is actually a discrete process will not give exact solutions at any one point, it does give correct solutions for quantities averaged over a large volume. In fact, if the parameters defining the equivalent homogeneous media are obtained by actual experiment, it is theorectically possible to write down a system of differential equations that will rigorously define the true average heat transfer rate per unit area through the packing.

There are two major works in this line. Van der Held[35] treated the general three dimensional problem by adding a radiation term to the

Fourier heat conduction equation,

$$K_c \nabla^2 T + 4\int_0^\infty n_\lambda^2 a_\lambda (I_\lambda - J_\lambda) d\lambda = \rho c_p \frac{\partial T}{\partial t} \qquad (7a)$$

where the second term represents the net accumulation of radiant energy of all wavelengths. At steady state, Van der Held obtained the following expression for an equivalent radiant conductivity at interior points of the packing,

$$K_r = \frac{4}{3} \frac{n^2 4\sigma}{a+s} T^3 \qquad (7b)$$

where n = refractive index of equivalent homogeneous media

a = absorption coefficient

s = scattering coefficient.

The other major work was by Hamaker[13] who, in 1947, suggested the two-flux treatment of the one dimensional problem. He proposed the following system of equations to treat simultaneous conduction and radiation,

$$\frac{di}{dx} = -(a + s_b) i + s_b j + a\sigma T$$

$$\frac{\partial j}{\partial x} = (a + s_b) j - s_b i - a\sigma T$$

$$K_c \frac{d^2 T}{dx^2} + a(i+j) - 2a\sigma T = 0$$

The first two equations describe the attenuation of a forward radiant flux, i, and a backward radiant flux, j. The third equation is an overall continuity equation for transfer of both conductive and radiative energies. Hamaker presented general solutions to the system of equations in terms of four arbitrary boundary constants, but the complete solution for the case of a finite bed was not given in detail. Since this present study is based on Hamaker's concepts, the system of equations,[8] were rederived, dimensionally analyzed, and solved in detail for the sake of completeness, (see Part II).

Experimental Studies

Majority of data reported in the literature for heat transfer in pack beds are limited to temperatures below 500°F. At such temperatures, radiation is relatively un-noticeable, and since these data have been amply summarized by Waddams[36] in 1944, Wilhelm, Johnson, Wynkoop, and Collier[38] in 1948, and Yagi and Kunii[40] in 1957. they will not be discussed here. Only some data for relatively higher temperatures are reviewed below.

In 1947, Lucks, Linebrink, and Johnson[22] made thermal conductivity measurements for packed beds of sands over a temperature range of 750°F to 2250°F. They reported that the overall conductivities of three tested samples increased with temperature, from values of 2.1 - 3.0 $\frac{\text{Btu in.}}{\text{hr.ft}^2\text{°F}}$ at 750°F to 3.2 - 8.8 $\frac{\text{Btu in.}}{\text{hr.ft.}^2\text{°F}}$ at 2250°F. No effort was made to separate out radiation contribution. Bell[2] in 1948 also reported data for sands, in a temperature range of 1000°F to 2000°F. Values obtained for overall conductivities were of the same order of magnitude as Lucks et al's. Again, no analysis was made to study radiant contributions.

Bunnell, Irvin, Olson, and Smith[4] investigated heat transfer in a two inch bed of 0.125 inch alumina cylinders, with air flow through the bed. Maximum test temperature was 400°C. Extrapolating their data to zero air velocity, an effective conductivity of 5 x k_a was obtained (k_a = true conductivity of air). Campbell and Huntington[5] also investigated packed bed with gas flow. Particles tested were silica-alumina cylinders, hydrated alumina cylinders, tabular alumina spheres, aluminum cylinders, and glass spheres, ranging in size from 0.194 to 1.0 inch. Test temperatures were between 200°F and 700°F. A single linear extrapolation to zero gas velocity was used to obtain an overall conductivity of 0.31 $\frac{\text{Btu}}{\text{hr.ft.°F}}$ for all test

particles. Maximum deviation of data points from this correlation seemed to be ± 51 percent. Campbell and Huntington also reported data for packed beds in vacuum. From this set of data they were able to qualitatively conclude that radiant contributions were already an "appreciable factor."

Yagi and Kunii[40] present data for a number of packings in still air, with particle sizes ranging from 0.18 to 11.0 mm. and temperatures up to 840°C. Maximum experimental scatter, for values of overall conductivity of the same packing, seemed to be approximately ± 13 percent, a very respectable precision for experimental work in this field. Schotte[33] has analyzed Yagi and Kunii's data according to his proposed equations and reported that at the highest temperature, radiation contribution accounts for about 80 percent of the total thermal conductivity.

Only recently has an experimental investigation designed to study radiant heat transfer in packed media been reported. Hill and Wilhelm[15] made local total-conductivity measurements on a quiescent bed of 3.8 mm. alumina spheres at temperatures up to 1000°C. The conduction-conductivity was arbitrarily set equal to total-conductivity at 0°C, then extended to higher temperatures by the correlation of Wilhelm et al.[38]. These conduction-conductivities were then subtracted from total-conductivities to obtain values for radiant-conductivities. By this means, it was estimated that radiant transfer contributes about ten percent to total heat transfer at room temperatures and about 55 percent at 1000°C. Accuracy of the measured conductivities was estimated to range from five to 25 percent.

PART II

ANALYTICAL DEVELOPMENT

GENERAL ONE-DIMENSIONAL CASE

As mentioned previously, the analysis of this study was based on concepts presented by Hamaker.[13] A more detailed derivation with some new interpretations are presented below in order to underline the basic assumptions, advantages, and disadvantages of this mode of treatment.

Radiant Energy Transfer

Heat transfer by radiation is inherently different from conductive or convective heat transfer. While the latter two are dependent on the conveyance of kinetic energy of molecular vibration, radiation is dependent on the transport of electromagnetic energy. As such, there are three basic phenomena that come into play in the transport of radiant flux through a media of packed particles--emission, absorption, and scattering.

At a position $\vec{r}$ in the media, the specific intensity of radiant flux of wavelength λ which is traveling in the direction $\vec{\Omega}$ may be denoted by

$$i_\lambda(\vec{r}, \vec{\Omega}), \quad \frac{\text{Btu}}{\text{hr. ft}^2\text{. steradian}}$$

and the power impinging on an elemental area dA due to radiant flux traveling in the elemental solid angle $d\Omega$, about the direction $\vec{\Omega}$, is then equal to

$$i_\lambda(\vec{r}, \vec{\Omega})\, d\Omega\, dA \cos\mu, \quad \frac{\text{Btu}}{\text{hr.}}$$

where μ = angle between $\vec{\Omega}$ and normal to dA.

The next step, basic in this treatment, is to assume that properties of the discrete particulate media may be averaged over a bulk volume to obtain pseudo-homogeneous properties. This representation is analogous to such concepts as the "average density" for a mixture of solids, and should be quite

good if a large enough sample is considered. Thus, while local point conductivities vary greatly from solid particle to void, the average conductivity over a large cross section is sensibly constant. On the basis of this assumption, the following bulk properties may be defined.

S_λ = monochromatic scattering cross section per unit volume, the effective cross sectional area presented by a unit volume of packing that scatters the incident radiant flux, units of ft^2/ft^3.

A_λ = monochromatic absorption cross section per unit volume, the effective cross sectional area presented by a unit volume of packing that absorbs incident radiant flux, units of ft^2/ft^3.

E_λ = monochromatic emission cross section per unit volume, the effective cross sectional area presented by a volume of packing for the emission of radiation, units of ft^2/ft^3.

Now consider a beam of radiant flux, $i_\lambda(\vec{r},\vec{\Omega})\, d\Omega\, dA$, as it passes through an elemental volume of packing, as illustrated in Figure 4. The changes in the intensity of $i_\lambda(\vec{r},\vec{\Omega})\, d\Omega\, dA$ as it traverses the differential length dl are as follows:

a) loss due to scattering and absorption = $i_\lambda(\vec{r},\vec{\Omega})\, d\Omega\, dA\, dl \times (S_\lambda + A_\lambda)$

b) gain due to emission = $P_{t\lambda} \frac{1}{4\pi} d\Omega\, dA\, dl \times (E_\lambda)$

c) gain due to scattering of other fluxes into $d\Omega$

$$= d\Omega\, dA\, dl \int_{\Omega'} i_\lambda(\vec{r},\vec{\Omega}')\, f_\lambda(\vec{\Omega},\vec{\Omega}')\, S_\lambda\, d\Omega'$$

where $P_{t\lambda}$ = Planck's radiation spectra for emission of wavelength λ at temperature t.

$f_\lambda(\vec{\Omega},\vec{\Omega}')$ = angular distribution of scattering, the fraction of scattered flux which came from direction $\vec{\Omega}'$ and is scattered into $\vec{\Omega}$.

$\int_{\Omega'} \text{----} d\Omega'$ = integration over all directions of Ω'.

The net change in $i_\lambda(\vec{r},\vec{\Omega})\,d\Omega\,dA$ is then,

$$\begin{aligned} d[i_\lambda(\vec{r},\vec{\Omega})\,d\Omega\,dA] = & -(S_\lambda + A_\lambda)\, i_\lambda(\vec{r},\vec{\Omega})\,d\Omega\,dA\,dl \\ & + (S_\lambda)\,d\Omega\,dA\,dl \int_{\Omega'} i_\lambda(\vec{r},\vec{\Omega}')\, f_\lambda(\vec{\Omega},\vec{\Omega}')\,d\Omega' \\ & + (E_\lambda)\, P_{t\lambda} \frac{1}{4\pi}\, d\Omega\, dA\, dl \end{aligned}$$

which may be rewritten as,

$$\begin{aligned} \frac{d}{dl}\left[i_\lambda(\vec{r},\vec{\Omega}) \right] = & -(S_\lambda + A_\lambda)\, i_\lambda(\vec{r},\vec{\Omega}) \\ & + (S_\lambda) \int_{\Omega'} i_\lambda(\vec{r},\vec{\Omega}')\, f_\lambda(\vec{\Omega},\vec{\Omega}')\,d\Omega' \\ & + (E_\lambda)\, P_{t\lambda} \frac{1}{4\pi} \end{aligned} \qquad (9)$$

The integro-differential Equation (9) is commonly called the transport equation.

In the Cartesian coordinate system of Figure 5,

$$i_\lambda(\vec{r},\vec{\Omega}) = i_\lambda(x,y,z,\theta,\phi)$$

and

$$\begin{aligned} \frac{di_\lambda(\vec{r},\vec{\Omega})}{dl} = & \frac{\partial i}{\partial x}\frac{\partial x}{\partial l} + \frac{\partial i}{\partial y}\frac{\partial y}{\partial l} + \frac{\partial i}{\partial z}\frac{\partial z}{\partial l} \\ & + \frac{\partial i}{\partial \theta}\frac{\partial \theta}{\partial l} + \frac{\partial i}{\partial \phi}\frac{\partial \phi}{\partial l} \end{aligned}$$

For the one dimensional case,

$$\frac{\partial i}{\partial y} = \frac{\partial i}{\partial z} = \frac{\partial i}{\partial \phi} = 0$$

and for any specific direction of $\vec{\Omega}$,

$$\frac{\partial \phi}{\partial l} = \frac{\partial \theta}{\partial l} = 0$$

Thus, $i_\lambda(\vec{r},\vec{\Omega}) = i_\lambda(x,\theta)$

$$\begin{aligned} \frac{di_\lambda(\vec{r},\vec{\Omega})}{dl} &= \frac{di_\lambda(x,\theta)}{dx} \cdot \frac{\partial x}{\partial l} \\ &= \cos\theta \quad \frac{di_\lambda(x,\theta)}{dx} \end{aligned} \qquad (10)$$

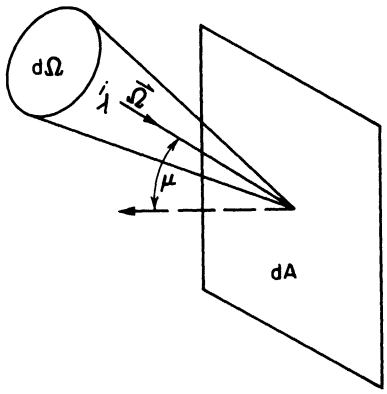

Figure 3. Illustration of Radiant Intensity

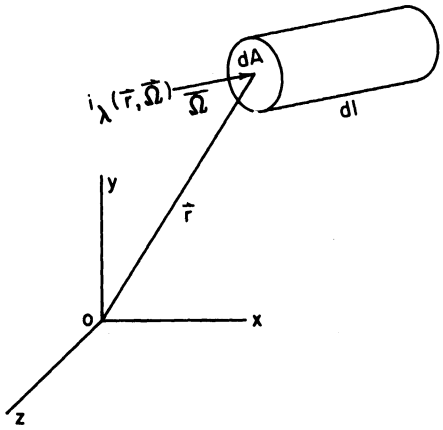

Figure 4. Traverse of Flux through Elemental Volume

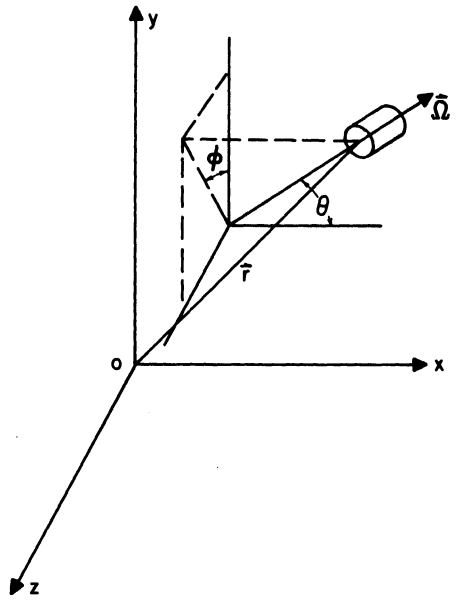

Figure 5. Cartesian Coordinate System

Substituting into Equation (9),

$$\cos\Theta \frac{di_\lambda(x,\Theta)}{dx} = -(S_\lambda + A_\lambda) i_\lambda(x,\Theta) + (S_\lambda)\int_{\Omega'} i_\lambda(x,\Theta') f_\lambda(\Theta,\Theta')\, d\Omega' + (E_\lambda) P_{t\lambda} \frac{1}{4\pi}$$

Evaluating the integral over the solid angle Ω',

$$\cos\Theta \frac{di_\lambda(x,\Theta)}{dx} = -(S_\lambda + A_\lambda) i_\lambda(x,\Theta) + (S_\lambda) 2\pi \int_{\Theta'=0}^{\pi} i_\lambda(x,\Theta') f_\lambda(\Theta,\Theta') \sin\Theta'\, d\Theta' + (E_\lambda) P_{t\lambda} \frac{1}{4\pi} \quad (11)$$

This energy balance is often written in terms of total intensity for black body radiation as,

$$\cos\Theta \frac{di_\infty(x,\Theta)}{dx} = -(S+A) i_\infty(x,\Theta) + (S) 2\pi \int_{\Theta'=0}^{\pi} i_\infty(x,\Theta') f(\Theta,\Theta') \sin\Theta'\, d\Theta' + (E) \frac{1}{2\pi} \sigma T^4 \quad (12)$$

$i_\infty(x,\Theta)$ = total specific intensity of all wavelengths

S, A, E, = total cross sections per unit volume of all wavelengths for scattering, absorption, and emission, respectively

σ = Stephen Boltzman constant

T = °R

$f(\Theta,\Theta')$ = aver. angular distribution function for all wavelengths.

The relationships between these black body parameters and the monochromatic parameters may be derived by integrating Equation (11) over all

wavelengths,

$$\cos\theta \frac{d}{dx}\int_0^\infty i_\lambda(x,\theta)\,d\lambda = -\int_0^\infty (S_\lambda + A_\lambda)\, i_\lambda(x,\theta)\,d\lambda + 2\pi\int_{\lambda=0}^{\infty}\int_{\theta'=0}^{\pi} S_\lambda\, i_\lambda(x,\theta')\, f_\lambda(\theta,\theta')\sin\theta'\,d\theta'\,d\lambda + \int_0^\infty E_\lambda P_{t\lambda}\,\frac{1}{4\pi}\,d\lambda \tag{13}$$

Comparing Equations (12) and (13), it is seen that,

$$i_\infty(x,\theta) = \int_0^\infty i_\lambda(x,\theta)\,d\lambda \tag{14}$$

$$S = \frac{\int_0^\infty S_\lambda i_\lambda(x,\theta)\,d\lambda}{\int_0^\infty i_\lambda(x,\theta)\,d\lambda} = \frac{1}{i_\infty(x,\theta)}\int_0^\infty S_\lambda i_\lambda(x,\theta)\,d\lambda \tag{15}$$

$$A = \frac{\int_0^\infty A_\lambda i_\lambda(x,\theta)\,d\lambda}{\int_0^\infty i_\lambda(x,\theta)\,d\lambda} = \frac{1}{i_\infty(x,\theta)}\int_0^\infty A_\lambda i_\lambda(x,\theta)\,d\lambda \tag{16}$$

$$E = \frac{\int_0^\infty E_\lambda P_{t\lambda}\,d\lambda}{\int_0^\infty P_{t\lambda}\,d\lambda} = \frac{1}{2\sigma T^4}\int_0^\infty E_\lambda P_{t\lambda}\,d\lambda \tag{17}$$

$$f(\theta,\theta') = \frac{\int_0^\infty S_\lambda i_\lambda(x,\theta)\, f_\lambda(\theta,\theta')\,d\lambda}{\int_0^\infty S_\lambda\, i_\lambda(x,\theta')\,d\lambda} = \frac{1}{S i_\infty(x,\theta')}\int_0^\infty S_\lambda i_\lambda(x,\theta') F_\lambda(\theta,\theta')\,d\lambda \tag{18}$$

Hamaker[13] started his analysis with the two-flux equations,

$$\begin{aligned}\frac{di}{dx} &= -(a+s_b)\,i + s_b j + a\sigma T^4 \\ \frac{dj}{dx} &= (a+s_b)\,j - s_b i - a\sigma T^4\end{aligned} \tag{8}$$

where i represents the flux of all radiant energy traveling in positive x direction and j represents the flux of all radiant energy traveling in negative x direction. The first terms in Equation (8) represent the net loss due to absorption and backward scattering. The second terms represent gain due to backscattering of the opposite flux, and the last terms represent gain due to thermal emission. The assumptions inherent in this system of equations, Equation (8), may be pointed out by integrating Equation (12) over forward and backward hemispheres.

Over forward hemisphere,

$$2\pi \frac{d}{dx}\int_0^{\frac{\pi}{2}} i_\infty(x,\theta)\cos\theta\sin\theta\,d\theta = -(S+A)\int_0^{\frac{\pi}{2}} i_\infty(x,\theta)\sin\theta\,d\theta \quad (19)$$
$$+ (S)(2\pi)^2\int_{\theta=0}^{\frac{\pi}{2}}\int_{\theta'=0}^{\pi} i_\infty(x,\theta')f(\theta,\theta')\sin\theta'\sin\theta\,d\theta'd\theta$$
$$+ (E)\sigma T^4\int_0^{\frac{\pi}{2}}\sin\theta\,d\theta$$

and over backward hemisphere,

$$2\pi \frac{d}{dx}\int_0^{\frac{3\pi}{2}} i_\infty(x,\theta)\cos\theta\sin\theta\,d\theta = -(S+A)\,2\pi\int_\pi^{\frac{3\pi}{2}} i_\infty(x,\theta)\sin\theta\,d\theta \quad (20)$$
$$+ (S)(2\pi)^2\int_{\theta=\pi}^{\frac{3\pi}{2}}\int_{\theta'=0}^{\pi} i_\infty(x,\theta')f(\theta,\theta')\sin\theta'\sin\theta\,d\theta'd\theta$$
$$+ (E)\sigma T^4\int_\pi^{\frac{3\pi}{2}}\sin\theta\,d\theta \quad .$$

Let,

$$i(x) = 2\pi\int_0^{\frac{\pi}{2}} i_\infty(x,\theta)\cos\theta\sin\theta\,d\theta \quad (21)$$

= radiant energy passing through a unit cross sectional area per unit time in +x direction

$$j(x) = 2\pi\int_\pi^{\frac{3\pi}{2}} i_\infty(x,\theta)\cos\theta\sin\theta\,d\theta \quad (22)$$

= radiant energy passing through a unit cross sectional area per unit time in -x direction

$$A_1 = 2\pi\frac{A}{i(x)}\int_0^{\frac{\pi}{2}} i_\infty(x,\theta)\sin\theta\,d\theta \quad (23)$$

$$A_2 = -2\pi\frac{A}{j(x)}\int_\pi^{\frac{3\pi}{2}} i_\infty(x,\theta)\sin\theta\,d\theta = 2\pi\frac{A}{j(x)}\int_0^{\frac{\pi}{2}} i_\infty(x,\theta+\pi)\sin\theta\,d\theta \quad (24)$$

$$S_1 = 2\pi\frac{S}{i}\int_0^{\frac{\pi}{2}} i_\infty(x,\theta)\sin\theta\,d\theta \quad (25)$$

$$S_2 = -2\pi\frac{S}{j}\int_\pi^{\frac{3\pi}{2}} i_\infty(x,\theta)\sin\theta\,d\theta = 2\pi\frac{S}{j}\int_0^{\frac{\pi}{2}} i_\infty(x,\theta+\pi)\sin\theta\,d\theta \quad (26)$$

$$S_{1F} = (2\pi)^2\frac{S}{i}\int_{\theta=0}^{\frac{\pi}{2}}\int_{\theta'=0}^{\frac{\pi}{2}} i_\infty(x,\theta')f(\theta,\theta')\sin\theta\sin\theta'\,d\theta\,d\theta' \quad (27)$$

$$S_{1B} = (2\pi)^2\frac{S}{j}\int_{\theta=0}^{\frac{\pi}{2}}\int_{\theta'=\frac{\pi}{2}}^{\pi} i_\infty(x,\theta')f(\theta,\theta')\sin\theta\sin\theta'\,d\theta\,d\theta' \quad (28)$$

$$S_{2F} = -(2\pi)^2\frac{S}{j}\int_{\theta=\pi}^{\frac{3\pi}{2}}\int_{\theta'=\frac{\pi}{2}}^{\pi} i_\infty(x,\theta')f(\theta,\theta')\sin\theta\sin\theta'\,d\theta\,d\theta'$$
$$= (2\pi)^2\frac{S}{j}\int_{\theta=0}^{\frac{\pi}{2}}\int_{\theta'=0}^{\frac{\pi}{2}} i_\infty(x,\theta'+\pi)f(\theta+\pi,\theta'+\pi)\sin\theta\sin\theta'\,d\theta\,d\theta' \quad (29)$$

$$S_{2B} = -(2\pi)^2\frac{S}{i}\int_{\theta=\pi}^{\frac{3\pi}{2}}\int_{\theta'=0}^{\frac{\pi}{2}} i_\infty(x,\theta')f(\theta,\theta')\sin\theta\sin\theta'\,d\theta\,d\theta'$$
$$= (2\pi)^2\frac{S}{i}\int_{\theta=0}^{\frac{\pi}{2}}\int_{\theta'=\frac{\pi}{2}}^{\pi} i_\infty(x,\theta'+\pi)f(\theta+\pi,\theta'+\pi)\sin\theta\sin\theta'\,d\theta\,d\theta' \quad (30)$$

Equations (19) and (20) may then be written as,

$$\frac{di(x)}{dx} = -S_1 i - A_1 i + S_{1F} i + S_{1B} j + E\sigma T^4 \tag{31}$$

and,

$$\frac{dj(x)}{dx} = S_2 j + A_2 j - S_{2F} j - S_{2B} i - E\sigma T^4 \tag{32}$$

By definition of angular scattering function,

$$\int_{\theta=0}^{\pi} \int_{\phi=0}^{2\pi} f(\theta, \theta') \sin\theta \, d\theta = 1 \tag{33}$$

and so,

$$S_1 i = 2\pi S \int_0^{\frac{\pi}{2}} i_\infty (x, \theta') \sin\theta' \, d\theta'$$

$$= 2\pi S \int_{\theta'=0}^{\frac{\pi}{2}} i_\infty (x, \theta') \sin\theta' \left[2\pi \int_{\theta=0}^{\frac{\pi}{2}} f(\theta, \theta') \sin\theta \, d\theta + 2\pi \int_{\theta=\frac{\pi}{2}}^{\pi} f(\theta, \theta') \sin\theta \, d\theta \right] d\theta'$$

$$S_1 i = (S_{1F} + S_{2B}) i \tag{34a}$$

similarly,

$$S_2 j = (S_{1B} + S_{2F}) j \tag{34b}$$

Therefore, Equations (31) and (32) reduce to,

$$\frac{di}{dx} = -(S_{2B} + A_1) i + S_{1B} j + E\sigma T^4 \tag{35}$$

$$-\frac{dj}{dx} = -(S_{1B} + A_2) j + S_{2B} i + E\sigma T^4 \tag{36}$$

Comparing Equations (35) and (36) with Equation (8), it is now readily seen that the conditions or approximations necessary for Hamaker's two-flux equations are as follows:

(a) $a = A_1 = A_2$

i.e.,
$$\frac{\int_0^{\frac{\pi}{2}} i_\infty (x, \theta) \sin\theta \, d\theta}{\int_0^{\frac{\pi}{2}} i_\infty (x, \theta) \sin\theta \cos\theta \, d\theta} = \frac{\int_0^{\frac{\pi}{2}} i_\infty (x, \theta+\pi) \sin\theta \, d\theta}{\int_0^{\frac{\pi}{2}} i_\infty (x, \theta+\pi) \sin\theta \cos\theta \, d\theta} \tag{37a}$$

(b) $s_b = S_{2B} = S_{1B}$

i.e.,
$$\frac{\int_{\theta=0}^{\frac{\pi}{2}} \int_{\theta'=\frac{\pi}{2}}^{\pi} i_\infty (x, \theta') f(\theta, \theta') \sin\theta \sin\theta' \, d\theta \, d\theta'}{\int_0^{\frac{\pi}{2}} i_\infty (x, \theta+\pi) \sin\theta \cos\theta \, d\theta} =$$

$$\frac{\int_{\theta=0}^{\frac{\pi}{2}} \int_{\theta'=\frac{\pi}{2}}^{\pi} i_\infty (x, \theta'+\pi) f(\theta+\pi, \theta'+\pi) \sin\theta \sin\theta' \, d\theta \, d\theta'}{\int_0^{\frac{\pi}{2}} i_\infty (x, \theta) \sin\theta \cos\theta \, d\theta} \tag{37b}$$

(c) $a = E$ (37c)

Condition (37c) is the equivalent of Kirchhoff's law and may be considered as satisfied. Conditions (37a) and (37b) are equivalent to the requirement that the fraction of radiant flux traveling in +x direction which gets absorbed or backscattered be the same as the fraction that would be absorbed or backscattered if the radiant flux has been traveling in -x direction. These conditions are sensibly satisfied for particles that are either symmetric or are randomly packed. Under these conditions, the two flux equations of Equation (8) may be considered to be valid.

Simultaneous Conductive and Radiative Transfer

For all packings of the particle-size and temperature ranges considered, conduction and radiation are the two important heat transfer mechanisms and occur simultaneously. The coupling between them is by the process of absorption and emission of radiant energy. The governing relationship may be obtained by a thermal energy balance about a differential element, $dA \cdot dx$, of the packed bed.

Net accumulation of energy due to conduction is given by the familiar Laplacian term,

$$k_c \frac{d^2T}{dx^2}$$

where k_c = bulk conduction-conductivity for packed media. The input of radiant energy is given by, $a(i + j)$ and the output of radiant energy is $2a(\sigma T^4)$. Thus the continuity equation of heat flow is

$$k_c \frac{d^2T}{dx^2} + a(i+j) - 2a\sigma T^4 = \rho_B c_B \frac{dT}{d\theta} \qquad (38)$$

where ρ_B = bulk density,

c_B = bulk heat capacity,

θ = time,

T = absolute temperature,

For steady state,

$$K_c \frac{d^2T}{dx^2} + a(i+j) - 2a\sigma T^4 = 0 \qquad (39)$$

Four boundary conditions are required in order to completely define the one-dimensional system of Figure 1. Two conditions usually known are the wall temperatures,

$$T(x=0) = T_1 \quad °R$$

$$T(x=L) = T_2 \quad °R$$

If the emissivities of the two walls are also known, then the other two boundary conditions may be written as a radiant energy balance at each wall,

$$i(x=0) = \epsilon_1 \sigma T_1^4 + (1-\epsilon_1) \cdot j(x=0)$$

$$j(x=L) = \epsilon_2 \sigma T_2^4 + (1-\epsilon_2) \cdot i(x=L)$$

where ϵ_1 = emissivity of wall at x = 0

ϵ_2 = emissivity of wall at x = L.

To summarize, one dimensional, steady state, coupled radiation and conduction heat transfer through packed media is described by the following three simultaneous differential equations and four boundary conditions:

$$\frac{di}{dx} = -(a+s_b)i + s_b j + a\sigma T^4 \qquad (40)$$

$$-\frac{dj}{dx} = -(a+s_b)j + s_b i + a\sigma T^4 \qquad (41)$$

$$K_c \frac{d^2T}{dx^2} + a(i+j) - 2a\sigma T^4 = 0 \qquad (42)$$

and,

$$T(x=0) = T_1 \qquad (43a)$$

$$T(x=L) = T_2 \qquad (43b)$$

$$i(x=0) = \epsilon_1 \sigma T_1^4 + (1-\epsilon_1) j(x=0) \qquad (43c)$$

$$j(x=L) = \epsilon_2 \sigma T_2^4 + (1-\epsilon_2) i(x=L) \qquad (43d)$$

The conductive heat transfer rate is,

$$Q_c = -K_c \frac{dT}{dx} \quad , \quad \frac{Btu}{hr.\ ft^2} \tag{44}$$

and the radiative heat transfer rate is,

$$Q_r = i - j \quad , \quad \frac{Btu}{hr.\ ft^2} \tag{45}$$

from which an equivalent radiant conductivity may be defined as,

$$k_r = \frac{Q_r}{-\frac{dT}{dx}} = \frac{i-j}{-\frac{dT}{dx}} \tag{46}$$

Dimensional Analysis

From Equations (40) to (43), it is seen that the four variables, i, j, T, and x are functions of eight parameters a, s_b, k_c, L, T_1, T_2, ϵ_1, and ϵ_2. It may be expected that some of the eight parameters could be combined to obtain a minimum number of parametric groups, affecting a very useful reduction in the amount of numerical work necessary to specify the general solution. This minimum number and the grouping of parameters may be obtained by the dimensional analysis technique of Hellums and Churchill[14], as follows.

For the four variables in the differential Equations (40) to (42), substitute the dimensionless quantities,

$$\begin{aligned} \tau &= \frac{T}{t_o} \\ X &= \frac{x}{x_o} \\ I &= \frac{i}{i_o} \\ J &= \frac{j}{j_o} \end{aligned} \tag{47}$$

where t_o, i_o, j_o, x_o are arbitrary constants to be specified later. Substituting into Equations (40) to (42) and boundary conditions (43),

$$\frac{dI}{dX} = -(a x_o + s_b x_o) I + \left(\frac{s_b x_o j_o}{i_o}\right) J + \left(\frac{a x_o \sigma t_o^4}{i_o}\right) \tau^4 \tag{48}$$

$$-\frac{dJ}{dX} = -(a x_o + s_b x_o) J + \left(\frac{s_b x_o i_o}{j_o}\right) I + \left(\frac{a x_o \sigma t_o^4}{j_o}\right) \tau^4 \tag{49}$$

$$\frac{d^2\tau}{dX^2} + \left(\frac{a x_o^2 i_o}{K_c t_o}\right) I + \left(\frac{a x_o^2 j_o}{K_c t_o}\right) J - 2\left(\frac{a x_o^2 \sigma t_o^4}{K_c t_o}\right) \tau^4 = 0 \qquad (50)$$

$$\tau(X=0) = \frac{T_1}{t_o} = \tau_1 \qquad (51a)$$

$$\tau\left(X=\frac{L}{x_o}\right) = \frac{T_2}{t_o} = \tau_2 \qquad (51b)$$

$$I(X=0) = \left(\frac{\epsilon_1 \sigma}{i_o}\right) \tau_1^4 + (1-\epsilon_1)\left(\frac{j_o}{i_o}\right) \cdot J(X=0) \qquad (51c)$$

$$J\left(X=\frac{L}{x_o}\right) = \left(\frac{\epsilon_2 \sigma}{j_o}\right) \tau_2^4 + (1-\epsilon_2)\left(\frac{i_o}{j_o}\right) \cdot I\left(X=\frac{L}{x_o}\right) \qquad (51d)$$

It is seen that there are ten independent groups of parameters which appear in Equations (48) to (51),

$$(a x_o) \;,\; (s_b x_o) \;,\; \left(\frac{\sigma t_o^3 x_o}{K_c}\right) \;,\; \left(\frac{L}{x_o}\right) \;,\; \left(\frac{T_1}{t_o}\right) \;,$$

$$\left(\frac{T_2}{t_o}\right) \;,\; \left(\frac{i_o}{j_o}\right) \;,\; \left(\frac{\sigma}{i_o}\right) \;,\; \epsilon_1 \;, \text{ and } \epsilon_2 \;.$$

Since four quantities, x_o, i_o, j_o, t_o, are arbitrary, it is evident that ultimately the physical problem can be defined in terms of just six groups of parameters. If the four arbitrary reference quantities are chosen to be,

$$\begin{aligned} x_o &= L \;, \text{ ft.} \\ t_o &= T_1 \;, \; ^\circ R \\ i_o &= \sigma T_1^4 \;, \; \frac{\text{Btu}}{\text{hr. ft}^2} \\ j_o &= \sigma T_1^4 \;, \; \frac{\text{Btu}}{\text{hr. ft}^2} \end{aligned} \qquad (52)$$

then the dimensionless variables are,

$$\begin{aligned} X &= \frac{x}{L} \\ \tau &= \frac{T}{T_1} \\ I &= \frac{i}{\sigma T_1^4} \\ J &= \frac{j}{\sigma T_1^4} \end{aligned} \qquad (53)$$

and the six independent parameter groups may be chosen to be,

$$\alpha = aL = \text{dimensionless absorption coefficient}$$

$$\beta = s_b L = \text{dimensionless backscattering coefficient}$$

$$\gamma = \frac{\sigma T_1^3 L}{K_c} = \text{dimensionless ratio of radiation to conduction from wall at } X = 0 \tag{54}$$

$$\delta = \left(\frac{T_1}{T_2}\right)^4 = \text{boundary temperature ratio}$$

$$\epsilon_1 = \text{boundary emissivity at } X = 0$$

$$\epsilon_2 = \text{boundary emissivity at } X = 1.$$

The system of Equations (40) to (42) may now be written in dimensionless form as,

$$\frac{dI}{dX} = -(\alpha + \beta) I + \beta J + \alpha \tau^4 \tag{55}$$

$$-\frac{dJ}{dX} = -(\alpha + \beta) J + \beta I + \alpha \tau^4 \tag{56}$$

$$\frac{d^2\tau}{dX^2} + \alpha\gamma (I + J - 2\tau^4) = 0 \tag{57}$$

and the corresponding boundary conditions would be,

$$\tau_1 (X=0) = 1 \tag{58a}$$

$$\tau_2 (X=1) = \delta^{-1/4} \tag{58b}$$

$$I(X=0) = \epsilon_1 + (1-\epsilon_1) \cdot J(X=0) \tag{58c}$$

$$J(X=1) = \epsilon_2 \delta^{-1} + (1-\epsilon_2) \cdot I(X=1) \tag{58d}$$

In terms of these dimensionless variables, Equations (44) to (46) may be re-written as,

$$Q_c(X) = -\frac{K_c T_1}{L} \frac{d\tau(X)}{dX} \tag{59}$$

$$Q_r(X) = \sigma T_1^4 [I(X) - J(X)] \tag{60}$$

and

$$K_r(X) = -\frac{\sigma L T_1^3 [I(X) - J(X)]}{\frac{d\tau}{dX}} \tag{61}$$

Approximate Solutions

The system of Equations (55) to (57) are nonlinear, and no exact solution has been found. However, a number of approximate solutions have been suggested by various authors for the equivalent system of Equations (40) to (42). These approximate solutions are rewritten below for the dimensionless system, Equations (55) to (57), and are reviewed with regard to regions of applicability.

Larkin and Churchill[20] obtained a solution by assuming that the temperature $\tau(X)$ may be approximated as a linear function of position. This allowed the nonlinear terms, $\alpha\tau^4$, to be replaced by a function in X so that Equations (55) to (57) becomes an ordinary system of nonhomogeneous linear differential equations. The solutions can then be written as,

$$I(X) = c_1 \sinh\left(X\sqrt{\eta^2-\beta^2}\right) + c_2 \cosh\left(X\sqrt{\eta^2-\beta^2}\right) + \tau^4 + \frac{4(\tau_1-\tau_2)\tau^3}{(\eta+\beta)} + \frac{12(\tau_1-\tau_2)^2\tau^2}{(\eta^2-\beta^2)} + \frac{24(\tau_1-\tau_2)^3\tau}{(\eta^2-\beta^2)(\eta+\beta)} + \frac{24(\tau_1-\tau_2)^4}{(\eta^2-\beta^2)^2} \tag{62}$$

$$J(X) = \frac{1}{\beta}\left(c_1\sqrt{\eta^2-\beta^2} + c_2\eta\right)\cosh\left(X\sqrt{\eta^2-\beta^2}\right) + \frac{1}{\beta}\left(c_2\sqrt{\eta^2-\beta^2} + c_1\eta\right)\sinh\left(X\sqrt{\eta^2-\beta^2}\right) + \tau^4 - \frac{4(\tau_1-\tau_2)\tau^3}{(\eta+\beta)} + \frac{12(\tau_1-\tau_2)^2\tau^2}{(\eta^2-\beta^2)} - \frac{24(\tau_1-\tau_2)^3\tau}{(\eta+\beta)(\eta^2-\beta^2)} + \frac{24(\tau_1-\tau_2)^4}{(\eta^2-\beta^2)^2} \tag{63}$$

where $\eta = \alpha + \beta$ = net attenuation coefficient, and c_1, c_2 are boundary constants to be determined from Equations (58c) and (58d).

The region of applicability for this solution may be found by examining Equation (57). The approximation,

$$\tau(X) = c_3 X + c_4, \quad \text{linear } X \text{ function} \tag{64}$$

c_3, c_4 = constants

is equivalent to the approximation that

$$\frac{d\tau}{dX} = c_3 = \text{constant}$$

$$\text{and } \frac{d^2\tau}{dX^2} = 0 \tag{65}$$

From Equation (57), it is seen that there are four cases which would satisfy this condition:

a) $\alpha \cong 0$

i.e., the packed media is sensibly nonabsorbent.

b) $\gamma \cong 0$

i.e., the ratio of radiation to conduction is sensibly zero.

c) $\alpha \neq 0$, $\gamma \neq 0$, $\gamma\alpha \rightarrow 0$

i.e., absorption and radiation both exist but are sufficiently small so that the product, $\gamma\alpha$, approaches zero.

d) $I + J \cong 2\tau^4$

i.e., the total radiant flux at any point is sensibly equal to the local thermal emission.

In practical cases, only conditions (a), (c), and (d) are of interest since the case of zero radiation degenerates to the usual Fourier conduction problem. For condition (a), another approach may be taken which leads to a simpler solution, as follows.

Assuming that the packed media is quite nonabsorbent,

$\alpha \cong 0$

$\alpha + \beta = \eta \cong \beta$

the nonlinear terms in Equations (55) to (57) drop out to give,

$$\frac{dI}{dX} = -\eta I + \eta J \tag{66}$$

$$-\frac{dJ}{dX} = -\eta J + \eta I \tag{67}$$

$$\frac{d^2\tau}{dX^2} = 0 \tag{68}$$

Note that while radiation and conduction can still occur simultaneously, they are no longer coupled in this case. The temperature function is obtained from Equation (68),

$$\tau(X) = c_3 X + c_4 \tag{64}$$

and evaluating the constants, c_3 and c_4, by boundary conditions (58a) and (58b)

$$\tau(X) = (\delta^{-1/4} - 1)X + 1 \quad . \tag{69}$$

Equations (66) and (67) may be solved rigorously to obtain the radiant fluxes,

$$I(X) = c_1 X + c_2 \tag{70}$$

$$J(X) = c_1 X + \frac{c_1}{\eta} + c_2 \quad . \tag{71}$$

Boundary constants c_1 and c_2 are evaluated from Equations (58c) and (58d) to obtain,

$$c_1 = \frac{\eta \epsilon_1 \epsilon_2 (\delta^{-1} - 1)}{\epsilon_1 + \epsilon_2 + \epsilon_1 \epsilon_2 (\eta - 1)} \tag{72}$$

$$c_2 = \frac{\epsilon_1 (1 + \eta \epsilon_2) - \epsilon_2 \delta^{-1} (1 - \epsilon_1)}{\epsilon_1 - \epsilon_2 + \epsilon_1 \epsilon_2 (\eta + 1)} \quad . \tag{73}$$

Substituting into Equations (60) and (61), the radiant heat transfer rate is found to be,

$$Q_r = \frac{\sigma T_1^4 \epsilon_1 \epsilon_2 (\delta - 1)}{\delta \left[\epsilon_1 + \epsilon_2 + \epsilon_1 \epsilon_2 (\eta - 1)\right]} \tag{74}$$

and the equivalent radiant conductivity is,

$$K_r = \frac{\sigma T_1^3 L (1 - \delta^{-1})}{(\eta - 1 + \epsilon_1^{-1} + \epsilon_2^{-1})(1 - \delta^{-1/4})} \quad . \tag{75}$$

Hamaker[13] proposed a solution based on approximating the fourth order temperature term by,

$$\tau^4 \cong \tau_o^4 + 4\tau_o^3(\tau - \tau_o) \tag{76}$$

where τ_o = some base temperature near the mean bed temperature. Hamaker's solution, transposed into dimensionless form is,

$$I(X) = A(1-\beta')e^{\sigma' X} + B(1+\beta')e^{-\sigma' X} + C(\sigma' X - \beta') + D \tag{77}$$

$$J(X) = A(1+\beta')e^{\sigma' X} + B(1-\beta')e^{-\sigma' X} + C(\sigma' X + \beta') + D \tag{78}$$

$$\tau^4(X) = -A\alpha' e^{\sigma' X} - B\alpha' e^{-\sigma' X} + C\sigma' X + D \tag{79}$$

where,

$$\sigma' = \sqrt{\alpha(8\gamma\tau_o^3 + \alpha + 2\beta)}$$
$$\alpha' = \frac{8\tau_o^3\gamma}{\alpha + 2\beta} \tag{80}$$
$$\beta' = \frac{\sigma'}{\alpha + 2\beta}$$

The four constants A, B, C, D were to be evaluated by boundary conditions. Since this evaluation was not given by Hamaker, it was necessary to do so in order to obtain a useful solution. Substituting functions (77) to (80) into the boundary Equation (58) and solving, the constants were determined to be,

$$A = \frac{b_2 c_1 - b_1 c_2}{a_1 b_2 - a_2 b_1} \tag{81}$$

$$B = \frac{a_1 c_2 - a_2 c_1}{a_1 b_2 - a_2 b_1} \tag{82}$$

$$C = \frac{1}{\sigma'}\left[\alpha'(e^{\sigma'} - 1)A + \alpha'(e^{-\sigma'} - 1)B - (1 - \delta^{-1})\right] \tag{83}$$

$$D = \alpha'[A + B] + 1 \tag{84}$$

where, $a_1 = \epsilon_1 (1+\alpha') - \beta' (2-\epsilon_1)\left[\frac{\alpha'}{\sigma'}(e^{\sigma'}-1) + 1\right]$ (85)

$b_1 = \epsilon_1 (1+\alpha') - \beta' (2-\epsilon_1)\left[\frac{\alpha'}{\sigma'}(e^{-\sigma'}-1) - 1\right]$ (86)

$c_1 = \frac{-(1-\delta^{-1})(2-\epsilon_1)}{(\alpha + 2\beta)}$ (87)

$a_2 = \epsilon_2 e^{\sigma'}(1+\alpha') + \beta' (2-\epsilon_2)\left[\frac{\alpha'}{\sigma'}(e^{\sigma'}-1) + e^{\sigma'}\right]$ (88)

$b_2 = \epsilon_2 e^{-\sigma'}(1+\alpha') + \beta' (2-\epsilon_2)\left[\frac{\alpha'}{\sigma'}(e^{-\sigma'}-1) - e^{-\sigma'}\right]$ (89)

$c_2 = \frac{(1-\delta^{-1})(2-\epsilon_2)}{(\alpha + 2\beta)}$ (90)

For large values of σ' , which is usually the case, it was found that many terms could be neglected and the above relations simplify to,

$a_1 = -\frac{\alpha'(2-\epsilon_1)}{\alpha+2\beta} e^{\sigma'}$ (91)

$b_1 = \epsilon_1 (1+\alpha') + \beta' (2-\epsilon_1)(\frac{\alpha'}{\sigma'} + 1)$ (92)

$c_1 = -\frac{(1-\delta^{-1})(2-\epsilon_1)}{\alpha + 2\beta}$ (93)

$a_2 = \left[\epsilon_2 (1+\alpha') + \beta' (2-\epsilon_2)(\frac{\alpha'}{\sigma'} + 1)\right] e^{\sigma'}$ (94)

$b_2 = -\frac{\alpha'(2-\epsilon_2)}{\alpha+2\beta}$ (95)

$c_2 = \frac{(1-\delta^{-1})(2-\epsilon_2)}{\alpha+2\beta}$ (96)

By this solution, the temperature gradient is no longer limited to a constant,

$$\frac{d\tau(X)}{dX} = \frac{1}{4\tau_0^3} \frac{d(\tau^4)}{dX}$$

and by differentiating Equation (79),

$$\frac{d\tau(X)}{dX} = \frac{\sigma'}{4\tau_0^3}\left[-A\alpha' e^{\sigma' X} + B\alpha' e^{-\sigma' X} + C\right] \quad (97)$$

The conduction heat transfer rate would then be,

$$Q_c(X) = -k_c \frac{T_1}{L} \frac{d\tau}{dX} \quad (59)$$

$$= -\frac{K_c T_1 \sigma'}{4L\tau_0^3}(-A\alpha' e^{\sigma' X} + B\alpha' e^{-\sigma' X} + C) . \quad (98)$$

The radiation heat transfer rate would be,

$$Q_r(X) = \sigma T_1^4 (I(X) - J(X)) \quad (60)$$

and by Equations (77) and (78),

$$Q_r(X) = 2\sigma T_1^4 \beta' \left(-Ae^{\sigma' X} + Be^{-\sigma' X} - C\right) \qquad (99)$$

The corresponding equivalent radiant conductivity is found by substitution into Equation (61),

$$K_r(X) = -\frac{Q_r}{\frac{\Pi}{L}\frac{d\tau}{dX}} \qquad (61)$$

$$= \frac{8\sigma T_1^3 \tau_0^3 L \beta'}{\sigma'}\left[\frac{Ae^{\sigma' X} - Be^{-\sigma' X} + C}{\alpha'\left(-Ae^{\sigma' X} + Be^{-\sigma' X}\right) + C}\right] . \qquad (100)$$

Equations (98) to (100) together with boundary functions (81) to (84) and (91) to (96) represent the complete solution in accordance with Hamaker's approximation. It should be noted that the approximation Equation (76) is the equivalent of a truncated Taylor series,

$$\tau^4 \cong \tau_0^4 + (\tau - \tau_0)\left[\frac{d\tau^4}{d\tau}\right]_{\tau_0} + \underbrace{\sum_{n=2}^{\infty} (\tau - \tau_0)^n \frac{1}{n!}\left[\frac{d^n \tau^4}{d\tau^n}\right]_{\tau_0}}_{\text{neglected}}$$

so that an estimate of the maximum error may be obtained from Taylor's remainder formula,

$$\Delta_m = \left[\frac{d^2\tau^4}{d\tau^2}\right]_{\tau_m} \frac{(\tau - \tau_0)^2}{2}$$

$$= 6\tau_m^2 (\tau - \tau_0)^2 \qquad (101)$$

where Δ_m is the maximum possible error in τ^4

and $\tau_m = \tau$ for $\tau > \tau_0$

$\tau_m = \tau_0$ for $\tau < \tau_0$

In general, this approximate solution is quite good for small values of δ, i.e., for small temperature differences. It is to be recommended for most practical applications, and especially for application where local details are of importance.

Radiant Conductivity for the Media

With the exception of the zero-absorptivity case, it is seen from the above solutions that I, J, τ, and Q_r are all functions of position and boundary conditions as well as of the packing properties. It is evident that any equivalent radiant conductivity, k_r, would be a property of the system rather than a physical property of the packed media itself, such as k_c is. Larkin and Churchill[20] have demonstrated that k_r for an optically thin system is highly dependent on the values of boundary temperatures and emissivities. This fact may also be seen from Equation (100). Therefore, a value of k_r is generally insufficient to specify the radiant transfer properties of a packed media. Rigorously speaking, only the two attenuation cross sections, a and s_b, are true radiant "properties" of the packed media and can be used as a measure of its transfer characteristic.

However, values of a and s_b have little physical meaning and does not provide a sense of the ease of transfer, as k_c does for conduction. Moreover, the relative importance of radiation and conduction is not evident from comparisons of a and s_b to k_c. What is desired is some sort of a conductance coefficient which would have physical meaning in terms of ease of radiant transfer and which would be a true "property" of the packed media itself--independent of boundary conditions.

Such a coefficient was found by examining the expression of radiant conductivity for interiors of thick packings, where boundary effects may be expected to be at a minimum. Equation (100) gives the local conductivity at any point as,

$$K_1(X) = \frac{8\sigma T_i^3 r_o^3 L \beta'}{\sigma'} \left[\frac{Ae^{\sigma' X} - Be^{-\sigma' X} + C}{-\alpha'(Ae^{\sigma' X} - Be^{-\sigma' X}) + C} \right] . \qquad (100)$$

Equations (81), (82), and (91) to (96) show that the two constants, A and B, are of the form,

$$A = d_1 e^{-\sigma'}$$

$$B = d_2$$

where d_1 and d_2 are nonexponential constants. The constant σ' is directly proportional to the thickness of packing, L, as seen by Equation (80). Thus, for interior regions of thick packings where,

$$L \text{ is large}$$

$$X \neq 0$$

$$X \neq 1 \quad ,$$

it is seen that,

$$A e^{\sigma' X} = d_1 e^{-\sigma'(1-X)} \longrightarrow 0$$

$$B e^{-\sigma' X} = d_2 e^{-\sigma' X} \longrightarrow 0$$

Therefore, the exponential terms of Equation (100) may be dropped,

$$\frac{-Q_r}{\frac{T_1}{L}\frac{d\tau}{dX}} = \frac{8\sigma T_1^3 \tau_0^3 L \beta'}{\sigma'}\left[\frac{(A e^{\sigma' X} - B e^{-\sigma' X}) + C}{\alpha'(-A e^{\sigma' X} + B e^{-\sigma' X}) + C}\right]$$

$$= \frac{8\sigma T_1^3 \tau_0^3 L \beta'}{\sigma'}$$

$$= \frac{8\sigma T_0^3}{a + 2s_b} \qquad (103)$$

Thus a quantity k_{ir} may be defined,

k_{ir} = interior radiant conductivity

$$= \frac{8\sigma T^3}{a + 2s_b} \quad , \quad \frac{Btu}{hr.ft.^\circ R} \qquad (104)$$

where T = operating temperature, °R.

This function, k_{ir}, is seen to be independent of boundary conditions and has the physical meaning of conductance. It provides a simple expression for characterizing radiant transfer properties for packed media and may be used as a guide to the relative importance of radiation and conduction by direct comparison with k_c. The expression, Equation (104), was also derived by Hamaker[13] by a different procedure, but its significance was not actually utilized.

EXPERIMENTAL CASE

In the experimental program of this investigation it was possible to modulate the transmission signal in such a way that only the direct and scattered radiant fluxes would be measured. Radiant energy which was absorbed and then re-emitted, along with any conducted energy, was not counted in the strength of the transmission signal. This modulated transmission led to simplified forms of the two-flux equations which could be solved rigorously. These simplified equations and their solution are described below.

Modulated Transmission Equations

In Equations (40) and (41), the $(a\sigma T^4)$ terms denote gain due to emitted radiant energy. If i_e and j_e are defined as radiant flux intensities for the experimental case, i.e., without emission flux, then the $(a\sigma T^4)$ terms may be dropped from the flux equations to give,

$$\frac{di_e}{dx} = -(a + s_b) i_e + s_b j_e = -a_n i_e + s_b j_e \tag{105}$$

$$-\frac{dj_e}{dx} = -(a + s_b) j_e + s_b i_e = -a_n j_e + s_b i_e \tag{106}$$

Boundary conditions for the experimental case are:

a) at $x = 0$, $i_e(0) = S_o$, a known input signal (107)

b) at $x = h$ ft., $j_e(h) = 0$, no reflection. (108)

These conditions represent black body boundaries with

$$\epsilon_1 = \epsilon_2 = 1$$

Solving Equations (105) and (106) simultaneously,

$$j_e = \frac{1}{s_b}\left[\frac{di_e}{dx} + a_n i_e\right] \tag{109}$$

$$\frac{dj_e}{dx} = \frac{1}{s_b}\left[\frac{d^2 i_e}{dx^2} + a_n \frac{di_e}{dx}\right] \tag{110}$$

and substituting into Equation (106),

$$\frac{d^2 i_e}{dx^2} - (a_n^2 - s_b^2)\, i_e = 0$$

or,

$$\frac{d^2 i_e}{dx^2} = m^2 i_e \tag{111}$$

where, $m^2 = a_n^2 - s_b^2$

$$m = \sqrt{a^2 + 2as_b}$$, always real.

The general solution of Equation (111) is,

$$i_e(x) = c_1 \cosh(mx) + c_2 \sinh(mx) \tag{112}$$

and

$$\frac{di_e(x)}{dx} = c_1 m \sinh(mx) + c_2 m \cosh(mx) \tag{113}$$

Substituting into Equation (109),

$$j_e(x) = \frac{1}{s_b}(c_1 m + c_2 a_n)\sinh(mx) + \frac{1}{s_b}(c_2 m + c_1 a_n)\cosh(mx) \tag{114}$$

The constants c_1 and c_2 may be evaluated from boundary conditions of Equations (107) and (108),

$$i_e(0) = S_o = c_1 \cosh(0) + c_2 \sinh(0)$$

$$c_1 = S_o$$

and

$$j_e(h) = 0 = (mS_o + c_2 a_n)\sinh(mh) + (c_2 m + a_n S_o)\cosh(mh)$$

$$c_2 = -S_o\left[\frac{m\sinh(mh) + a_n\cosh(mh)}{m\cosh(mh) + a_n\sinh(mh)}\right].$$

Thus the flux transmitted through a bed of depth h is,

$$i_e(h) = S_o\left[\cosh(mh) - \frac{m\sinh(mh) + a_n\cosh(mh)}{m\cosh(mh) + a_n\sinh(mh)}\sinh(mh)\right]$$

$$= S_o\left[\frac{m}{m\cosh(mh) + a_n\sinh(mh)}\right]$$

Since S_o is the flux incident on the bed at $x = 0$, a normalized transmitted flux may be defined as,

$$S_n(h) = \frac{i_e(h)}{i_e(0)} = \frac{i_e(h)}{S_o}$$
$$= \frac{m}{m\cosh(mh) + a_n \sinh(mh)} \qquad (115)$$

Equation (115) is the analytical model used to fit experimental measurements of S_n and h.

PART III

EXPERIMENTAL INVESTIGATION

DESCRIPTION

Background

Equations (99), (100), and (80) of the previous section show that the radiant heat transfer characteristics of any packed system may be described in terms of two attenuation cross sections for the packed media, a and s_b. If values of these two parameters are known, together with boundary temperatures and emissivities, then the local radiant heat transfer rate may be obtained by Equation (99) and the corresponding radiant "conductivity" would be given by Equation (100). The interior radiant conductivity, k_{ir}, solely a property of the packed media, may also be described in terms of a and s_b according to Equation (104).

The obvious next step would be to obtain measured values of a and s_b for all types of particles. Ultimately, it would be desirable to be able to predict values of a and s_b from basic particle properties. At the present time, no measurements of a and s_b have been reported for packed beds. Some measurements for fibrous insulation at temperatures below 1000°F are reported by Larkin and Churchill[20] from a study of radiant heat transfer in porous insulations. The experimental investigation of this present study was designed to obtain sample measurements of a and s_b for a range of packings, at temperatures up to 2000°F.

Method

The experimental method was based on the same black body transmission technique as that used by Larkin and Churchill[20]. A variable temperature source provided black body radiation which was passed through the test bed of packed particles. The intensities of flux transmitted through various depths of the bed were measured by a thermopile detector and normalized with respect to the flux intensity at zero bed depth.

By mechanical chopping, the input signal from the source was modulated to approximate a ten cycle per second square wave. The total flux that impinged on the detector could be considered to be of four types:

a) the flux that traveled through the bed by direct transmission through voids,

b) the flux that traveled through the bed by multiple scattering off the particles,

c) the flux due to absorption of radiant energy which was converted to thermal energy and then re-emitted as radiant energy at the temperature of the particles, and

d) the random background flux from external sources.

The background flux (d) was of random intensity and may be considered to have a constant root-mean-square value, V_B, as shown in Figure 6. The absorbed radiant flux had a ten cps time function, but the thermal inertia of the particles damped out this function so that the re-emitted flux (c) had sensibly a constant intensity, V_E. The transmitted and scattered fluxes, (a) and (b), traveled through the bed at the speed of light and therefore would retain the square wave function, causing a ten cps response, V_T, at the detector. All these fluxes are additive so that the total intensity at the detector was of the type shown in Figure 6. The detector was designed to provide a voltage output directly proportional to the intensity of radiant flux impinging on it, so that quantities V_T, V_E, and V_B may be treated directly as the voltage signal outputs from the detector.

The detector signal was first passed through a primary transformer which served to eliminate all D.C. portions of the voltage. This sensibly shifted the horizontal axis of Figure 6 so that V_E and V_B were eliminated from the signal and only the V_T signal passed on through to the amplifier. A narrow band amplifier was used which could be finely turned to amplify only

V_T = transmitted and scattered flux signal

V_E = emitted flux signal

V_B = background flux signal

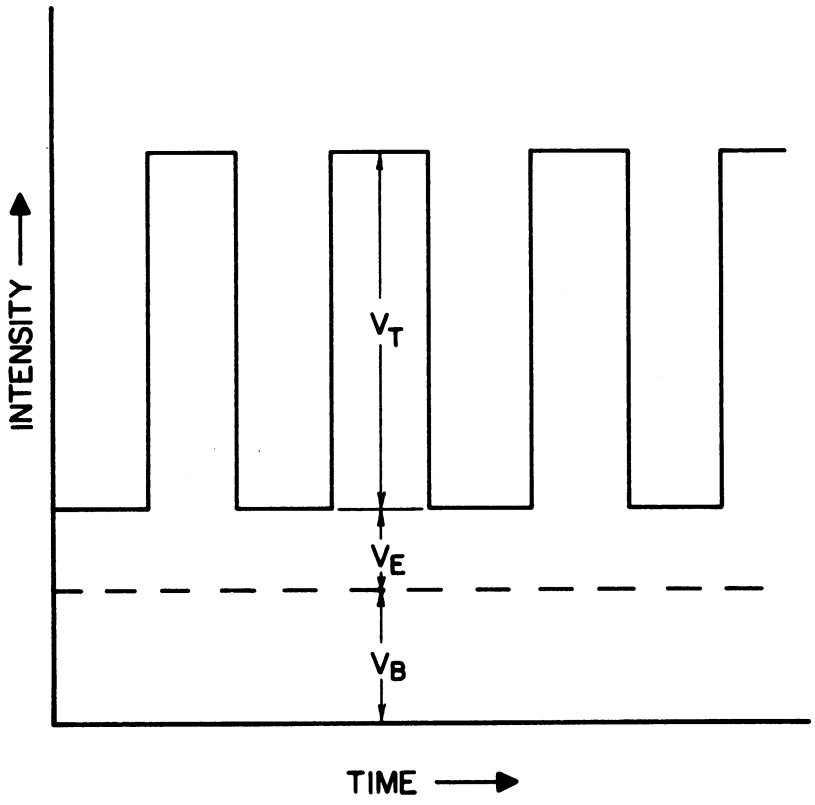

Figure 6. Flux Impinging on Detector.

ten cps signals. This served to filter out any additional random frequencies which might have passed through the primary transformer. Thus the final signal output of the amplifier was proportional to solely the V_T portion of the radiant fluxes impinging upon the detector. Normalizing $V_T(h)$ with respect to $V_T(h=0)$, a direct measure of the quantity $S_n(h)$ was obtained,

$$\frac{V_T(h)}{V_T(h=0)} = \frac{S(h)}{S_o(h=0)} = S_n(h) \qquad (116)$$

By measuring $V_T(h)$ at several packed depths, h, a set of data points of $S_n(h)$ versus h was obtained. Using two of these points, a first-guess approximation for m and a_n could then be calculated by Equations (178) and (179). These values were then used to initiate an iterative regression. Equations (146), (165), and (166) were used to obtain progressively closer estimates of the true regression values of m and a_n corresponding to a minimum Φ error, based on the model of Equation (115). The attenuation cross sections, a and s_b, were then calculated from these converged values of m and a_n by Equations (174) and (175). Derivations of these regression equations are given in the Appendix.

It should be noted that while the source temperature and the black body radiation spectrum were variable, the test beds' temperatures remained sensibly constant at room level. In most practical applications this would not be the case, as packed beds are commonly operated at temperatures close to wall temperatures. This dissimilarity is not as serious as it may seem to be. Temperature affects absorption and scattering in two ways: (a) by changing wave length spectrum of the radiation, and (b) by changing physical properties of the packing. Of the two, the spectrum change is the more important. Physical properties of the solids are not expected to change greatly over the temperature range considered. In the experimental work,

the spectrum effect was reproduced by the variable-temperature source, and it was only the relatively minor effect of physical property change that was not accounted for.

Apparatus

The apparatus assembly used in the experimental studies is schematically represented in Figure 7 and a photograph is presented in Figure 8. Details are given below.

The black body source was basically an open-end tubular furnace, as shown in Figure 9. The core was a silicon carbide (Norton's Crystolon RC-138 mix) tube closed at one end, of three inches internal diameter, 27 inches length, and 1/2 inch thick wall. Silicon carbide was chosen as the material because of its high emissivity, mechanical strength at elevated temperatures, good thermal conductivity, and low electrical conductivity. The first and third qualities were necessary in order to obtain uniform black body radiation and the other two properties were desirable for constructional ease. Heating coils of 18 gauge Chromel-A (nickel-chromium) were externally wound on the core and set in refractory cement (Norton's RA 1055). The coils were in three 20 foot length sections, each with its own Variac power control and ammeter. This sectional power control allowed local temperature adjustments to obtain uniform wall temperatures. Since heat loss was greatest at the top open end, heating coils were wound proportionally closer at that end. Thus the top 20 feet section of coils covered only 5.4 inches of the core, the middle section covered 8.1 inches, and the bottom section covered 13.5 inches. Each section was designed to provide a maximum of two kilowatts power input at 135 volts A.C. With this set-up, it was found possible to maintain wall temperatures uniform within 5°F from top to bottom, at temperatures up to 2000°F.

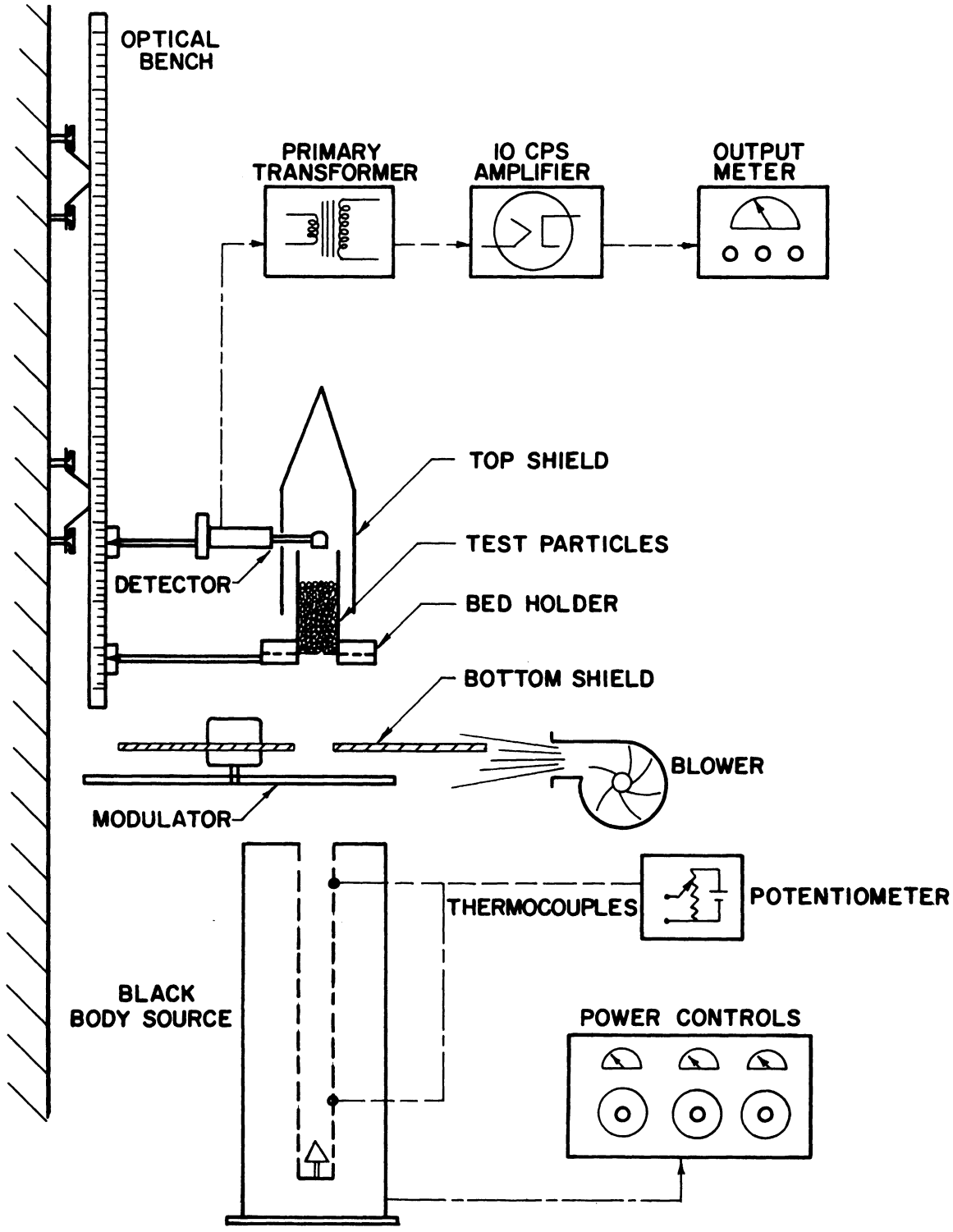

Figure 7. Diagram of Apparatus

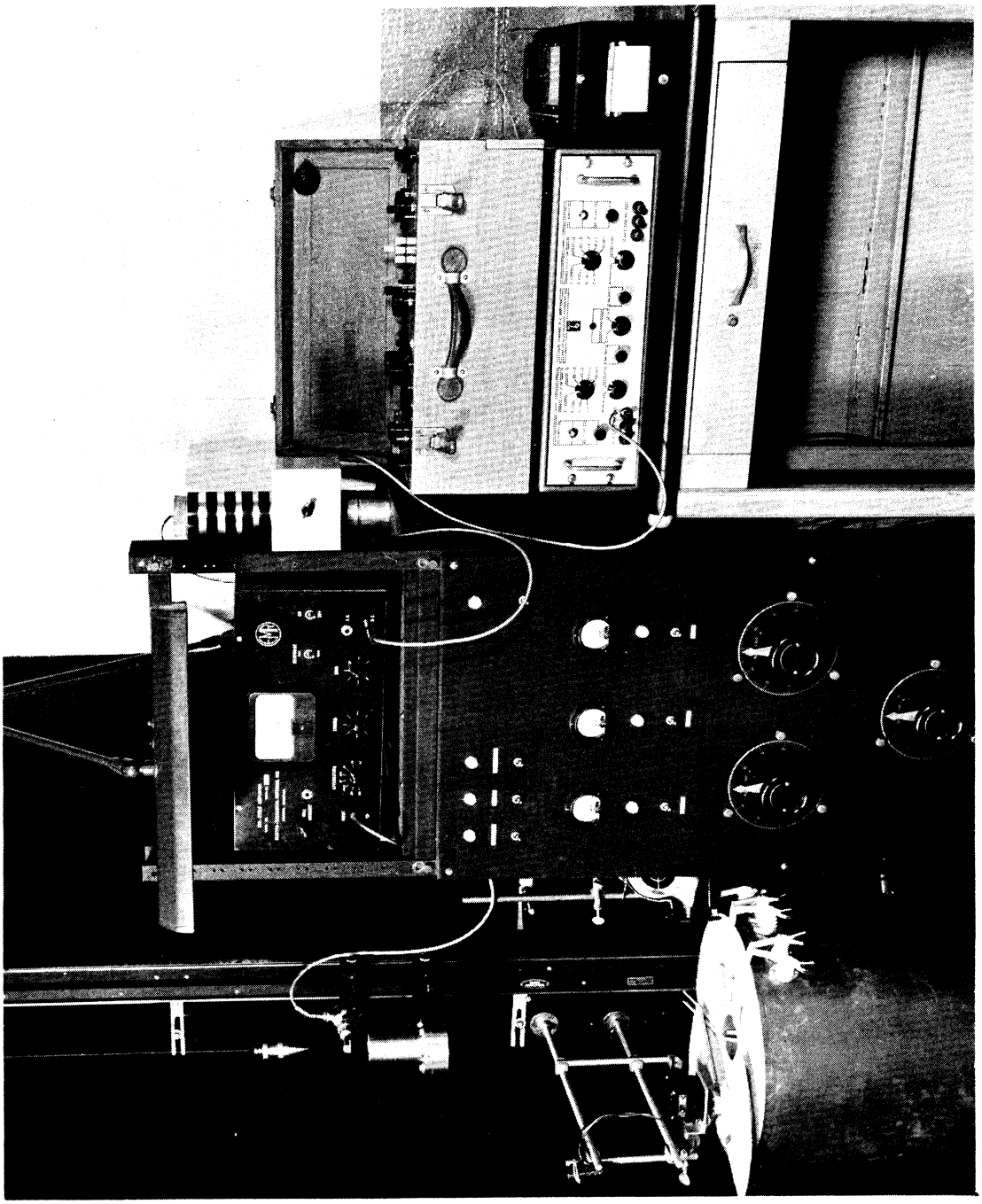

Figure 8. Photograph of Equipment

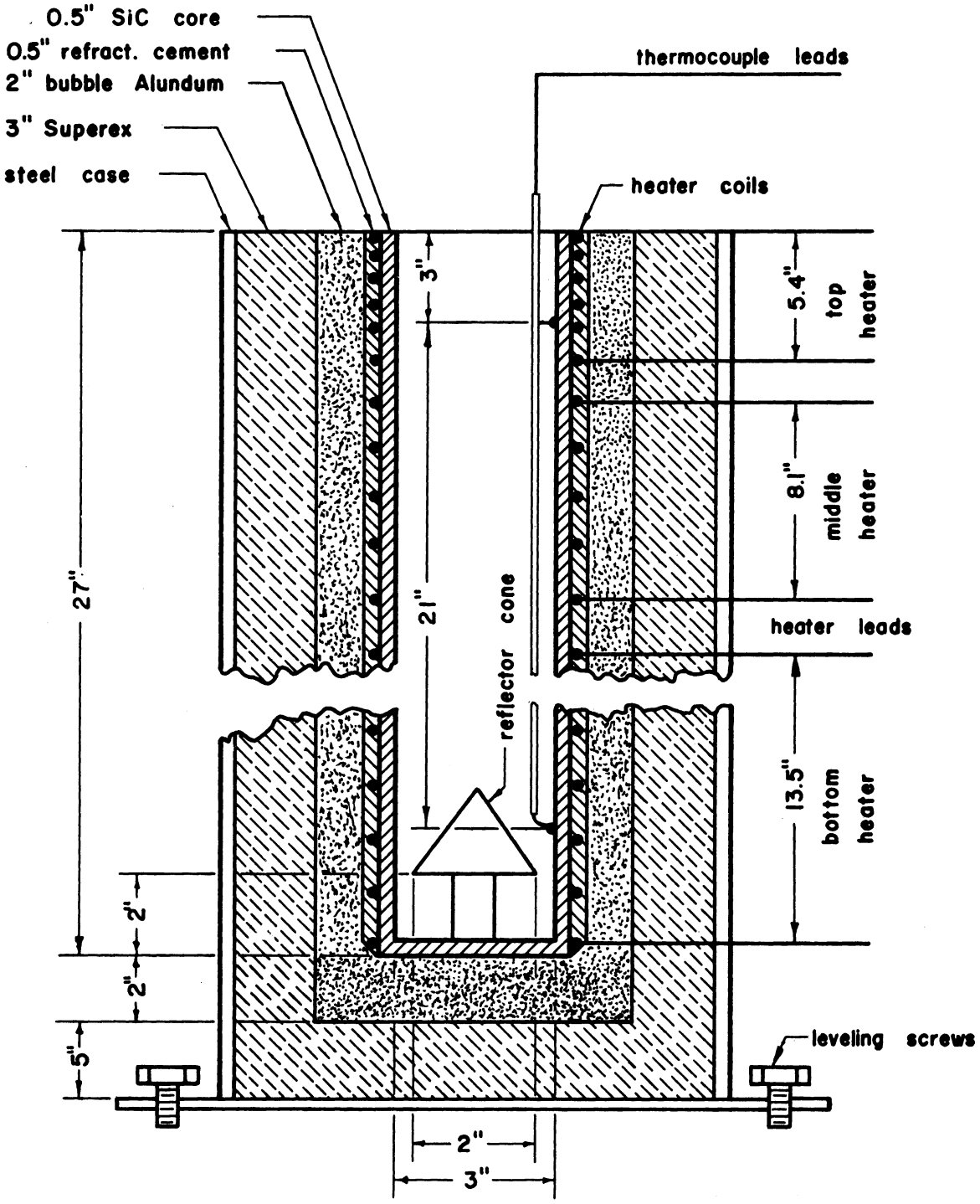

Figure 9. Details of Source

A 2-1/2 inch diameter reflector-cone of aluminum oxide (Norton's Alundum RA 321) was set inside the core, raised a height of two inches from the bottom. This cone served to prevent a direct view of core bottom and thus increased the overall emissivity of the enclosure. It also presented a surface temperature closer to wall temperature than could be attained by the core bottom.

Two types of insulations were set around the outside of the core. The inner high-temperature insulation was of bubble alundum (Norton's E163). It was packed to a thickness of two inches around and under the core. Preformed diatomaceous silica blocks (Johns-Manvill's Superex) were used for the external low-temperature insulation. Side blocks were of three inches thickness and bottom blocks were of 5-1/2 inches thickness. The entire assembly of core and insulations was set in a 1/16 inch steel casing.

Core wall temperatures were measured by two chromel-alumel thermocouples, set three inches and 24 inches from the top of the core. The thermocouples were led in through ceramic insulators, and the hot junctions were kept in contact with the core wall by spring tension. Cold junction was kept at 32°F by an ice bath. Thermocouple EMF's were measured by a standard Leeds and Northrup potentiometer. The thermocouple assembly was not calibrated as only 5°F precision was required.

The test bed was designed to approximate a one-dimensional system. Rigorously, this would require a bed of infinite lateral dimensions. Physically, this could be approached by the use of mirror walls which would provide perfect reflection of any side radiant fluxes so that net transfer would be zero in lateral directions. The actual test bed was constructed of a two inch diameter aluminum tube, highly polished on the inside. This tube was set on a screen which was in turn clamped between

two annular aluminum rings, as shown in Figure 10. The test particles were then packed in the tube, on top of the supporting screen. Tubes of various lengths, from one inch to five inches, and two different screens, one of NBS mesh 30 and one of NBS mesh 18 were used during the course of the experiments. The entire bed assembly was clamped to runners on an optical bench track, which was mounted vertically on the wall.

The detector used in this study was the same as that used by Larkin and Churchill[20], custom built by Charles M. Reeder and Company. Its sensing element consisted of bismuth-antimony-tellurium thermocouples with a gold-black filmed junction. Element response to ten cps signal was specified as approximately 64 percent of D.C. The total sensing junction had cross sectional dimensions of approximately 0.1 x 0.15 inches. The element was mounted in an evacuated brass case with a potassium bromide window. All electrical leads were shielded to minimize noise signals. The junction was so fixed in its case that the sensing element could be positioned a few millimeters below the rim of the bed tube, as shown in Figure 11. The entire detector case was also clamped to runners on the optical bench. The ruled scale of the optical bench served to measure relative positions of detector, bed, and source. When not in use, the detector was kept in a dessicator in order to prevent fogging of the KBr window.

Voltage signals from the detector were passed through a primary transformer. Thermador Corporation's type HG-3 with 90 db. magnetic shielding was used. This primary transformer served the dual purpose of eliminating D.C. signals and of providing a 1:102 step-up in ten cps signal strength.

Output from the transformer was then fed to a ten cps narrow band amplifier, Electro-Mechanical Research's model 33A. This amplifier featured

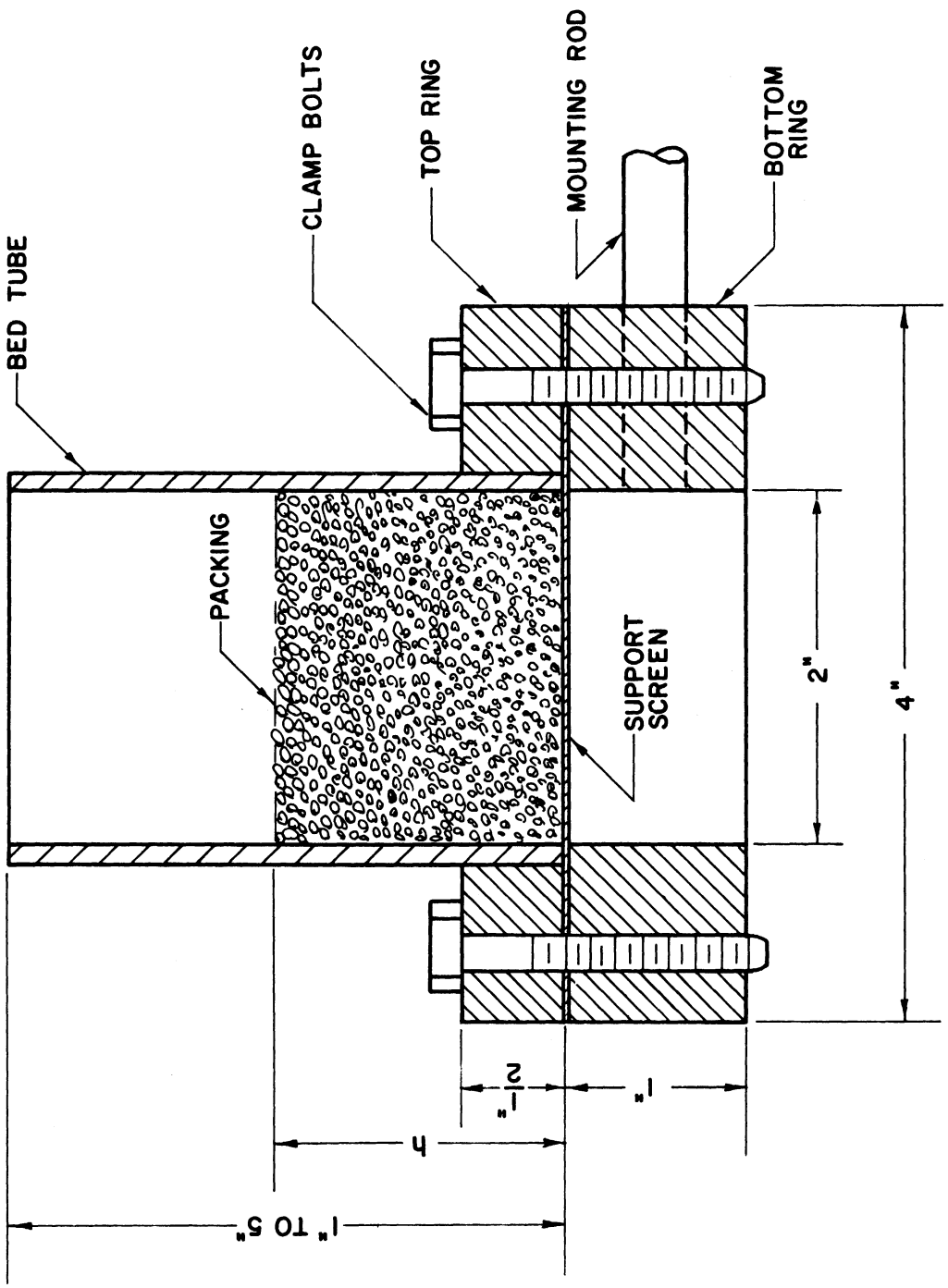

Figure 10. Details of Bed Assembly

a maximum sensitivity of one microvolt for full scale deflection with an overall voltage gain of 6×10^6. Band width was specified as one cycle to either side of ten cps at half power points. Thus, sensibly only the ten cps portion of the signal from the detector would be amplified and measured. A calibrated attenuator having a total ratio of 1000 to one was incorporated in the amplifier, together with an uncalibrated gain control. Output could be measured by either a build-in milliammeter or by externally connected recorders. The built-in meter was of variable range and had a specified accuracy of better than $\pm$ two percent of full scale. By judicious use of the calibrated attenuator and the dual range of the meter, it was found possible to maintain precision at the $\pm$ two percent value for almost all readings. Several external recorders of both millivolt and milliampere types were tried, but precisions were found to be less than that of the built-in meter. All readings of the final experiments were taken from the meter.

Modulation of original source signal was accomplished by mechanical chopping. A double bladed chopper was constructed out of asbestos sheeting attached to a wire frame. The bottom face of the blade was covered with aluminum foil to reduce absorption of energy from the hot source. The blade was shaped to have equal open and closed spaces in order to maximize signal response of the amplifier. Rotated by a 300 rpm synchronous motor, the chopper provided a close approximation to the desired square wave, ten cps, pulse signal.

A blower was mounted to circulate air across the space between the source and the test bed. This served the dual purpose of (a) preventing convective heating of the bed and (b) of cooling the modulator and shields.

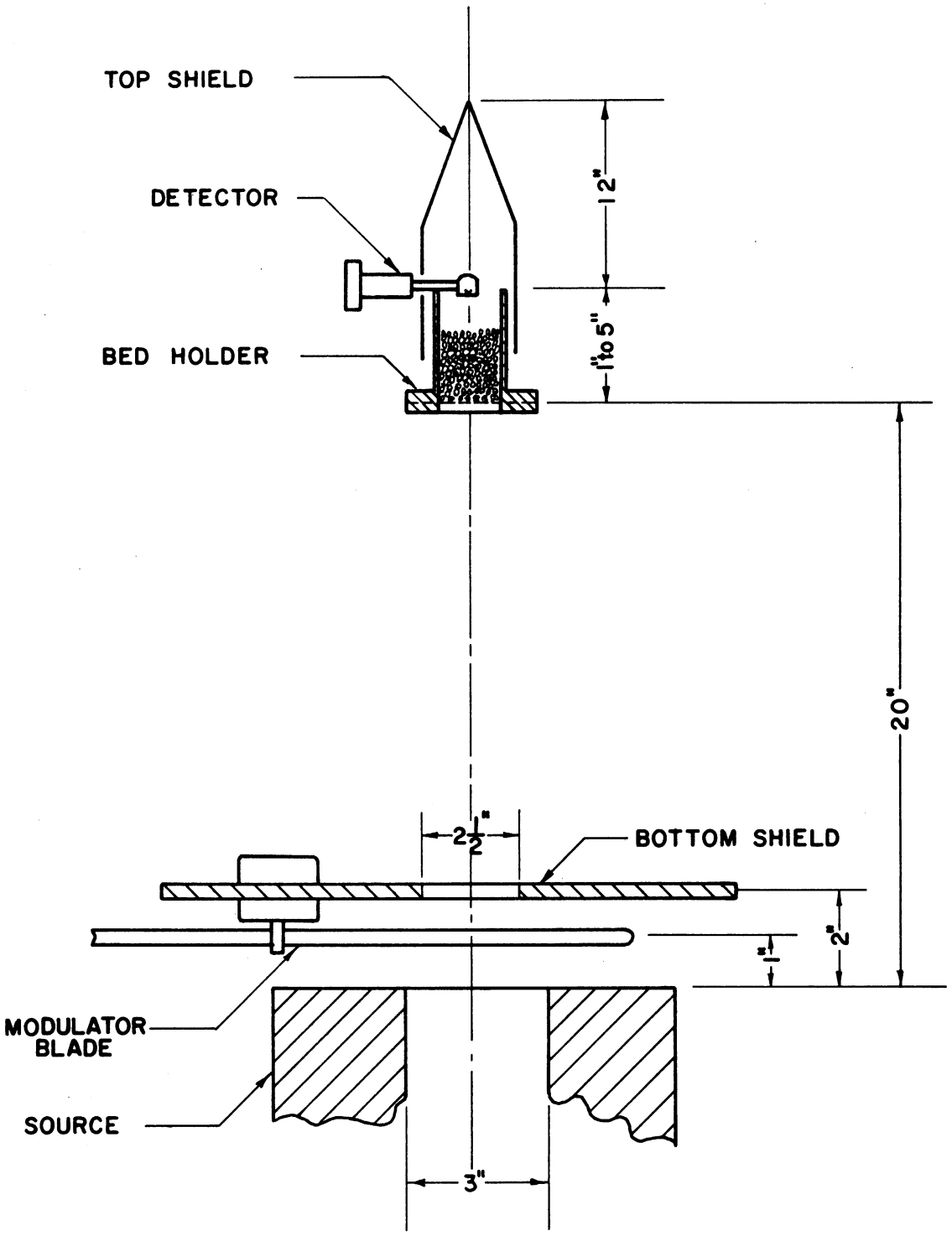

Figure 11. Relative Positions of Apparatus

Walls and control panels around the equipment were painted a dull black to approximate the condition of black body boundaries, as assumed in the derivation of Equation (115). However, it was discovered that still enough radiation from the source reflected off the surroundings to noticeably affect readings. To prevent this, two shields had to be installed. The bottom shield, with a 2-1/2 inch hole centered over the source, served to block edge radiant fluxes from the source. It was constructed of 1/4 inch beaver board with aluminum sheeting on the bottom and painted dull-black on top. The top shield was constructed out of dull-black felt cardboard, having a surface of high absorptivity. It was conically shaped to fit over the top of the bed and served to prevent any secondary reflections off walls and ceilings from reaching the detector. Relative positions of the apparatus and the placing of the shields for actual experimental conditions are indicated in Figure 11.

Test Particles

Twelve different packing particles were tested. They are listed and described under code names in the following table.

TABLE I

Test Particles

Code Name	Description
GS-3	solid glass spheres, 3mm. in nominal diameter, supplied by Kimble Glass Co.
GS-4	solid glass shperes, 4mm. in nominal diameter, supplied by Kimble Glass Co.
GS-5	solid glass spheres, 5mm. in nominal diameter, supplied by Kimble Glass Co.
AS-3/16	solid aluminum oxide spheres, 3/16 inch in nominal diameter, Norton's RA 5291.

TABLE I (cont'd)

Code Name	Description
AP-1/8	aluminum oxide pellets, cylindrically shaped, 1/8 inch diameter x 1/8 inch length nominal size, Norton's SA 103.
AP-5/32	aluminum oxide pellets, cylindrically shaped, 5/32 inch diameter x 5/32 inch length nominal size, Norton's SA 103.
AP-3/16	aluminum oxide pellets, cylindrically shaped, 3/16 inch diameter x 3/16 inch length nominal size, Norton's SA 103.
SS-1/8	carbon-steel spheres, 1/8 inch diameter, polished surface, Hoover's grade D balls.
SS-3/16	carbon-steel spheres, 3/16 inch diameter, polished surface, Hoover's grade D balls.
AG-4	aluminum oxide grain, mesh 4, irregularly shaped, nominal size 6.6 mm., Norton's number 38 Alundum.
AG-16	aluminum oxide grain, mesh 16, irregularly shaped, nominal size 1.7 mm., Norton's number 38 Alundum.
CG-16	silicon carbide grain, mesh 16, irregularly shaped, nominal size 1.7 mm., Norton Crystolon (regular grade).

All further references to the test particles will be by these code names. Properties of the packings, such as particle emissivity, particle conductivity, bulk density, and void fraction, are given in Table XII, in the Appendix. Figure 12 presents a photograph of samples of the test particle.

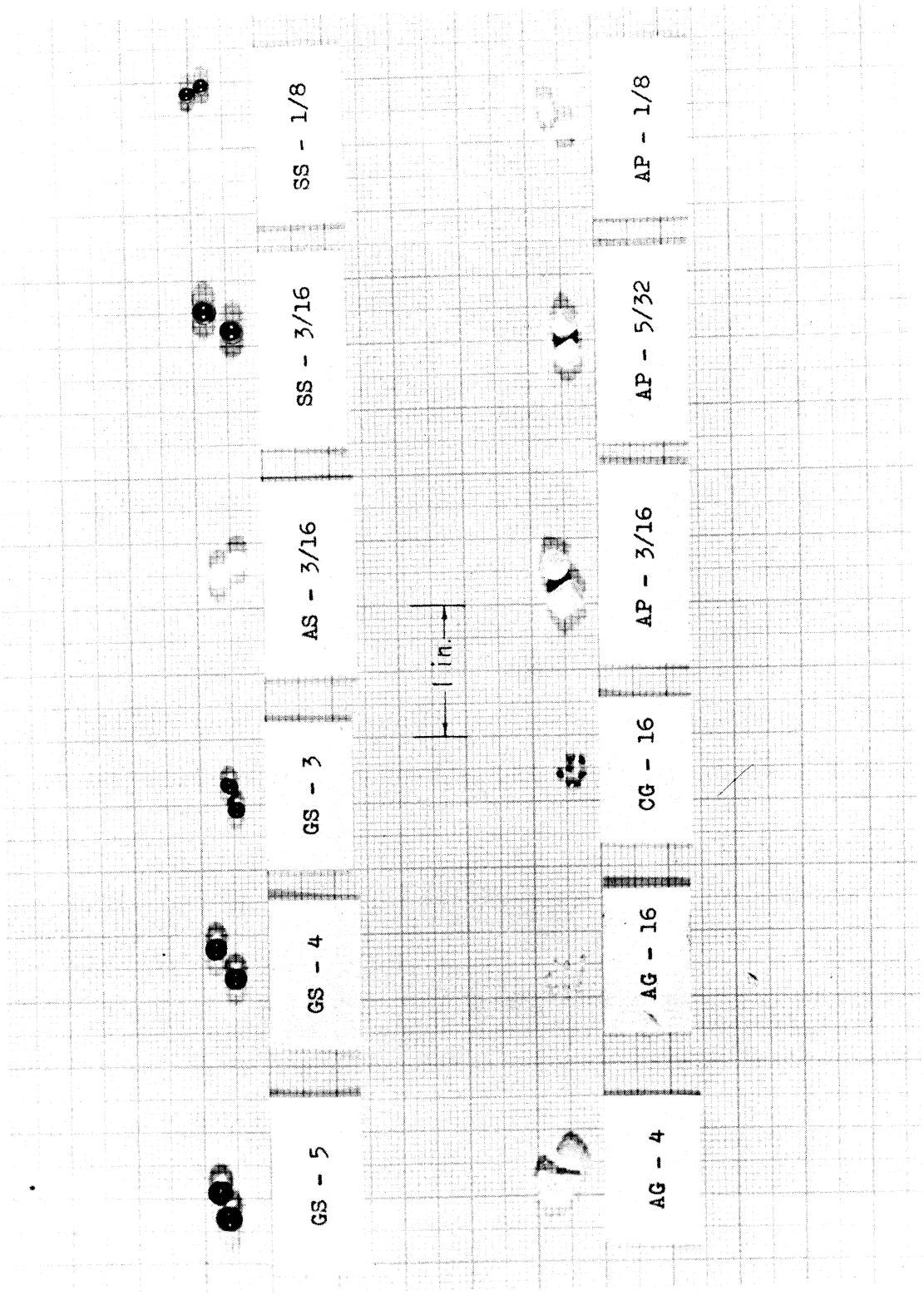

Figure 12. Photograph of Test Particles

PROCEDURES

The experimental data required were values of normalized transmissions, $S_n(h)$, at a number of packed heights, h. Three quantities had to be measured for this data: (a) bed height, h, (b) incident flux intensity, $S_o(h = 0)$, and (c) transmitted flux intensity, S(h). Assuming a linear detector and a constant amplifier gain, the measured voltage signals $V_T(h)$ and $V_T(0)$ would be directly proportional to S(h) and S_o, respectively. In this case it would be valid to treat the amplifier outputs, V_T, directly as the quantity S(h), since the normalized ratio is the same,

$$S_n(h) = \frac{S(h)}{S_o(h=0)} = \frac{V_T(h)}{V_T(h=0)} \qquad (116)$$

This simplification will be utilized in all further discussions. Details of the procedures used to measure h, S_o, and S were as follows.

Measurement of Bed Height

Bed height, h, was defined as the bulk packed height through which the radiant flux was transmitted. It was necessary to use bulk height rather than actual packing height since the latter could not be specified to better than $\pm D_p$.

To obtain measurements of h, it was first necessary to determine bulk density, ρ_B, for each type of packing. This was accomplished by packing a bed tube to the brim and weighing the entire assembly. Then, subtracting the tare and knowing the dimensions of the bed tube, it was possible to obtain a value of ρ_B as,

$$\rho_B = \frac{\text{(weight packing \& tube)-(weight tube)}}{\frac{1}{4}\pi D^2 \times H} \qquad (117)$$

where D = tube I.D.

H = tube height, ft.

For each packing, the above determination was made with several different tubes of varying heights. In all cases, the variation of ρ_B between determinations was only of the order of 1%. The arithmatic mean was then used as the true ρ_B for the packing. These values are given in Table XII of the Appendix.

In an experimental run, incremental samples of the packing would be weighed out previous to the test. These incremental samples were then added to the bed during the course of the test. The bulk height for the j-th data joint would thus be,

$$h_j = \frac{4}{\pi D^2 \rho_B} \sum_{i=1}^{j} \Delta W_i \qquad (118)$$

where ΔW_i = i-th incremental sample.

Measurement of Transmission Flux

The modulated transmission, S(h), was read from the output meter of the amplifier. At a packing height, h, the detector would be centered over the bed as shown in Figure 11 and the shields placed in position. With the source set at the desired temperature and the chopper turned on, the amplifier attenuator and meter range would be adjusted to bring reading on scale. At steady state, the meter reading, R_m, and attenuator ratio, A_t, would be recorded. All meter readings, for all data points were then adjusted to a common basis of unit attenuation by,

$$R = \frac{R_m}{A_t} \qquad (119)$$

During the course of each run, background signal would be measured by covering the bottom of the bed with an opaque piece of transcite and taking a reading on the meter. This reading, R_b, normalized to unit attenuation as with R, was considered to be a valid measure of all stray background signals. The true transmission signal was then given by,

$$S(h_j) = R_j - R_b \qquad (120)$$

In the actual experiments, the bed would be repacked and the value of $S(h_j)$ measured two to four times at each packed height, h_j. The arithmatic mean value of $S(h_j)$ was then used as the true signal value for that data point.

Measurement of Incident Flux

For a one dimensional bed, the flux incident at the bottom of the packing would be the same as that reaching the detector if the bed had no packing. In the experiment, $S(h=0)$, the zero packing signal, was measured and used as the normalizing incident flux, S_o.

A difficulty in measuring $S(h=0)$ directly was that at temperatures above 800°F, the flux intensities without packing were so high that all readings were off scale even at maximum amplifier attenuation. While this problem could have been avoided by increasing the distance between source and bed, this was not desirable since the signal with packing would then be too low for accurate measurement.

In the experiments, two aids were used to obtain values of S_o. First, a standard screen was placed over the source opening of the bottom shield, serving to reduce the flux intensity by a constant factor. This screen was calibrated at temperatures up to 2000°F and the factor was determined to be 5.80, independent of temperature, bed location, and source opening.

A second aid was the signal-temperature relationship. It was found by actual measurements at temperatures up to 1700°F, that a plot of S_o versus source temperature raised to the fourth power, T_s^4, could be quite accurately correlated by a straight line. This correlation was then extrapolated to 2000°F in order to obtain values of S_o at the higher temperatures. Thus, the actual values of S_o used in the experiments were determined as,

$$S_o = 5.80 \times S_o^* \qquad (121)$$

where S_o^* = signal value from temperature correlation, with standard screen.

Procedure of Test Runs

To summarize, the procedure of a typical test run was as follows:

1. Determine bulk density of test packing, ρ_B .
2. Weigh out incremental packing samples, ΔW_i.
3. Heat up source to desired uniform temperature.
4. Align source, modulator, bed, detector, and shields (by plumb line).
5. Start modulation and wait for source temperature to attain steady state.
6. Obtain value of S_o, by meter reading if below 1700°F, by correlation if above 1700°F.
7. Measure background signal, R_b.
8. Dump and pack into bed the first incremental sample, ΔW.
9. Measure transmission flux reading, R.
10. Repack bed and repeat step 9 for two or three times.
11. Take average of all values from step 10 as the true value of R.
12. Add next incremental sample and repeat steps 9 to 11 for next data point.
13. Continue till all samples have been added or till transmission falls too low for accurate measurement.
14. Re-measure background signal, R_b.

15. Calculate $S(h)$ for each data point by Equation (120), using arithmatic average of R_b.

16. Obtain normalized transmission, $S_n(h)$, by Equation (116).

17. Plot $S_n(h)$ versus h for desired transmission curve.

EQUIPMENT CHECKS AND CALIBRATIONS

The analytical development and experimental method described in the previous sections were based on several assumptions regarding equipment characteristics. These assumptions were checked by either experimental tests or by calculations wherever possible. These checks, along with equipment calibration, are described below.

Black Body Behavior of Source

The attenuation cross sections, a and s_b, were defined as total cross sections for radiation of all wavelengths, i.e., for black body radiation. Therefore, it was necessary that the experimental source approximate black body behavior as closely as possible. In theory, an opening in an enclosure approaches black body behavior as the opening decreases in size, since any radiation falling on the opening would tend to be trapped within the enclosure. In practical applications where an extended source is required, the opening has a finite area so that a fraction of incident radiation would be reflected back out. The absorptivity (or emissity) of such an enclosure would evidently be equal to

ϵ_s = 1 - (fraction of incident radiation reflected back out).

For any real enclosure, ϵ_s would be a function of enclosure size and shape, opening size, shape, and location, and emissivity of wall inside enclosure. Gouffe[12] has derived equations for calculating effective enclosure emissivities from these parameters. His result for cylindrical enclosures may be written as,

$$\epsilon_s = \frac{\epsilon_w}{\epsilon_w\left(1 - \frac{A_o}{A_w}\right) + \frac{A_o}{A_w}}\left[1 + (1-\epsilon_w)\left(\frac{A_o}{A_w} - \frac{A_o}{A'}\right)\right] \qquad (122)$$

where ϵ_s = effective emissivity of enclosure

ϵ_W = emissivity of wall inside enclosure

A_o = area of opening

A_W = area of wall of enclosure

A' = area of equivalent sphere with diameter equal to length of the enclosure.

Applying Equation (122) to the source enclosure of this study;

ϵ_W = emissivity of silicon carbide

$= 0.9$

$A_o = \frac{1}{4}\pi \times 3^2 = 7.06$ sq. in.

$A_W = (\frac{1}{4}\pi \times 3^2) + (\pi \times 3 \times 27) = 262$ sq. in.

$A' = \pi \times 27^2 = 2{,}290$ sq. in.

$\frac{A_o}{A_W} = 0.0271$

$\frac{A_o}{A'} = 0.0031$

$$\epsilon_s = \frac{0.9}{0.9\,(1-.0271) + .0271}\,[1 + (1-.9)(.0271 - .0031)]$$

$= 0.994$.

Thus it is seen that the effective emissivity of the test source was better than 0.99. This was judged to be sufficiently close to black body behavior.

Linearity of Measurement System

A linear detector and amplification system was required in order to obtain meaningful transmission curves. Basically, it was required that the final meter reading be directly proportional to the flux intensity impinging on the detector. The experimental system was checked for this characteristic by means of the reciprocal-distance-squared law.

It is well known that flux intensity decreases as the reciprocal of the square of the distance from a point source. Therefore, if the detector should be placed at various distances from a point source and an output-meter

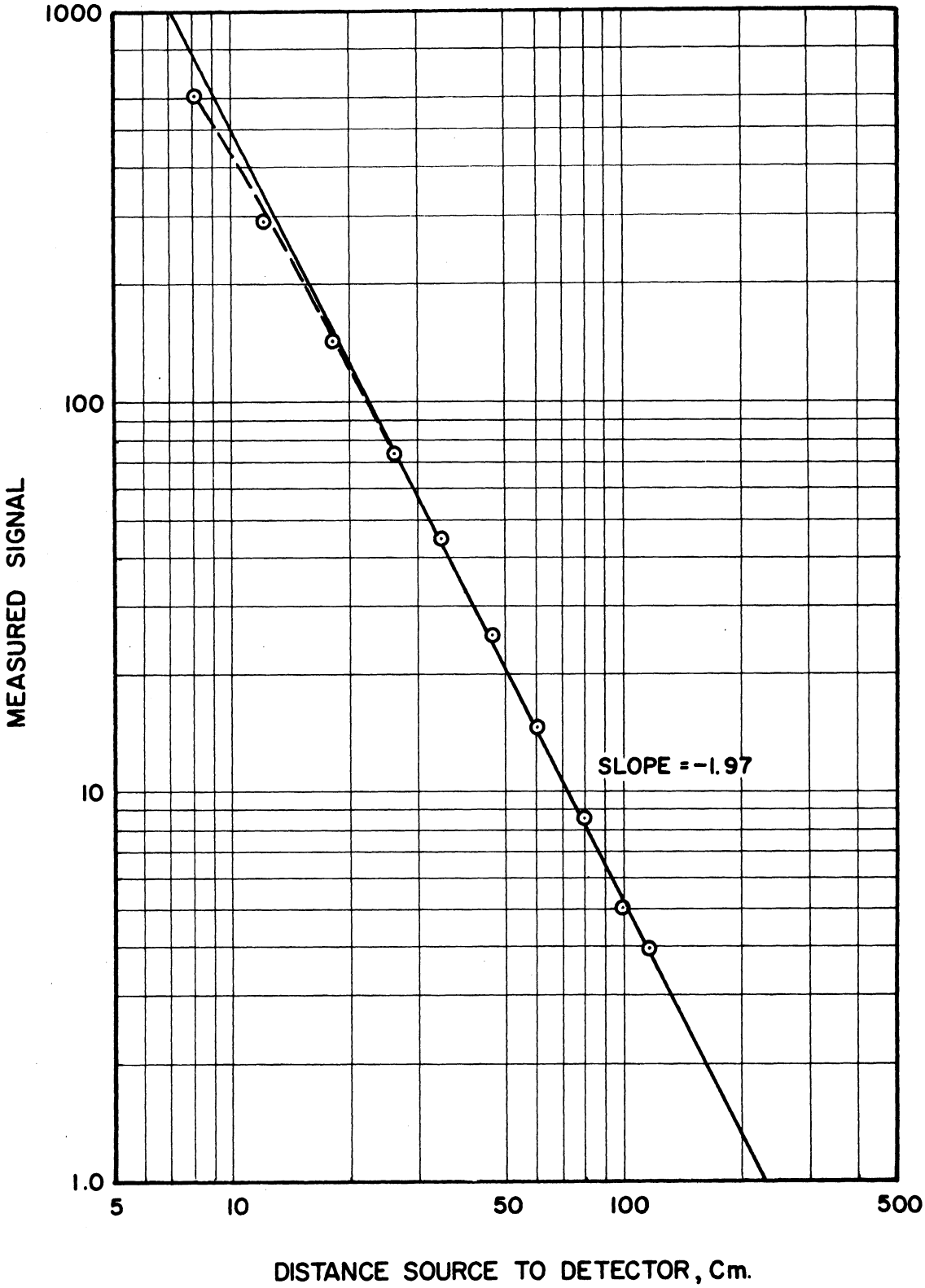

Figure 13. System Linearity Check

reading taken at each distance, then a log-log plot of meter reading versus distance would be a straight line of slope -2 for a truly linear system. In actual test, only an approximate point source would be practical, so that the straight line relationship might only be expected at large distances.

To check the experimental system, the black body source was heated to 354°F and a half inch circular opening in the bottom shield centered over it to serve as the approximate point source. The detector was then placed at various distances from the opening, along the optical bench. The packed bed frame was removed for this test. Detector signal at each distance was then read from the amplifier-output-meter and plotted against distance in Figure 13. Numerical values are listed in Table VIII of the Appendix.

It is seen that the plot of Figure 11 does approach a straight line at large distances. Asymptotic slope of the straight line portion was measured to be -1.97, well within experimental accuracy to the expected value of -2. It was therefore concluded that the detector and amplification circuit was sensibly a linear system.

Temperature Response of Measurement System

The total radiant intensity absorbed by a grey body detector from a grey body source is given by,

$$i = G\sigma(\epsilon_s T_s^4 - a_d T_d^4) \qquad (123)$$

where G = geometric factor

T_s = source temperature, °R

T_d = detector temperature, °R

ϵ_s = source emissivity

a_d = detector absorptivity

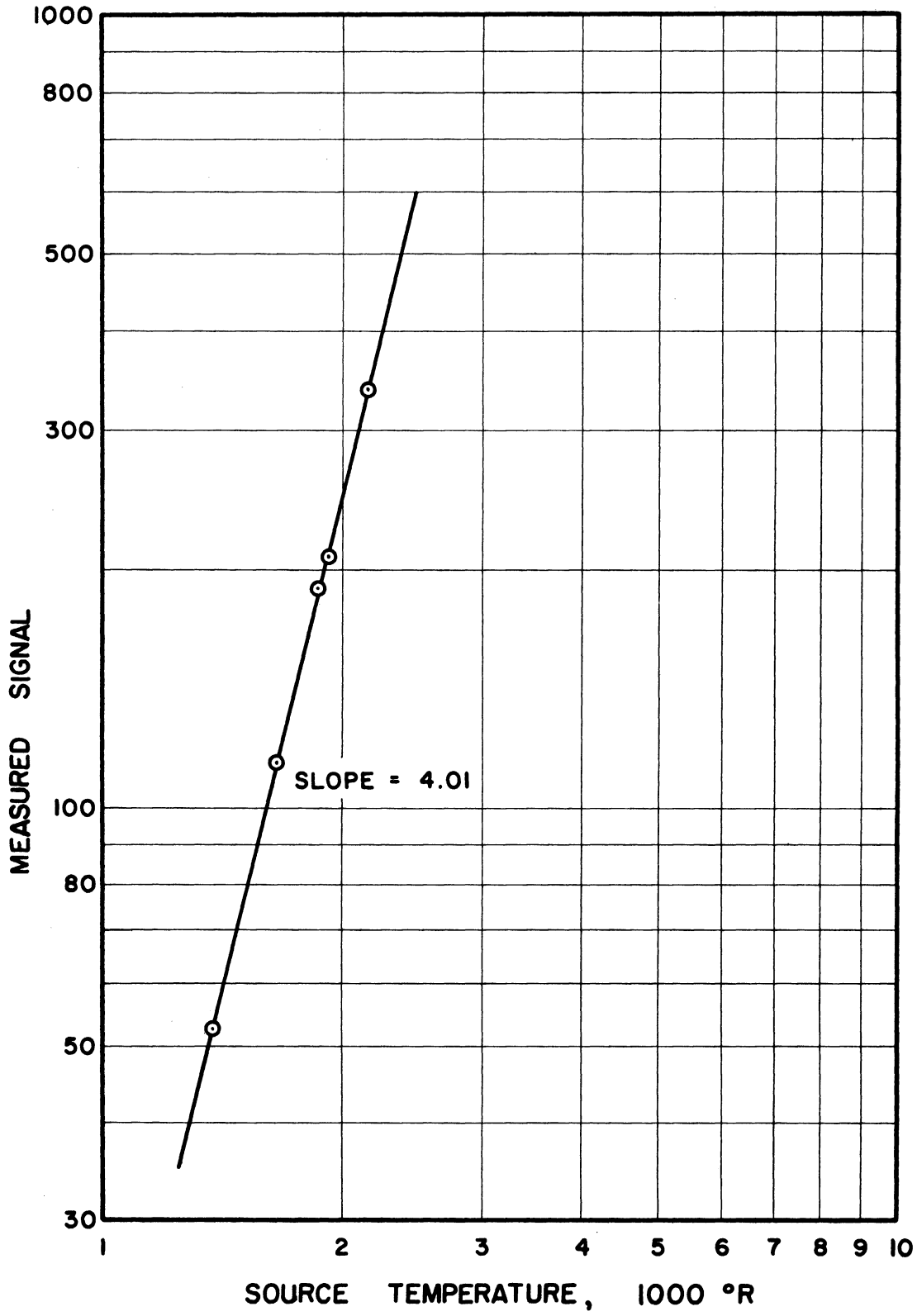

Figure 14. Temperature Response of System

Since the experimental source was a black body and the detector system was linear, Equation (123) takes the form,

$$R_m \sim (T_s^4 - a_d T_d^4) \qquad (124)$$

where R_m = output meter reading.

For $T_s \gg T_d$, Equation (124) would be approximated by

$$R_m \sim T_s^4 \qquad (125)$$

or, $\log R_m = 4 \log T_s + \text{const.}$

Test values of R_m and T_s were obtained on the experimental equipment, with bed in place but with no packing. Source temperature was varied from 900°F to 1700°F and the results are tabulated in Table VII. Plotted on log-log coordinates in Figure 14, it is seen that a straight line is obtained as required by Equation (125). Slope of the line was determined to be 4.01, very close to the expected value of 4.0.

Effect of Support Screen

In the experimental test beds, a bottom screen was used to support the packings, as shown in Figure 10. The assumption was that by normalizing all transmission measurements of packing and screen to that of screen alone, the attenuation effect of the screen itself would cancel out. This assumption would be valid if the screen attenuation remained constant, independent of the presence or absence of packings.

To check this assumption and to obtain an order-of-magnitude estimate of the screen effect, two test runs were performed with identical packings but with two widely different screens. Runs 10 and 14 were both made with GS-3 packing, at a source temperature of 1200°F, and with a four inch length bed tube.

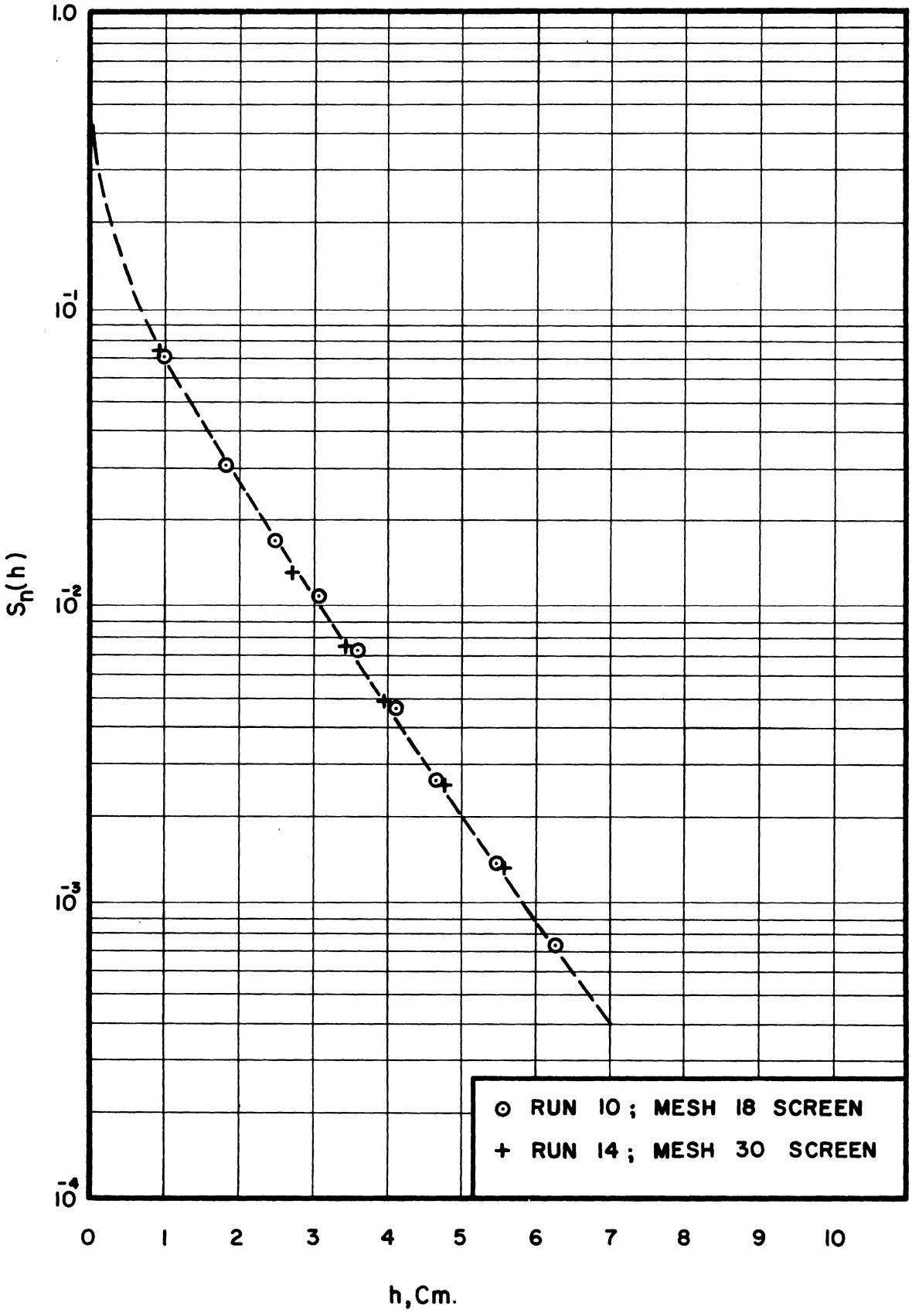

Figure 15. Effect of Support Screen

The two screens used were:

	Material	NBS Mesh	Opening, mm.	Wire diam., mm.
Run 10	copper	18	1.00	0.43
Run 14	brass	30	0.59	0.29

The data points for these two runs are plotted together on Figure 15 and it is seen that the two runs represent quite similar transmission curves. The regression values of a and s_b and the corresponding k_{ir} were determined to be:

	$a \frac{ft^2}{ft^3}$	$s_b \frac{ft^2}{ft^3}$	$k_{ir} \frac{Btu}{hr.ft.°F}$	diff. in k_{ir}
Run 10	0.96	343	0.091	7.6%
Run 14	0.84	372	0.084	

The 7.6 percent variation in conductivity is of a noticeable magnitude and may place a limit on the validity of the experimental data. Indications are that the screen effect was probably one of the relatively important drawbacks of the experimental set up. However, this order of magnitude variation is still quite acceptable when compared with general experimental precision commonly reported for packed bed characterizations.

Wall Absorption

It was desired to have the bed walls approximate mirrow-walls as closely as possible, i.e., to have zero absorptivity. Any real wall has some finite absorptivity which would tend to decrease flux intensity. However, effect of this flux decrease on transmission curves is only secondary since normalization tends to cancel out the absorption factor. In fact, if wall absorption with packing is the same as without packing, then the normalized

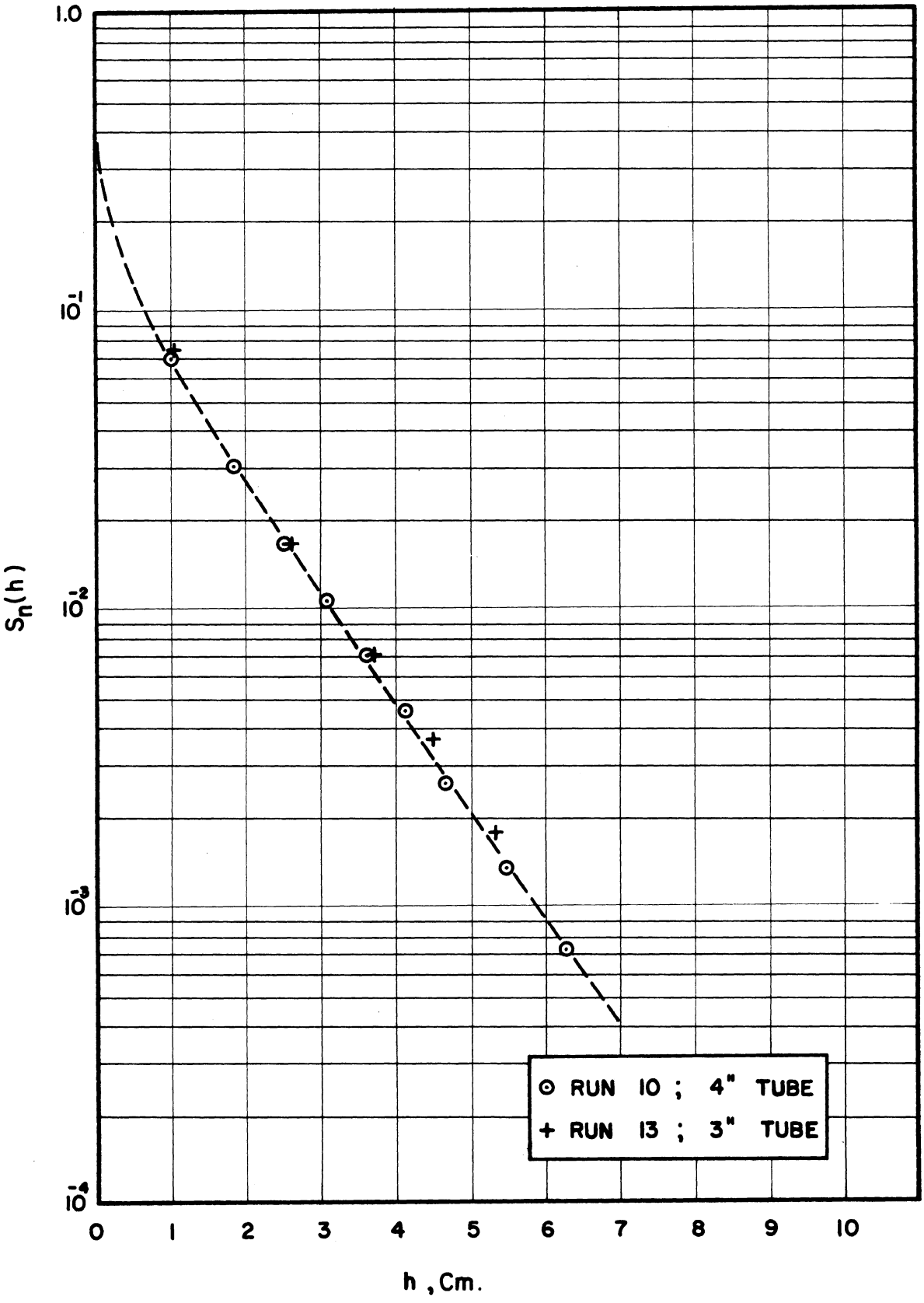

Figure 16. Effect of Tube Wall Length

transmissions, $S_n(h)$, are not affected at all. In real cases, packing materials change the angular distribution of flux and so the total flux absorbed by the bed wall will not be the same for packed as for empty beds.

To obtain an estimate of the effect of wall absorption, two runs were made under identical conditions but with bed tubes of different lengths. Runs 10 and 13 were both made with GS-3 packing at 1200°F. A four inch length bed tube was used for Run 13 and a three inch length tube was used for Run 14. If wall absorption were important, then the 30 percent change in wall length might be expected to show a noticeable effect on the transmission curves.

Data points of Runs 10 and 13 are plotted together on Figure 16. It is seen that the points coincide quite closely on sensibly one transmission curve. Values of parameters obtained by regression were:

	$a \frac{ft^2}{ft^3}$	$s_b \frac{ft^2}{ft^3}$	$k_{ir} \frac{Btu}{hr.ft.°F}$	Diff. in k_{ir}
Run 10	0.96	343	0.091	1.1%
Run 13	0.88	341	0.092	

The agreement is seen to be remarkably good, indicating that wall absorption effects were probably neglegible.

Lateral Variations

The correlation model, Equation (115), was based on the one dimensional case, where it was assumed that there were no variations in either packing properties or flux intensities in the lateral directions. In the actual case, there were three types of variations that could have been expected. First, the bottom face of the packed bed might not have been uniformly illuminated by the incident flux. This could be due to either nonuniformity of the extended source or due to differences in distance between

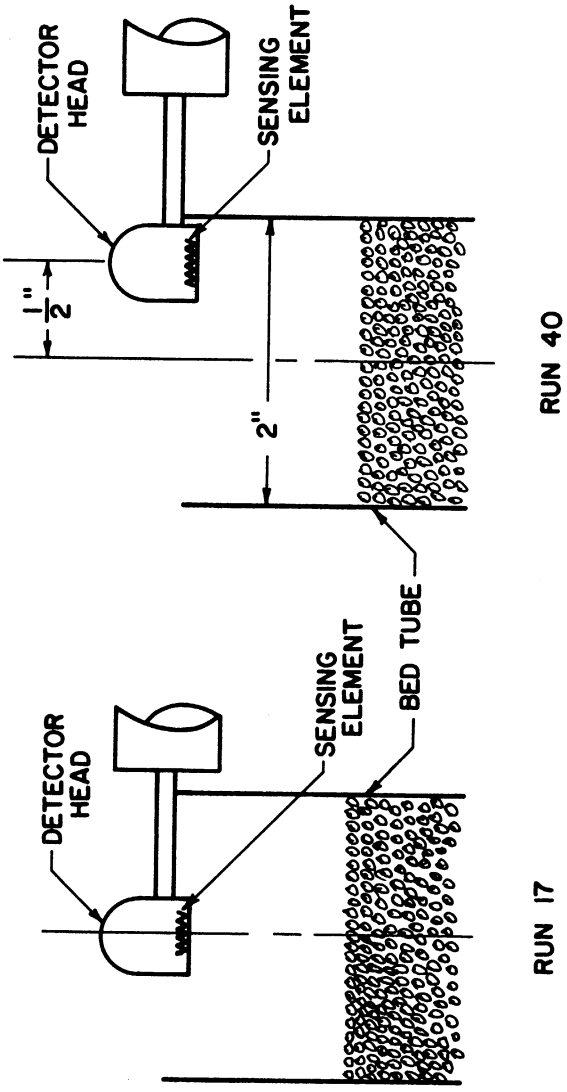

Figure 17. Placement of Detector in Lateral Variation Test

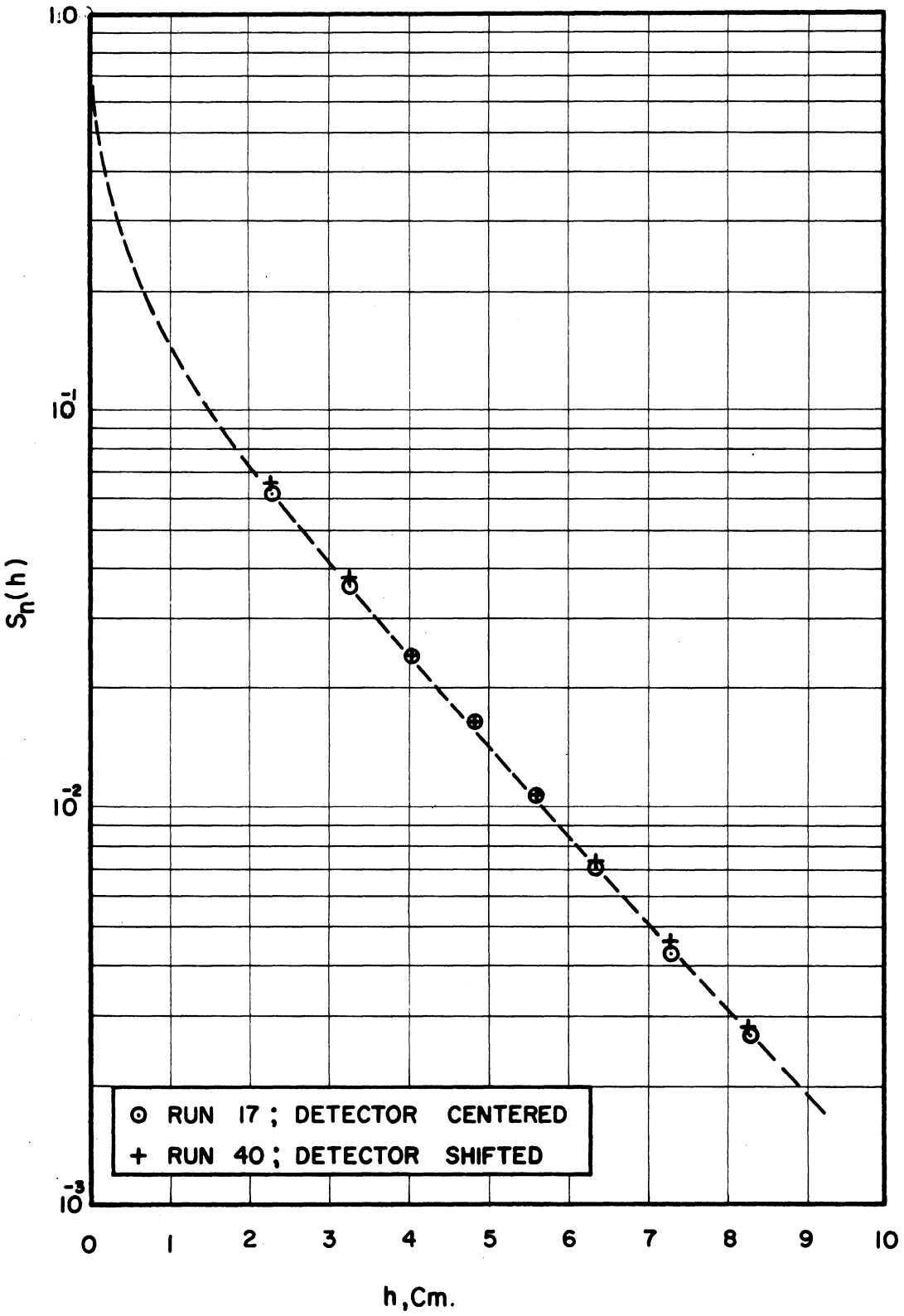

Figure 18. Effect of Lateral Variation

source and various points of the bed face. Second, any absorption loss at wall would cause a decrease in flux intensity in the vicinity of the wall. Third, it is expected that local void fraction would be greater near the wall than in the bulk of the bed.

A measure of the overall lateral effect was obtained by making a run (Run 40) with the detector placed off center over the bed. The results were then compared to a similar run (Run 17) with detector placed in the normal center position, as illustrated in Figure 17.

In Run 40, the detector was shifted off center as much as constructional features allowed, a distance of approximately one quarter of tube diameter. Both runs were made with GS-5 packing and at a source temperature of 1600°F. The data are plotted together on Figure 18. Values of regression parameters corresponding to the two runs were found to be:

	$a \frac{ft^2}{ft^3}$	$s_b \frac{ft^2}{ft^3}$	$k_{ir} \frac{Btu}{hr.ft.°F}$	Diff. in k_{ir}
Run 17	0.81	151	0.396	1.2%
Run 40	0.80	149	0.401	

Once again, the agreement in transmission curves and regression parameters are seen to be very good. It was concluded therefore that effect of lateral variations on experimental results was negligible.

Calibration of Standard Screen

The standard screen used for measurement of incident flux had to be calibrated for two functions:

a) for values of the ratio $F_s = \frac{S_o}{S_o^*}$,

where, S_o = true incident flux intensity

S_o^* = incident flux intensity measured through standard screen.

b) for values of S_o^* at various source temperatures.

Values of the ratio F_s were obtained by direct measurements of $S(h=0)$ with and without the standard screen. It was expected that F_s would be a constant independent of bed position, area of source opening, and source temperature. To be certain, measurements were made at a number of bed positions, with several different source areas, and over a range of temperatures. In Figure 19, F_s is plotted versus bed position for different source areas, at two parameters of temperature. It is seen that the best correlation is a straight horizontal line for each temperature, indicating that F_s was truly independent of bed position and source size. In Figure 20, the average value of F_s at each source temperature is plotted against temperature. It is seen that at temperatures below 800°F, F_s was not independent of temperature but decreased with decreasing temperature. Above 800°F, F_s was constant at a mean value of 5.80, independent of source temperature. Since all experimental runs were made at temperatures of 800°F or higher, this constant value of 5.80 was taken as the value for F_s.

As explained in a previous section, it was necessary to obtain a calibrated correlation of S_o^* versus temperature for extrapolation to higher temperatures where S_o^* and S_o could not be measured directly. To use such a correlation, it was necessary to maintain constant gain at the amplifier and to have consistent placement of bed and detector. Under such conditions, S_o^* would be a function only of source temperature, bed tube length, and type of bed support screen. Experimental measurements for S_o^* were obtained over a temperature range of 600°F to 1700°F, for two different bed tube lengths and with the mesh 30 support screen. Numerical values are tabulated in the Appendix, Table X. In Figure 21, S_o^* (in terms of meter readings) is plotted against source temperature (in °R raised to the fourth power). It is seen

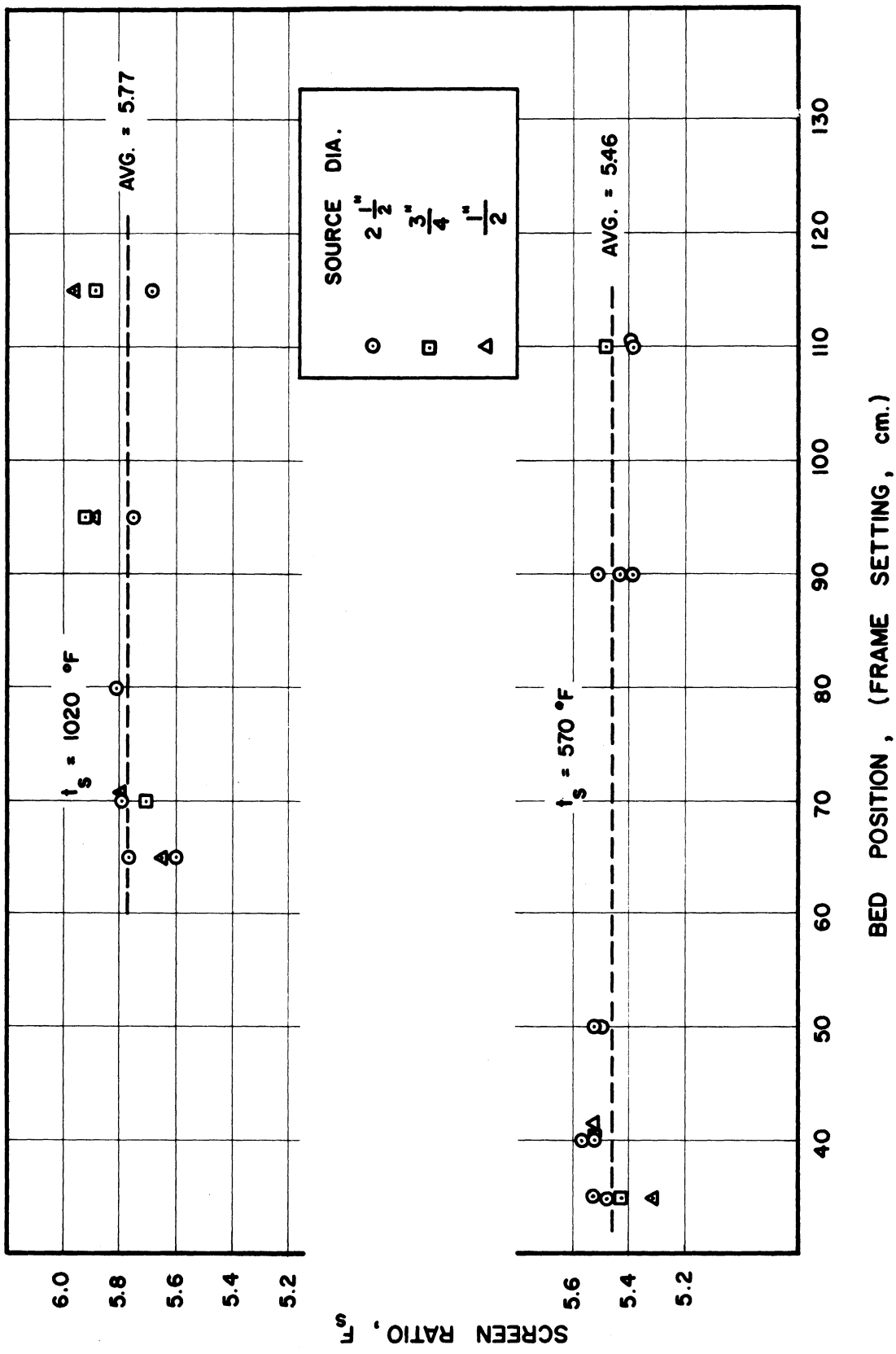

Figure 19. Position and Source Area Dependence of F_s

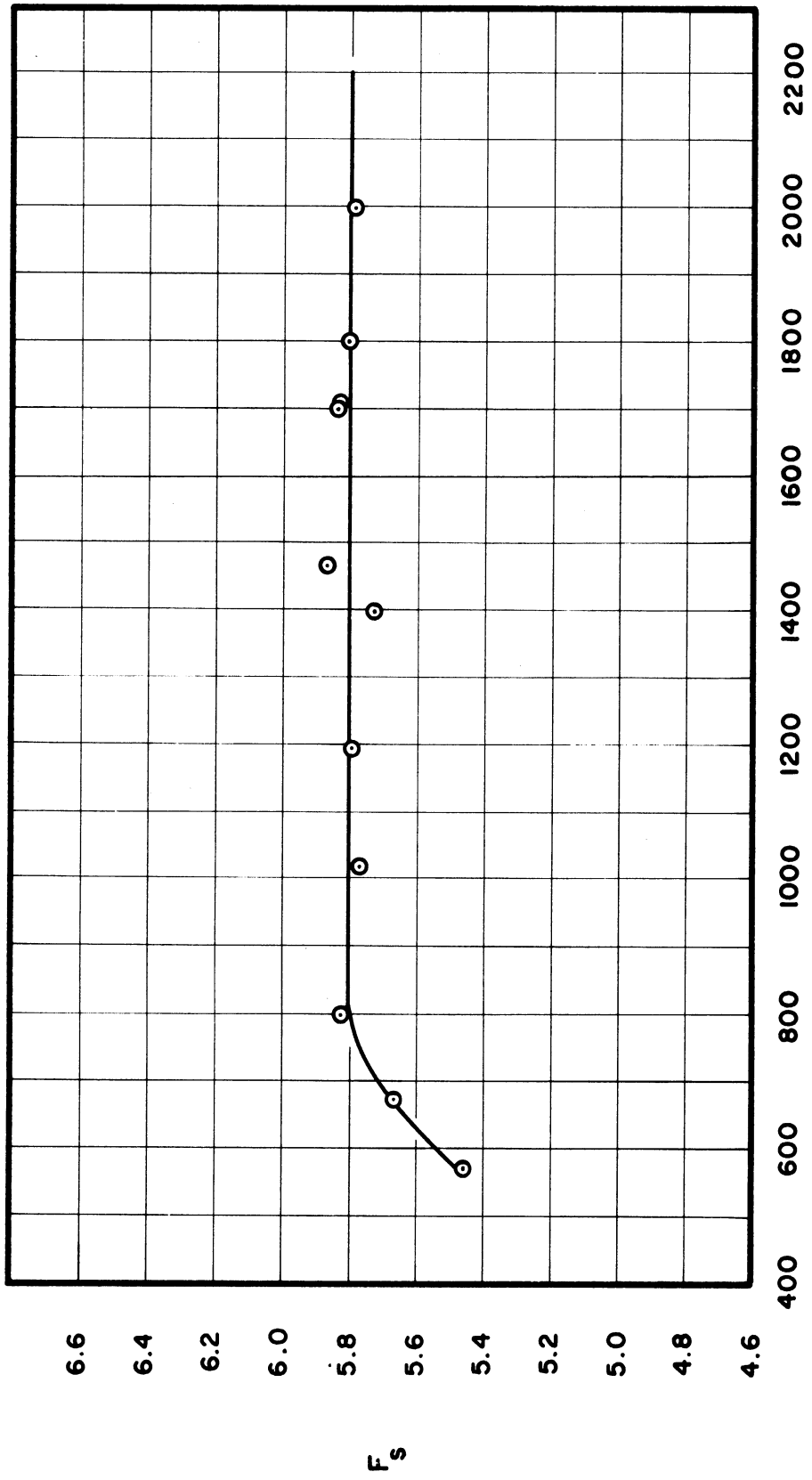

Figure 20. Temperature Dependence of F_s

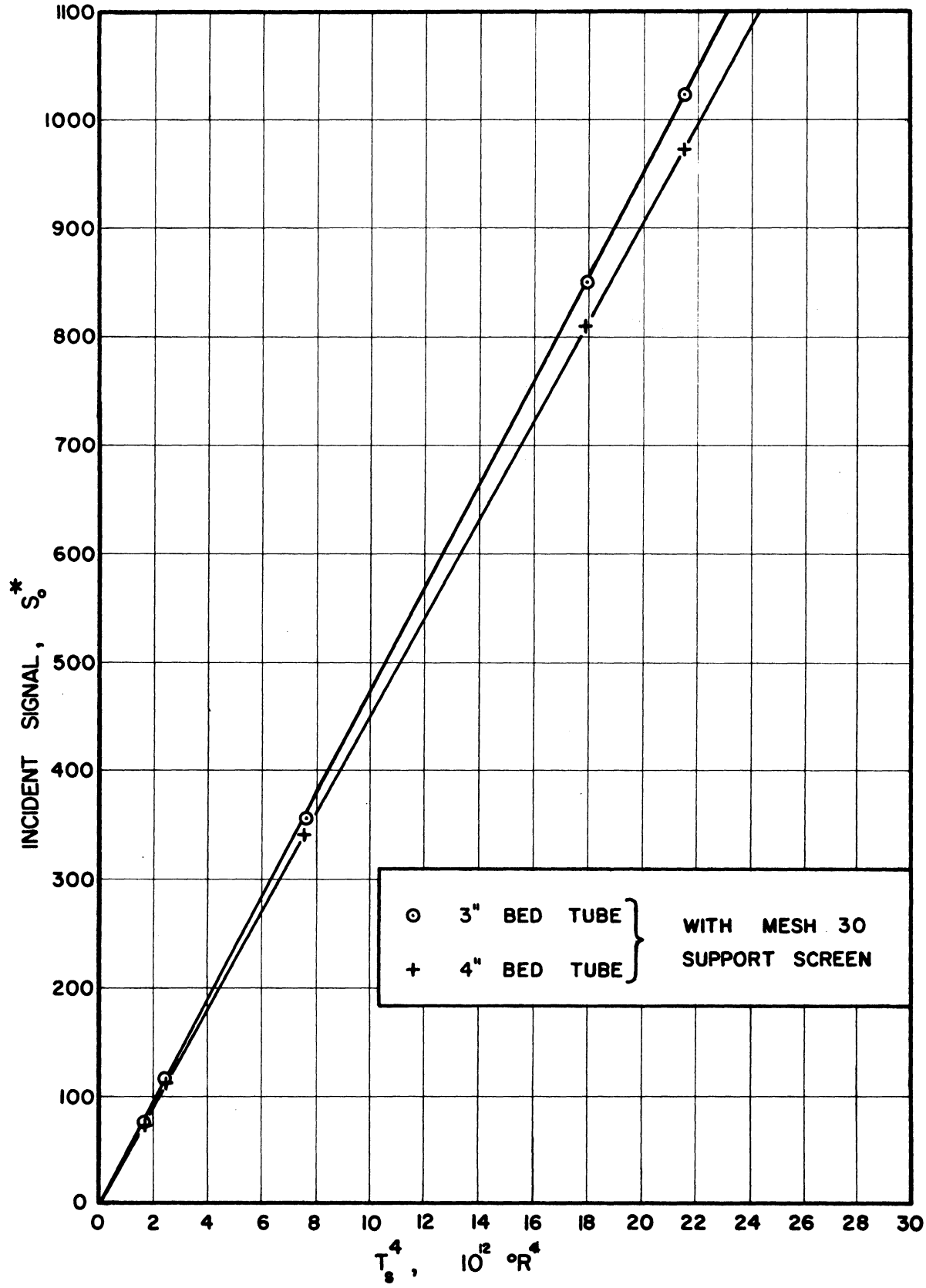

Figure 21. Temperature Calibration for S_o^*

that linear correlations fitted the data points very well. For the four inch bed tube, the dependence of S_o^* on source temperature was correlated by

$$S_o^*(T_s) = 44.8 \times (T_s\,°R)^4 \times 10^{-12} \qquad (126)$$

and for the three inch bed tube, by,

$$S_o^*(T_s) = 47.4 \times (T_s\,°R)^4 \times 10^{-12} \qquad (127)$$

where S_o^* is given in terms of meter readings normalized to unit attenuation at the amplifier. Relations (126) and (127) were used to obtain values of S_o^* at temperatures above 1700°F.

It should be noted that the data points of Figures 20 and 21 were obtained over a period of two months. This showed that the standard screen was sensibly not affected by the atmosphere or by handling and that the correlations could be used over a period of several months without recalibration.

RESULTS AND DISCUSSION

Transmission Curves

A total of fifty-two runs were made with twelve different packings. For the glass particles (GS-3, GS-4, GS-5) it was possible to obtain measurements down to 800°F. For the other opaque particles (AS-3/16, AP-1/8, AP-5/32, AP-3/16, SS-1/8, SS-3/16, AG-4, AG-16, CG-16) it was possible to obtain accurate measurements only at temperatures above 1500°F. The data for valid runs are presented in Table VI of the Appendix.

As explained in the Description section, the final transmission value for each packing height was obtained from the arithmatic average of several measurements, with the bed being repacked between each measurement. These average transmission values are plotted as data points in Figures 22-33. Each figure represents one type of packing, with parameters of source temperature. Runs were made for the glass particles at temperatures of 800°F, 1200°F, 1600°F, 1800°F, and 2000°F. For all other particles, runs were made at 1600°F, 1800°F, and 2000°F. It is seen that for every run, the natural log of $S_n(h)$ did approach a linear dependence on h at large values of h. Therefore, Equations (178) and (179) were valid for estimating first-guess values of m and a_n.

By regression formulas developed in the Appendix, transmission curves were fitted to the data points according to Equation (115). These curves are plotted on Figures 22-33 to show the degree of correlation with data points. It is evident that the two-flux model of Equation (115) was very successful in fitting the experimental data. In every run, the regression curve seemed to be coincident with the "best curve" that could

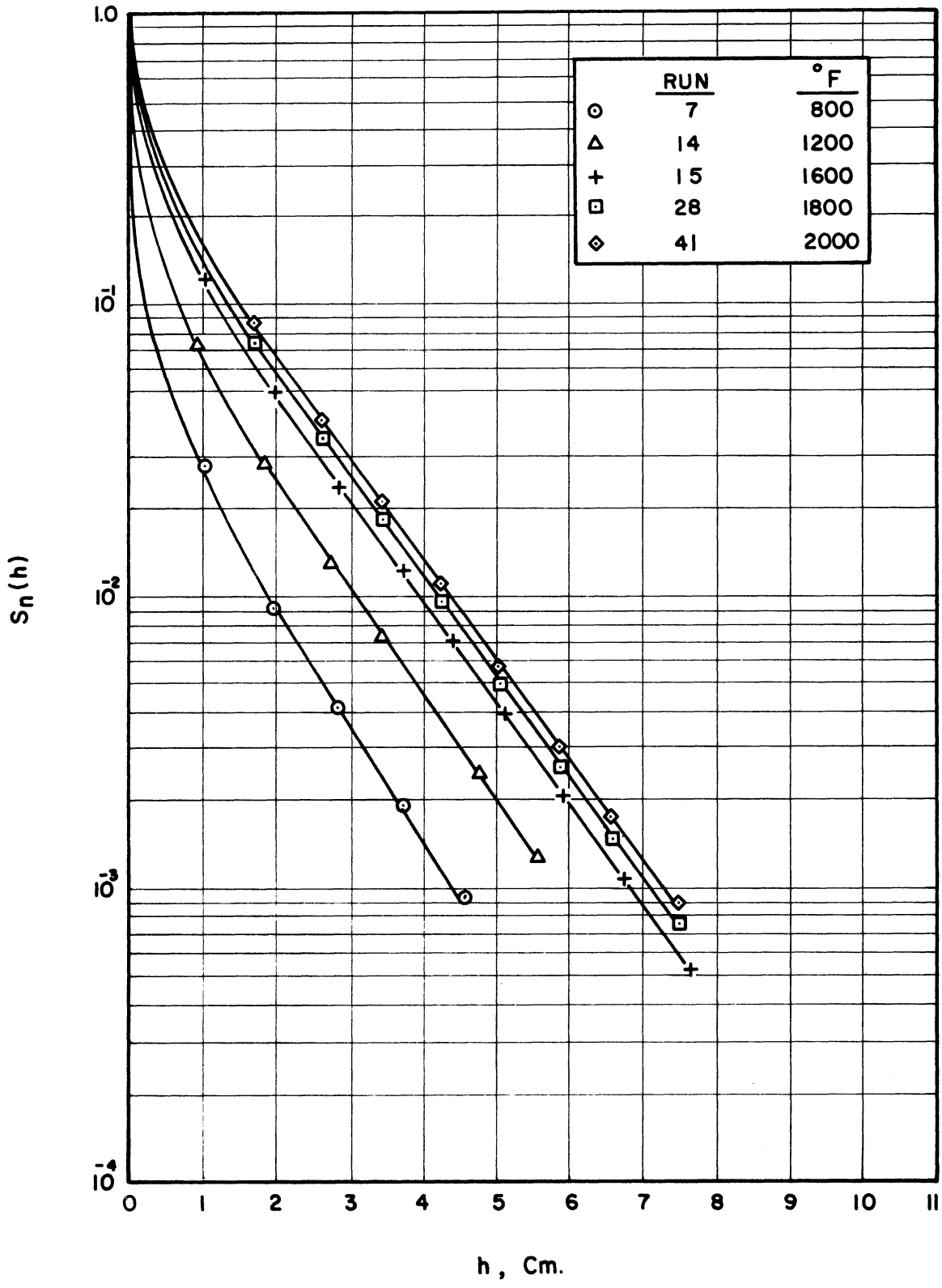

Figure 22. Transmission Curves for GS-3

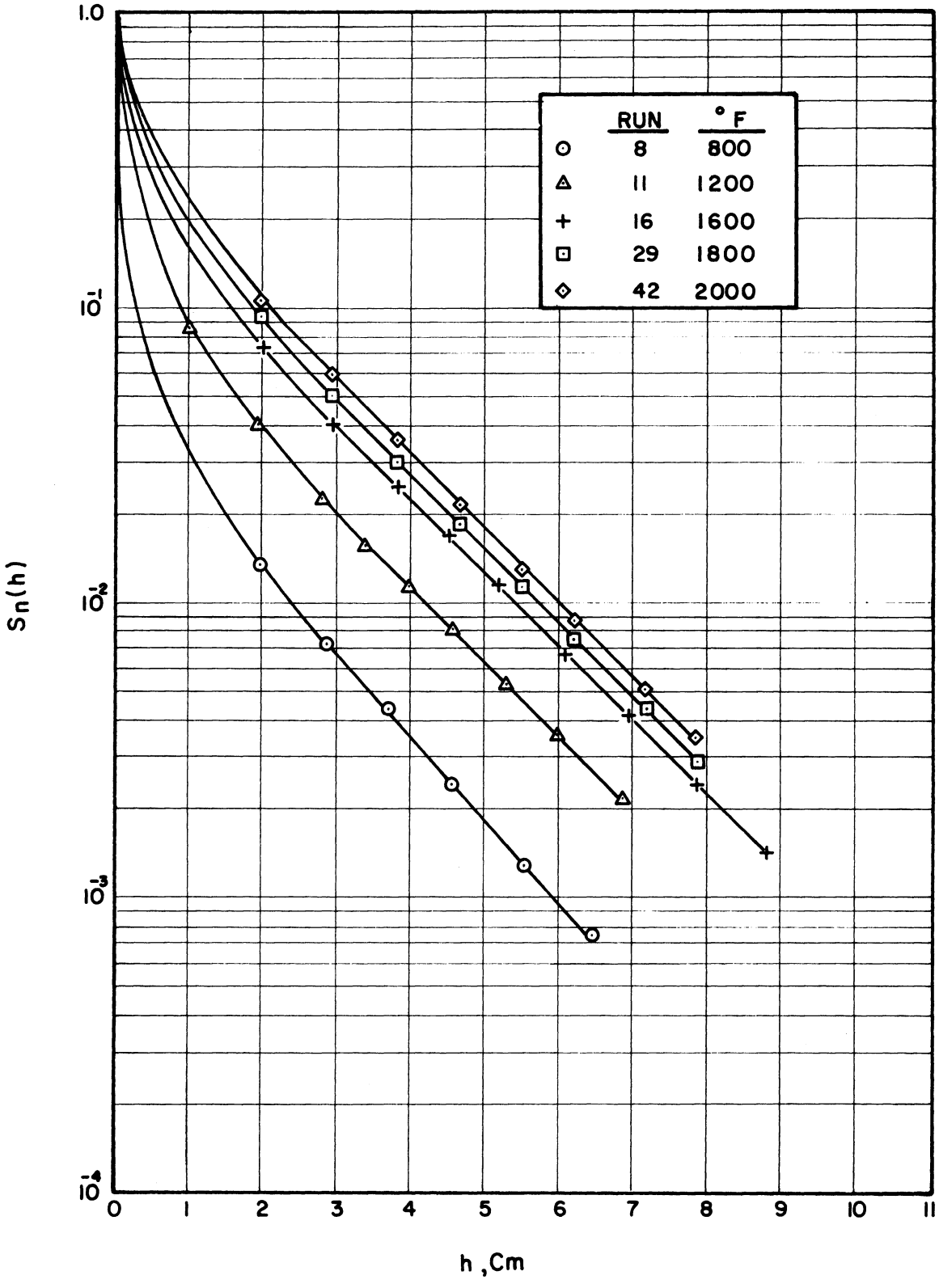

Figure 23. Transmission Curves for GS-4

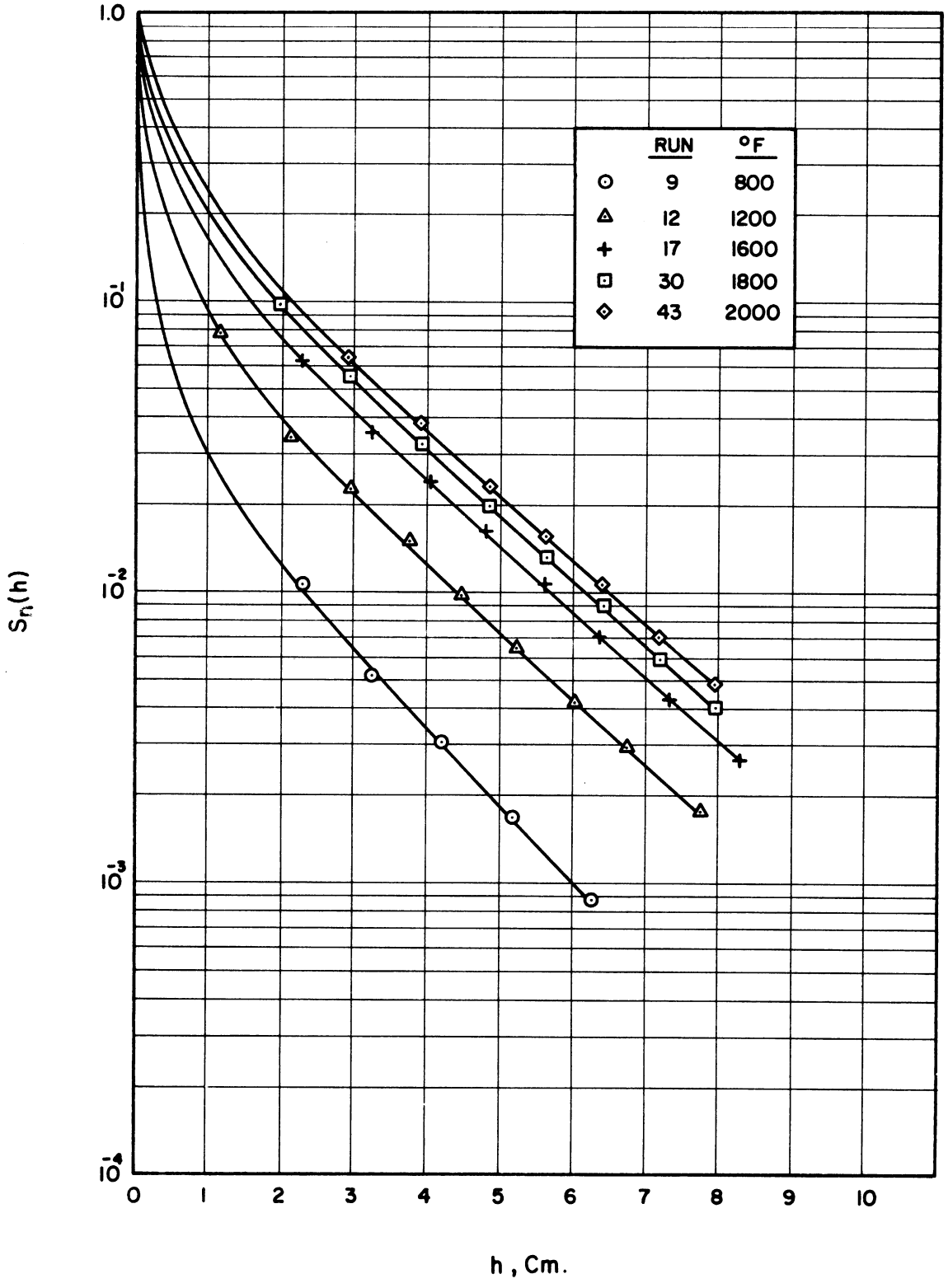

Figure 24. Transmission Curves for GS-5

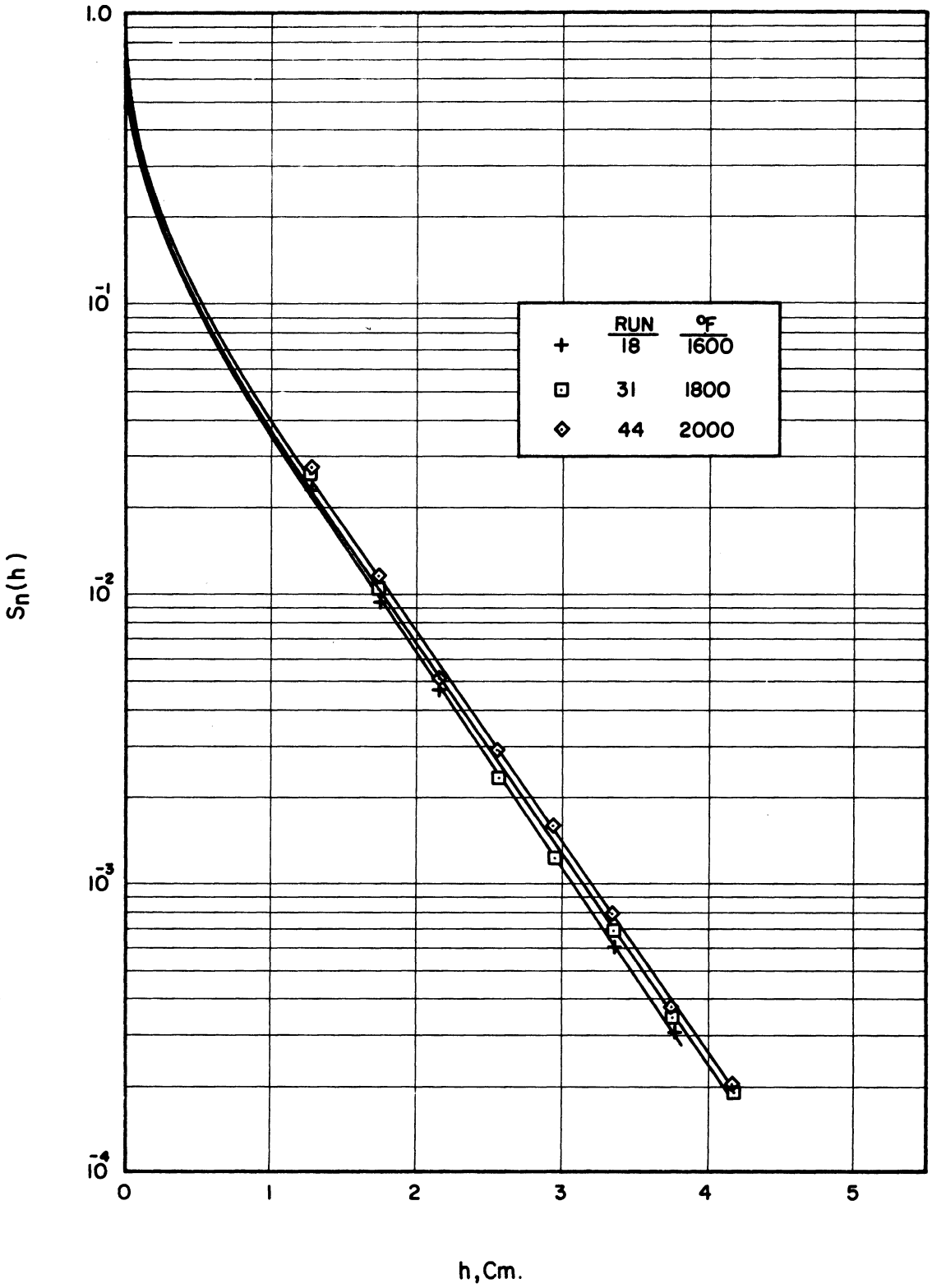

Figure 25. Transmission Curves for AS-3/16

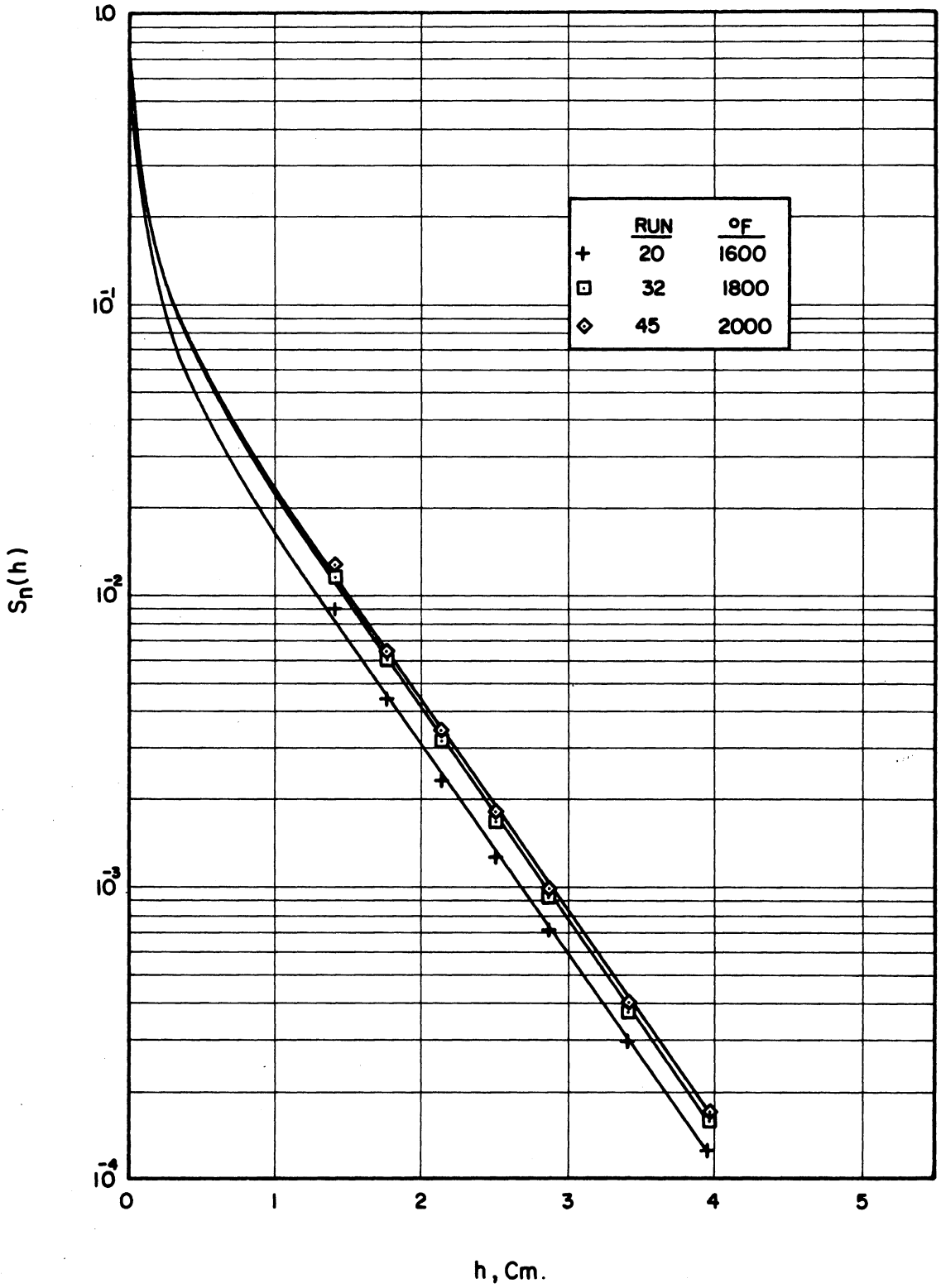

Figure 26. Transmission Curves for AP-1/8

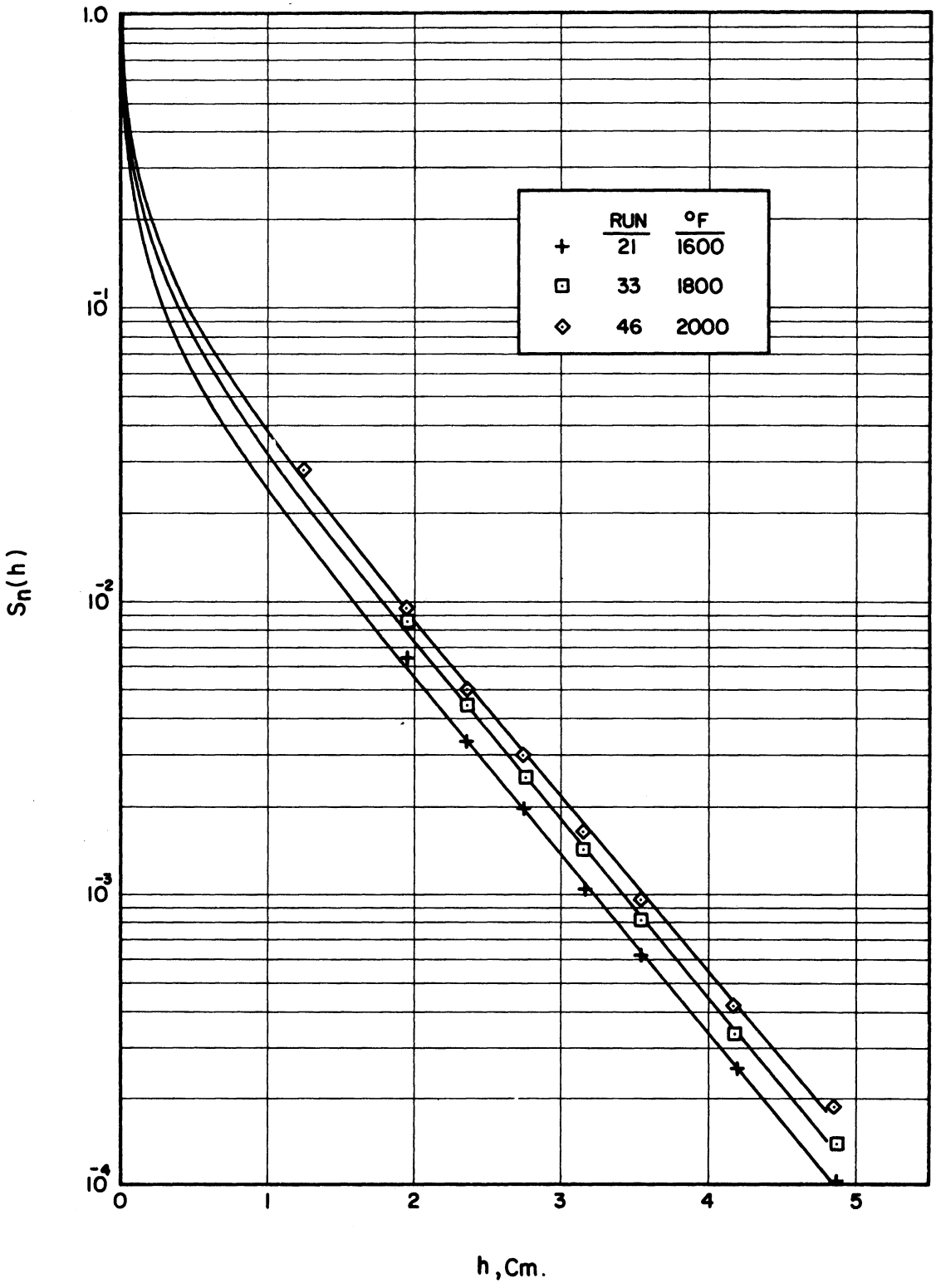

Figure 27. Transmission Curves for AP-5/32

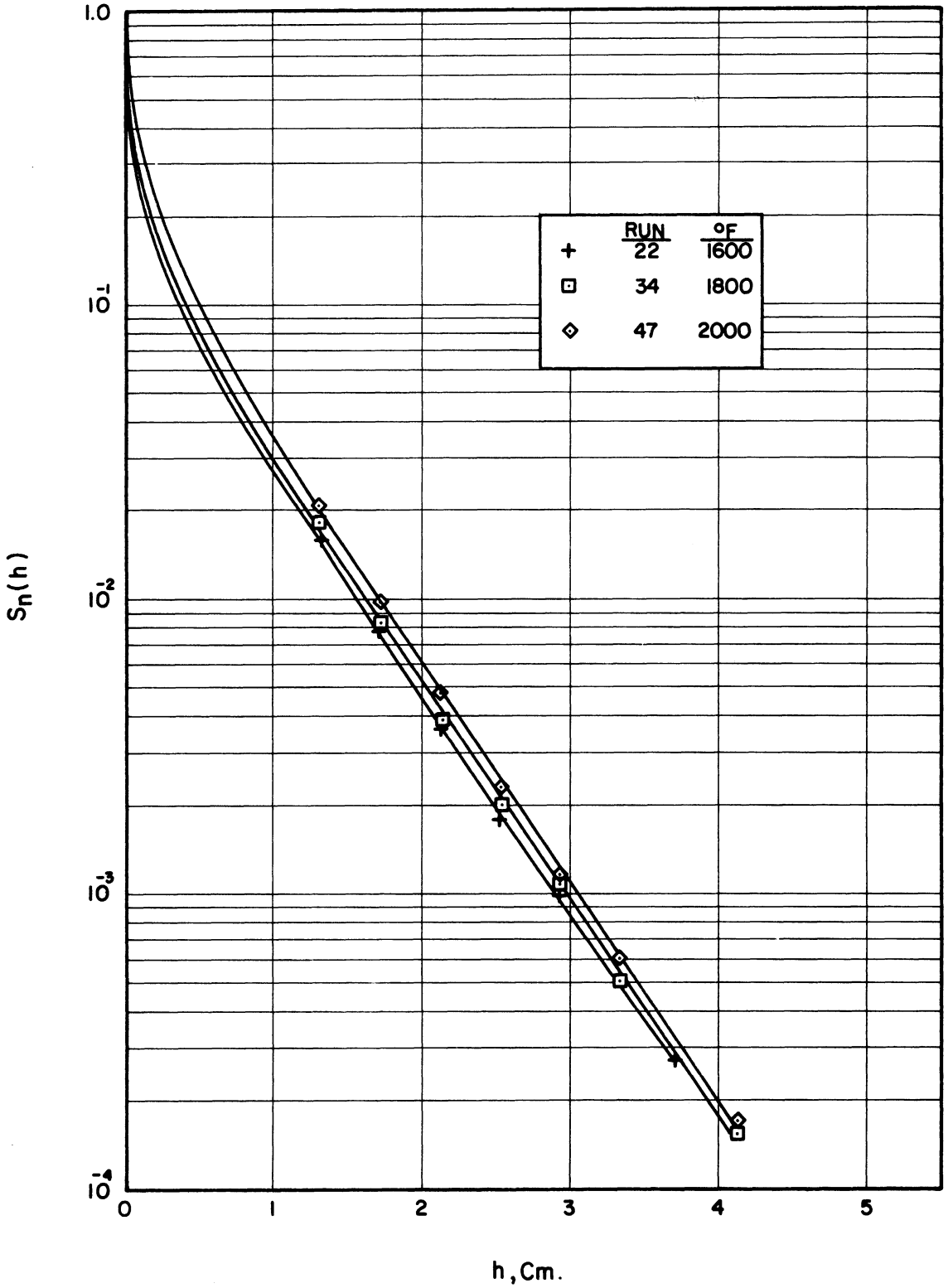

Figure 28. Transmission Curves for AP-3/16

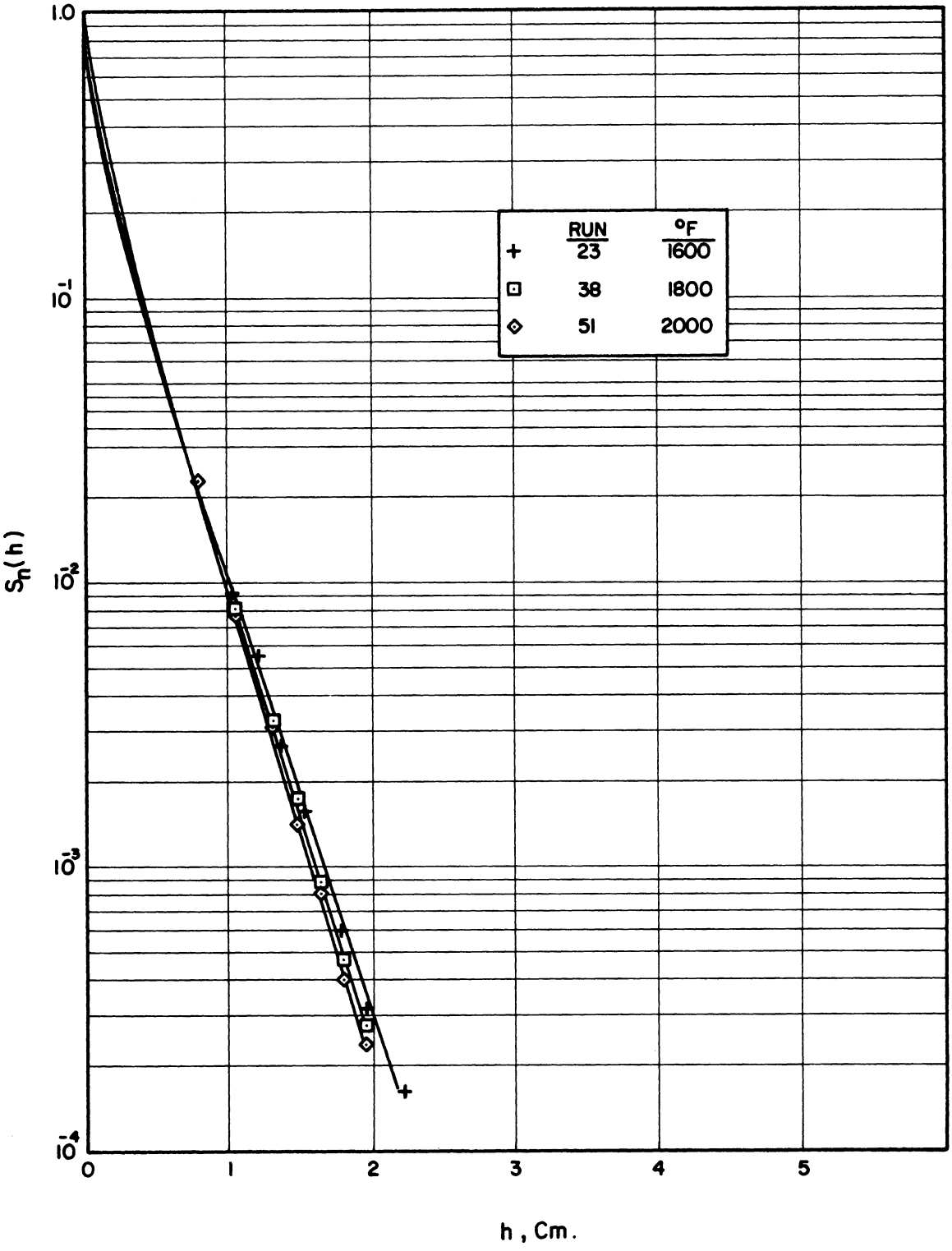

Figure 29. Transmission Curves for SS-1/8

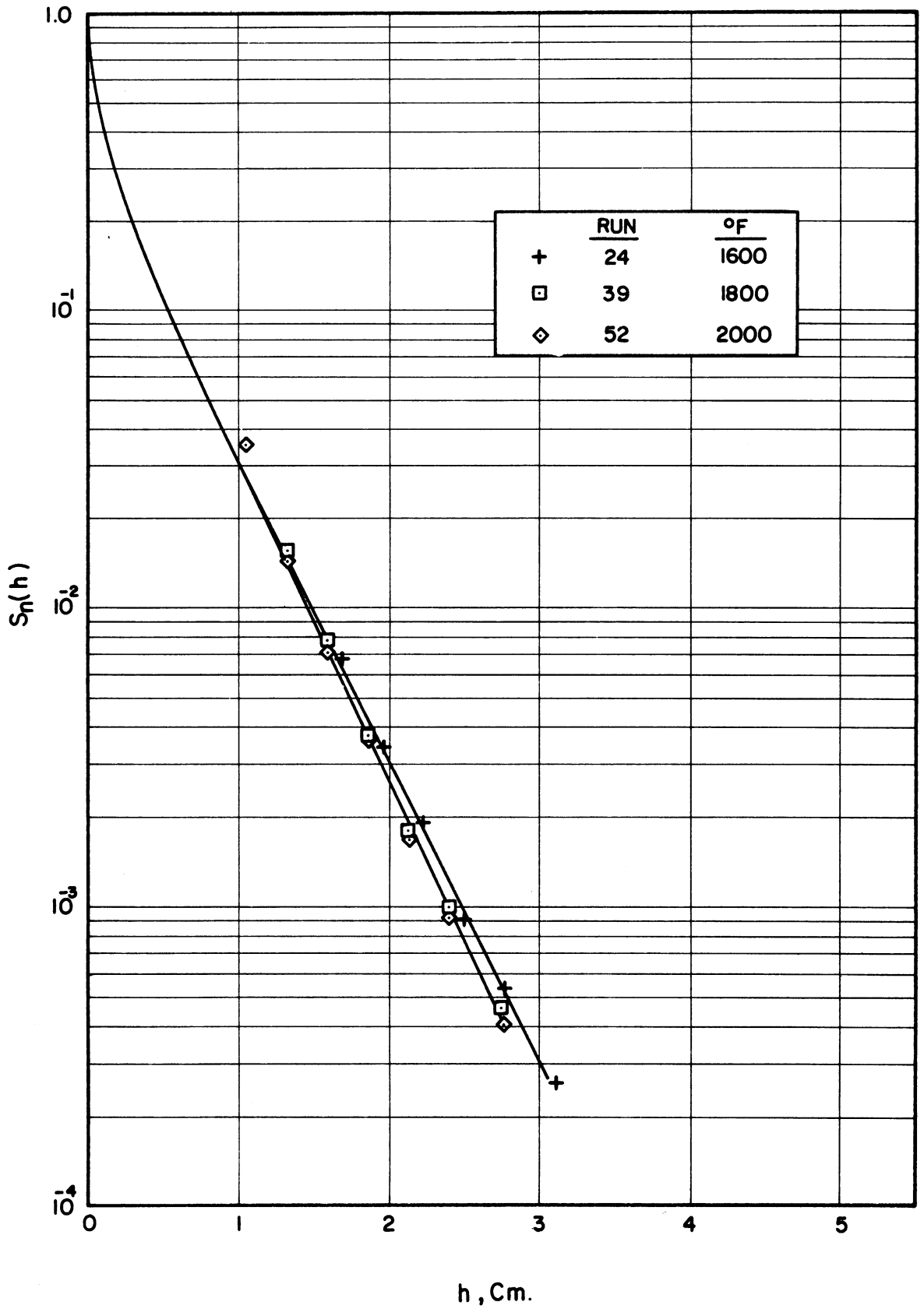

Figure 30. Transmission Curves for SS-3/16

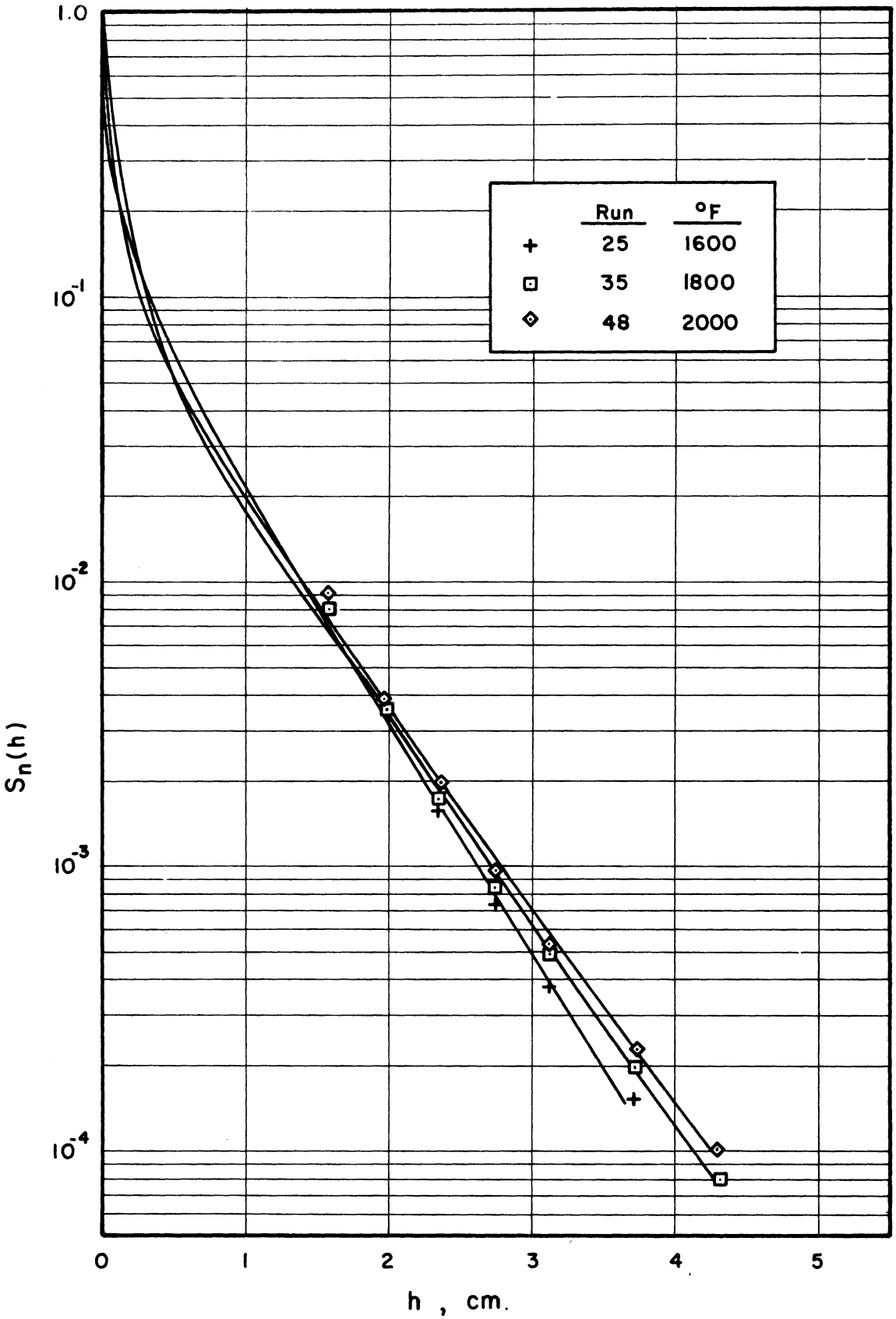

Figure 31. Transmission Curves for AG-4

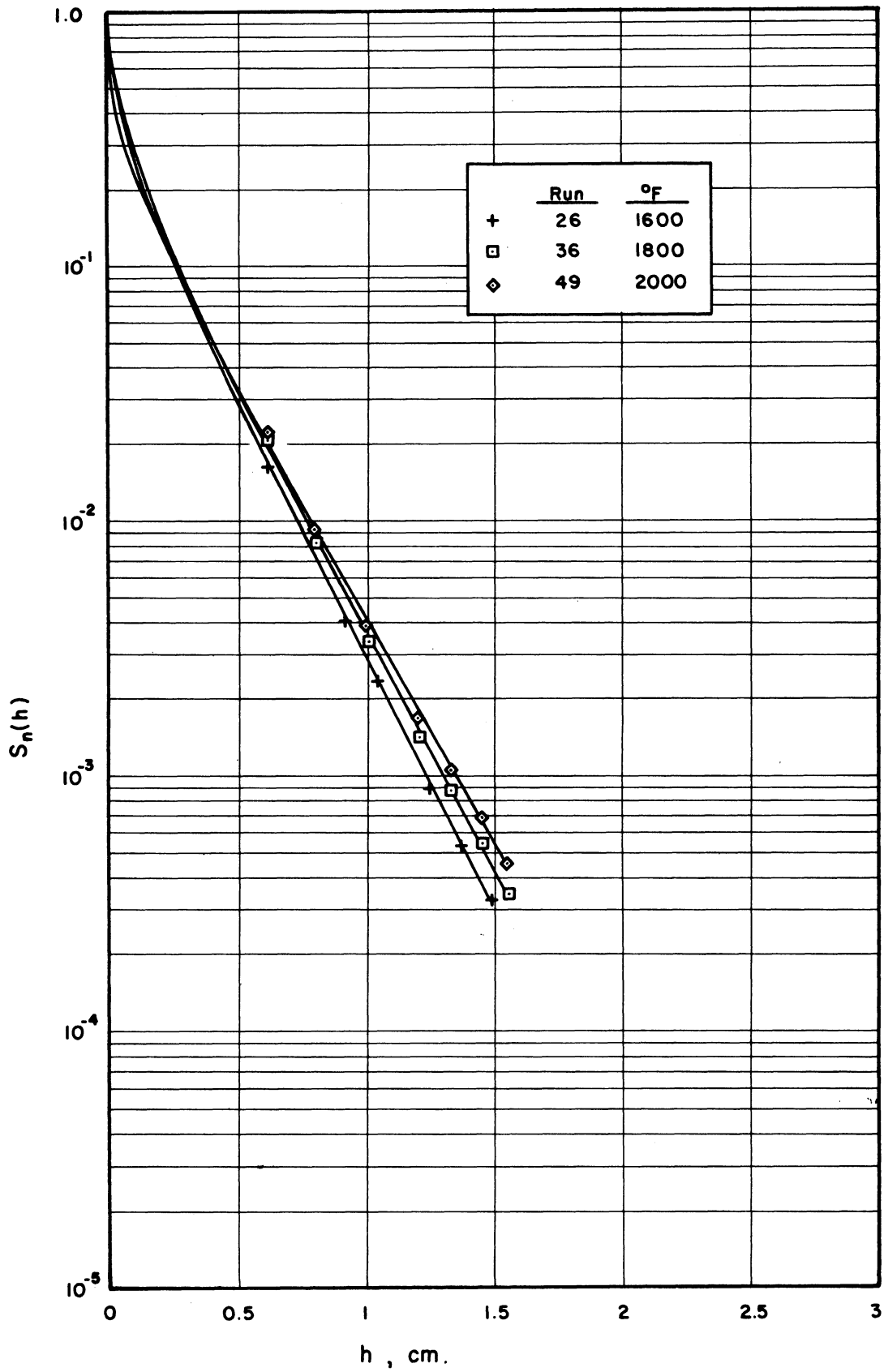

Figure 32. Transmission Curves for AG-16

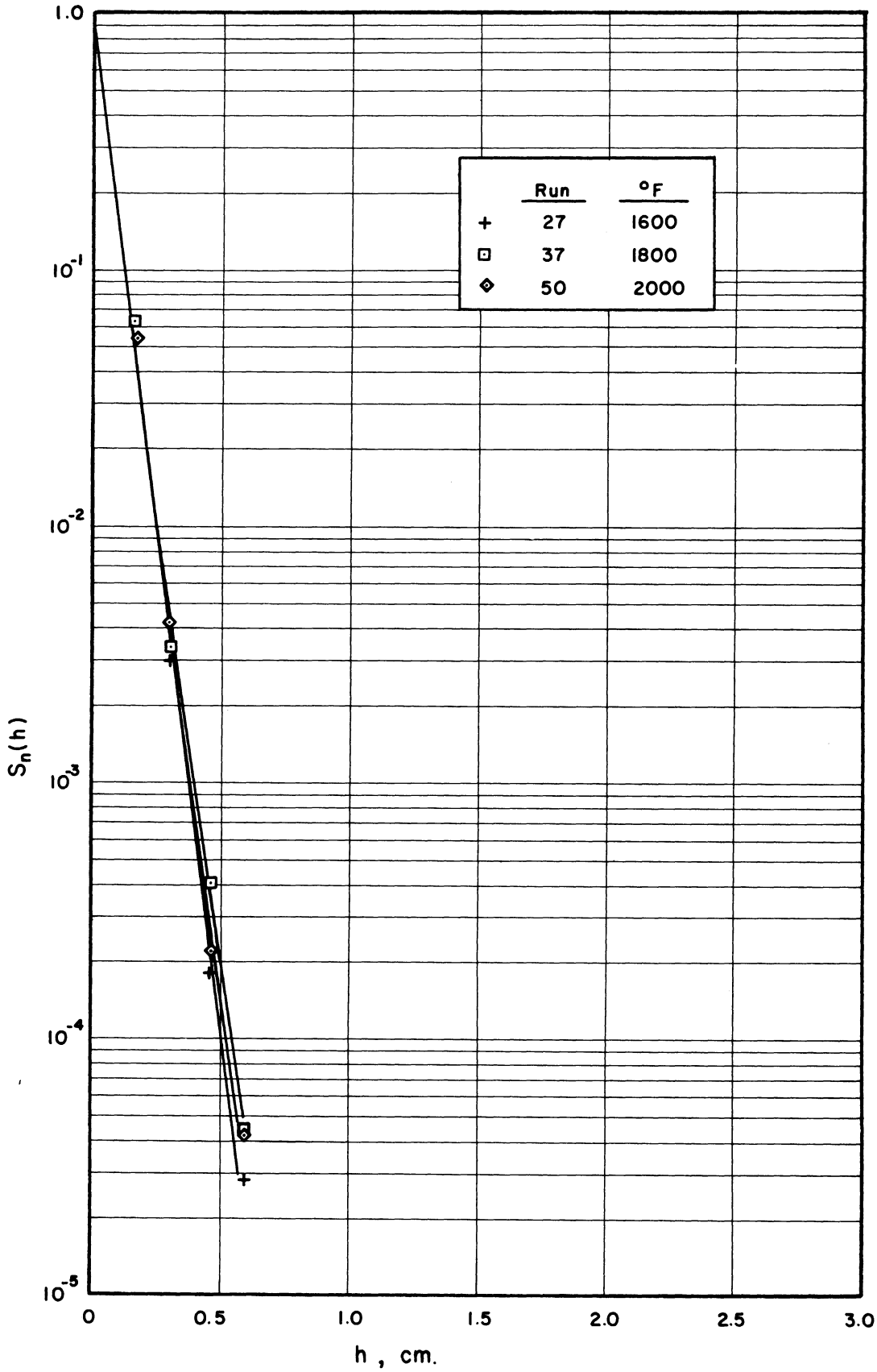

Figure 33. Transmission Curves for CG-16

have been drawn through the data points by eye. This fact is also evident from Table XI which compares the transmissions calculated from the regression curves to the experimental transmissions. The differences between the calculated and experimental values are seen to be generally small, of the order of 2-8%, and to be fairly well divided between positive and negative differences.

A statistical measure of the correlation fit may be obtained from the standard deviation, defined as

$$\delta_s = 100 \sqrt{\frac{\Phi}{n}} \quad \% \tag{128}$$

where

Φ is given by Equation (143)

n = number of data points used in correlation.

Standard deviation, δ_s, has the physical significance that in 100 measurements of S_n, 95 of the measurements may be expected to fall within $\pm 2 \delta_s \sqrt{\frac{n}{n-1}}$ % of the value predicted by the correlation. Standard deviation values for the transmission curves are given in Table XI. It is seen that the deviations were lowest for glass particles and highest for silicon carbide particles. This verified an experimental characteristic which was noticeable during operation--that precision and reproducibility were best for packings with high transmissions.

Several trends should be noted about the transmission curves of Figures 22-33. First, it is seen that the curves for glass particles show the greatest separation between temperatures. This is consistent with the fact that glass transmissivity is highly dependent on wavelength of the radiation. At 800°F, the wavelength of maximum intensity is 4.9 microns,

to which glass is mostly opaque. At 2000°F, the wavelength of maximum intensity is reduced to 2.2 microns which is almost in the optical range, and to which glass is much more transparent. The transmission curves for all the other test particles, which remain opaque to radiation of all wavelengths, do not show as wide a separation between temperatures.

It is also seen that transmission curves for packings of high absorptivity tend to have steep slopes and to approximate straight lines. This is as expected since a packing of infinite absorptivity would have zero transmission, and the transmission curve would approach the limit of a vertical straight line. Among the test particles, CG-16 approached the closest to this limiting case. A side effect of steep transmission curves is the tendency to increase standard deviations since a small variation in h would correspond to a large variation in S_n. This may be seen from the curves for CG-16, Figure 33, which approach all data points quite closely yet have relatively high standard deviations of 18-27%.

Attenuation Cross Sections

The main objective of this experimental investigation was to obtain values of the attenuation cross sections, a and s_b, for a number of typical packings. The values of these parameters determined by regression, for the twelve packings tested, are listed in Table II below. These values correspond to the transmission curves of Figures 22-33.

The relative importance of absorption and back scattering is immediately evident from examination of Table II. For all test packings except CG-16, it is seen that back scattering is definitely the major mechanism of attenuation. This is especially true for the alundum and glass

TABLE II

ATTENUATION CROSS SECTIONS

Packing Particle	t_s (°F)	Run	a $(\frac{ft^2}{ft^3})$	s_b $(\frac{ft^2}{ft^3})$
GS-3	800	7	0.390	977
	1200	14	0.843	372
	1200	10	0.969	343
	1200	13	0.884	342
	1600	15	1.54	190
	1800	28	1.88	153
	2000	41	2.21	129
GS-4	800	8	0.209	878
	1200	11	0.521	298
	1600	16	0.988	149
	1800	29	1.33	114
	2000	42	1.59	95.0
GS-5	800	9	0.178	952
	1200	12	0.437	296
	1600	17	0.812	151
	1600	40	0.804	149
	1800	30	1.09	114
	2000	43	1.24	96.8
AS-3/16	1600	18	2.74	496
	1800	31	2.70	483
	2000	44	2.84	449
AP-1/8	1600	20	1.06	1190
	1800	32	1.49	860
	2000	45	1.47	847
AP-5/32	1600	21	1.00	906
	1800	33	1.32	682
	2000	46	1.54	576
AP-3/16	1600	22	1.96	682
	1800	34	2.18	614
	2000	47	2.77	496
AG-16	1600	26	12.7	779
	1800	36	10.6	811
	2000	49	9.37	837

TABLE II (CONT'D)

Packing Particle	t (°F)	Run	a ($\frac{ft^2}{ft^3}$)	s_b ($\frac{ft^2}{ft^3}$)
AG-4	1600	25	2.05	789
	1800	35	1.16	1090
	2000	48	1.20	1010
CG-16	1600	27	272	420
	1800	37	107	1050
	2000	50	192	627
SS-1/8	1600	23	13.1	450
	1800	38	17.0	387
	2000	51	20.5	343
SS-3/16	1600	24	6.66	370
	1800	39	8.70	322
	2000	52	9.26	314

particles (spheres, pellets and grains), all of which have absorption cross sections of less than 2% the value of the back scattering cross sections. For these packings it would be valid to assume that the medium is sensibly non-absorbent and to use Equations (74) and (75) to describe radiant heat transfer. The absorption cross sections are significant for steel spheres--having values of approximately 2-7% of that of back scattering cross sections. Silicon carbide packings are seen to have the greatest absorption cross sections, as might be expected since SiC particles with its black surface have a very high emissivity. The magnitudes of the absorption cross sections for CG-16 were determined to be approximately 5-60% of the magnitudes of scattering cross sections. Equations (75) and (74) can not be applied to packings with such high absorptivities, so it is recommended that the approximate Equations (99)

and (100) be used in describing radiant heat transfer for steel or silicon carbide packed media.

Radiant Conductivities

The internal radiant conductivity, k_{ir}, was calculated for each of the test runs by Equation (104). These values are useful in obtaining an estimate of the relative ease of radiant heat transfer in the different packings. In Table III, representative values of k_{ir} for each packing are tabulated, in approximate decreasing order.

TABLE III

RADIANT CONDUCTIVITIES (k_{ir} $\frac{\text{Btu}}{\text{hr.ft.}^\circ\text{F}}$)

Packing Particle	Temperature °F				
	800	1200	1600	1800	2000
GS-5	0.0144	0.106	0.401	0.693	1.05
GS-4	0.0156	0.105	0.401	0.689	1.06
GS-3	0.0140	0.0840	0.314	0.515	0.785
SS-3/16			0.161	0.243	0.320
SS-1/8			0.131	0.200	0.289
AS-3/16			0.120	0.163	0.227
AP-3/16			0.0877	0.129	0.205
AP-5/32			0.0661	0.116	0.177
CG-16			0.108	0.0714	0.141
AG-16			0.0762	0.0968	0.121
AP-1/8			0.0504	0.0918	0.120
AG-4			0.0758	0.0729	0.101

Several general trends are evident from Table III:

(a) k_{ir} increases in the order -- alundum, steel, silicon carbide, and glass.

(b) k_{ir} increases for increasing temperature.

(c) k_{ir} increases for increasing particle size.

Packings of glass particles are seen to be the best radiant "conductors", especially at higher temperatures. Physically, this can be explained in terms of the transmission of low wavelength radiation, which is effectively counted as part of the unattenuated flux in Equations (55) and (56). For opaque particles, the conductivity results from a balance between back scattering and absorption. For alumina, which has a high surface reflectivity, attenuation is largely controlled by the large back scattering cross section, accounting for the relatively low conductivities. For silicon carbide and steel particles, absorption becomes important and the attenuation must be attributed to both back scattering and absorption. Increasing emissivity of solid increases absorption cross sections but decreases scattering cross sections. The overall effect generally is to increase radiant conductivities.

The second two trends of k_{ir}, increasing with increasing temperature and particle size, are as expected. Almost all analytic works predict an increase in radiant conductivity for higher temperatures and larger particles, as shown by Equation (5) from Schotte's[33] study, Equation (6) from Rosseland's[31] study, and Equation (3) from Laubitz's[21] study. Of the two, the temperature effect was definitely more pronounced. These two trends, showing the effects of temperature and particle size, are discussed in greater detail in later sections.

Relative Importance of Radiation and Conduction

The ratio of heat transfer by radiation to that by conduction is of practical interest in defining the conditions where radiant transfer becomes important. Previously, this ratio had been experimentally determined

for only one packing -- Hill and Wilhelm's[15] alumina spheres. From the experimental measurements of this present study, it was possible to determine the radiation-conduction ratios for all twelve of the packings tested.

Conductive heat transfer is commonly specified by a bulk conductivity, k_c. Wilhelm et al.[38] have proposed a semi-empirical method for calculating k_c, based on Schuman and Voss' model.[34] By means of this method, values of k_c were obtained for the test beds. The ratios k_{ir}/k_c were then determined and used as a measure of the relative importance of radiation and conduction. Details of the calculation are given in the Appendix and the results are shown in Table IV.

Some representative radiation-conduction ratios have been plotted against temperature in Figures 34 and 35. Figure 34 shows the effects of different particle materials and shapes. Glass spheres are seen to have the largest ratios and to have the greatest temperature sensitivity. For packings of 5 mm. glass spheres, radiation accounts for 50% of total heat transfer at a temperature of 1300°F. At higher temperature, the ratio increases rapidly so that at 2000°F, radiation accounts for 85% of all heat transfer. The packings of opaque particles are seen to have much lower radiation-conduction ratios, which are also less sensitive to temperature. At 1600°F, the radiant heat transfers are all less than 50% of total heat transfer, for 3/16 steel spheres, 3/16 alumina cylinders, 3/16 alumina spheres, and mesh 4 silicon carbide grains. At 2000°F, the radiant transfers increase to 61% and 58% for alumina cylinders and spheres respectively, while for the steel spheres and silicon carbide grains, the radiant transfers are still below 50%, at 45% and 35% respectively.

TABLE IV

RADIATION TO CONDUCTION RATIO

	800 °F			1200 °F			1600 °F			1800 °F			2000 °F		
	k_c	k_{ir}	$\frac{k_{ir}}{k_c}$	k_c	k_{ir}	$\frac{k_{ir}}{k_c}$	k_c	k_{ir}	$\frac{k_{ir}}{k_c}$	k_c	k_{ir}	$\frac{k_{ir}}{k_c}$	k_c	k_{ir}	$\frac{k_{ir}}{k_c}$
GS-3	.136	.014	0.10	.151	.091	0.60	.167	.314	1.88	.173	.515	2.98	.178	.785	4.41
GS-4	.136	.015	0.12	.151	.105	0.70	.167	.401	2.40	.173	.689	3.98	.178	1.06	5.96
GS-5	.136	.014	0.10	.151	.106	0.70	.167	.396	2.37	.173	.693	4.01	.178	1.05	5.90
AS-3/16							.154	.120	0.78	.161	.163	1.01	.168	.227	1.35
AP-1/8							.098	.050	0.51	.103	.092	0.89	.131	.120	0.92
AP-5/32							.098	.066	0.67	.103	.116	1.26	.131	.177	1.35
AP-3/16							.098	.088	0.89	.103	.129	1.25	.131	.205	1.56
AG-16							.132	.076	0.58	.138	.097	0.70	.144	.121	0.84
AG-4							.115	.076	0.66	.121	.073	0.60	.126	.101	0.80
CG-16							.246	.108	0.44	.254	.071	0.29	.259	.141	0.54
SS-1/8							.354	.131	0.37	.372	.200	0.54	.389	.289	0.74
SS-3/16							.354	.161	0.45	.372	.243	0.65	.389	.320	0.82

Units of $k = \frac{\text{B.T.U.}}{\text{hr.ft.}^\circ\text{F}}$

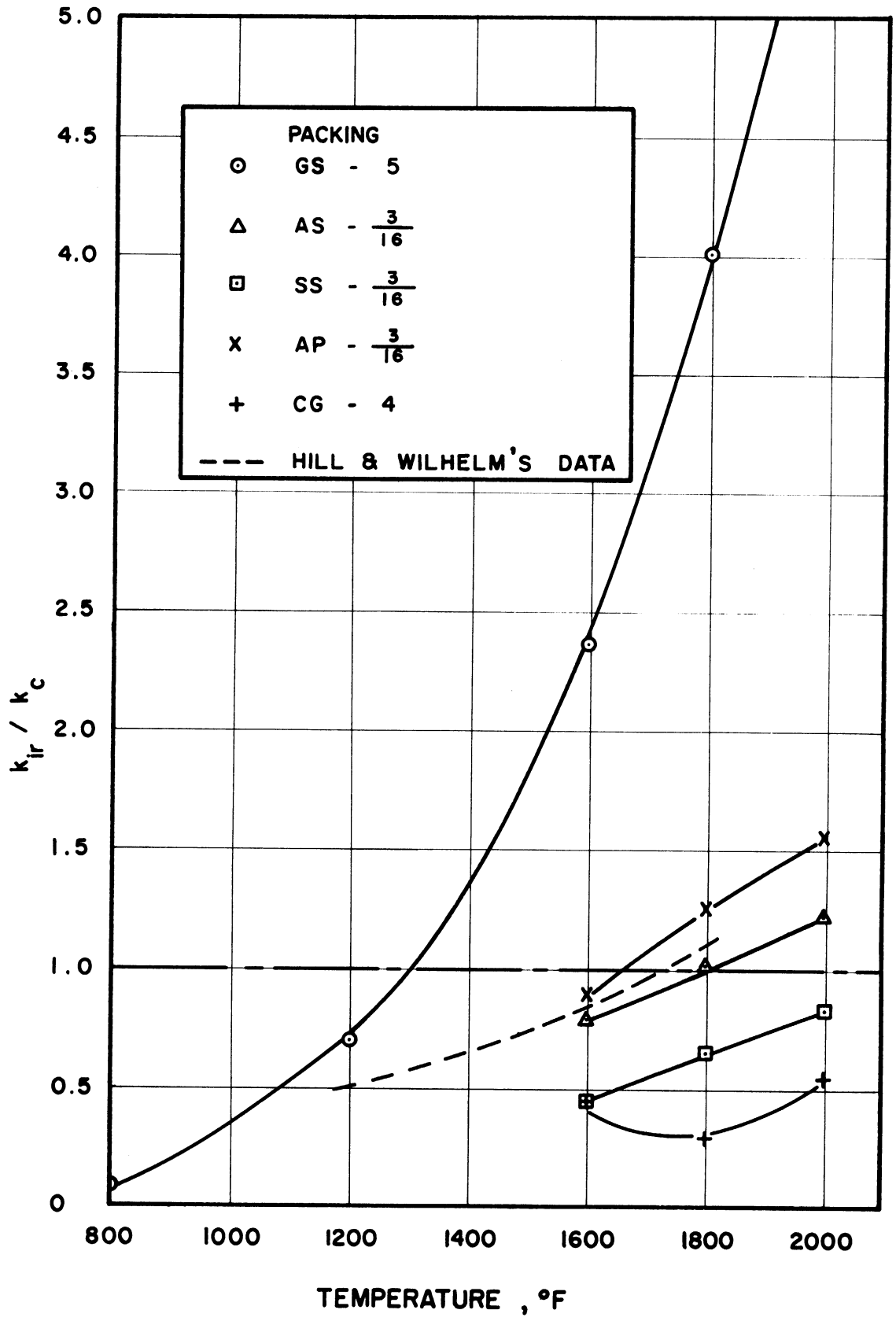

Figure 34. Radiation to Conduction Ratio

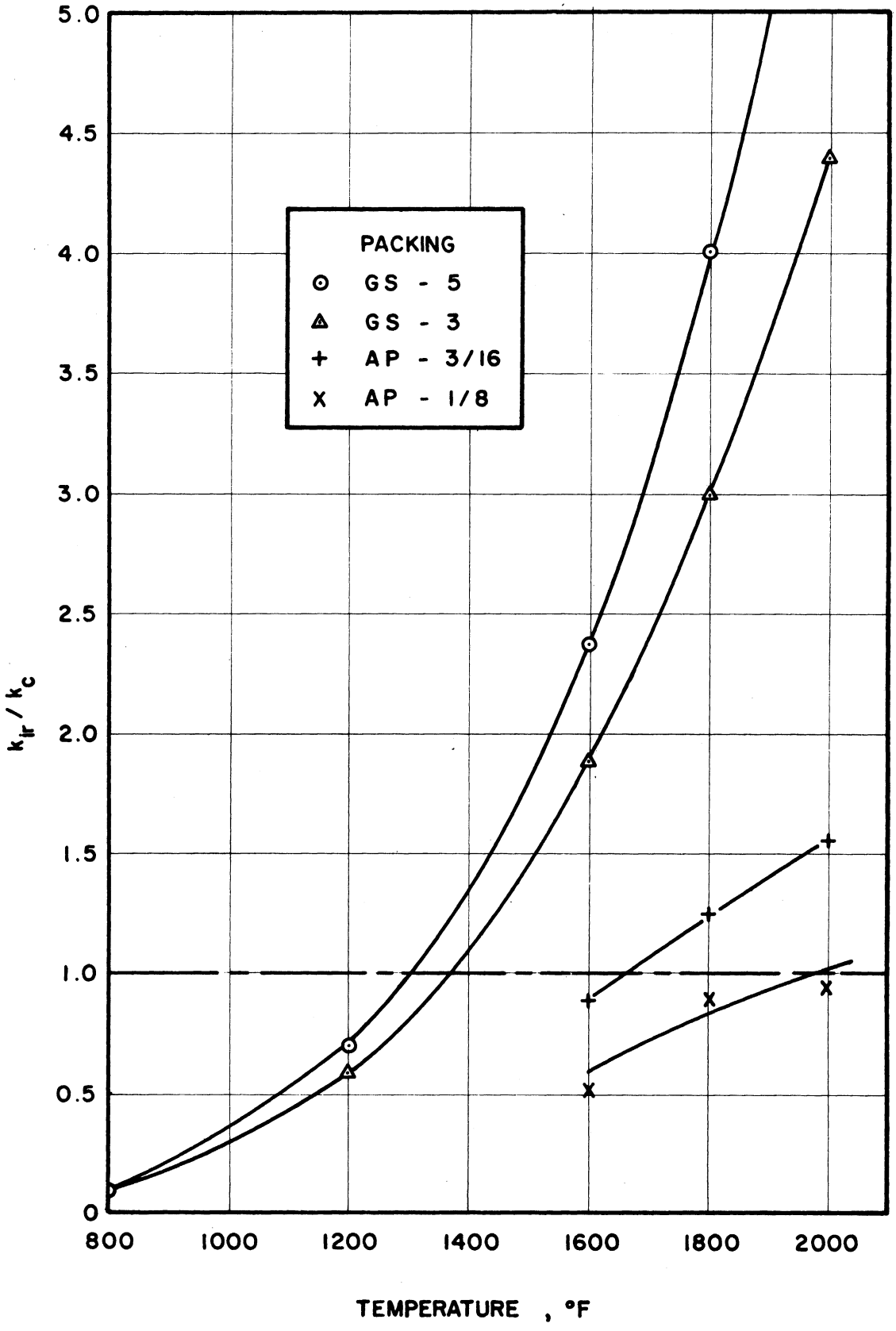

Figure 35. Radiation to Conduction Ratio

Hill and Wilhelm's data[15] have been replotted on Figure 34 for comparison. It is seen that their values, which were obtained for 3.8 mm. alumina spheres, agree quite well with the data for 3/16 inch (4.8 mm) alumina spheres of this investigation.

Figure 35 shows the effect of particle size. Two types of particles are presented -- glass spheres and alumina cylinders. In both cases, it is seen that radiant transfer is more important for larger particles. Thus at a temperature of 1600°F, radiation accounts for 65% of all heat transfer for 3 mm. glass spheres, but accounts for 73% for 5 mm. glass spheres. Similarly, the fraction increases from 34% to 47% in changing from 1/8 inch alumina cylinders to 3/16 inch alumina cylinders. This dependence on particle size is more pronounced at high temperatures than at low temperatures, as shown by the increased divergence of curves in Figure 33 at higher temperatures.

In general, the results indicate that radiation starts to become important at temperatures of about 1000°F. The radiant heat transfer becomes increasingly important relative to conductive transfer as temperature increases, and becomes dominant at temperatures of about 1400°F to 2200°F.

Comparison With Analytic Estimates

As mentioned in Part I, a number of authors have proposed equations for estimating radiant conductivities of particulate media. To compare these analytical estimates with the experimental data, radiant conductivities were calculated by three of these proposed equations for packings of AP-1/8, SS-3/16, and GS-3 particles. The equations used were:

(a) Damköhler[6] - Argo and Smith[1],

$$k_1 = 4\sigma\left(\frac{\epsilon}{2-\epsilon}\right) D_p T^3 \qquad (2b)$$

(b) Schotte[33]

$$k_2 = \frac{1 - \delta_p}{\frac{1}{k_s} \quad \frac{1}{k_r^\circ}} + \delta_p k_r^\circ \tag{5}$$

where $k_r^\circ = 4\sigma \epsilon D_p T^3$

(c) Rosseland[31] - Bosworth[3]

$$k_3 = \frac{4}{3} \sigma l T^3 \tag{6}$$

where

l = mean free path = D_p

Details of the calculations are given in the Appendix. Results have been plotted together with experimental conductivities on Figures 36, 37, 38.

It is seen that the agreement is generally not very good, either among analytic estimates themselves or between estimates and data. While the order of magnitudes are the same, variations range through factors of 0 - 8. The estimated values are seen to be all too high for the two opaque packings. For the glass packing, the estimates are seen to be too high at low temperatures and too low at high temperatures.

One possible explanation for the poor agreement is that all the analytic estimates were based on extremely simple models, as described in Part I. The models assumed no interaction between particles, which actually may not be valid for packed media where the particles are in physical contact. It is conceivable that two particles together would have a larger effective scattering cross section than the two particles separately, due to the greatly reduced free path length in vicinities of contact points. Such a situation would of course reduce the equivalent conductivity of the

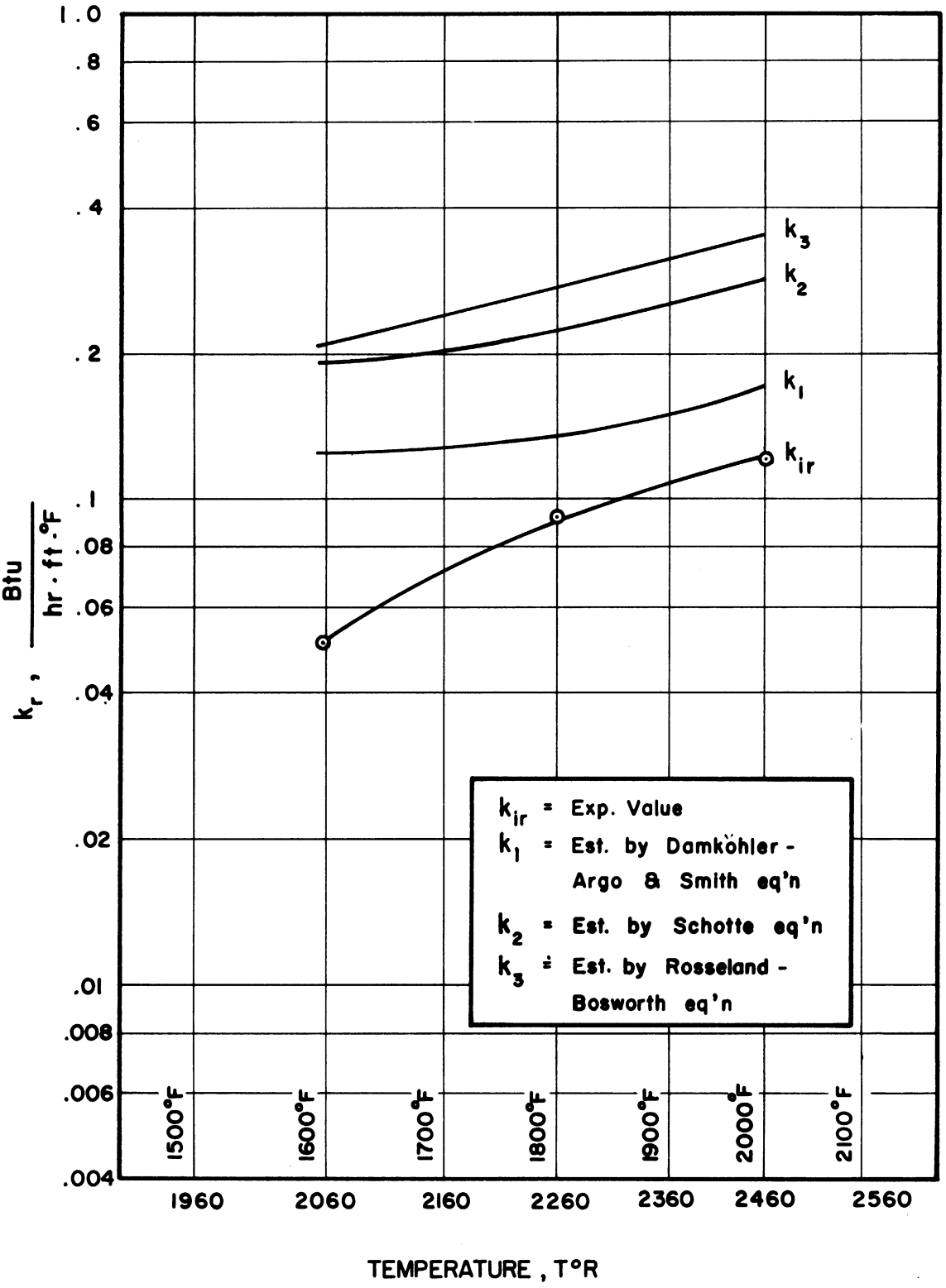

Figure 36. Comparison with Analytic Estimates for AP-1/8

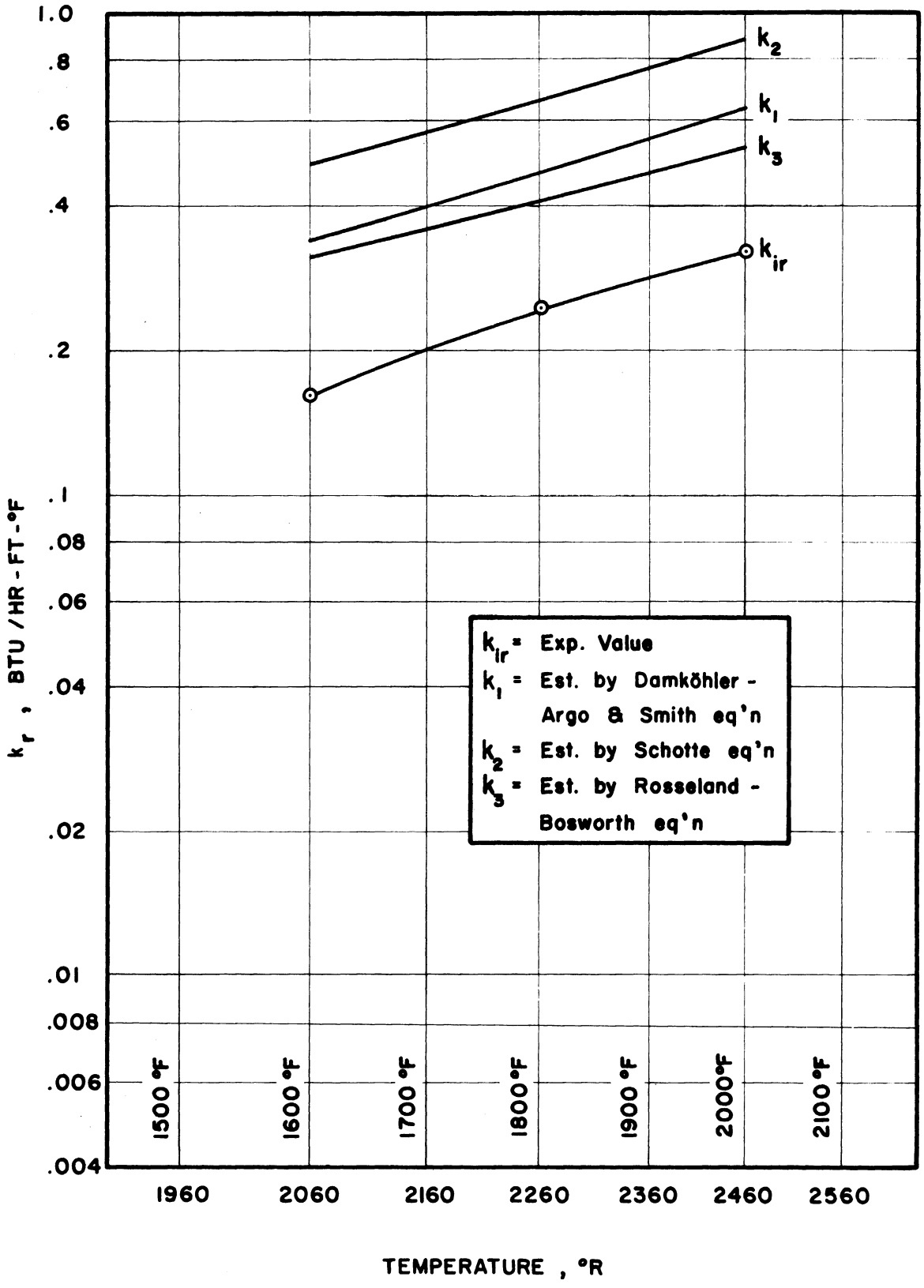

Figure 37. Comparison with Analytic Estimates for SS-3/16

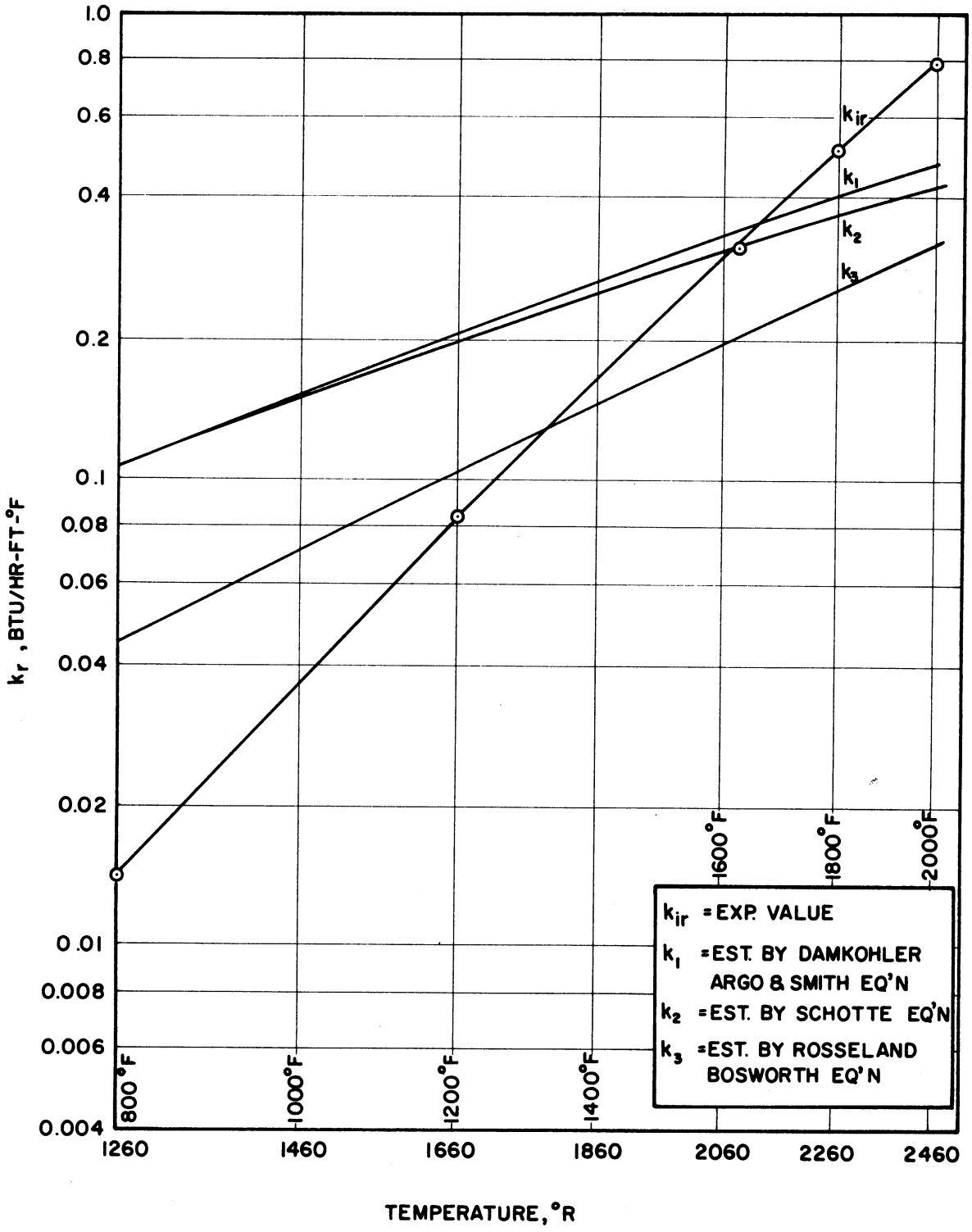

Figure 38. Comparison with Analytic Estimates for GS-3

packed media, accounting for the low values obtained experimentally. One possible way to modify the analytic expressions in order to account for this increased attenuation is to use an effective particle diameter, D_p', which is smaller than the actual particle diameter, D_p. This would serve to reduce the conductivities calculated by all three of the analytic estimates.

A second factor, that may account for part of the failure of the analytic estimates, is that none of the three estimates allowed for particle transmission. Thus the estimated conductivities fell too low for glass packings at high temperatures, where a fair portion of the flux transport may occur by direct transmission through the glass particles. To correct for this, some equivalent conductivity due to transmission would have to be added to the present expressions (2b), (5), and (6). This additive term would be expected to be directly proportional to material transmissivity which would in turn be a function of radiation temperature. The combined effect of the two suggested corrections, i.e., using D_p' and an additive k_r of transmission, would be to lower estimated conductivities for opaque particles and to raise estimated conductivities for transparent particles. Such a modification would bring much better agreement between predictions and data, as evident from Figures 36-38.

It is interesting to note that most of the analytic expressions for radiant conductivity are of the form,

$$k_r \cong 4\sigma D_p T^3 \times K \qquad (129)$$

where K is some arbitrary function given by the specific analysis. This similarity between the various expressions have been noted previously by

Gorring and Churchill[11] and by Hill and Wilhelm.[15] The entire problem of predicting radiant conductivities may be reduced to a problem of finding the correct K function.

In the three analytic models tested, the function K is seen to be:

(a) Damköhler - Argo and Smith,

$$K = \frac{\epsilon}{2 - \epsilon} \tag{130}$$

(b) Schotte,

$$K = \epsilon \tag{131}$$

(c) Rosseland - Bosworth

$$K = \frac{1}{3} \tag{132}$$

The K function may also be separated out from the expression for k_{ir}, Equation (104), as follows.

$$K = \frac{k_{ir}}{4 \sigma D_p T^3}$$

$$= \frac{8 \sigma T^3}{(a + 2 s_b)(4 \sigma D_p T^3)}$$

$$= \frac{2}{a + 2 s_b D_p} \tag{133}$$

Comparing Equation (133) to Equations (130) - (132), it is seen that the K functions given by the three analytic models are basically too simple to handle the true situation. Rosseland and Bosworth's function is a set constant, while Schotte's and Damkohler - Argo - Smith's functions are dependent only on emissivity. In the real case, it is expected that K

would be a function of temperature of radiation, void fraction of packing, particle shape, size, and transmissivity as well as of emissivity. Thus, any close agreement between the analytic estimates and true conductivities would actually be fortuitous. The only exact method of obtaining K functions and conductivities at this time is to experimentally measure the attenuation cross sections, a and s_b, and applying Equations (133) and (104), as was done in this study.

Effect of Temperature

All analytic expressions for radiant heat transfer predict that radiant conductivity would have a third-power temperature dependence. Equations (2b), (5), and (6) are typical examples. By Hamaker's formulation, k_{ir} would also be proportional to T^3 if s_b and a were temperature independent, as seen by Equation (104). However, the experimental data show that for most of the test packings, s_b and a were affected by the temperature of the radiation. This is evident from Figures 39-50, where the experimental values of s_b, a, and k_{ir} have been plotted against temperature for each test packing.

As mentioned previously, the effect of temperature was most pronounced for glass particles. As an example, the value of s_b changed from 977 to 129 and the value of a changed from 0.4 to 2.2 for GS-3 packing over a temperature range of 800°F to 2000°F. The variation of s_b and a were much less for the other opaque packings. Some typical values are:

	s_b (ft^{-1})		a (ft^{-1})	
	1600°F	2000°F	1600°F	2000°F
AS-3/16	496	449	2.7	2.8
AP-1/8	1190	847	1.1	1.5
AG-16	779	837	12.7	9.4
SS-1/8	450	343	13.1	20.5

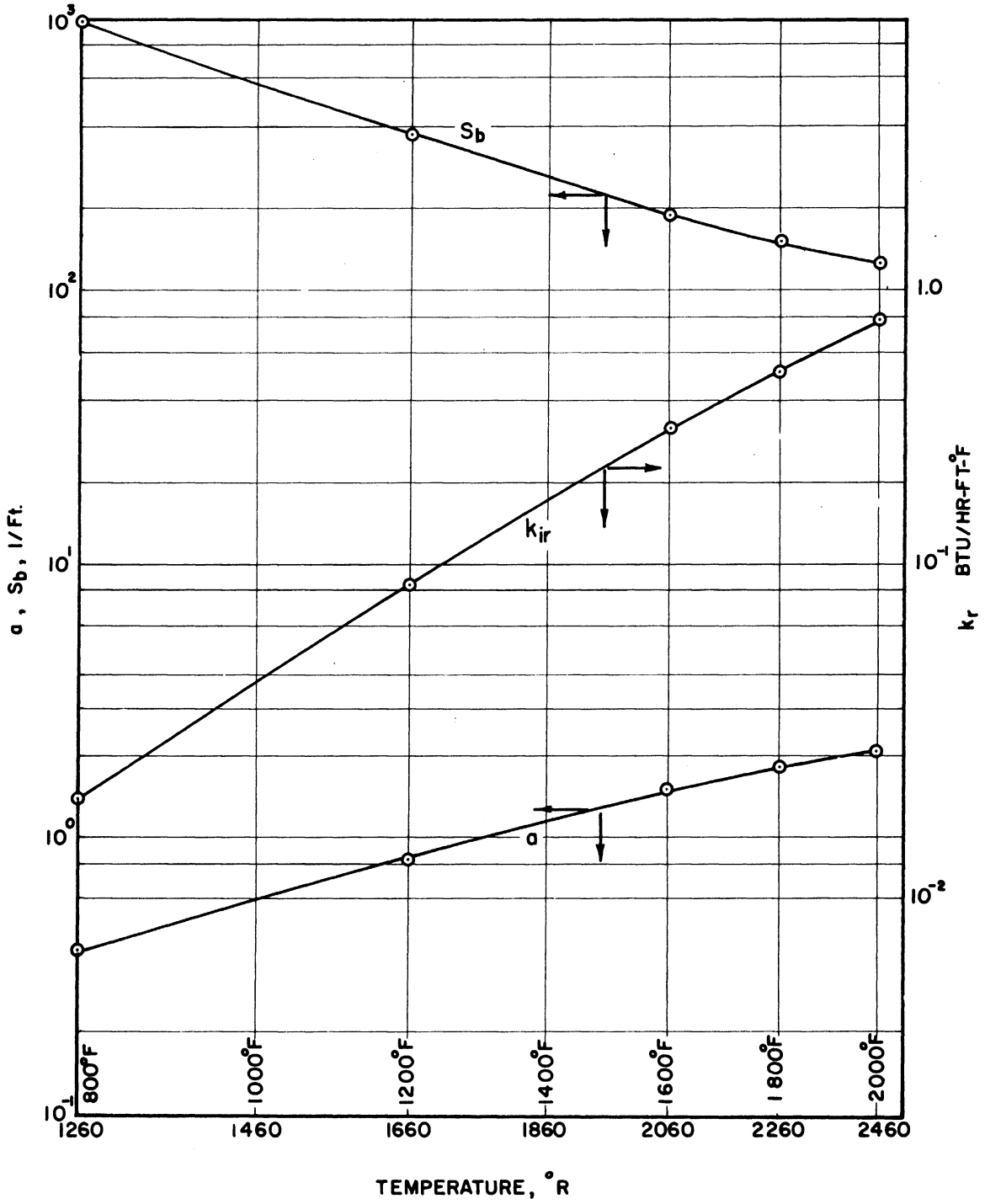

Figure 39. Temperature Effect for GS-3

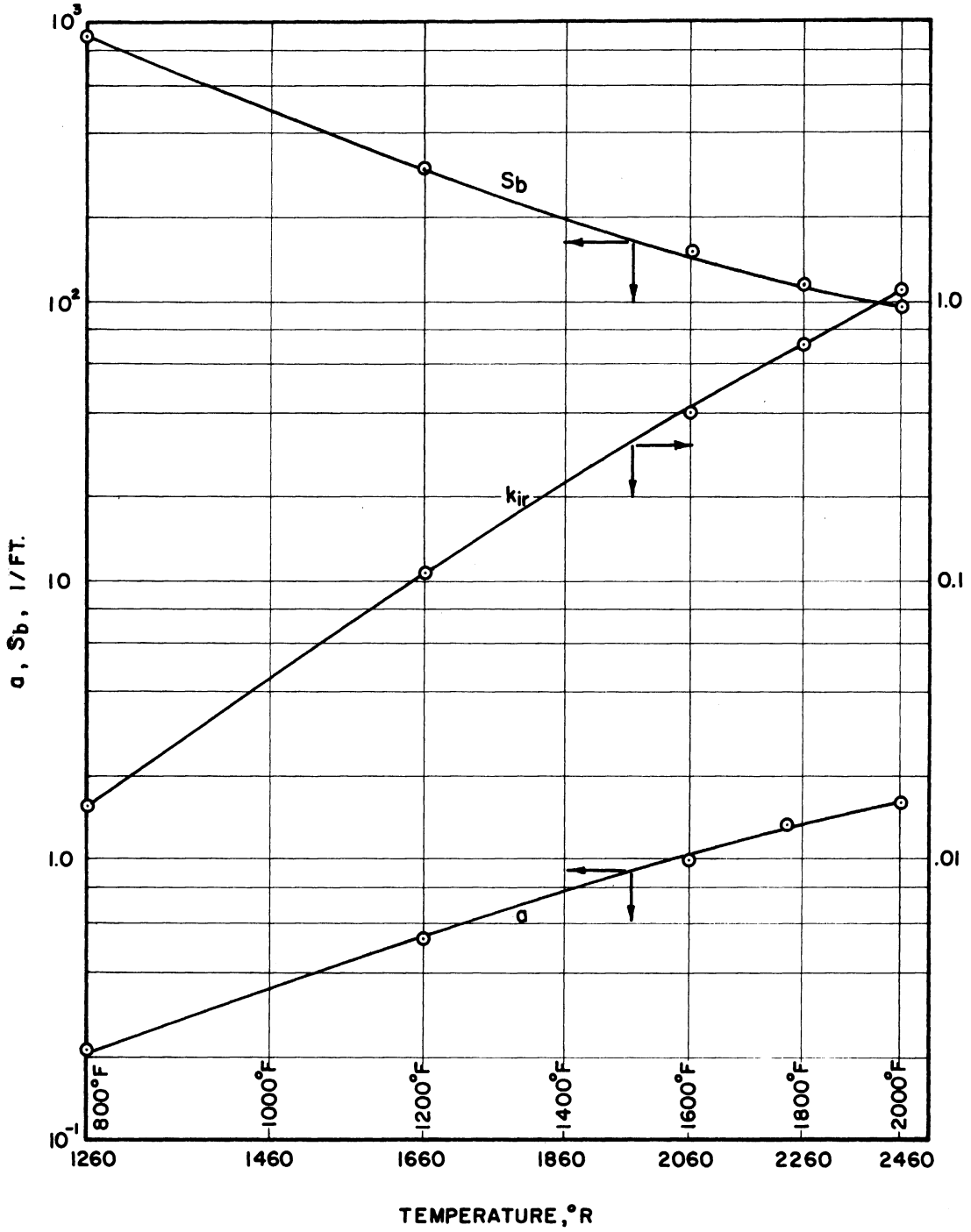

Figure 40. Temperature Effect for GS-4

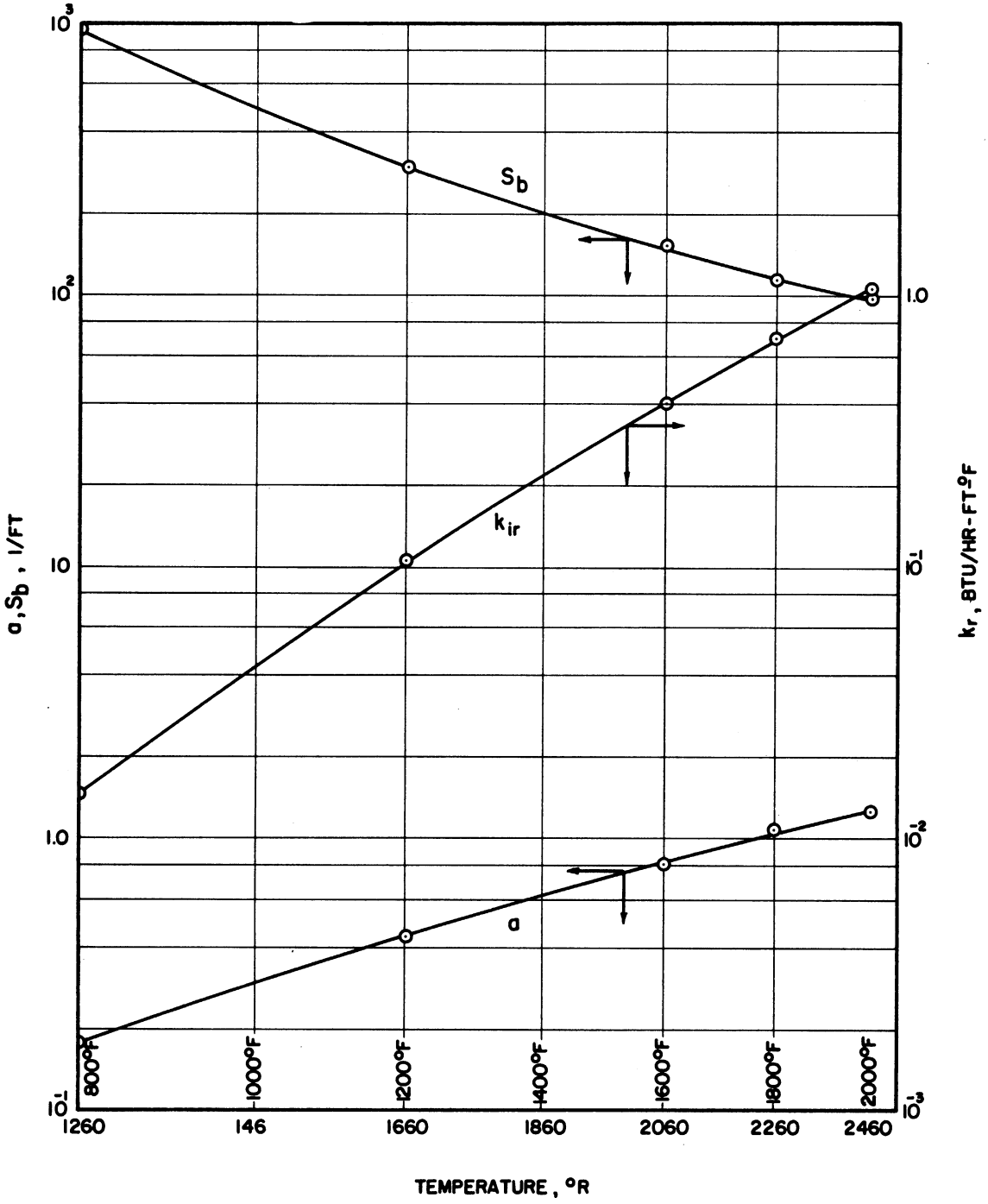

Figure 41. Temperature Effect for GS-5

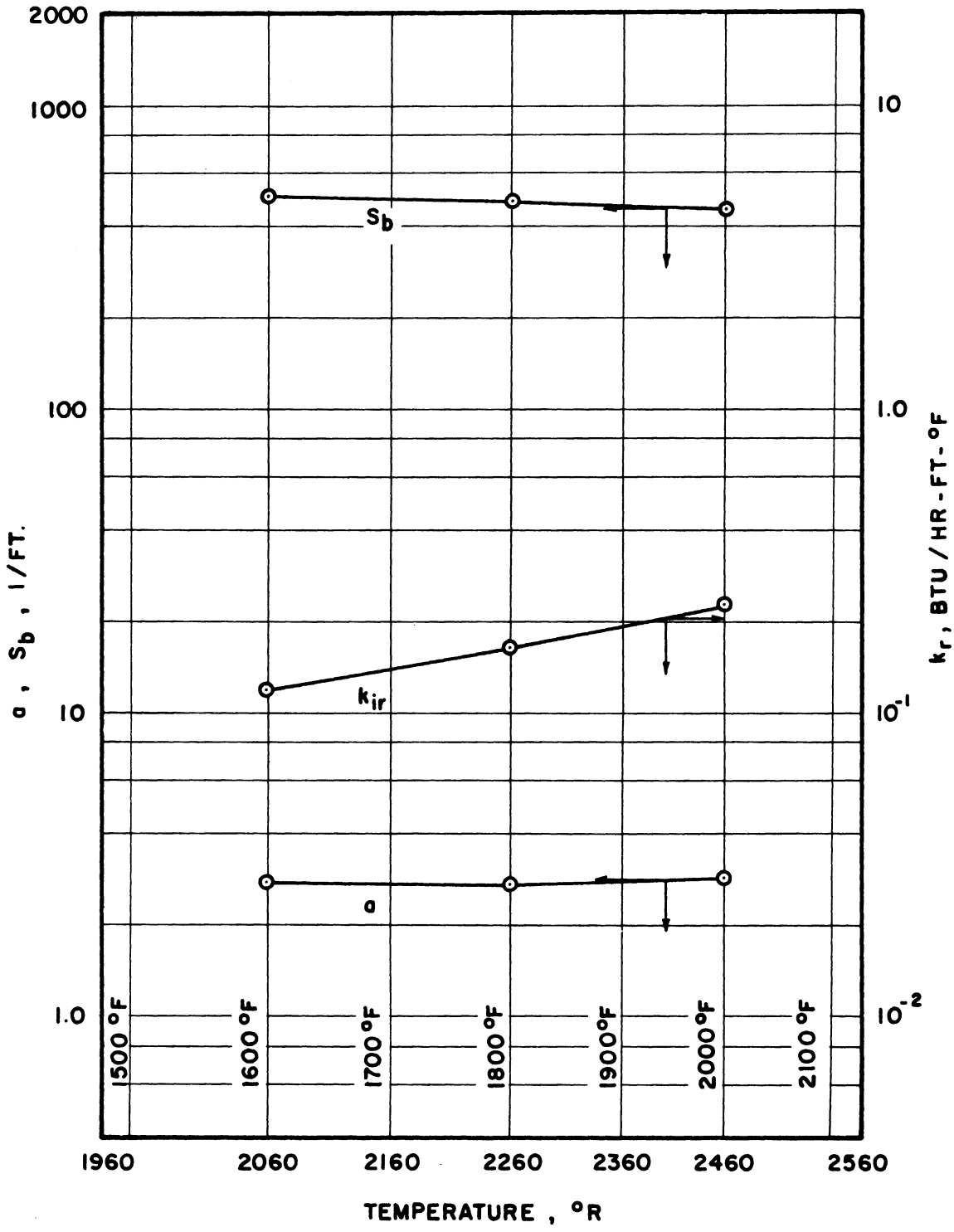

Figure 42. Temperature Effect for AS-3/16

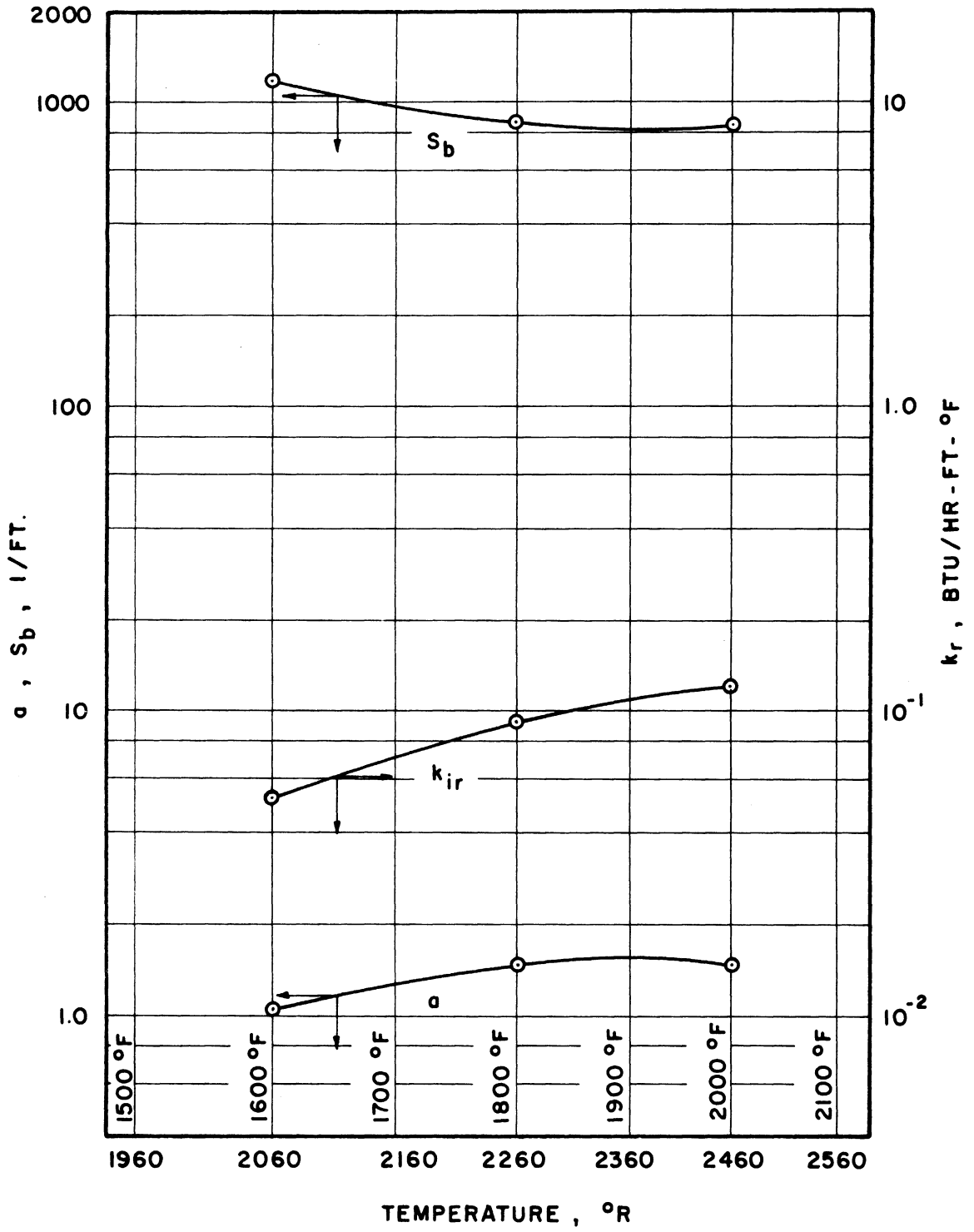

Figure 43. Temperature Effect for AP-1/8

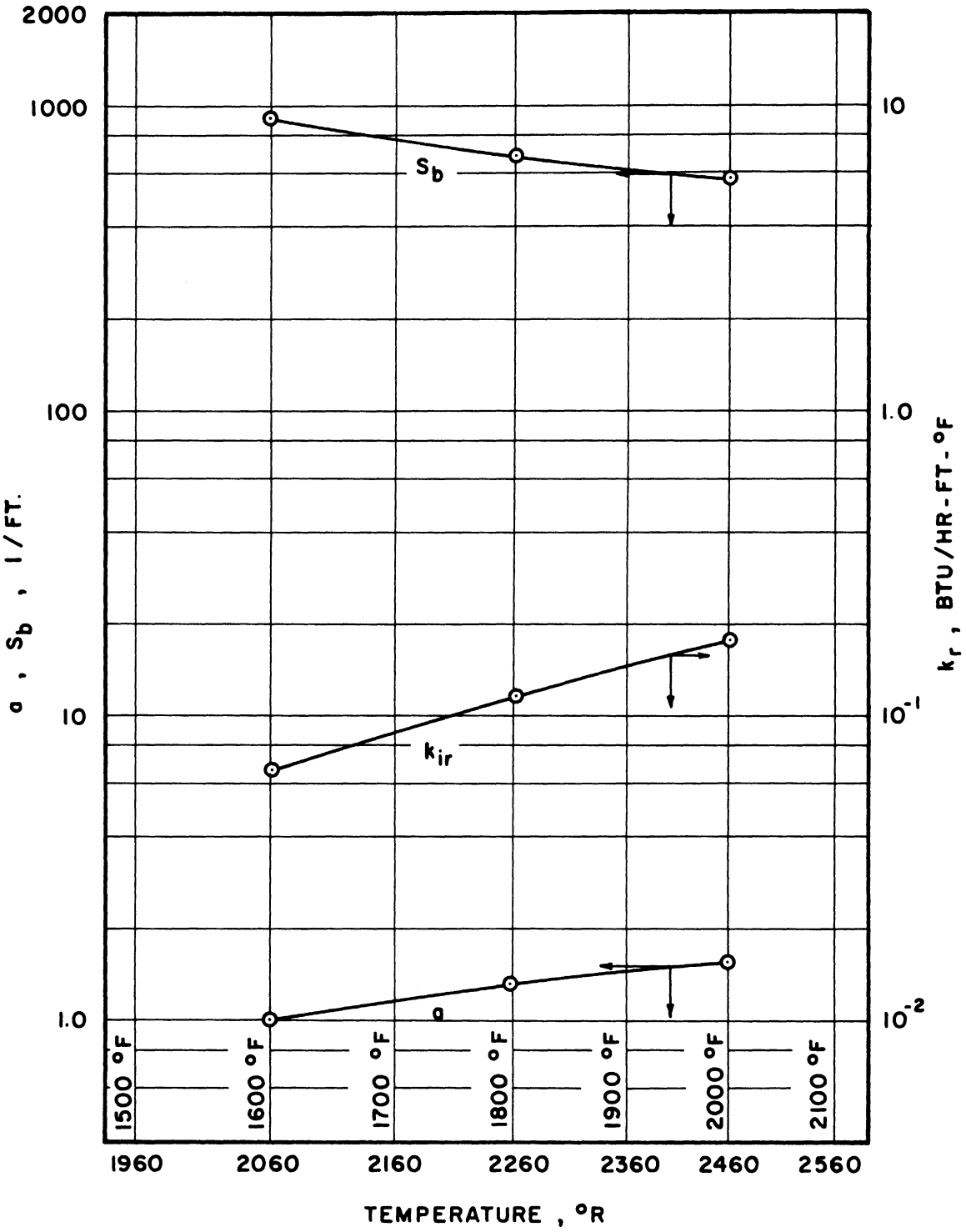

Figure 44. Temperature Effect for AP-5/32

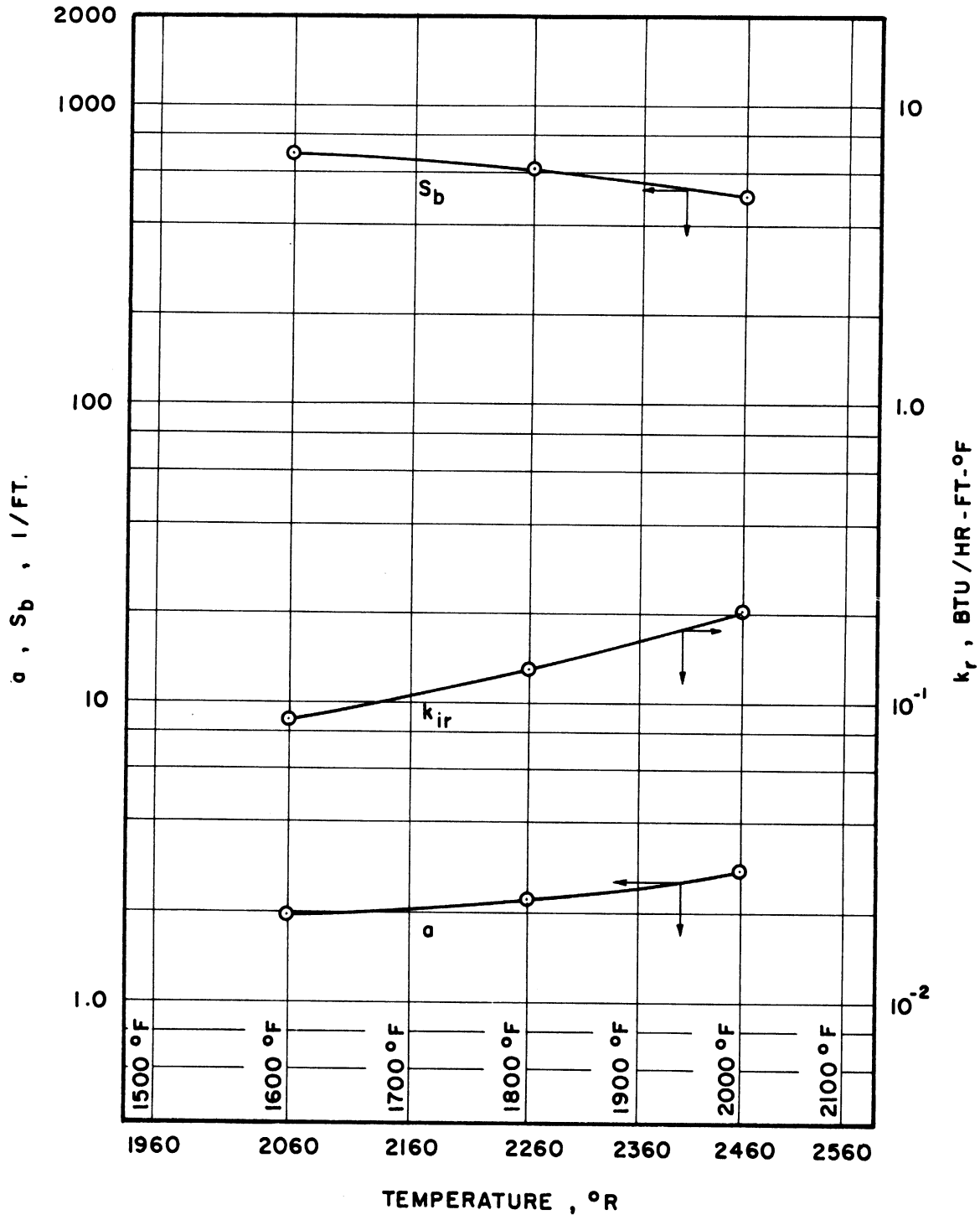

Figure 45. Temperature Effect for AP-3/16

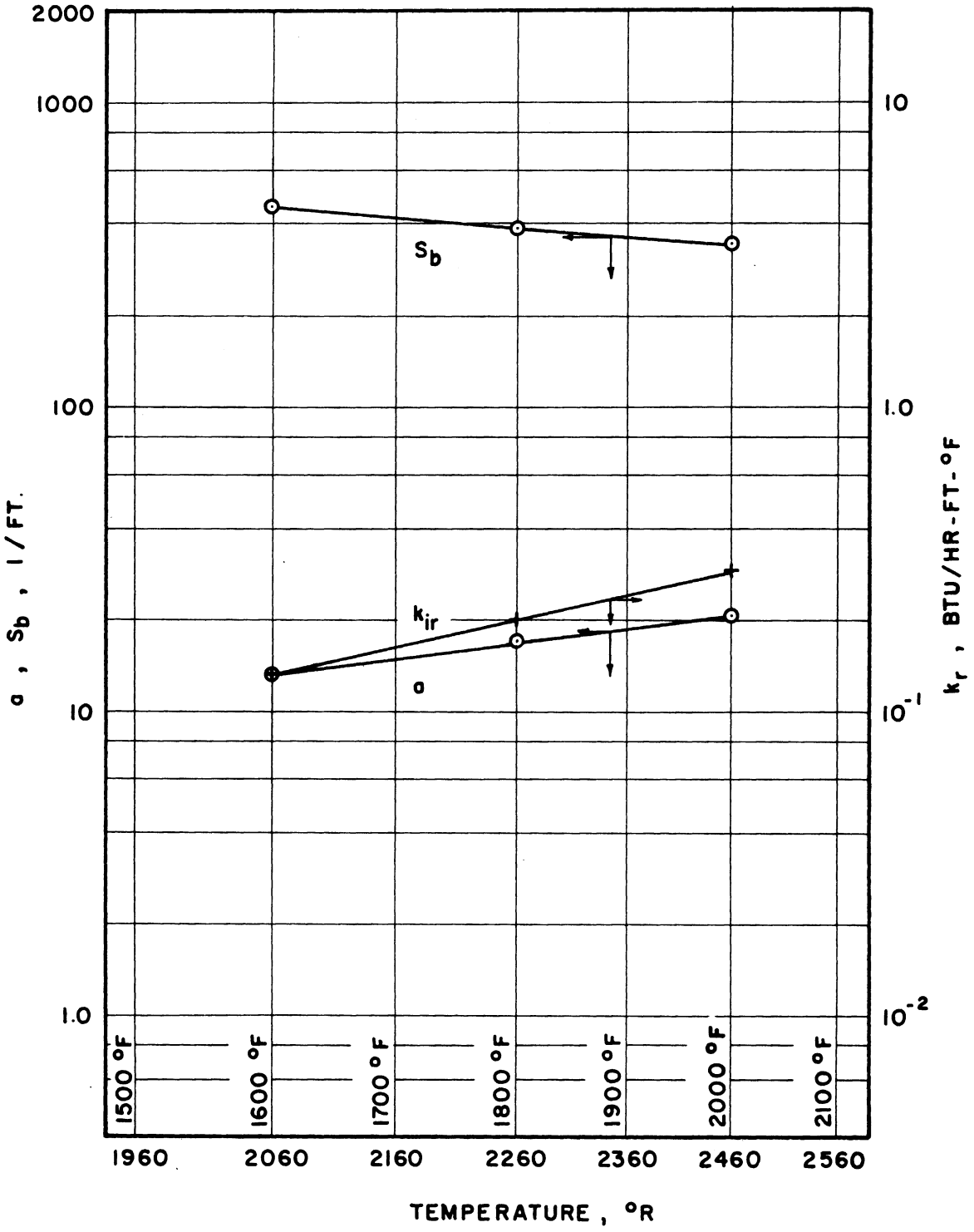

Figure 46. Temperature Effect for SS-1/8

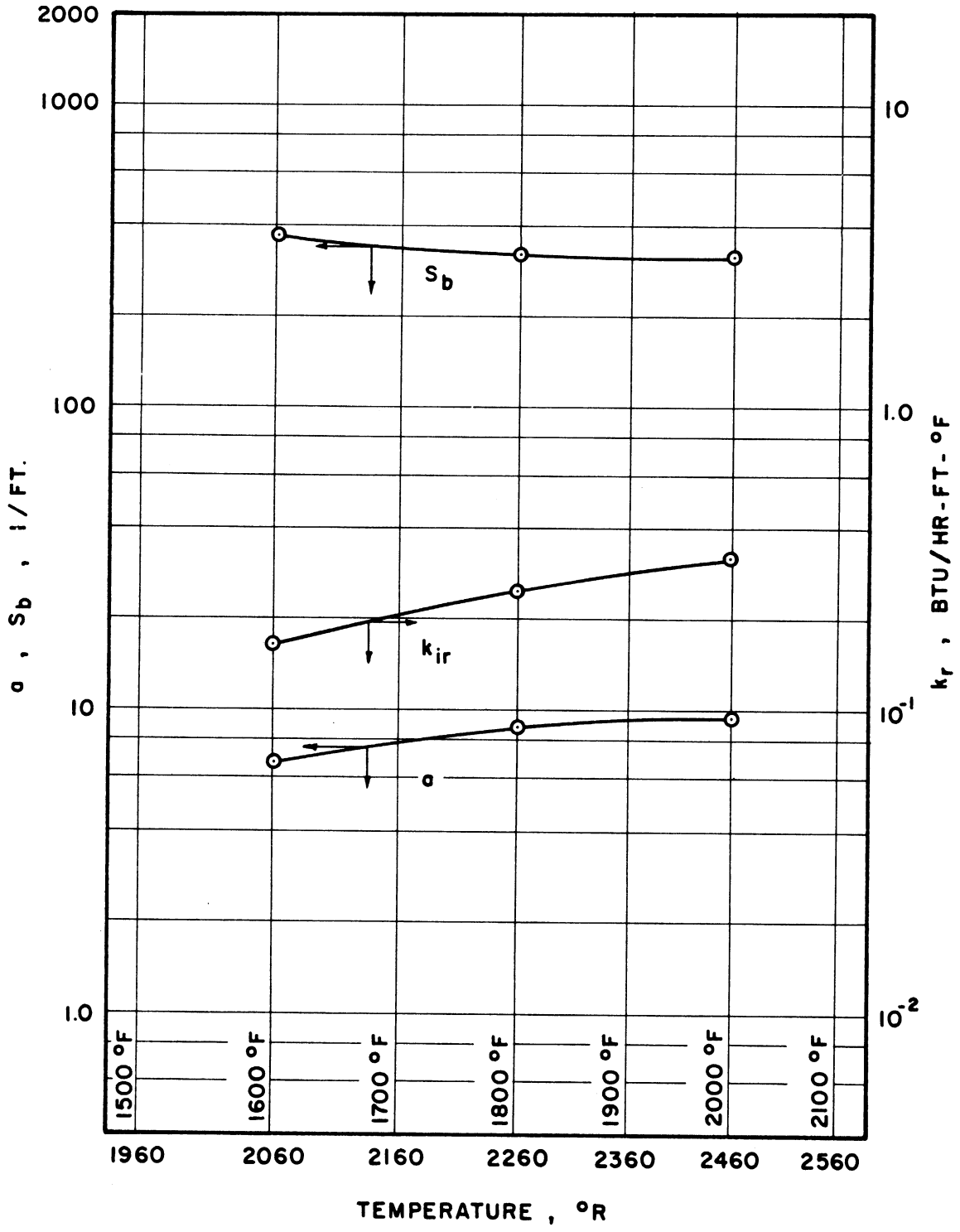

Figure 47. Temperature Effect for SS-3/16

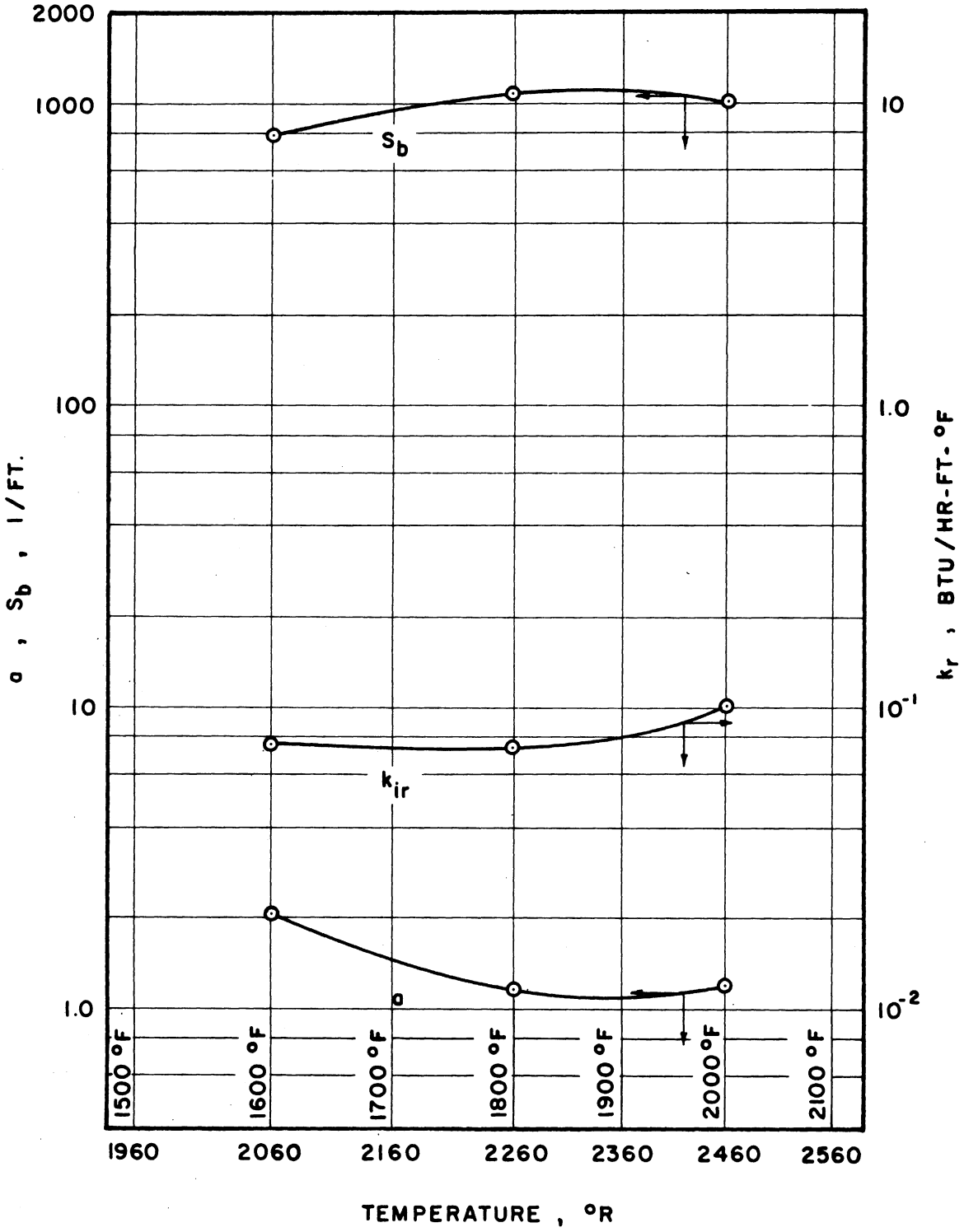

Figure 48. Temperature Effect for AG-4

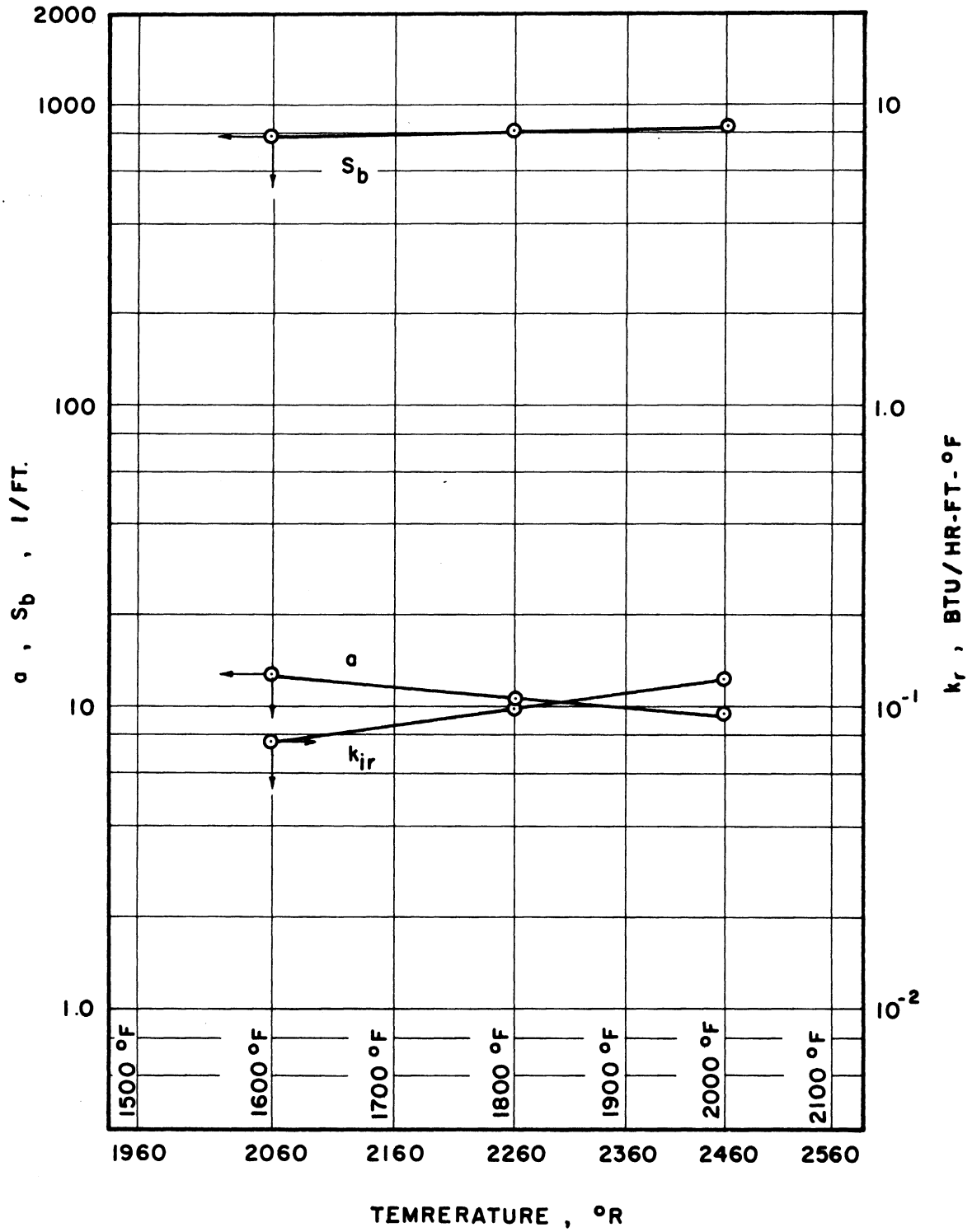

Figure 49. Temperature Effect for AG-16

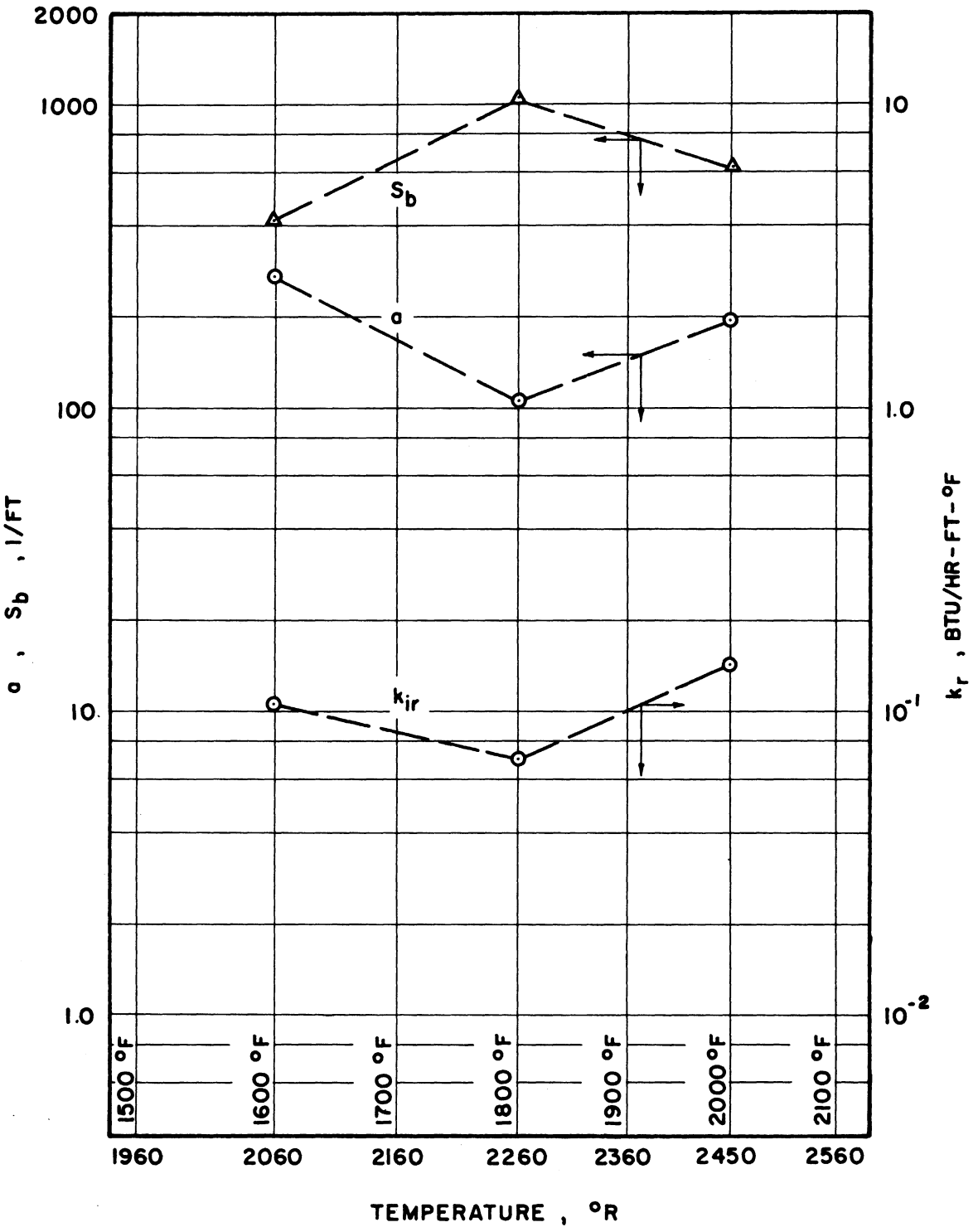

Figure 50. Temperature Effect for CG-16

It is evident that the attenuation cross section, s_b and a, may not be assumed to be temperature independent. Therefore the temperature dependence of k_{ir} may not be an exact third power function. This effect was also found in Larkin and Churchill's[20] work. Assuming a general power function,

$$k_{ir} \sim T^p \tag{134}$$

the value of p would be different from 3.0 for packings where s_b and a are temperature dependent. Some sample values have been determined, for the test packings, over a temperature range of 1600°F to 2000°F and are listed in Table V.

TABLE V

TEMPERATURE DEPENDENCE OF k_{ir}

Packing Particle	$k_{ir}\left(\frac{\text{Btu}}{\text{hr.ft.°F}}\right)$ 1600°F	2000°F	p
GS-3	0.314	0.785	5.2
GS-4	0.401	1.06	5.5
GS-5	0.401	1.05	5.5
AS-3/16	0.120	0.227	3.6
AP-1/8	0.050	0.120	4.9
AP-5/32	0.066	0.177	5.6
AP-3/16	0.088	0.205	4.8
AG-4	0.076	0.101	1.6
AG-16	0.076	0.121	2.6
CG-16	0.108	0.141	1.6
SS-1/8	0.131	0.289	4.5
SS-3/16	0.161	0.320	3.9

It is seen that the powers, p, are quite different from a constant value of 3. For the grain packings AG-16, AG-4, and CG-16, the values of p are less than 3. This is due to s_b increasing with temperature, opposing

the effect of the T^3 term in Equation (104). For all other packings, attenuation cross sections decrease with temperature, serving to magnify the temperature dependence of k_{ir}, as indicated by p values greater than 3.

Effect of Packing Properties

The data showed a number of qualitative trends in the effects of packing properties on radiant heat transfer. The most important single effect was that of particle transmissivity, as demonstrated by the large change in s_b and a for glass particles between opaque conditions (low temperatures) and transparent conditions (high temperatures). This effect has been described in previous sections and will not be discussed further here.

Probably the second most important effect was that due to particle shape. This effect is hard to define since there are no quantitative means of characterizing particle shape. It is necessary to use some secondary property which is related to particle shape and which can be measured. One possibility is void fraction of the packed media, a property that is dependent on particle shape. To test this possibility, the data for AS-3/16, AP-3/16, and AG-4 were compared. These three test packings are of the same material and particle size, differing only in particle shape. Experimental values of s_b and a for these three packings are plotted against void fractions in Figures 51 and 52. It is seen that the results are irregular, with no evident trend. This is taken to mean that there is some other factor connected with particle shape which overshadows the effect of void fraction. It would be of interest to isolate and define this factor by more detailed investigations in the future.

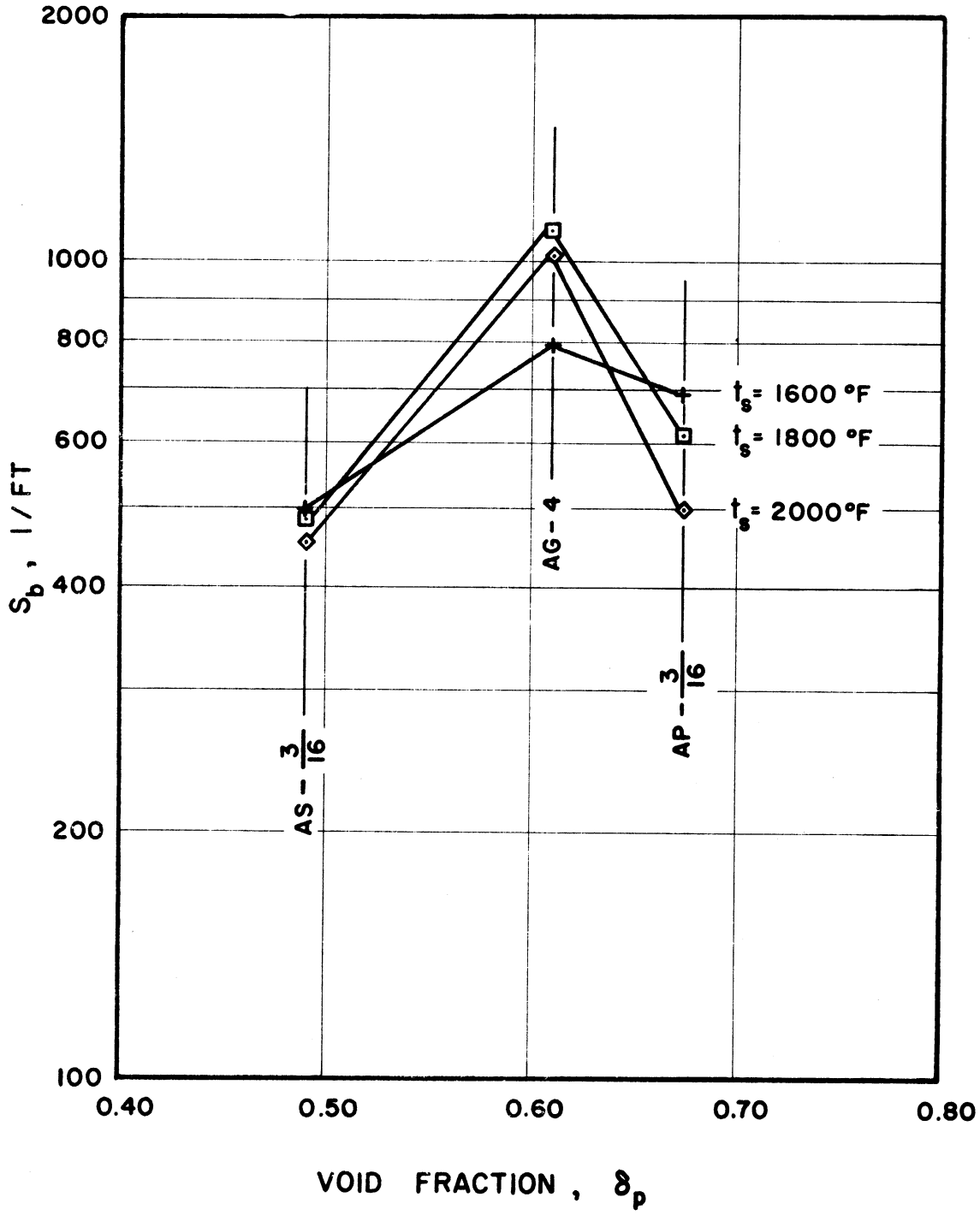

Figure 51. Effect of Void Fraction on Scattering Cross Section

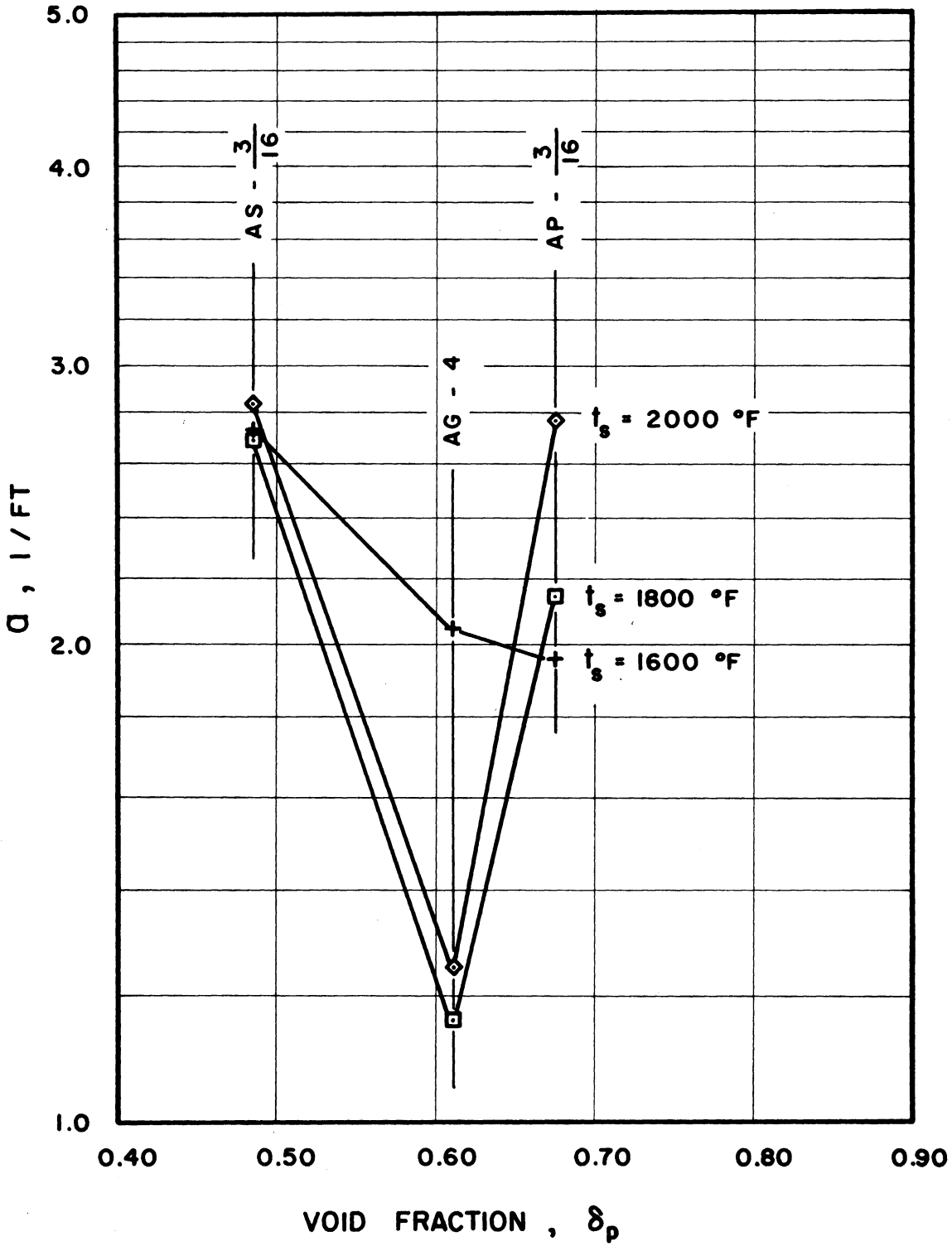

Figure 52. Effect of Void Fraction on Absorption Cross Section

Particle emissivity was found to have a noticeable effect on attenuation cross sections. Among the packings tested, there were two pairs which could be used to demonstrate this emissivity effect: (a) AS-3/16 and SS-3/16, (b) AG-16 and CG-16. The two packings in each pair are of the same particle shape and size, differing only in emissivities. Values of the cross sections for these four packings, at three temperatures, have been plotted against emissivity on Figure 53. The lines connect particles of each pair. General trends are seen to be: (a) s_b decreases with increasing emissivity, (b) a increases with increasing emissivity. This is consistent with physical expectations since a black, high emissivity, surface has lower reflectivity and higher absorptivity.

One last noticeable effect was that of particle size. Figures 54 and 55 show the variation of s_b and a, respectively, with equivalent particle diameter. The lines connect data points for particles of the same material and shape, differing only in size. It should be noted that particle diameters were known only nominally so that these plots can only be interpreted qualitatively. It is seen that the trend for s_b is to decrease with increasing particle size, as may be expected since the number of particles per unit volume decreases for larger particles. The trend for absorption cross section, a, is not as clear -- decreasing for GS and SS packings but increasing for AP packings. The total effect on radiant conductivity, k_{ir}, is shown by Figures 56 and 57. A quite definite trend is evident. Conductivities are seen to increase with increasing particle size for all three types of packings and for all the temperatures tested. The effect also seems to be more pronounced at larger particle sizes and at higher temperatures.

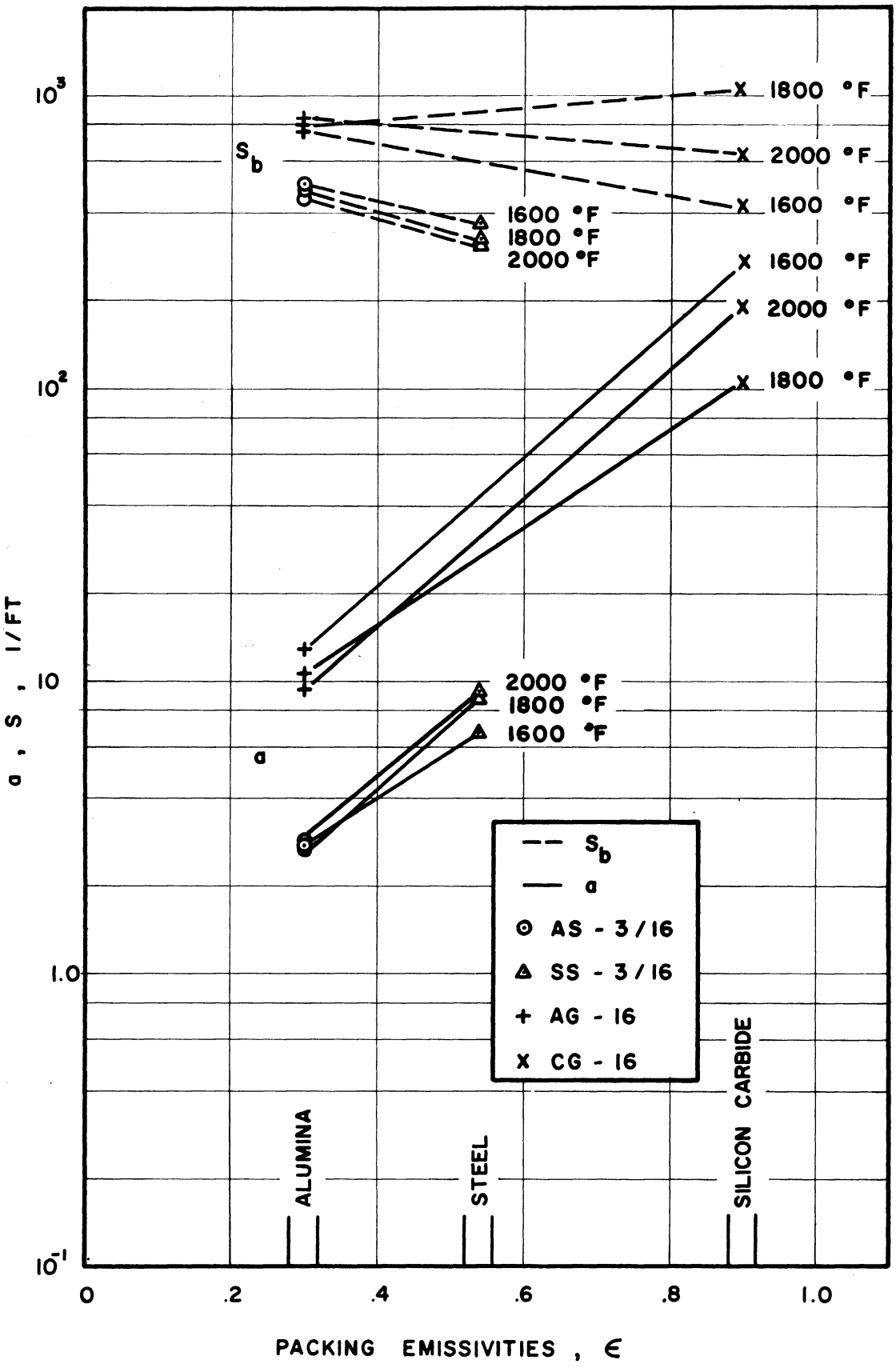

Figure 53. Effect of Emissivity

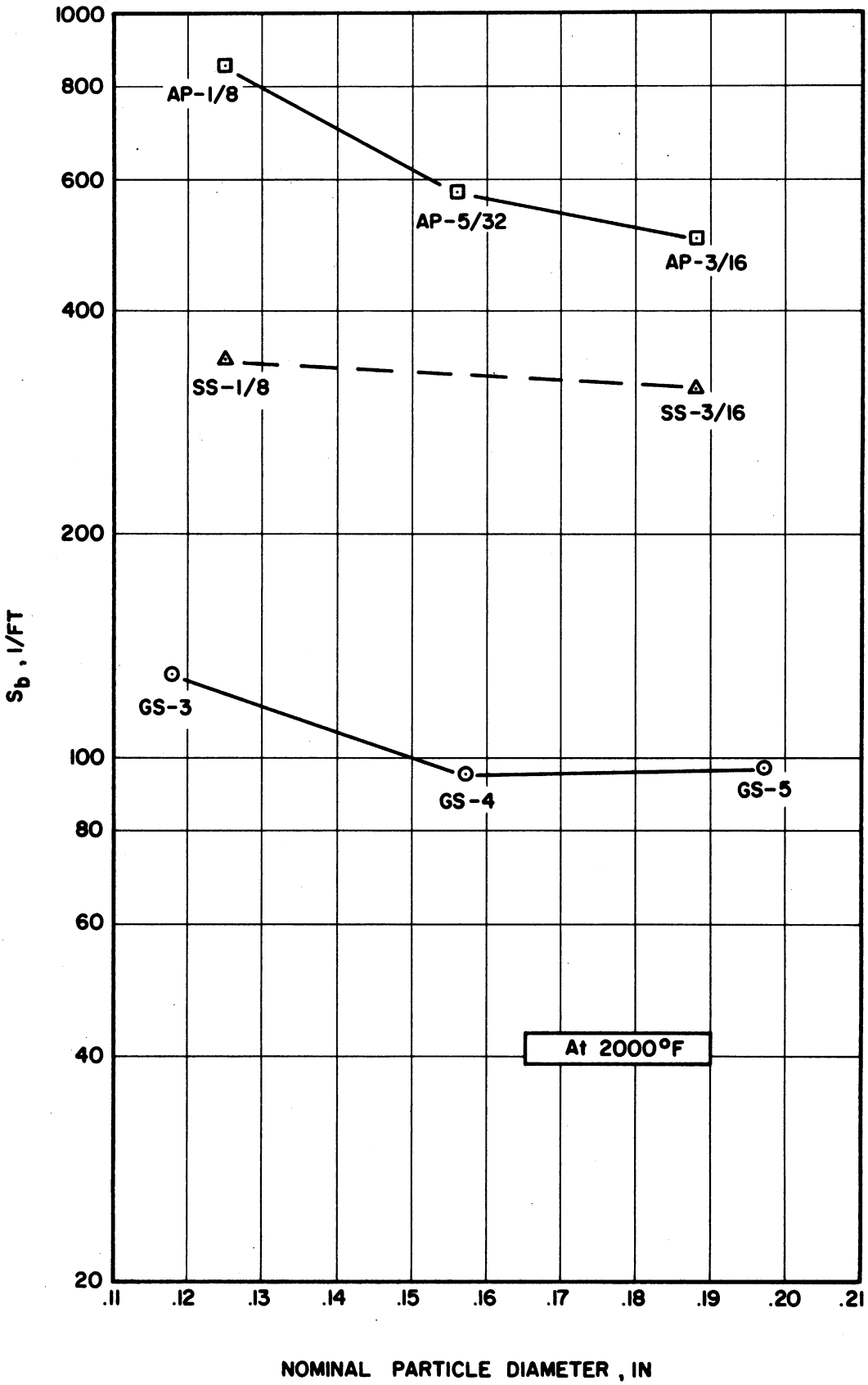

Figure 54. Effect of Particle Size on Scattering Cross Section

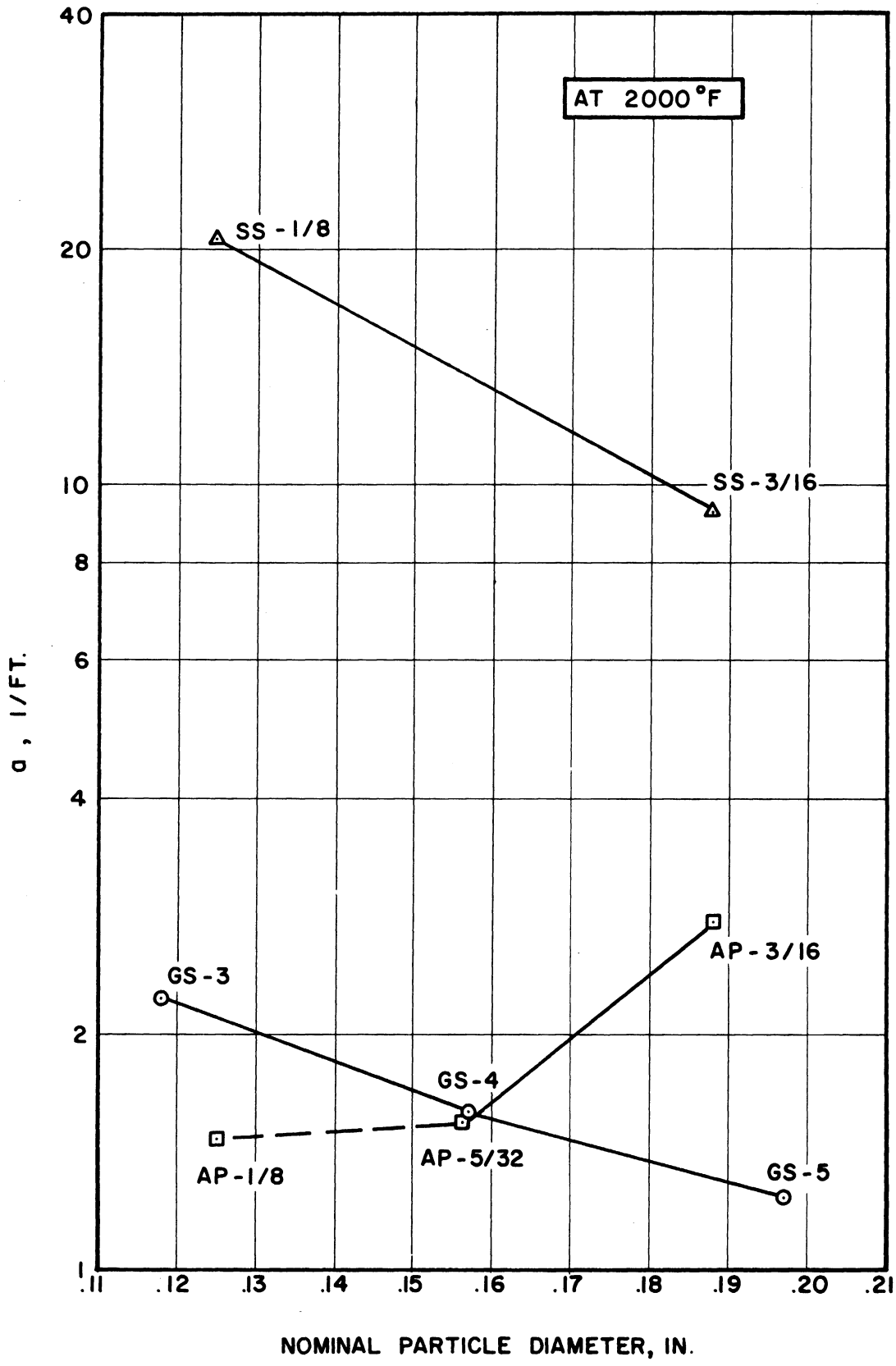

Figure 55. Effect of Particle Size on Absorption Cross Section

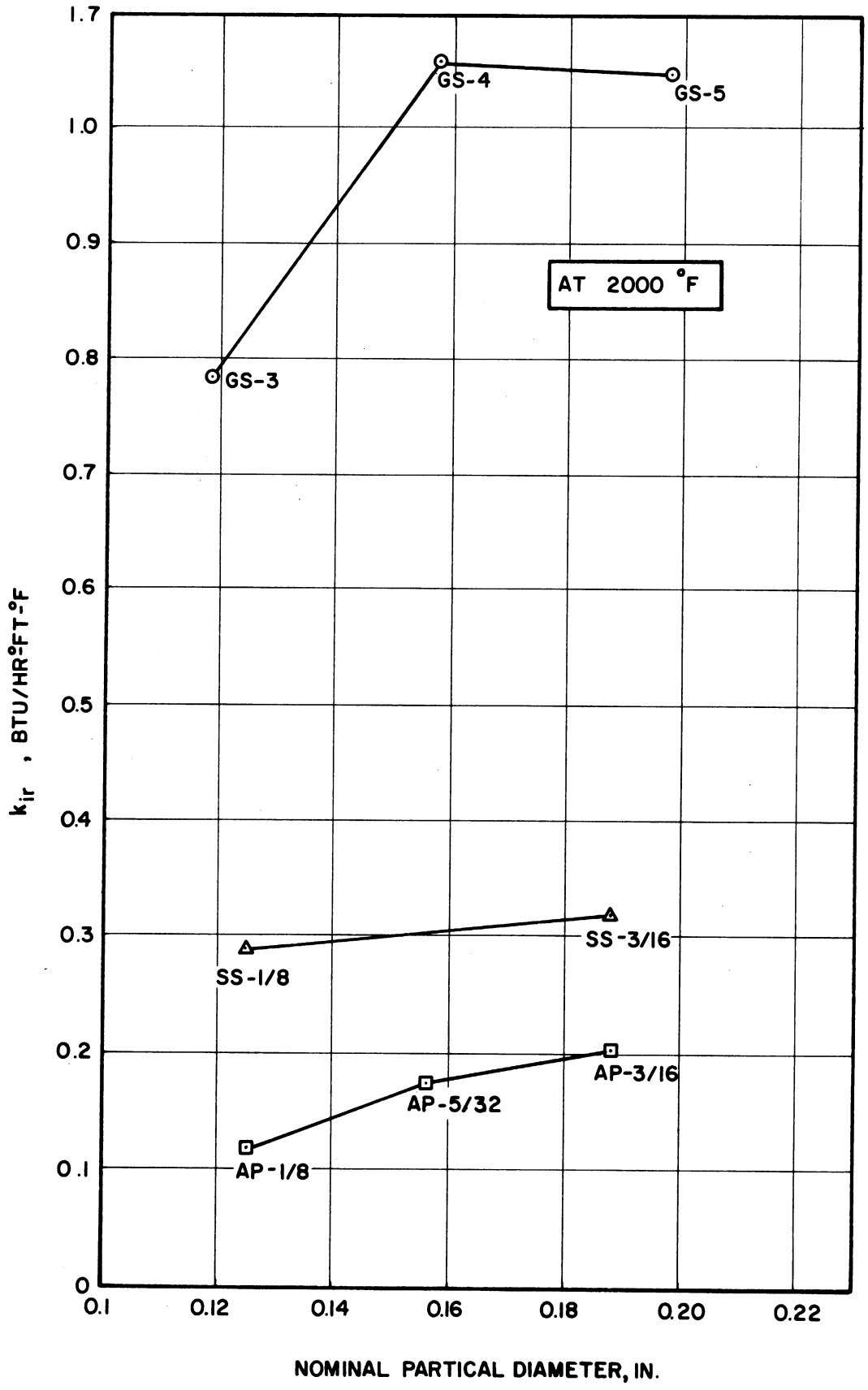

Figure 56. Effect of Particle Size on k_{ir} Parameters of Material

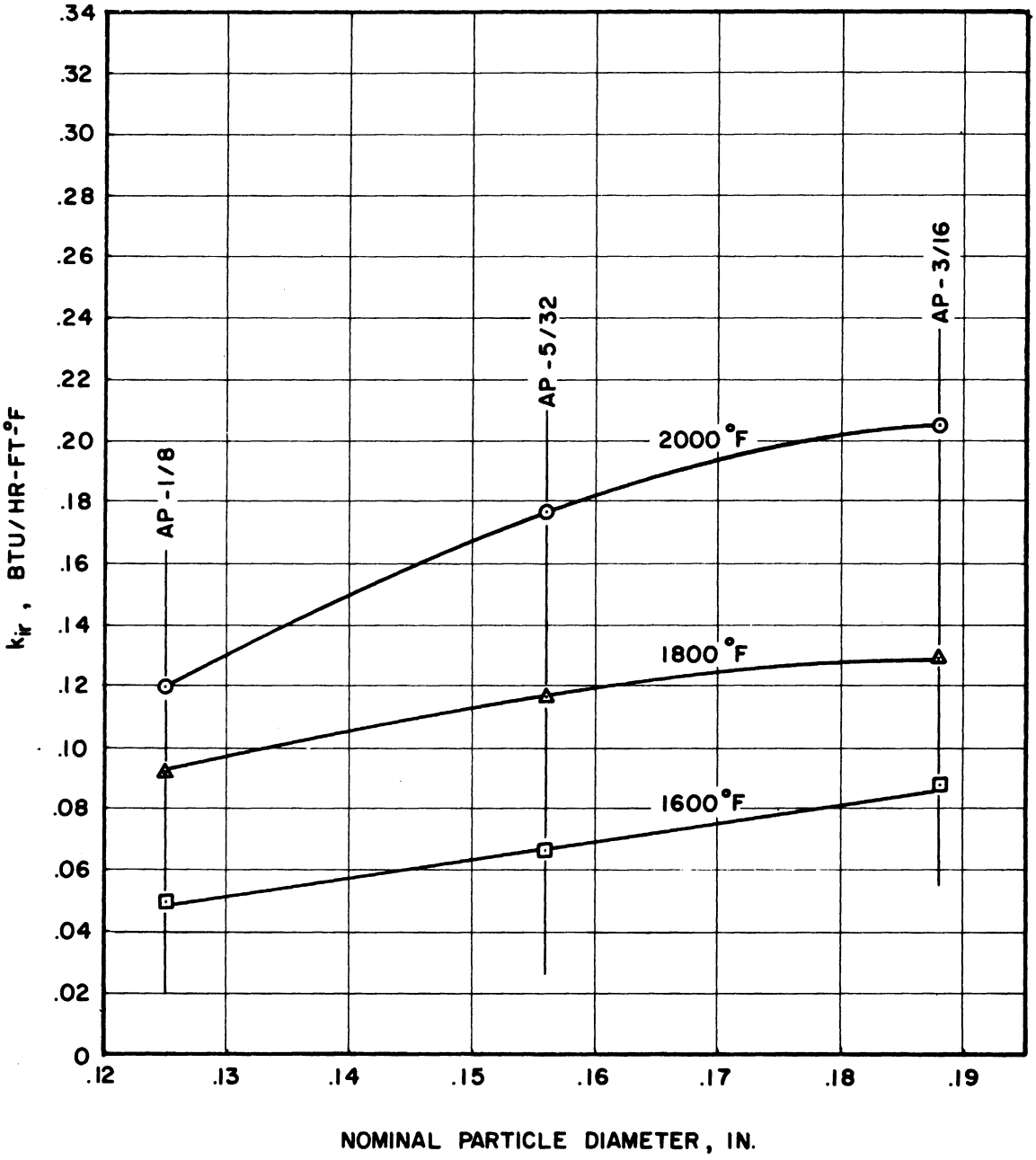

Figure 57. Effect of Particle Size on k_{ir}, Parameters of Temperature

Correlation of Attenuation Parameters

As mentioned previously, it ultimately would be desirable to have quantitative correlations for attenuation cross sections, s_b and a, in terms of the physical properties of the materials and the geometrical properties of the systems. With such correlations, it would be possible to predict s_b and a, and so to estimate radiant conductivity for any packing of any material. The pertinent physical properties are not known in sufficient detail to obtain quantitative correlation from the data of this study. Measurement of these properties would be a task of the same magnitude as the thesis. A number of correlations were attempted between the measured cross sections and the available literature values of the microscopic properties, i.e., emissivity and transmissivity. However, due to the high degree of uncertainty and incompleteness in the literature values and also to the complexity of interacting effects of geometry (roughness, shape, size, etc.) and these microscopic properties, no simple correlations were evident.

Two graphical correlations, Figures 58 and 59, are presented to enable interpolation and extrapolation of the experimental data for prediction of attenuation cross sections for other packings. Such predictions are obviously subject to considerable uncertainty but at least indicate first order effects.

The attenuation cross sections are correlated in the form of dimensionless parameters,

$$C_a = \frac{a D_p}{1 - \delta_p} \tag{135}$$

$$C_s = \frac{s_b D_p}{1 - \delta_p} \tag{136}$$

since it was expected that s_b and a would be both directly proportional to the total projected area of particles per unit volume. Thus, to a first order estimate,

$$C_a \sim a \times \frac{4}{\pi D_p^2} \times \frac{\pi D_p^3}{6(1-\delta_p)} \quad , \quad \text{independent of } D_p \text{ and } \delta_p \qquad (137)$$

$$C_s \sim s_b \times \frac{4}{\pi D_p^2} \times \frac{\pi D_p^3}{6(1-\delta_p)} \quad , \quad \text{independent of } D_p \text{ and } \delta_p \qquad (138)$$

In general, the attenuation cross sections are functions of particle size, shape, emissivity, transmissivity, and of radiation wave length. The effects of the last three factors are in turn functions of temperature of radiation, particle size, shape, and material. These secondary functional dependences are quite complex in their interactions so that the dependence on D_p and δ_p can not be entirely eliminated by the use of the parameters C_a and C_s.

Thus,

$$C_a = f_1(\text{shape}, D_p, \delta_p, \varepsilon, \text{transmissivity}, \lambda.) \text{ for all materials} \qquad (139)$$

or

$$C_a = f_2(\text{shape}, D_p, \delta_p, T) \text{ for a specific material,} \qquad (140)$$

and

$$C_s = g_1(\text{shape}, D_p, \delta_p, \varepsilon, \text{transmissivity}, \lambda) \text{ for all materials} \qquad (141)$$

or

$$C_s = g_2(\text{shape}, D_p, \delta_p, T) \text{ for a specific material.} \qquad (142)$$

Correlations with literature values of emissivity and transmissivity were attempted for the type of f_1 and g_1 functions, for all materials. A general trend of third power dependence on emissivity was evident. However, the degree of complexity necessary for the f_1 and g_1 correlations were

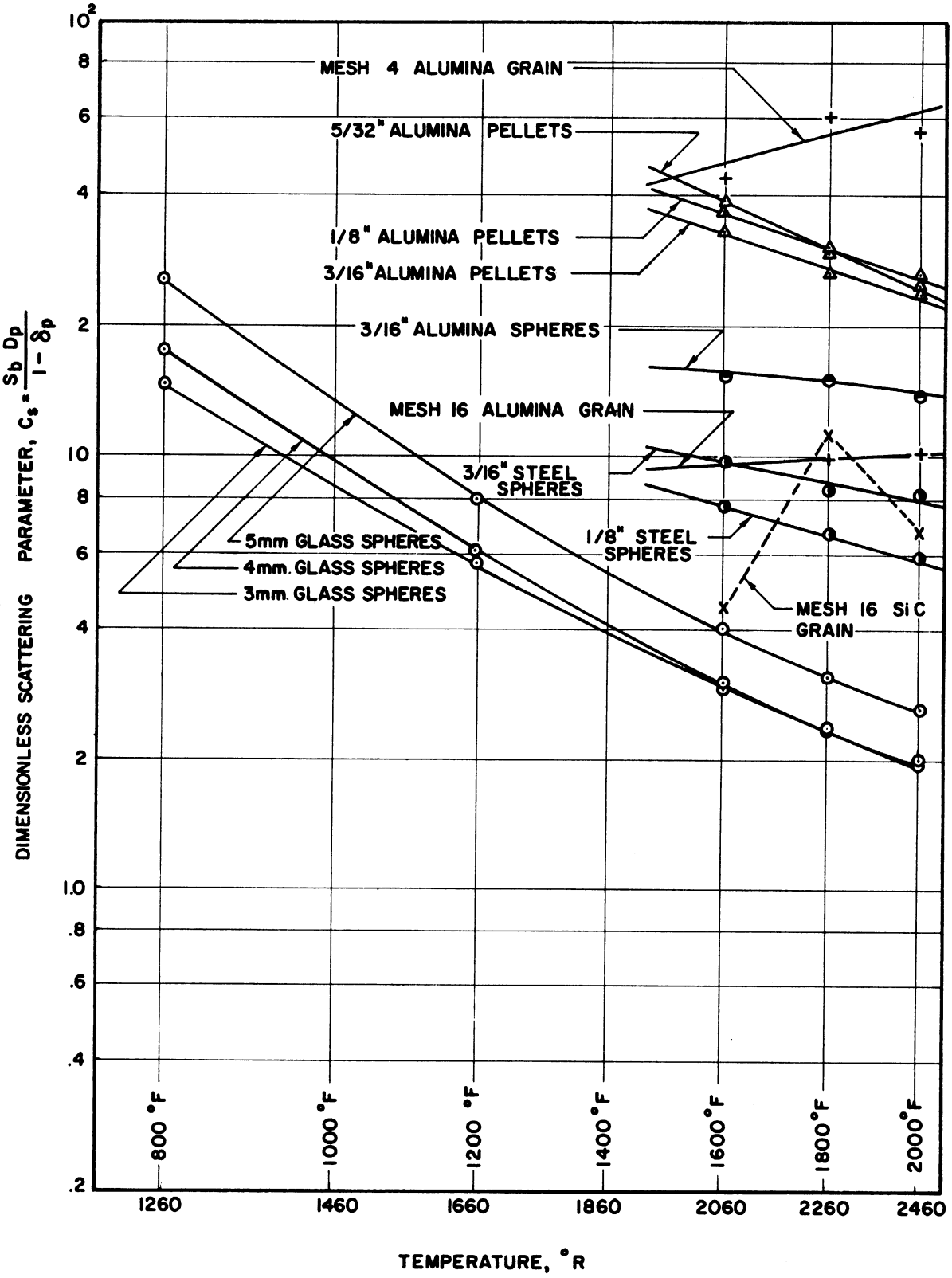

Figure 58. Correlation of Scattering Parameter

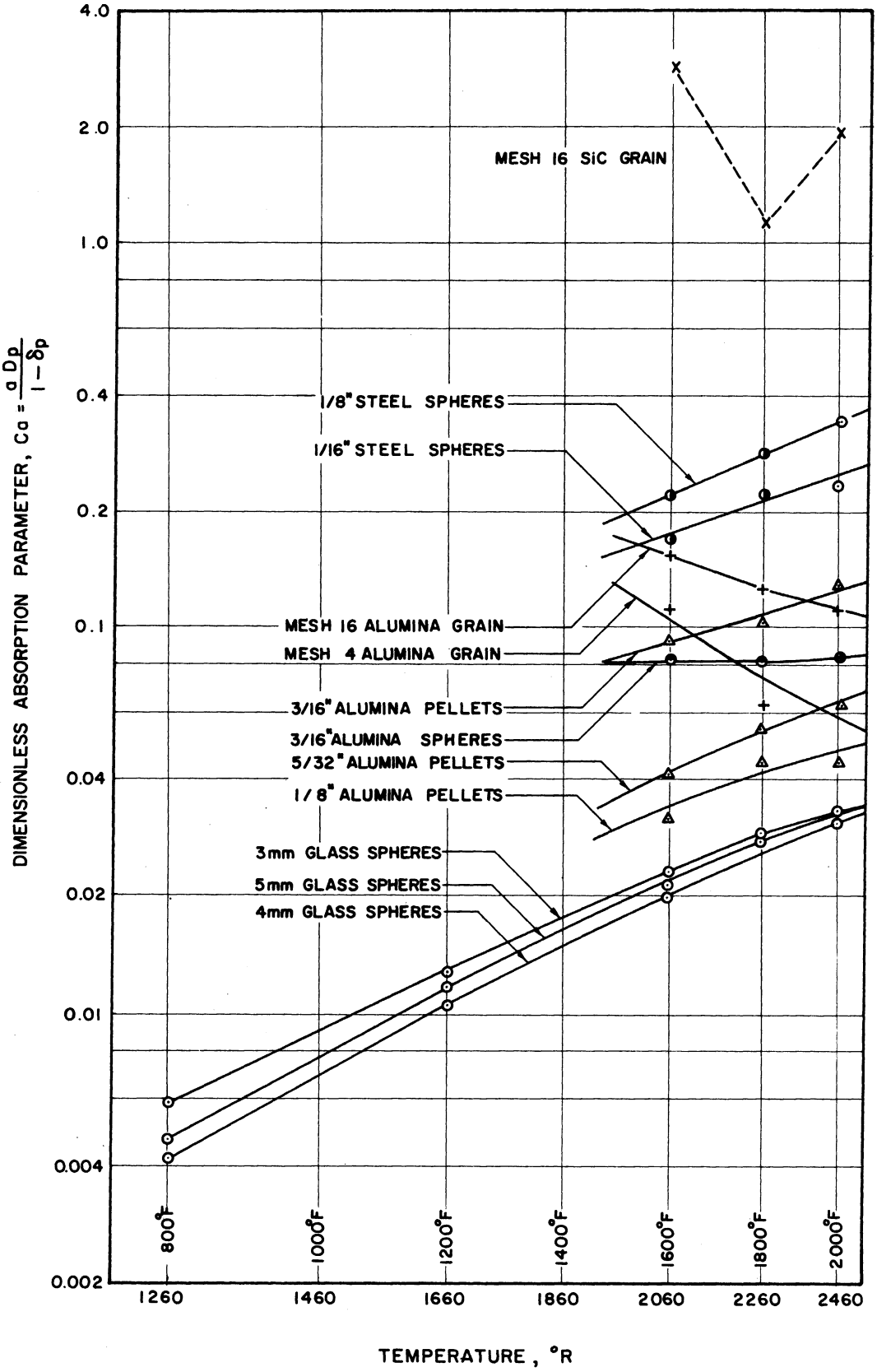

Figure 59. Correlation of Absorption Parameter

higher than could be justified, in view of the uncertainties introduced by using literature values of physical properties. The final graphical correlations of the f_2 and g_2 type were found to be more suitable.

The correlation plots of C_s and C_a versus T, Figures 58 and 59, give parametric curves for packings of different shape, material, size, and void fraction. To use the correlation plots, it is necessary to interpolate between each of the four factors. Values of these factors for the curves are given in Table XII of the Appendix.

It should be noted that the data for silicon carbide grain (CG-16) have a relatively high degree of uncertainity. The maximum and minimum exhibited by C_s and C_a, respectively, may be due to data scatter and may not be actual phenomena.

As an example of the use of these correlations, the radiant conductivity, k_{ir}, for packings of 5/32 inch steel spheres at 1700°F was estimated to be 0.184 Btu/hr.ft.°F. Details of this example are given in the Appendix.

Experimental Precision

The absolute accuracy of the experimental data could not be determined due to a lack of other data for comparison. However, it is known that the values obtained were of the correct order of magnitudes, as indicated by the comparisons with analytic estimates and by the good agreement of k_{ir}/k_c ratio with Hill and Wilhelm's[15] values.

Internal experimental precision was judged to be quite good, relative to the usual precisions reported for experimental work in this field. As examples of usual precisions, the maximum scatter of Campbell

and Huntington's[5] data was approximately ± 50%, Yagi and Kunii's[40] was ± 13%, and Hill and Wilhelm's[15] was ± 20%. A common cause of this high scatter is that packed bed properties are often quite sensitive to the particle arrangement, so that repacking a bed would result in a substantial change in the data obtained. The experimental method of this study has the advantage of allowing easy repacking. It was thus possible to take measurements over a number of packings at each bulk height, resulting in an average measurement of much greater precision.

There are several things which may be taken as indications of the degree of precision obtained. First, the standard deviations in Table XI provide a measure of the variations in transmission measurements within each run. It is evident that the degree of precision obtained was dependent on the type of packing. Best precision was obtained with glass packings, whose standard deviations were of the order 0.5% to 5%. Standard deviations for most of the test particles were around 2% to 10%.

An indication of run-to-run precision may be obtained by examining Figures 39-50. In these figures, each point on the k_{ir} curve represents a separate run. Therefore, the scatter of these points from the smoothed curve would be a measure of the overall precision in the experimental values of k_{ir}. The worst case was that of CG-16, which shows a scatter of approximately ± 20%. The second worst case was that of AG-4 which shows a scatter of ± 10%. All the other cases show surprisingly good precision, with scattering in the order of only 1 or 2 per cent.

A final indication of experimental precision may be obtained by comparing Runs 10 to 13 and Runs 17 to 40. Each pair of runs were

made for one type of packing at one source temperature, but each run was a separate measurement, with the equipment being shut down and reassembled between runs. Therefore, Runs 13 and 40 may be regarded as reproducibility checks of Runs 10 and 17, respectively. The variations in the measured k_{ir} are seen to be only 1.1% between runs 10 and 13, and 1.2% between runs 40 and 17. This degree of reproducibility was considered to be quite sufficient.

PART IV

SUMMARY AND CONCLUSIONS

SUMMARY AND CONCLUSIONS

This study was undertaken to investigate radiant heat transfer in beds of packed particles. The analysis and experimental method were formulated for the one-dimensional steady-state case, but the experimentally measured parameters are applicable to general problems of radiant transfer in packed media of any geometry.

Hamaker's two-flux model[13] was taken as the basis for a defining set of nonlinear differential equations, Equations (40) to (42). Transport properties of the packed media were specified in terms of an absorption cross section, a, and back scattering cross section, s_b. The assumptions inherent in this method of treatment were derived by integration of the general vectorial transport equation of monochromatic radiation. A dimensional analysis was made on the differential equations and boundary conditions to determine the minimum number of variables and parametric groups necessary to specify the one dimensional system. Various approximate solutions to the system of nonlinear differential equations were also examined, completed where necessary, and catagorized in terms of the following regions of applicability:

a) cases of linear temperature distribution,

b) cases of negligible absorption,

c) cases of small temperature differences, and

d) cases of no re-radiation.

The attenuation cross sections, s_b and a, were experimentally measured for the twelve types of packings listed in Table I. The experimental method was based on transmission measurements of modulated black-body radiation. Values of s_b and a were obtained from the transmission measurements by regression on Equation (115), using an IBM 704 digital computer for the necessary iterative calculation.

An equivalent radiant conductivity, k_{ir}, was defined in terms of the attenuation cross sections, s_b and a, and was calculated for each of the test packings at every experimental temperature. This radiant conductivity was then compared to conduction conductivity, k_c, for each test packing in order to determine the relative importance of radiation and conduction as heat transfer mechanisms. Values of k_c were estimated by means of Schumann and Voss' correlation[34] with Wilhelm et al.'s modification[38].

The experimentally obtained radiant conductivities, k_{ir}, were also used to check a number of analytic estimates. Radiant conductivities estimated by equations of Damköhler-Argo & Smith[1], Schotte[33], and Rosseland - Bosworth[3] were graphically compared to k_{ir} for packings of glass spheres, steel spheres, and aluminum oxide pellets.

The effects of (a) temperature of radiation, (b) void fraction of packing, (c) size of particles, and (d) emissivity of particle surface, on s_b, a, and k_{ir}, were graphically indicated. Though a number of qualitative trends were evident, it was not possible to obtain quantitative correlations because the pertinent physical properties of the packings were not known in sufficient detail. However, two graphical correlations, Figures 58 and 59, are presented to enable interpolation and extrapolation of the experimental data for first-order estimation of attenuation cross sections for other packings.

The main conclusions resulting from this study may be summarized as follows:

a) the problem of steady state, one dimensional, simultaneous, radiative and conductive heat transfer in packed media may be specified by a minimum of four dimensionless variables, defined by the system of Equation (53), and six dimensionless parameters, defined by the system of Equation (54).

b) Equation (115), the solution of the two-flux model for the case of no re-radiation, correlates transmission measurements of modulated flux very well. Average standard deviation of the regressed transmission curves from experimental data points was only 5.6 percent for the 46 valid runs of this study.

c) Values of the absorption cross section (a), the back scattering cross section (s_b), and the equivalent radiant conductivity (k_{ir}), range widely between various types of packings. For example, at 2000°F, the lowest and highest values of a were 1.20 and 192 (1/ft.) respectively, among the twelve packings tested. Similarly, s_b ranged from a low of 95.0 to a high of 1,010 (1/ft.), and k_{ir} ranged from a low of 0.101 to a high of 1.06 (Btu/hr. ft. °F).

d) Back scattering is the major mechanism of attenuation for radiant transport in packings of glass, aluminum oxide, and steel particles. For packings of silicon carbide particles, both absorption and back scattering are important as attenuating mechanisms.

e) Radiation becomes important, relative to conduction, at temperatures of approximately 1000°F and becomes predominant at temperatures of about 2000°F. Thus, at 2000°F, radiation was found to account for approximately 35 percent of the total heat transfer for packings of mesh 4 silicon carbide grains, 45 percent for 3/16 inch steel spheres, 60 percent for 3/16 inch aluminum oxide cylinders, and 85 percent for 5mm. glass spheres.

f) The temperature dependence of radiant conductivities may be substantially different from the simple third power dependence commonly assumed. In the range of 1600°F to 2000°F, values of the exponent of temperature was found to be less than three for packings of grains

and to be greater than three for packings of spheres and cylinders.

g) Radiant conductivity increases with increasing particle transmissivity and size.

h) Increasing particle emissivity increases absorption cross sections and decreases scattering cross sections. The overall effect is generally to increase radiant conductivities.

i) Equations available in the literature for predicting radiant conductivities a priori are generally too simplified to give better than order of magnitude estimates. The three equations tested were found to differ from experimental values by as much as factors of eight.

j) This experimental method, based on transmission measurements of modulated radiant flux, is shown to be applicable to studies of radiant transport properties of close packed media. It is the only method presently known that can isolate radiant transfer from conductive and convective transfer for individual examination.

The major contribution of this study is in providing the first direct measurements of radiant heat transfer properties of packed media. The data obtained for the twelve test packings and the various trends which they showed are the first experimental information available for calculation of radiant heat transfer in packed media. In future investigations, it may well be fruitful to isolate and individually study the effects of various particle properties and system geometrics, with the ultimate goal of obtaining complete quantitative correlations for predicting radiant transfer properties of any packed system.

APPENDIX

DATA REGRESSION EQUATIONS

Experimental measurements supplied values of S_n as a function of h. From this, it was desired to obtain values of a and s_b by regression on Equation (115). As the fractional deviation (rather than absolute deviation) was approximately equal for all data points in a run, the least square error requirement specified was that

$$\Phi = \sum_{j=1}^{n} \left[\frac{S_n(h_j) - S_n'(h_j)}{S_n(h_j)} \right]^2 \qquad (143)$$

be minimized. In Equation (143), n denotes the number of data points, $S_n(h_j)$ is the experimental value of S_n for jth data point, and $S_n'(h_j)$ is the correlation value of S_n at h_j.

Since Equation (115) is a nonlinear model, analytic regression was not possible, and it was necessary to resort to iterative methods. A number of numerical regression methods were attempted, including straight-log iteration, steepest-descent iteration, and truncated Taylor series iteration. The Taylor series method was found to be most satisfactory in giving fast convergence and was the method finally used. The necessary relationships may be developed as follows.

Consider a run with n data points. There exists some value of m and a_n such that Φ is at a minimum, where Φ is defined by Equation (143) and S_n' is to be calculated by Equation (144),

$$S_n'(h_j) = f_j(m, a_n) = \frac{m}{m \cosh(mh_j) + a_n \sinh(mh_j)} \qquad (144)$$

At the ith iteration, the ith approximate value of m and a_n differs

from this true value by,

$$\Delta m^i = m - m^i$$
$$\Delta a_n^i = a_n - a_n{}^i \tag{145}$$

where m and a_n are the true converged values corresponding to minimal Φ, and m^i and a_n^i are the ith approximations. Evidently for the i+1 iteration, the best values would be,

$$m^{i+1} = m^i + \Delta m^i$$
$$a_n^{i+1} = a_n^{i+1} + \Delta a_n^i \tag{146}$$

However, the quantities Δm^i and Δa_n^i are unknown and only an estimate of their values can be obtained, as follows.

For the ith approximation,

$$\Phi^i = \sum_{j=1}^{n} \left[\frac{S_n(h_j) - f_j^i}{S_n(h_j)} \right] \tag{147}$$

where,

$$f_j^i = f_j^i(m^i, a_n^i) = \frac{m^i}{m^i \cosh(m^i h_j) + a_n^i \sinh(m^i h_j)} \tag{148}$$

For any specific set of data points, Φ^i may be considered as a two dimensional function of the variables m^i and a_n^i. At the desired minimum point,

$$\Phi^i \longrightarrow \Phi$$
$$a_n^i \longrightarrow a_n$$
$$m^i \longrightarrow m$$
$$f_j^i \longrightarrow f_j$$

and also,

$$\frac{\partial \Phi^i}{\partial m^i} \longrightarrow \frac{\partial \Phi}{\partial m^i} = 0 \tag{149}$$

$$\frac{\partial \Phi^i}{\partial a_n^i} \longrightarrow \frac{\partial \Phi}{\partial a_n^i} = 0 \tag{150}$$

By Equation (145),

$$\frac{\partial \Phi}{\partial m^i} = \frac{\partial \Phi}{\partial \Delta m^i} = 0 \tag{151}$$

$$\frac{\partial \Phi}{\partial a_n^i} = \frac{\partial \Phi}{\partial \Delta a_n^i} = 0 \tag{152}$$

since m and a_n are fixed constants for any specific data set.

Then from Equation (147),

$$\frac{\partial \Phi}{\partial \Delta m^i} = \sum_{j=1}^{n} \frac{\partial}{\partial \Delta m^i} \left[\frac{S_n(h_j) - f_j}{S_n(h_j)} \right]^2 = 0$$

$$= -2 \sum_{j=1}^{n} \left(\frac{1}{S_n(h_j)}\right)^2 (S_n(h_j) - f_j)\left(\frac{\partial f_j}{\partial \Delta m^i}\right) = 0 \tag{153}$$

$$\frac{\partial \Phi}{\partial \Delta a_n^i} = -2 \sum_{j=1}^{n} \left(\frac{1}{S_n(h_j)}\right)^2 (S_n(h_j) - f_j)\left(\frac{\partial f_j}{\partial \Delta m^i}\right) = 0 \tag{154}$$

to continue, $f_j(m, a_n)$ is expanded in a Taylor series about m^i and a_n^i,

$$f_j(m, a_n) = f_j^i + \Delta m^i \left(\frac{\partial f_j}{\partial m}\right)_i + \Delta a_n^i \left(\frac{\partial f_j}{\partial m}\right)_i$$

$$+ \frac{1}{2}(\Delta m^i)^2 \left(\frac{\partial^2 f_j}{\partial m^2}\right)_i + \frac{1}{2}(\Delta a_n^i)^2 \left(\frac{\partial^2 f_j}{\partial a_n^2}\right)_i + \ldots \tag{155}$$

where,

$$f_j(m, a_n) = S_n'(h_j, m, a_n) \tag{156}$$

$$f_j^i(m^i, a_n^i) = S_n'(h_j, m^i, a_n^i) \tag{157}$$

$$\left(\frac{\partial f_j}{\partial m}\right)_i = \left.\frac{\partial f_j}{\partial m}\right]_{m^i, a_n^i, h_j} \tag{158}$$

$$\left(\frac{\partial f_j}{\partial a_n}\right)_i = \left.\frac{\partial f_j}{\partial a_n}\right]_{m^i, a_n^i, h_j} \tag{159}$$

If the approximations, m^i and a_n^i, are close to the true values, m and a_n, then the higher order terms of Equation (155) may be neglected to give the truncated Taylor series,

$$f_j(m, a_n) = f_j^i + \Delta m^i \left(\frac{\partial f_j}{\partial m}\right)_i + \Delta a_n^i \left(\frac{\partial f_j}{\partial a_n}\right)_i \quad . \tag{160}$$

From which,

$$\frac{\partial f_j}{\partial \Delta m^i} = \left(\frac{\partial f_j}{\partial m}\right)_i \tag{161}$$

$$\frac{\partial f_j}{\partial \Delta a_n^i} = \left(\frac{\partial f_j}{\partial a_n}\right)_i \quad . \tag{162}$$

Substituting Equations (160) to (162) into Equation (153),

$$\frac{\partial \Phi}{\partial \Delta m^i} = 0 = -2 \sum_{j=1}^{n} \frac{1}{S_n^2(h_j)} \left[S_n(h_j) - f_j^i - \Delta m^i \left(\frac{\partial f_j}{\partial m}\right)_i - \Delta a_n^i \left(\frac{\partial f_j}{\partial a_n}\right)_i \right] \cdot \left(\frac{\partial f_j}{\partial m}\right)_i \tag{163}$$

and substituting into Equation (154),

$$\frac{\partial \Phi}{\partial \Delta a_n^i} = 0 = -2 \sum_{j=1}^{n} \frac{1}{S_n^2(h_j)} \left[S_n(h_j) - f_j^i - \Delta m^i \left(\frac{\partial f_j}{\partial m}\right)_i - \Delta a_n^i \left(\frac{\partial f_j}{\partial a_n}\right)_i \right] \cdot \left(\frac{\partial f_j}{\partial a_n}\right)_i \tag{164}$$

Equations (163) and (164) can be solved simultaneously to obtain,

$$\Delta m^i = \frac{Dm}{D} \tag{165}$$

$$\Delta a_n^i = \frac{Da}{D} \tag{166}$$

where,

$$D = \begin{vmatrix} \sum_{j=1}^{n} \frac{1}{S_n^2(h_j)} \left(\frac{\partial f_j}{\partial m}\right)_i^2 & \sum_{j=1}^{n} \frac{1}{S_n^2(h_j)} \left(\frac{\partial f_j}{\partial m}\right)_i \left(\frac{\partial f_j}{\partial a_n}\right)_i \\ \sum_{j=1}^{n} \frac{1}{S_n^2(h_j)} \left(\frac{\partial f_j}{\partial m}\right)_i \left(\frac{\partial f_j}{\partial a_n}\right)_i & \sum_{j=1}^{n} \frac{1}{S_n^2(h_j)} \left(\frac{\partial f_j}{\partial a_n}\right)_i^2 \end{vmatrix} \tag{167}$$

$$D_m = \begin{vmatrix} \sum_{j=1}^{n} \frac{S_n(h_j) - f_j^i}{S_n^2(h_j)} \left(\frac{\partial f_j}{\partial m}\right)_i & \sum_{j=1}^{n} \frac{1}{S_n^2(h_j)} \left(\frac{\partial f_j}{\partial m}\right)_i \left(\frac{\partial f_j}{\partial a_n}\right)_i \\ \sum_{j=1}^{n} \frac{S_n(h_j) - f_j^i}{S_n^2(h_j)} \left(\frac{\partial f_j}{\partial a_n}\right)_i & \sum_{j=1}^{n} \frac{1}{S_n^2(h_j)} \left(\frac{\partial f_j}{\partial a_n}\right)_i^2 \end{vmatrix} \tag{168}$$

$$D_a = \begin{vmatrix} \sum_{j=1}^{n} \frac{1}{S_n^2(h_j)} \left(\frac{\partial f_j}{\partial m}\right)_i^2 & \sum_{j=1}^{n} \frac{S_n(h_j) - f_j^i}{S_n^2(h_j)} \left(\frac{\partial f_j}{\partial m}\right)_i \\ \sum_{j=1}^{n} \frac{1}{S_n^2(h_j)} \left(\frac{\partial f_j}{\partial m}\right)_i \left(\frac{\partial f_j}{\partial a_n}\right)_i & \sum_{j=1}^{n} \frac{S_n(h_j) - f_j^i}{S_n^2(h_j)} \left(\frac{\partial f_j}{\partial a_n}\right)_i \end{vmatrix} \tag{169}$$

In these determinants,

$$S_n(h_j) = \text{experimental value of } S_n \text{ at } h_j \tag{170}$$

$$f_j^i = \frac{m^i}{m^i \cosh(m^i h_j) + a_n^i \sinh(m^i h_j)} \tag{171}$$

$$\left(\frac{\partial f_j}{\partial m}\right)_i = \frac{(m^i a_n^i h_j)\cosh(m^i h_j) + (m^{i2} h_j - a_n^i)\sinh(m^i h_j)}{-\left[m^i \cosh(m^i h_j) + a_n^i \sinh(m^i h_j)\right]^2} \tag{172}$$

and,

$$\left(\frac{\partial f_j}{\partial a_n}\right)_i = \frac{m^i \sinh(m^i h_j)}{-\left[m^i \cosh(m^i h_j) + a_n^i \sinh(m^i h_j)\right]^2} \quad . \tag{173}$$

Thus at the end of the ith iteration, the values of Δm^i and Δa_n^i may be estimated by Equations (165) and (166), with the relationships of Equations (170) to (173). The (i+1) approximation for m and a_n is then given by Equation (146). This iterative procedure may be continued until m and a_n converge to as many significant figures as desired. The values of radiation parameters a and s_b can then be calculated from these converged values by,

$$s_b = \sqrt{a_n^2 - m^2} \tag{174}$$

$$a = a_n - s_b \tag{175}$$

To initiate the iterative regression, it was necessary to obtain a fairly accurate first-guess for values of a_n and m. This may be done by

writing Equation (115) in exponential form,

$$S_n(h) = \frac{m}{m\cosh(mh) + a_n \sinh(mh)} \tag{115}$$

$$= \frac{2m}{(m + a_n)e^{mh} + (m - a_n)e^{-mh}} \tag{176}$$

At large values of h,

$$e^{-mh} \longrightarrow 0$$

and Equation (176) may be approximated as,

$$S_n(h) = \frac{2m}{(m+a_n)e^{mh}}$$

or

$$\ln(S_n(h)) = \ln\left(\frac{2m}{m+a_n}\right) - mh \tag{177}$$

By using two experimental data points at relatively large h, a first approximation can then be obtained from Equation (177) as,

$$m^\circ = \frac{1}{h_2 - h_1} \ln\left[\frac{S_n(h_1)}{S_n(h_2)}\right] \tag{178}$$

$$a_n^\circ = 2m^\circ e^{-m^\circ h_2}\left(\frac{1}{S_n(h_2)}\right) - m^\circ \tag{179}$$

In the actual experimental study, this first approximation calculation and the subsequent iterative regressions were programmed for computation on the IBM 704 digital computer. These programs are described in the last section of the Appendix.

SAMPLE CALCULATIONS

The data of Run 41, for GS-3 at 2000°F, are worked out below as an illustrative sample calculation. The results for all other runs were determined in a similar manner.

Regression For Transmission Curve

The original test run data are tabulated in Table VI. There are eight data points for Run 41, with packing height, h, ranging from 1.72 cm. to 7.49 cm. Using the sixth and eighth data points, first-guess values for a_n and m were calculated by Equations (178) and (179) as,

$$m^\circ = \frac{\ln\left(\frac{.00299}{.000879}\right)}{7.49 - 5.87}$$

$$= 0.756$$

$$a_n^\circ = \left[2 \times 0.756 \times e^{-(0.756 \times 7.49)} \times \left(\frac{1}{.000879}\right)\right] - 0.756$$

$$= 0.523 \quad cm^{-1} .$$

Calculated transmissions, $S_n'(h)$, corresponding to these values of a_n and m were obtained from Equation (144) for each packing height. The Φ error was then calculated by Equation (147) and from that the standard deviation was determined by Equation (128) to be,

$$\delta_s^\circ = 100 \left(\frac{\Phi}{8}\right)^{\frac{1}{2}} \%$$

$$= 7.77 \%$$

Corresponding to Equations (167) to (169), the values of the following three determinants were calculated,

$$D = 4.43$$

$$D_m = 0.143$$

$$D_a = -4.682$$

and the adjustments were determined to be, by Equations (165) and (166),

$$\Delta m^\circ = \frac{Dm}{D} = \frac{.143}{4.43} = 0.0322$$

$$\Delta a_n^\circ = \frac{Da}{D} = \frac{4.682}{4.43} = -1.06$$

Therefore, for the next iteration,

$$m' = m^\circ + \Delta m^\circ = 0.756 + 0.0322 = 0.788 \quad (146)$$

$$a_n' = m^\circ + \Delta a_n^\circ = 5.32 - 1.06 = 4.17 \quad (146)$$

and the corresponding standard deviation was found to be,

$$\delta_s' = 2.56\%$$

Continuing this iterative regression, the following values were obtained at successive iterations:

Iteration	$m\left(\frac{1}{cm}\right)$	$a_n\left(\frac{1}{cm}\right)$	$\delta_s(\%)$	$\Delta m\left(\frac{1}{cm}\right)$	$\Delta a_n\left(\frac{1}{cm}\right)$
0	0.756	5.23	7.77	.0322	-1.057
1	0.788	4.17	2.56	-.0014	0.120
2	0.787	4.29	1.68	-.0005	0.003
3	0.786	4.30	1.67	.0000	0.000
4	0.786	4.30	1.67	.0000	0.000

It is seen that convergence to three significant figures was obtained at the end of the fourth iteration, giving final regressed values of m and a_n as,

$$m = 0.786 \text{ cm}^{-1} \quad \text{or} \quad 24.1 \text{ ft.}^{-1}$$

$$a_n = 4.30 \text{ cm}^{-1} \quad \text{or} \quad 131 \text{ ft.}^{-1}.$$

The calculated transmissions, $S'_n(h)$, corresponding to these regressed parameters were then calculated by Equation (144) and may be compared to the experimental transmissions, $S_n(h)$, as follows:

h, (cm)	$S_n(h)$	$S'_n(h)$	$S_n - S'_n$
1.72	.0856	.0839	.0017
2.62	.0394	.0397	- .0004
3.43	.0212	.0209	.0003
4.25	.0108	.0109	- .0001
5.07	.00569	.00574	- .00005
5.87	.00299	.00306	- .00007
6.58	.00175	.00175	.00000
7.49	.00088	.00086	.00002

The experimental values, $S_n(h)$, are plotted as data points and the calculated values, $S'_n(h)$, are represented by the transmission curve on Figure 22. The fit is seen to be quite satisfactory. The standard deviation of this converged regression was found to be 1.67 percent.

The attenuation cross sections corresponding to these regressed values of m and a_n were calculated by Equations (174) and (175) to obtain,

$$S_b = \sqrt{a_n^2 - m^2}$$

$$= \sqrt{131^2 - 24.1^2} = 129 \text{ ft.}^{-1}$$

$$a = a_n - S_b$$

$$= 130.97 - 128.76 = 2.21 \text{ ft.}^{-1}$$

The transmission values obtained by such regressions for all runs are listed in Table XI.

Radiation to Conduction Ratios

By Schumann and Voss' correlation[34] with Wilhelm et al.'s modification[38], the conduction-conductivity of a packed medium may be estimated from the equation

$$k_c = k_c' + \Delta \qquad (180)$$

where k_c' = conductivity given by Schumann and Voss' graphical correlation

Δ = Wilhelm et al's correction.

The graphical correlation for k_c' presents it in the ratio, k_c'/k_g, as a function of k_s/k_g for parameters of δ_p, where

k_s = conductivity of solid

k_g = conductivity of gas

δ_p = void fraction of packing.

In Table XII, the values of k_s and δ_p for GS-3 at 2000°F are given as 0.63 $\frac{\text{Btu}}{\text{hr.ft.°F}}$ and 0.350, respectively. The conductivity of air at high temperatures is given by Glassman and Bonilla[10]. The values used were:

	800°F	1200°F	1600°F	1800°F	2000°F
k_g $\frac{\text{Btu}}{\text{hr.ft.°F}}$ =	0.0303	0.0369	0.0427	0.0454	0.0480

Thus for GS-3 at 2000°F,

$$k_s/k_g = \frac{0.63}{0.0480} = 13.1$$

and from Schumann and Voss' correlation,

$$k_c'/k_g = 3.7$$

$$k_c' = 0.178$$

Wilhelm's correction was calculated by,

$$\Delta = \left[\text{antilog} \left(0.859 + 0.0129 \times \frac{\kappa_s}{\delta}\right)\right] \times 10^{-5}$$

$$= \left[\text{antilog} \left(0.859 + 0.0129 \times \frac{0.63}{0.35}\right)\right] \times 10^{-5}$$

$$= 0.00076$$

Therefore, the bulk conductivity, k_c, for GS-3 at 2000°F was determined to be,

$$k_c = 0.178 + 0.00076$$

$$= 0.178 \ \frac{\text{Btu}}{\text{hr.ft.°F}}$$

The radiant conductivity was calculated as

$$k_{ir} = \frac{8\sigma T^3}{a + 2s_b}$$

$$= \frac{8 \times 1.713 \times 10^{-9} \times 2460^3}{2.21 + 2(129)} \qquad (104)$$

$$= 0.785 \ \frac{\text{Btu}}{\text{hr.ft.°F}}$$

The ratio of radiation to conduction was thus,

$$\frac{k_{ir}}{k_c} = \frac{0.785}{0.178}$$

$$= 4.41$$

Analytic Estimates

The three analytical estimates of radiant conductivity were calculated as follows.

Estimate of Damköhler[6] and Argo & Smith[1],

$$k_{r1} = 4\sigma \left(\frac{\epsilon}{2-\epsilon}\right) D_p T^3 \qquad (2b)$$

where ϵ = particle emissivity.

Estimate of Schotte[33],

$$k_{r2} = \frac{1-\delta}{\frac{1}{\kappa_s} + \frac{1}{k_r^\circ}} + \delta k_r^\circ \qquad (5)$$

$$k_r^\circ = 4\sigma\epsilon D_p T^3$$

Estimate of Rosseland[31] and Bosworth[3],

$$k_{r3} = \frac{4}{3}\sigma D_p T^3 \qquad (6)$$

For GS-3 at 2000°F:

a) $k_{r1} = 4 \times 1.713 \times 10^{-9}\left(\frac{0.65}{2-0.65}\right) \times 0.00983 \times 2460^3$

$$= 0.483 \quad \frac{\text{Btu}}{\text{hr.ft.°F}}$$

b) $k_r^\circ = 4 \times 1.713 \times 10^{-9} \times 0.65 \times 0.00983 \times 2460^3$

$$= 0.652$$

$$k_{r2} = \frac{1 - 0.35}{\frac{1}{0.63} + \frac{1}{0.652}} + 0.35\ (0.652)$$

$$= 0.436 \quad \frac{\text{Btu}}{\text{hr.ft.°F}}$$

c) $k_{r3} = \frac{4}{3} \times 1.713 \times 10^{-9} \times 0.00983 \times 2460^3$

$$= 0.334 \quad \frac{\text{Btu}}{\text{hr.ft.°F}}$$

Estimation of Conductivity from Correlation

To demonstrate how the graphical correlations, Figures 58 and 59, may be used to estimate radiant transfer properties of some packing not tested in this study, an example is worked out below for 5/32 inch diameter steel spheres operating at a temperature of 1700°F.

Figures 58 and 59 present smoothed curves of C_s and C_a for steel spheres of 1/8 inch and 3/16 inch diameters. Since 5/32 inch steel spheres have approximately the same emissivity, shape, material, and bulk void fraction as these two tested packings, it is necessary only to interpolate for size and temperature. Interpolating between curves at 1700°F, a value of 8.0 is obtained for C_s from Figure 58 and a value of 0.23 for C_a from

Figure 59. Attenuation cross sections may then be calculated as,

$$s_b = c_s \times \frac{1-\delta_p}{D_p}$$

$$= 8.0 \times \frac{1-.395}{.0131}$$

$$= 370 \quad ft.^{-1}$$

$$a = c_a \times \frac{1-\delta_p}{D_p}$$

$$= 0.23 \times \frac{1-.395}{.0131}$$

$$= 10.6 \quad ft.^{-1}$$

The radiant conductivity at interior of a packing of 5/32 inch steel spheres at 1700°F may be thus estimated as,

$$K_{ir} = \frac{8\sigma T^3}{a + 2s_b}$$

$$= \frac{8 \times 1.713 \times 10^{-9} \times 2160^3}{10.6 + 2(370)}$$

$$= 0.184 \frac{Btu}{hr.ft.^\circ F} .$$

EXPERIMENTAL DATA

Test Run Data

Experimental data for the valid test runs are given below in Table VI. Values of background reading, R_B, are the average values for each run. The column of S gives the transmission reading minus background; $S = R - R_B$. S_n denotes flux signal normalized with respect to input flux; $S_n = S/S_o$. Source temperatures are nominal values, with possible variations of ± 5°F.

TABLE VI

Test Run Data

Run	Description	ΔW gm.	h cm.	S	Avg. S	Avg. S_n
7	GS-3	0	0	836	836	1
	t_s=800°F	26.25	1.01	24.4	23.6	0.0282
	S_o=836			22.8		
	R_B=0.13			23.7		
		24.40	1.95	7.52	7.56	0.00904
				7.62		
				7.55		
		22.80	2.83	3.49	3.44	0.00415
				3.43		
				3.40		
		23.25	3.72	1.57	1.58	0.00189
				1.59		
		21.30	4.54	0.77	0.78	0.00093
				0.79		
8	GS-4	0	0	830	830	1
	t_s=800°F	26.75	1.03	31.9	34.1	0.0411*
	S_o=830			35.1		
	R_B=0.13			35.3		
		24.30	1.97	10.7	11.1	0.0134
				11.2		
				11.4		
		22.80	2.85	6.07	6.01	0.00724
				5.95		
				6.02		
		22.25	3.70	3.69	3.59	0.00432
				3.52		
				3.57		

TABLE VI (cont'd)

Test Run Data

Run	Description	ΔW gm.	h cm.	S	Avg. S	Avg. S_n
		22.50	4.57	2.07 2.02	2.04	0.00246
		24.55	5.51	1.07 1.07	1.07	0.00129
		24.55	6.46	0.60 0.63	0.62	0.00075
9	GS-5 t_s=800°F S_o=855 R_B=0.13	0	0	855	855	1
		29.15	1.20	30.6 25.4 26.8	27.6	0.0323*
		26.35	2.29	8.82 9.37 9.12	9.10	0.0106
		23.15	3.24	4.37 4.47	4.42	0.00517
		23.55	4.21	2.57 2.60	2.60	0.00304
		23.80	5.19	1.41 1.41	1.41	0.00165
		26.30	6.27	0.76 0.75	0.75	0.00087
10	GS-3 t_s=1200°F S_o=2,560 R_B=0.06	26.25	1.01	182 175 173	177	0.0690
		21.35	1.83	79.0 74.5 78.6	77.0	0.0301
		18.30	2.54	42.1 42.5	42.3	0.0165
		13.80	3.07	27.7 27.6	27.7	0.0108
		13.65	3.59	18.0 18.0	18.0	0.00703
		13.75	4.12	11.4 11.7	11.5	0.00449
		13.50	4.64	6.54 6.64	6.59	0.00257
		21.00	5.45	3.50 3.39 3.44	3.44	0.00134
		20.90	6.26	1.82 1.81	1.82	0.000711

TABLE VI (cont'd)

Test Run Data

Run	Description	ΔW gm.	h cm.	S	Avg. S	Avg. S_n
11	GS-4 t_s=1200°F S_o=2,610 R_B=0.06	26.75	1.03	238 217 228	228	0.0874
		22.80	1.91	109 103	106	0.0406
		22.25	2.76	59.5 60.2	59.8	0.0229
		15.55	3.36	41.2 41.9	41.5	0.0159
		15.70	3.97	30.4 29.1	29.7	0.0114
		15.95	4.58	21.0 21.5	21.3	0.00816
		17.80	5.27	13.9 13.7	13.8	0.00529
		17.85	5.95	9.35 9.19	9.27	0.00355
		22.55	6.82	5.66 5.72	5.69	0.00218
12	GS-5 t_s=1200°F S_o=2,590 R_B=0.06	29.15	1.20	203 203	203	0.0784
		23.55	2.17	87.8 88.0	87.9	0.0339
		18.80	2.95	59.5 59.0	59.2	0.0229
		18.80	3.72	38.8 38.5	38.6	0.0149
		18.25	4.47	25.4 24.3 26.0	25.2	0.00973
		18.75	5.24	16.8 16.4	16.6	0.00641
		18.80	6.02	10.9 10.7	10.8	0.00417
		18.50	6.78	7.39 7.64	7.51	0.00290
		23.15	7.74	4.54 4.66	4.60	0.00178
13	GS-3 t_s=1200°F S_o=2,780 R_B=0.06	26.25	1.01	203 212 198	204	0.0734
		23.15	1.90	80.8 83.0 84.0	82.6	0.0297

TABLE VI (cont'd)

Test Run Data

Run	Description	ΔW gm.	h cm.	S	Avg. S	Avg. S_n
		18.50	2.61	45.2 45.0	45.1	0.0162
		13.80	3.15	29.2 29.6	29.4	0.0106
		13.75	3.67	19.3 19.4	19.3	0.00694
		21.35	4.50	9.79 9.96	9.88	0.00360
		22.80	5.37	4.89 4.89	4.89	0.00176
14	GS-3 t_s=1200°F S_o=1,980 R_B=0.06	24.40	0.94	148 142 146	145	0.0732
		23.70	1.85	57.4 56.1	56.7	0.0386
		23.25	2.75	25.6 25.6	25.6	0.0129
		18.30	3.45	14.5 14.5	14.5	0.00732
		13.65	3.98	9.34 9.55	9.44	0.00477
		20.90	4.78	4.90 4.94	4.92	0.00248
		21.00	5.59	2.50 2.56	2.53	0.00128
15	GS-3 t_s=1600°F S_o=4,680 R_B=0.09	26.25	1.01	535 600 565	567	0.121
		24.40	1.95	227 233 226	229	0.0490
		23.70	2.86	110 107	108	0.0231
		21.35	3.68	55.9 56.1	56.0	0.0120
		18.30	4.39	32.0 32.0	32.0	0.00684
		18.50	5.10	18.0 18.1	18.1	0.00387
		20.90	5.81	9.52 9.52	9.52	0.00204
		21.30	6.73	5.01 4.91	4.95	0.00106
		23.25	7.62	2.41 2.49	2.45	0.000524

TABLE VI (cont'd)

Test Run Data

Run	Description	ΔW gm.	h cm.	D	Avg. S	Avg. S_n
16	GS-4 t_s=1600°F S_o=4,680 R_B=0.09	51.40	1.98	340 341	340	0.0727
		24.65	2.93	187 183 185	185	0.0396
		22.50	3.79	114 120	117	0.0250
		17.80	4.48	78.3 80.1	79.2	0.0169
		17.85	5.17	54.0 53.5	53.8	0.0115
		22.80	6.04	32.1 30.8 32.2	31.7	0.00678
		22.25	6.90	19.4 19.4	19.4	0.00415
		24.35	7.83	11.4 11.3	11.4	0.00244
		24.55	8.79	6.89 6.77	6.83	0.00146
17	GS-5 t_s=1600°F S_o=4,680 R_B=0.07	55.50	2.29	292 288	290	0.0620
		23.80	3.27	165 169	167	0.0357
		18.80	4.04	112 112	112	0.0240
		18.80	4.82	76.5 76.1	76.3	0.0163
		18.75	5.59	50.0 49.5	49.7	0.0106
		18.80	6.36	33.2 32.8	33.0	0.00706
		23.55	7.33	20.0 20.0	20.0	0.00428
		23.15	8.29	12.4 12.6	12.5	0.00267
18	AS-3/16 t_s=1600°F S_o=4,680 R_B=0.13	27.70	0.77	311 300	305	0.0652*
		17.70	1.27	105 109	107	0.0229
		17.20	1.75	42.0 44.4 44.4	43.6	0.00933
		14.65	2.16	21.7 21.6	21.7	0.00464

TABLE VI (cont'd)

Test Run Data

Run	Description	ΔW gm.	h cm.	S	Avg. S	Avg. S_n
		14.65	2.56	10.6 10.6	10.6	0.00227
		14.35	2.97	5.57 5.48	5.53	0.00118
		14.20	3.36	2.72 2.90	2.81	0.000601
		14.90	3.78	1.42	1.42	0.000304
20	AP-1/8 t_s=1600°F S_o=4,680 R_B=0.12	19.30	0.81	160 163 163	162	0.0347*
		14.25	1.41	40.7 41.7 42.6	41.7	0.00892
		8.55	1.76	20.5 20.7	20.6	0.00441
		8.80	2.13	10.7 10.9	10.8	0.00231
		8.80	2.50	5.88 5.88	5.88	0.00126
		8.60	2.86	3.35 3.35	3.35	0.000717
		13.05	3.41	1.34 1.41 1.39	1.38	0.000295
		13.20	3.96	0.54 0.60 0.63	0.59	0.000126
21	AP-5/32 t_s=1600°F S_o=4,680 R_B=0.14	27.50	1.28	96.2 104 103	101	0.0216*
		14.25	1.94	27.5 29.4 31.8 30.9	29.9	0.00640
		8.95	2.35	15.0 16.0 15.8	15.6	0.00334
		8.45	2.75	8.36 9.18 9.41	8.98	0.00192
		8.75	3.15	4.71 5.06 4.60 4.96	4.83	0.00103

TABLE VI (cont'd)

Test Run Data

Run	Description	ΔW gm.	h cm.	S	Avg. S	Avg. S_n
		8.20	3.53	2.90 2.06 2.76	2.91	0.000622
		14.30	4.19	1.20 1.16 1.18	1.18	0.000252
		14.45	4.87	0.53 0.46 0.49	0.493	0.000105
22	AP-3/16 t_s=1600°F S_o=4,680 R_B=0.10	30.70	1.33	74.9 72.9 72.4	73.4	0.0157
		9.30	1.73	36.7 36.9	36.8	0.00787
		9.25	2.13	16.0 17.6 16.2	16.6	0.00355
		9.25	2.53	7.85 8.50 8.40	8.25	0.00176
		9.35	2.94	4.55 4.20 4.89	4.55	0.000973
		17.75	3.71	1.23 1.32 1.29	1.28	0.000274
23	SS-1/8 t_s=1600°F S_o=4,950 R_B=0.13	45.10	0.53	405 470 440	438	0.0885*
		22.60	0.79	192 128 160 170	163	0.0329*
		22.15	1.05	46.4 48.7 42.9 44.6	45.7	0.00923
		13.20	1.21	26.7 26.6 28.2	27.2	0.00549
		14.00	1.37	13.6 12.3 12.6 13.8	13.1	0.00265

TABLE VI (cont'd)

Test Run Data

Run	Description	ΔW gm.	h cm.	S	Avg. S	Avg. S_n
		13.85	1.53	7.97 7.62 6.86 8.57	7.75	0.00157
		22.45	1.79	3.07 2.92 2.67	2.89	0.000584
		13.70	1.96	1.57 1.45 1.67	1.56	0.000315
		22.35	2.22	0.86 0.72 0.78	0.787	0.000159
24	SS-3/16 t_s=1600°F S_o=4,950 R_B=0.13	141.60	1.69	33.4	33.4	0.00675
		22.70	1.96	17.3 17.3 16.2 15.5	16.6	0.00335
		22.15	2.22	9.82 8.88 9.32	9.34	0.00189
		22.70	2.49	4.17 4.60 4.54	4.44	0.000897
		22.55	2.76	2.53 2.47 2.79	2.60	0.000525
		30.40	3.12	1.29 1.20 1.67	1.25	0.000253
25	AG-4 t_s=1600°F S_o=4,950 R_B=0.10	27.20	0.98	169 186 166	174	0.0351*
		16.70	1.58	38.0 37.4 37.9 38.9	38.1	0.00770
		10.95	1.98	16.6 16.3 18.0	17.0	0.00343
		10.70	2.36	7.85 7.33 8.00	7.73	0.00156

TABLE VI (cont'd)

Test Run Data

Run	Description	ΔW gm.	h cm.	S	Avg. S	Avg. S_n
		10.65	2.74	3.70 3.54 3.57	3.60	0.000727
		10.60	3.12	1.95 1.88 1.75	1.86	0.000376
		16.35	3.72	0.73 0.75	0.74	0.000149
26	AG-16 t_s=1600°F S_o=4,950 R_B=0.09	13.85	0.42	232 233 236	234	0.0473
		6.45	0.62	80.4 80.1	80.2	0.0162
		6.35	0.81	29.7 29.6	29.7	0.00600*
		3.90	0.93	20.2 20.1	20.1	0.00406
		3.85	1.05	11.6 11.5	11.6	0.00234
		6.45	1.25	4.41 4.36	4.39	0.000887
		3.95	1.37	2.55 2.67	2.61	0.000527
		3.85	1.49	1.60 1.62	1.61	0.000325
27	CG-16 t_s=1600°F S_o=4,950 R_B=0.08	4.85	0.161	403 230	317	0.0640
		4.35	0.305	14.0 14.8 15.0	14.6	0.00295
		4.60	0.458	0.92 0.86	0.89	0.000180
		4.20	0.600	0.14 0.14	0.14	0.000028
28	GS-3 t_s=1800°F S_o=6,780 R_B=0.09	44.75	1.72	500 492	496	0.0729
		23.25	2.62	228 238 239	235	0.0345
		21.00	3.43	123 123	123	0.0181
		21.35	4.25	64.1 64.4	64.3	0.00945

TABLE VI (cont'd)

Test Run Data

Run	Description	ΔW gm.	h cm.	S	Avg. S	Avg. S_n
		21.30	5.07	33.9 33.5	33.7	0.00495
		20.90	5.87	17.8 17.6	17.7	0.00260
		18.30	6.58	10.0 10.1	10.1	0.00148
		23.70	7.49	5.01 5.09	5.05	0.000742
29	GS-4 t_s=1800°F S_o=6,780 R_B=0.09	51.10	1.97	628 630	629	0.0925
		24.55	2.91	339 350	345	0.0507
		22.50	3.78	207 203	205	0.0301
		22.80	4.65	123 126	125	0.0184
		22.25	5.51	77.4 75.5 77.1	76.7	0.0113
		17.80	6.20	51.5 50.8	51.2	0.00753
		24.85	7.16	29.9 29.6	29.8	0.00438
		17.85	7.84	19.9 19.8	19.8	0.00291
30	GS-5 t_s=1800°F S_o=6,780 R_B=0.10	47.40	1.95	652 679 672	668	0.0982
		23.80	2.93	381 357 391	376	0.0553
		23.55	3.91	227 214 223	221	0.0325
		23.15	4.86	130 137 134	134	0.0197
		18.80	5.63	89.7 87.1	88.4	0.0130
		18.80	6.41	59.9 61.6	60.8	0.00894
		18.75	7.18	41.4 39.0 38.9	39.8	0.00585

TABLE VI (cont'd)

Test Run Data

Run	Description	ΔW gm.	h cm.	S	Avg. S	Avg. S_n
		18.50	7.94	27.4 27.4	27.4	0.00403
31	AS-3/16 t_s=1800°F	27.70	0.77	499 514	507	0.0745 *
	S_o=6,780 R_B=0.15	17.70	1.27	175 190 166	177	0.0260
		17.20	1.75	66.5 72.5 68.9	69.3	0.0102
		14.65	2.16	33.9 33.8 34.8	34.2	0.00503
		14.65	2.56	17.0 15.7 15.2	16.0	0.00235
		14.35	2.97	8.22 7.87 8.38	8.16	0.00120
		14.20	3.36	4.70 4.58	4.64	0.000680
		14.90	3.78	2.37 2.37 2.35	2.36	0.000347
		14.50	4.18	1.30 1.25	1.28	0.000188
32	AP-1/8 t_s=1800°F	19.30	0.81	299 250 295	281	0.0391 *
	S_o=7,192 R_B=0.37	14.25	1.41	86.9 83.5 78.7	83.0	0.0115
		8.55	1.76	39.6 41.8 47.7 43.8	43.2	0.00600
		8.80	2.13	22.1 23.6 22.6	22.8	0.00317
		8.80	2.50	11.9 12.0 11.6	11.8	0.00164
		8.60	2.86	6.85 6.68 6.58	6.70	0.000931

TABLE VI (cont'd)

Test Run Data

Run	Description	ΔW gm.	h cm.	S	Avg. S	Avg. S_n	
		13.50	3.43	2.58 2.63 2.73	2.65	0.000368	
		13.05	3.98	1.06 1.16 1.20	1.14	0.000158	
33	AP-5/32 t_s=1800°F S_o=7,192 R_B=0.33	27.50	1.28	171 188 168	176	0.0245	*
		14.25	1.94	57.2 66.5 59.7	61.1	0.00849	
		8.95	2.35	30.6 31.7 31.8	31.4	0.00436	
		8.45	2.75	17.9 18.0 17.9	17.9	0.00249	
		8.75	3.15	10.1 10.1 10.0	10.1	0.00140	
		8.20	3.53	5.90 5.72 5.89	5.84	0.000812	
		14.30	4.19	2.40 2.33 2.47	2.40	0.000334	
		14.45	4.87	1.00 1.07 0.95	1.01	0.000140	
34	AP-3/16 t_s=1800°F S_o=6,780 R_B=0.18	30.70	1.33	118 125 122	122	0.0179	
		9.50	1.74	54.0 57.7 52.9	54.9	0.00807	
		9.30	2.14	24.1 25.8 28.1	26.0	0.00382	
		9.30	2.55	13.3 14.1 12.6	13.3	0.00196	
		9.20	2.94	6.91 7.41 7.24	7.19	0.00106	

TABLE VI (cont'd)

Test Run Data

Run	Description	ΔW gm.	h cm.	S	Avg. S	Avg. S_n	
		9.40	3.35	3.27 3.58 3.37	3.39	0.000498	
		17.70	4.12	1.04 1.05 1.00	1.03	0.000151	
35	AG-4 t_s=1800°F S_o=6,780 R_B=0.14	27.20	0.98	260 259 270	263	0.0387	*
		16.70	1.58	54.9 55.0 50.7	53.6	0.00788	
		10.95	1.98	22.9 25.0 24.1	24.0	0.00353	
		10.70	2.36	11.5 12.1 11.9	11.8	0.00173	
		10.65	2.74	5.55 5.47 6.08	5.70	0.000838	
		10.60	3.12	3.16 3.46 3.36	3.33	0.000490	
		16.95	3.74	1.40 1.37 1.26	1.34	0.000197	
		16.55	4.33	0.54 0.54	0.54	0.000079	
36	AG-16 t_s=1800°F S_o=7,190 R_B=0.18	13.85	0.42	432 470 451	451	0.0627	*
		6.45	0.62	148 149	148	0.0206	
		6.35	0.81	57.9 59.9	58.9	0.00819	
		6.45	1.01	23.5 24.0	23.8	0.00331	
		6.50	1.21	10.0 10.2	10.1	0.00140	
		3.90	1.33	6.07 6.52 6.44	6.34	0.000881	
		3.85	1.45	3.92 3.83	3.88	0.000539	
		3.95	1.56	2.44 2.46	2.45	0.000341	

TABLE VI (cont'd)

Test Run Data

Run	Description	ΔW gm.	h cm.	S	Avg. S	Avg. S_n
37	CG-16 t_s=1800°F S_o=7,190 R_B=0.08	4.85	0.161	495 395	495	0.0619
		4.35	0.305	29.0 19.0	24.0	0.00334
		4.60	0.458	2.37 3.42	2.90	.000403
		4.20	0.600	0.44 0.19	0.32	0.000044
38	SS-1/8 t_s=1800°F S_o=7,192 R_B=0.23	45.10	0.30	530 590 690 620	608	0.0845*
		22.60	0.79	263 208 191	221	0.0307*
		22.15	1.05	52.3 60.8 60.3	57.8	0.00803
		22.45	1.31	24.5 20.8 24.7	23.3	0.00324
		13.20	1.47	14.3 11.0 11.9	12.4	0.00172
		14.00	1.63	6.29 6.47 6.17	6.31	0.000877
		13.85	1.79	3.23 3.37 3.40	3.33	0.000463
		13.70	1.96	1.85 1.95 2.12	1.97	0.000274
39	SS-3/16 t_s=1800°F S_o=6,780 R_B=0.24	88.00	1.05	218 228 267	238	0.0350*
		22.65	1.32	103 97.4 110	103	0.0151
		22.70	1.59	51.8 44.8 61.9	52.8	0.00776
		22.15	1.85	24.2 25.1 25.0	24.8	0.00365

TABLE VI (cont'd)

Test Run Data

Run	Description	ΔW gm.	h cm.	S	Avg. S	Avg. S_n
		22.70	2.12	11.9 11.4 13.1	12.1	0.00178
		22.55	2.39	6.76 6.66 6.71	6.71	0.000986
		30.90	2.76	2.86 3.26 3.21	3.11	0.000457
40	GS-5 t_s=1600°F S_o=4,362 R_B=1.0	55.50	2.29	263 273 310	282	0.0647
		23.80	3.27	163 166	164	0.0376
		18.80	4.04	103 105	104	0.0238
		18.80	4.82	72.0 69.5	70.8	0.0162
		18.75	5.59	46.8 46.4	46.6	0.0107
		18.80	6.36	31.7 31.3	31.5	0.00722
		23.55	7.33	20.2 20.2	20.2	0.00461
		23.15	8.29	12.1 12.5	12.3	0.00282
41	GS-3 t_s=2000°F S_o=9,520 R_B=0.10	44.75	1.72	820 810	815	0.9
		23.25	2.62	372 379	375	0.0394
		21.00	3.43	200 203	202	0.0212
		21.35	4.25	103 103	103	0.0108
		21.30	5.07	54.0 54.3	54.2	0.00569
		20.90	5.87	28.7 28.4	28.5	0.00299
		18.30	6.58	16.7 16.6	16.7	0.00175
		23.70	7.49	8.40 8.35	8.37	0.000879
42	GS-4 t_s=2000°F S_o=9,520	51.10	1.97	976 1050 1010	1012	0.106

TABLE VI (cont'd)

Test Run Data

Run	Description	ΔW gm.	h cm.	S	Avg. S	Avg. S_n
	R_B=0.11	24.55	2.91	562 565	563	0.0591
		22.50	3.78	345 343	344	0.0361
		22.80	4.65	205 207	206	0.0216
		22.25	5.51	123 126	124	0.0130
		17.80	6.20	82.7 83.9	83.3	0.00875
		24.85	7.16	48.0 47.9	48.0	0.00504
		17.85	7.84	32.9 33.2	33.0	0.00347
43	GS-5 t_s=2000°F S_o=9,520 R_B=0.11	71.20	2.93	591 611 616	606	0.0636
		23.55	3.91	368 362	365	0.0383
		23.15	4.86	217 222	219	0.0230
		18.80	5.63	148 149	149	0.0156
		18.80	6.41	101 99.6	100	0.0105
		18.75	7.18	66.7 67.4	67.1	0.00705
		18.50	7.94	46.6 45.1	45.9	0.00482
44	AS-3/16 t_s=2000°F S_o=9,520 R_B=0.27	45.40	1.26	262 264 261	262	0.0275
		17.20	1.75	101 102	102	0.0107
		14.65	2.16	48.3 47.3	47.8	0.00502
		14.65	2.56	27.5 27.7	27.6	0.00290
		14.35	2.97	15.0 15.0	15.0	0.00158
		14.20	3.36	7.50 7.20 7.75	7.48	0.000785

TABLE VI (cont'd)

Test Run Data

Run	Description	ΔW gm.	h cm.	S	Avg. S	Avg. S_n
		14.90	3.78	3.70 3.32 3.63	3.55	0.000373
		14.50	4.18	1.87 1.91 1.90	1.89	0.000198
45	AP-1/8 t_s=2000°F S_o=10,100 R_B=0.38	33.55	1.41	120 121 135	125	0.0124
		8.55	1.76	64.0 64.2	64.1	0.00637
		8.80	2.13	34.7 33.2	34.0	0.00338
		8.80	2.50	17.3 17.3	17.3	0.00172
		8.60	2.86	9.30 9.70	9.50	0.000944
		13.50	3.43	3.70 4.10	3.90	0.000388
		13.05	3.98	1.50 1.65 1.70	1.62	0.000161
		13.20	4.53	0.67 0.69 0.85	0.74	0.000074
46	AP-5/32 t_s=2000°F S_o=10,100 R_B=0.20	27.50	1.28	282 272 292	282	0.0280
		14.25	1.94	97.0 91.0 90.9	93.0	0.00924
		8.95	2.35	49.2 51.7 50.8	50.6	0.00503
		8.45	2.75	29.5 30.3 30.4	30.1	0.00299
		8.75	3.15	16.4 16.3	16.4	0.00163
		8.20	3.53	8.95 10.1	9.53	0.000947
		14.30	4.18	4.20 4.20	4.20	0.000417
		14.45	4.87	2.05 1.83 1.77	1.88	0.000187

TABLE VI (cont'd)

Test Run Data

Run	Description	ΔW gm.	h cm.	S	Avg. S	Avg. S_n
47	AP-3/16 t_s=2000°F S_o=9,520 R_B=0.22	30.70	1.33	188 199 208	198	0.0208
		9.50	1.74	87.1 93.0 94.0	91.4	0.00960
		9.30	2.14	41.8 46.5 50.0 43.0	45.3	0.00476
		9.30	2.55	20.8 22.0 21.0	21.3	0.00224
		9.20	2.94	10.1 10.1 11.6	10.6	0.00111
		9.40	3.35	5.80 5.70 5.78	5.76	0.000605
		17.70	4.12	1.63 1.73 1.48	1.61	0.000169
48	AG-4 t_s=2000°F S_o=9,520 R_B=0.15	43.90	1.58	86.3 91.0 81.6	86.3	0.00906
		10.95	1.98	35.0 37.0 39.9	37.3	0.00392
		10.70	2.36	18.2 19.2 17.8	18.4	0.00193
		10.65	2.74	9.40 9.00 9.08	9.16	0.000962
		10.60	3.12	4.80 5.20 5.10	5.03	0.000528
		16.95	3.74	2.08 2.22 2.10	2.13	0.000224
		16.55	4.33	0.95 0.97 0.93	0.95	0.000100

TABLE VI (cont'd)

Test Run Data

Run	Description	ΔW gm.	h cm.	S	Avg. S	Avg. S_n
49	AG-16 t_s=2000°F S_o=10,100 R_B=0.17	20.30	0.62	215 220 226	220	0.0219
		6.35	0.81	93.0 91.7 90.8	91.8	0.00912
		6.45	1.01	38.2 38.2	38.2	0.00380
		6.50	1.21	17.2 16.9	17.0	0.00169
		3.90	1.33	10.3 10.8	10.5	0.00104
		3.85	1.45	7.00 6.65	6.80	0.000676
		3.95	1.56	4.53 4.58	4.55	0.000452
50	CG-16 t_s=2000°F S_o=10,100 R_B=0.10	4.85	0.161	531 534	532	0.0529
		4.35	0.305	52.1 34.1 34.1 49.0	42.3	0.00420
		4.60	0.458	1.70 2.90 2.75	2.12	0.000211
		4.20	0.600	0.27 0.63 0.33 0.47	0.43	0.000043
51	SS-1/8 t_s=2000°F S_o=10,100 R_B=0.24	67.70	0.79	242 236 213	230	0.0229*
		22.15	1.05	73.0 67.0 90.0 83.0	78.3	0.00778
		22.45	1.31	40.2 32.0 30.2 24.4	31.7	0.00315
		13.20	1.47	12.9 14.5 14.4	13.9	0.00138
		14.00	1.63	8.20 7.05 9.80 7.16	8.05	0.000800

TABLE VI (cont'd)

Test Run Data

Run	Description	ΔW gm.	h cm.	S	Avg. S	Avg. S_n
		13.85	1.79	3.65 4.06 4.16	3.96	0.000394
		13.70	1.96	2.53 2.36 2.14	2.34	0.000233
52	SS-3/16 t_s=2000°F S_o=9,520 R_B=0.24	88.0	1.05	289 390 366 294	335	0.0352*
		22.65	1.32	168 123 120	137	0.0144
		22.70	1.59	67.0 67.8 65.5	66.8	0.00701
		22.15	1.85	31.9 36.1 38.5 31.0	34.4	0.00361
		22.70	2.12	14.8 18.0 16.4	16.4	0.00172
		22.55	2.39	8.90 8.60 8.40	8.63	0.000906
		30.90	2.76	3.96 3.78 3.66 3.51	3.73	0.000392

NOTE: Some data points were thought to be redundant or were evidently out of line with respect to other points of the same run. These points were considered to be invalid and have been marked by an asterisk, *, in the above table. They were not included in regression calculations.

Temperature Response Data

Data for the response of the detector and amplification system are presented below. R denotes the measured signal corresponding to a source temperature of T_S. Signals are expressed as output-meter readings, normalized to unit attenuation of the amplifier. The data was obtained with a 2-1/2" source opening (in the bottom shield), 3" length bed tube, mesh 18 support screen, and with the bed frame at a distance of 95 cm above the bottom shield. These data are plotted on Figure 14.

TABLE VII

TEMPERATURE RESPONSE DATA

Source Temperature (T_S)		Measured Signal
°F	°R	R
915	1375	52.4
1187	1647	114
1402	1862	189
1464	1924	208
1704	2164	335

Linearity Check Data

Data for the linearity check on the measurement system are presented below. All measurements were made at a source temperature of 354°F. Source opening (in the bottom shield) was 1/2 inch in diameter. The distance between this opening and the detector is tabulated under "Distance", in units of centimeters. The corresponding signal measured is given in terms of output-meter readings, R_m. These data are plotted on Figure 13.

TABLE VIII

LINEARITY CHECK DATA

Distance, cm	Measured Signal, R_m
8	605
12	290
12	287
18	142
26	74.0
34	44.5
46	25.0
60	14.7
80	8.4
100	5.0
116	3.9

Screen Ratio Calibration Data

Calibration data for the standard ratio, F_s, are presented below. The notations of the headings are:

t_s = temperature of source, °F

Opening = diameter of source opening in bottom shielf, inches

Setting = setting of bed holder on mounting track

S_o = incident flux intensity measured without standard screen

S_o^* = incident flux intensity measured through standard screen

$F_s = S_o \div S_o^*$

Avg. F_s = the average value of F_s for one source temperature

TABLE IX

SCREEN RATIO CALIBRATION DATA

t_s, °F	Opening	Setting	S_o	S_o^*	F_s	Avg. F_s
570	0.50	35	99.8	18.8	5.31	5.46
	0.75		300	55.3	5.42	
	2.50		995	182	5.47	
			800	145	5.52	
	0.50	40	1000	181	5.52	
	0.75		1005	182	5.52	
	2.50		1000	180	5.52	
			845	152	5.56	
		50	1000	182	5.52	
			500	91.0	5.49	
		90	299	55.5	5.39	
			645	117	5.51	
			200	36.8	5.43	
		110	100	18.6	5.38	
			149	27.7	5.38	
	0.75		29.6	5.40	5.48	
677	2.50	50	552	97.3	5.67	5.67
			992	174	5.70	
			541	95.1	5.69	
			985	174	5.66	
			429	76.0	5.64	
			1000	175	5.71	
			410	72.9	5.63	

TABLE IX (CONT'D)

t_s, °F	Opening	Setting	S_o	S_o*	F_s	Avg. F_s
800	2.50	50	674	115	5.86	5.82
			1000	173	5.78	
			648	111	5.84	
			856	147	5.82	
			884	152	5.82	
1020	2.50	65	990	172	5.76	5.77
	0.75		100	17.9	5.59	
	0.50		100	17.7	5.65	
	2.50	70	845	146	5.79	
	0.75		299	52.5	5.70	
	0.50		95.5	16.5	5.79	
	2.50	80	802	138	5.81	
		95	504	87.7	5.75	
	0.75		222	37.5	5.92	
	0.50		97.5	16.5	5.91	
	2.50	115	995	175	5.69	
			475	83.4	5.68	
	0.75		94.0	16.0	5.88	
	0.50		46.5	7.80	5.96	
	2.50		900	157	5.73	
1200	0.75	50	982	171	5.74	5.78
	2.50	90	802	138	5.81	
			810	139	5.83	
	0.75	50	252	43.9	5.74	
1400	2.50	110	900	160	5.63	5.72
	0.75		75.5	13.2	5.72	
		80	284	50.0	5.68	
	0.50	50	206	36.0	5.72	
	0.75		1003	172	5.83	
1465	0.75	70	990	168	5.89	5.86
	0.50		574	96.5	5.95	
	2.50	110	1023	178	5.75	
	0.75		270	46.0	5.87	
	0.50		52.5	8.95	5.85	
1700	0.75	110	296	51.0	5.80	5.83
	0.50		68.1	11.5	5.92	
	0.75	80	800	137	5.84	
	0.50		138	23.8	5.80	
	0.75	60	970	167	5.81	
	0.50		1000	172	5.81	

TABLE IX (CONT'D)

t_s, °F	Opening	Setting	S_o	S_o*	F_s	Avg. F_s
1710	0.75	110	272	46.5	5.85	5.83
	0.50		282	48.3	5.90	
	0.75	80	493	84.8	5.81	
	0.50		710	120	5.92	
	0.75	60	1000	173	5.78	
	0.50		196	34.2	5.73	
1800	0.75	50	980	171	5.73	5.80
			710	122	5.82	
			1000	173	5.78	
			599	102	5.87	
2000	0.75	50	908	157	5.78	5.78

Screen Temperature Calibration Data

Data for calibration of input signal measured through standard screen, S_o^*, as a function of source temperature are presented below. All measurements were with mesh 30 support screen. Parameters of two different bed tubes are presented. These data are plotted on Figure 21.

TABLE X

Screen Temperature Calibration Data

Bed Tube Length, inches	Source Temperature t_s, °F	Source Temperature T_s^4, °R^4	Signal S_o^*
3	678	1.68×10^{12}	76
	798	2.50	115
	1200	7.59	355
	1599	18.0	850
	1696	21.6	1020
4	677	1.67×10^{12}	73
	800	2.52	111
	1200	7.59	339
	1599	18.0	810
	1696	21.6	971

TRANSMISSION VALUES FROM REGRESSION

At any packing height, h, the transmission of modulated flux may be calculated by Equation (115), using the converged values of s_b and a obtained by regression. These calculated transmissions, $S_n'(h)$, are tabulated below and compared to the experimentally measured transmissions, $S_n(h)$. The difference, $S_n - S_n'$, is then a measure of the fit obtained by the regressed transmission curves. The values of S_n are plotted as data points and the values of S_n' are represented by solid curves on Figures 22-33. Standard deviations, δ_s, are also tabulated below.

Table XI

Transmission Values from Regression

Run	s_b, ft^{-1}	a, ft^{-1}	δ_s, %	h, cm.	S_n	S_n'	$S_n - S_n'$
7	977	0.390	5.07	1.01	.0282	.0259	.0023
				1.95	.00904	.00966	-.00062
				2.83	.00415	.00426	-.00011
				3.72	.00189	.00189	.00000
				4.54	.00093	.00090	.00003
8	878	0.209	2.14	1.97	.0134	.0135	-.0001
				2.85	.00724	.00731	-.00007
				3.70	.00432	.00421	.00011
				4.57	.00246	.00242	.00004
				5.51	.00129	.00134	-.00005
				6.46	.000750	.000737	.000013
9	952	0.178	3.33	2.29	.0106	.0101	.0005
				3.24	.00517	.00547	-.00030
				4.21	.00304	.00300	.00004
				5.19	.00165	.00166	-.00001
				6.27	.000870	.000861	.000009
10	343	0.969	3.81	1.01	.0690	.0703	-.0013
				1.83	.0301	.0308	-.0007
				2.54	.0165	.0164	.0001
				3.07	.0108	.0104	.0004
				3.59	.00703	.00669	.00034
				4.12	.00449	.00427	.00022
				4.64	.00257	.00275	-.00018
				5.45	.00134	.00138	-.00004
				6.26	.000711	.000697	.000014

Table XI (Cont'd)

Transmission Values from Regression

Run	s_b, ft^{-1}	a, ft^{-1}	δ_s, %	h, cm.	S_n	S_n'	S_n-S_n'
11	298	0.521	1.99	1.03	.0874	.0843	.0031
				1.91	.0406	.0410	-.0004
				2.76	.0229	.0235	-.0006
				3.36	.0159	.0163	-.0004
				3.97	.0114	.0113	.0001
				4.58	.00816	.00793	.00023
				5.27	.00529	.00531	-.00002
				5.95	.00355	.00358	-.00003
				6.82	.00218	.00216	.00002
12	296	0.437	3.46	1.20	.0784	.0732	.0052
				2.17	.0339	.0360	-.0021
				2.95	.0229	.0226	.0003
				3.72	.0149	.0147	.0002
				4.47	.00973	.00981	-.00008
				5.24	.00641	.00650	-.00009
				6.02	.00417	.00430	-.00013
				6.78	.00290	.00288	.00002
				7.74	.00178	.00173	.00005
13	342	0.884	1.47	1.01	.0734	.0714	.0020
				1.90	.0297	.0301	-.0004
				2.61	.0162	.0165	-.0003
				3.15	.0106	.0106	.0000
				3.67	.00694	.00695	-.00001
				4.50	.00360	.00355	.00005
				5.37	.00176	.00176	.00000
14	373	0.843	1.46	0.940	.0732	.0714	.0018
				1.85	.0286	.0287	-.0001
				2.75	.0129	.0132	-.0003
				3.45	.00732	.00739	-.00007
				3.98	.00477	.00477	.00000
				4.78	.00248	.00247	.00001
				5.59	.00128	.00127	.00001
15	190	1.54	0.647	1.01	.121	.119	.002
				1.95	.0490	.0493	-.0003
				2.86	.0231	.0233	-.0002
				3.68	.0120	.0120	.0000
				4.39	.00684	.00683	.00001
				5.10	.00387	.00388	-.00001
				5.91	.00204	.00204	.00000
				6.73	.00106	.00106	.00000
				7.62	.000524	.000522	.000002

Table XI (Cont'd)

Transmission Values from Regression

Run	s_b, ft^{-1}	a, ft^{-1}	δ_s, %	h, cm.	S_n	S_n'	$S_n - S_n'$
16	149	0.988	1.85	1.98	.0727	.0736	-.0009
				2.93	.0396	.0406	-.0010
				3.79	.0250	.0245	.0005
				4.48	.0169	.0165	.0004
				5.17	.0115	.0112	.0003
				6.04	.00678	.00683	-.00005
				6.90	.00415	.00420	-.00005
				7.83	.00244	.00249	-.00005
				8.79	.00146	.00145	.00001
17	151	0.812	1.33	2.29	.0620	.0626	-.0006
				3.27	.0357	.0359	-.0002
				4.04	.0240	.0238	.0002
				4.82	.0163	.0158	.0005
				5.59	.0106	.0106	.0000
				6.36	.00706	.00714	-.00008
				7.33	.00428	.00434	-.00006
				8.29	.00267	.00265	.00002
18	496	2.74	2.93	1.27	.0229	.0218	.0011
				1.75	.00933	.00950	-.00017
				2.16	.00464	.00470	-.00006
				2.56	.00227	.00237	-.00010
				2.97	.00118	.00118	.00000
				3.36	.000601	.000603	-.000002
				3.78	.000304	.000294	-.000010
20	1188	1.06	5.16	1.41	.00892	.00802	.00090
				1.76	.00441	.00448	-.00007
				2.13	.00231	.00243	-.00012
				2.50	.00126	.00132	-.00006
				2.86	.000717	.000730	-.000013
				3.41	.000295	.000295	.000000
				3.96	.000126	.000119	.000007
21	906	1.00	4.38	1.94	.00640	.00598	.00042
				2.35	.00334	.00336	-.00002
				2.75	.00192	.00192	.00000
				3.15	.00103	.00109	-.00006
				3.53	.000622	.000643	-.000021
				4.19	.000252	.000255	-.000003
				4.87	.000105	.0000986	.0000064
22	682	1.96	5.96	1.33	.0157	.0149	.0008
				1.73	.00787	.00748	.00039
				2.13	.00355	.00378	-.00023
				2.53	.00176	.00192	-.00016
				2.94	.000973	.000956	.000017
				3.71	.000274	.000259	.000015

Table XI (Cont'd)

Transmission Values from Regression

Run	s_b, ft^{-1}	a, ft^{-1}	δ_s, %	h, cm.	S_n	S_n'	$S_n - S_n'$
18	496	2.74	2.93	1.27	.0229	.0218	.0011
				1.75	.00933	.00950	-.00017
				2.16	.00464	.00470	-.00006
				2.56	.00227	.00237	-.00010
				2.97	.00118	.00118	.00000
				3.36	.000601	.000603	-.000002
				3.78	.000304	.000294	-.000010
20	1188	1.06	5.16	1.41	.00892	.00802	.00090
				1.76	.00441	.00448	-.00007
				2.13	.00231	.00243	-.00012
				2.50	.00126	.00132	-.00006
				2.86	.000717	.000730	-.000013
				3.41	.000295	.00295	.000000
				3.96	.000126	.000119	.000007
21	906	1.00	4.38	1.94	.00640	.00598	.00042
				2.35	.00334	.00336	-.00002
				2.75	.00192	.00192	.00000
				3.15	.00103	.00109	-.00006
				3.53	.000622	.000643	-.000021
				4.19	.000252	.000255	-.000003
				4.87	.000105	.0000986	.0000064
22	682	1.96	5.96	1.33	.0157	.0149	.0008
				1.73	.00787	.00748	.00039
				2.13	.00355	.00378	-.00023
				2.53	.00176	.00192	-.00016
				2.94	.000973	.000956	.000017
				3.71	.000274	.000259	.000015
23	450	13.1	8.43	1.05	.00923	.00888	.00035
				1.21	.00549	.00500	.00049
				1.37	.00265	.00282	-.00017
				1.53	.00157	.00159	-.00002
				1.79	.000584	.000627	-.000043
				1.96	.000315	.000341	-.000026
				2.22	.000159	.000134	.000025
24	370	6.66	6.26	1.69	.00675	.00633	.00042
				1.96	.00335	.00339	-.00004
				2.22	.00189	.00186	.00003
				2.49	.000897	.000996	-.000099
				2.76	.000525	.000533	-.000008
				3.12	.000253	.000232	.000021

Table XI (Cont'd)

Transmission Values from Regression

Run	s_b, ft^{-1}	a, ft^{-1}	δ_s, %	h, cm.	S_n	S_n'	$S_n - S_n'$
25	789	2.05	8.41	1.58	.00770	.00704	.00066
				1.98	.00343	.00333	.00010
				2.36	.00156	.00164	-.00008
				2.74	.000727	.000804	-.000077
				3.12	.000376	.000396	-.000020
				3.72	.000149	.000129	.000020
26	779	12.7	4.58	0.420	.0473	.0439	.0034
				0.620	.0162	.0172	-.0010
				0.930	.00406	.00408	-.00002
				1.05	.00234	.00234	.00000
				1.25	.000887	.000927	-.000040
				1.37	.000527	.000532	-.000005
				1.49	.000325	.000305	.000020
27	420	272.	25.2	0.160	.0640	.0494	.0146
				0.310	.00295	.00330	-.00035
				0.460	.000180	.000221	-.000041
				0.600	.0000280	.0000176	.0000104
28	153	1.88	0.784	1.72	.0729	.0729	.0000
				2.62	.0345	.0345	.0000
				3.43	.0181	.0181	.0000
				4.25	.00945	.00943	.00002
				5.07	.00495	.00494	.00001
				5.87	.00260	.00262	-.00002
				6.58	.00148	.00150	-.00002
				7.49	.000742	.000731	.000011
29	114	1.33	0.734	1.97	.0925	.0921	.0004
				2.91	.0507	.0509	-.0002
				3.78	.0301	.0304	-.0003
				4.65	.0184	.0184	.0000
				5.51	.0113	.0112	.0001
				6.20	.00753	.00753	.00000
				7.16	.00438	.00434	.00004
				7.84	.00291	.00294	-.00003
30	114	1.08	0.909	1.95	.0982	.0981	.0001
				2.93	.0553	.0552	.0001
				3.91	.0324	.0325	.0000
				4.86	.0197	.0197	.0000
				5.63	.0130	.0132	-.0002
				6.41	.00894	.00881	.00013
				7.18	.00585	.00592	-.00007
				7.94	.00403	.00400	.00003

Table XI (Cont'd)

Transmission Values from Regression

Run	s_b, ft^{-1}	a, ft^{-1}	δ_s, %	h, cm.	S_n	S_n'	$S_n - S_n'$
31	483	2.70	7.27	1.27	.0260	.0229	.0031
				1.75	.0102	.0101	.0001
				2.16	.00503	.00509	-.00006
				2.56	.00235	.00260	-.00025
				2.97	.00120	.00131	-.00011
				3.36	.000682	.000679	.000003
				3.78	.000347	.000336	.000011
				4.18	.000188	.000172	.000016
32	860	1.49	4.26	1.41	.0115	.0107	.0008
				1.76	.00600	.00597	.00003
				2.13	.00317	.00322	-.00005
				2.50	.00164	.00174	-.00010
				2.86	.000931	.000957	-.000026
				3.43	.000368	.000371	-.000003
				3.98	.000158	.000149	.000009
33	682	1.32	4.40	1.94	.00849	.00785	.00064
				2.35	.00436	.00442	-.00006
				2.75	.00249	.00253	-.00004
				3.15	.00140	.00145	-.00005
				3.53	.000812	.000851	-.000039
				4.19	.000334	.000339	-.000005
				4.87	.000140	.000131	.000009
34	614	2.18	5.45	1.33	.0179	.0163	.0016
				1.74	.00807	.00807	.00000
				2.14	.00382	.00408	-.00026
				2.55	.00196	.00203	-.00007
				2.94	.00106	.00105	.00001
				3.35	.000498	.000521	-.000023
				4.12	.000151	.000141	.000010
35	1090	1.16	10.2	1.58	.00788	.00659	.00129
				1.98	.00353	.00340	.00013
				2.36	.00173	.00182	-.00009
				2.74	.000838	.000973	-.000135
				3.12	.000490	.000521	-.000031
				3.74	.000197	.000188	.000009
				4.33	.0000790	.0000711	.0000079
36	811	10.6	4.77	0.620	.0206	.0190	.0016
				0.810	.00819	.00834	-.00015
				1.01	.00331	.00351	-.00020
				1.21	.00140	.00148	-.00008
				1.33	.000880	.000881	-.000001
				1.45	.000539	.000524	.000015
				1.56	.000341	.000326	.000015

Table XI (Cont'd)

Transmission Values from Regression

Run	s_b, ft^{-1}	a, ft^{-1}	δ_s, %	h, cm.	S_n	S_n'	$S_n - S_n'$
37	1054	107	18.6	0.160	.0619	.0460	.0159
				0.310	.00334	.00418	-.00084
				0.460	.000403	.000380	.000023
				0.600	.0000440	.0000407	.0000033
38	387	17.0	4.71	1.05	.00803	.00824	-.00021
				1.31	.00324	.00306	.00018
				1.47	.00172	.00167	.00005
				1.63	.000877	.000908	-.000031
				1.79	.000463	.000494	-.000031
				1.96	.000274	.000259	.000015
39	322	8.70	7.57	1.32	.0151	.0143	.0008
				1.59	.00776	.00731	.00045
				1.85	.00365	.00385	-.00020
				2.12	.00178	.00197	-.00019
				2.39	.000986	.00101	-.000024
				2.76	.000457	.000406	.000051
40	149	0.804	2.09	2.29	.0647	.0636	.0011
				3.26	.0376	.0366	.0010
				4.04	.0238	.0244	-.0006
				4.82	.0162	.0163	-.0001
				5.59	.0107	.0110	-.0003
				6.36	.00722	.00740	-.00018
				7.33	.00461	.00451	.00010
				8.29	.00282	.00277	.00005
41	129	2.21	1.67	1.72	.0856	.0839	.0017
				2.62	.0394	.0399	-.0005
				3.43	.0212	.0209	.0003
				4.25	.0108	.0109	-.0001
				5.07	.00569	.00574	-.00005
				5.87	.00299	.00306	-.00007
				6.58	.00175	.00175	.00000
				7.49	.000879	.000856	.000023
42	95.0	1.59	0.886	1.97	.106	.107	-.001
				2.91	.0591	.0593	-.0002
				3.78	.0361	.0355	.0006
				4.65	.0216	.0214	.0002
				5.51	.0130	.0131	-.0001
				6.20	.00875	.00881	-.00006
				7.16	.00504	.00508	-.00004
				7.84	.00347	.00344	.00003

Table XI (Cont'd)

Transmission Values from Regression

Run	s_b, ft^{-1}	a, ft^{-1}	δ_s, %	h, cm.	S_n	S_n'	S_n-S_n'
43	96.8	1.24	0.556	2.93	.0636	.0639	-.0003
				3.91	.0383	.0379	.0004
				4.86	.0230	.0232	-.0002
				5.63	.0156	.0156	.0000
				6.41	.0105	.0105	.0000
				7.18	.00705	.00708	-.00003
				7.94	.00482	.00481	.00001
44	449	2.84	6.25	1.27	.0275	.0248	.0027
				1.75	.0107	.0111	-.0004
				2.16	.00502	.00561	-.00059
				2.56	.00290	.00289	.00001
				2.97	.00158	.00146	.00012
				3.36	.000785	.000766	.000019
				3.78	.000373	.000382	-.000009
				4.18	.000198	.000197	.000001
45	847	1.47	6.72	1.41	.0124	.0111	.0013
				1.76	.00637	.00622	.00015
				2.13	.00338	.00338	.00000
				2.50	.00172	.00184	-.00012
				2.86	.000944	.00102	-.000076
				3.43	.000388	.000401	-.000013
				3.98	.000161	.000163	-.000002
				4.53	.0000740	.0000660	.0000080
46	576	1.54	8.45	1.28	.0280	.0238	.0042
				1.94	.00924	.00934	-.00010
				2.35	.00503	.00528	-.00025
				2.75	.00299	.00304	-.00005
				3.15	.00163	.00175	-.00012
				3.53	.000947	.00103	-.000083
				4.19	.000417	.000414	.000003
				4.87	.000187	.000162	.000025
47	496	2.77	5.22	1.33	.0208	.0194	.0014
				1.74	.00960	.00953	.00007
				2.14	.00476	.00478	-.00002
				2.55	.00224	.00236	-.00012
				2.94	.00111	.00120	-.00009
				3.35	.000605	.000594	.000011
				4.12	.000169	.000158	.000011
48	1010	1.20	12.4	1.58	.00906	.00723	.00183
				1.98	.00392	.00377	.00015
				2.36	.00193	.00203	-.00010

Table XI (Cont'd)

Transmission Values from Regression

Run	s_b, ft^{-1}	a, ft^{-1}	δ_s, %	h, cm.	S_n	S_n'	S_n-S_n'
				2.74	.000962	.00110	-.000138
				3.12	.000528	.000594	-.000066
				3.74	.000224	.000218	.000006
				4.33	.000100	.0000837	.0000163
49	837	9.37	5.31	0.620	.0219	.0202	.0017
				0.810	.00912	.00920	-.00008
				1.01	.00380	.00404	-.00024
				1.21	.00169	.00177	-.00008
				1.33	.00104	.00108	-.00004
				1.45	.000676	.000659	.000017
				1.56	.000452	.000419	.000033
50	627	192	27.3	0.160	.0529	.0494	.0035
				0.310	.00420	.00370	.00050
				0.460	.000211	.000277	-.000066
				0.600	.0000430	.0000247	.0000183
51	343	20.5	6.97	1.05	.00778	.00785	-.00007
				1.31	.00315	.00281	.00034
				1.47	.00138	.00149	-.00011
				1.63	.000800	.000794	.000006
				1.79	.000394	.000422	-.000028
				1.96	.000233	.000215	.000018
52	314	9.26	4.37	1.32	.0144	.0138	.0006
				1.59	.00701	.00699	.0002
				1.85	.00361	.00363	-.00002
				2.12	.00172	.00184	-.00012
				2.39	.000906	.000930	-.000024
				2.76	.000392	.000366	.000026

PROPERTIES OF TEST PACKINGS

Some properties of the test particles are listed below. These are the values used in the correlations presented previously. Many of the properties had to be estimated from limited data available in the literature. Reference numbers are given for such items. Some bulk properties were determined experimentally and these are marked by a superscript "e". Other properties were obtained from manufacturer's specifications. These are marked by a superscript "m".

D_p = nominal equivalent diameter, ft.

Material = basic material of solid particle.

k_s = conductivity of solid particle, Btu/hr.ft.°F.

ϵ = emissivity of solid particle.

ρ_s = density of solid particle, gm./cc.

ρ_B = bulk density of randomly packed particles, gm/cc.

δ_p = void fraction of packing.

TABLE XII

PROPERTIES OF TEST PACKINGS

Particle	Material	D_p	800°F k_s	800°F ϵ	1200°F k_s	1200°F ϵ	1600°F k_s	1600°F ϵ	1800°F k_s	1800°F ϵ	2000°F k_s	2000°F ϵ	ρ_s	ρ_B	δ_p
GS-3	boro-silicate glass[m]	0.0098[m]	0.63[24]	0.9[24]	0.63[24]	0.8[24]	0.63[24]		0.63[24]		0.63[24]		2.23[28]	1.45[e]	0.35[e]
GS-4		0.0131[m]												1.45[e]	0.35[e]
GS-5		0.0164[m]												1.36[e]	0.39[e]
AS-3/16	Al_2O_3[m]	0.0157[m]					2.22[25]	0.32[25]	2.29[25]	0.28[25]	2.36[25]	0.28[25]	3.95[25]	2.01[e]	0.49[e]
AP-1/8		0.0104[m]												1.34[e]	0.66[e]
AP-5/32		0.0130[m]												1.21[e]	0.69[e]
AP-3/16		0.0157[m]												1.29[e]	0.67[e]
SS-1/8	carbon steel[m]	0.0104[m]					17[24]	0.5[24]	16[24]	0.6[24]	15[24]	0.6[24]	7.83[16]	4.76[e]	0.39[e]
SS-3/16		0.0157[m]												4.72[e]	0.40[e]
AG-4	Al_2O_3[m]	0.0216[m]					2.22[25]	0.32[25]	2.29[25]	0.28[25]	2.36[25]	0.28[25]	3.95[26]	1.55[e]	0.61[e]
AG-16		0.0056[m]												1.83[e]	0.54[e]
CG-16	SiC[m]	0.0056[m]					8.75[25]	0.88[25]	8.25[25]	0.91[25]	7.75[25]	0.92[25]	3.20[26]	1.68[e]	0.48[e]

COMPUTER PROGRAMS

Data regression for values of the attenuation cross sections was performed on an IBM 704 digital computer. The necessary equations have been developed in a previous section. The actual programs are presented here. Computation was carried out in two parts:

a. regression on Equation (115) for values of a_n and m,

b. calculation of S_b and a from the converged values of a_n and m by Equations (174) and (175).

Schematic flow diagrams and Fortran statements of the programs are presented below.

FLOW DIAGRAM FOR ITERATIVE REGRESSION:

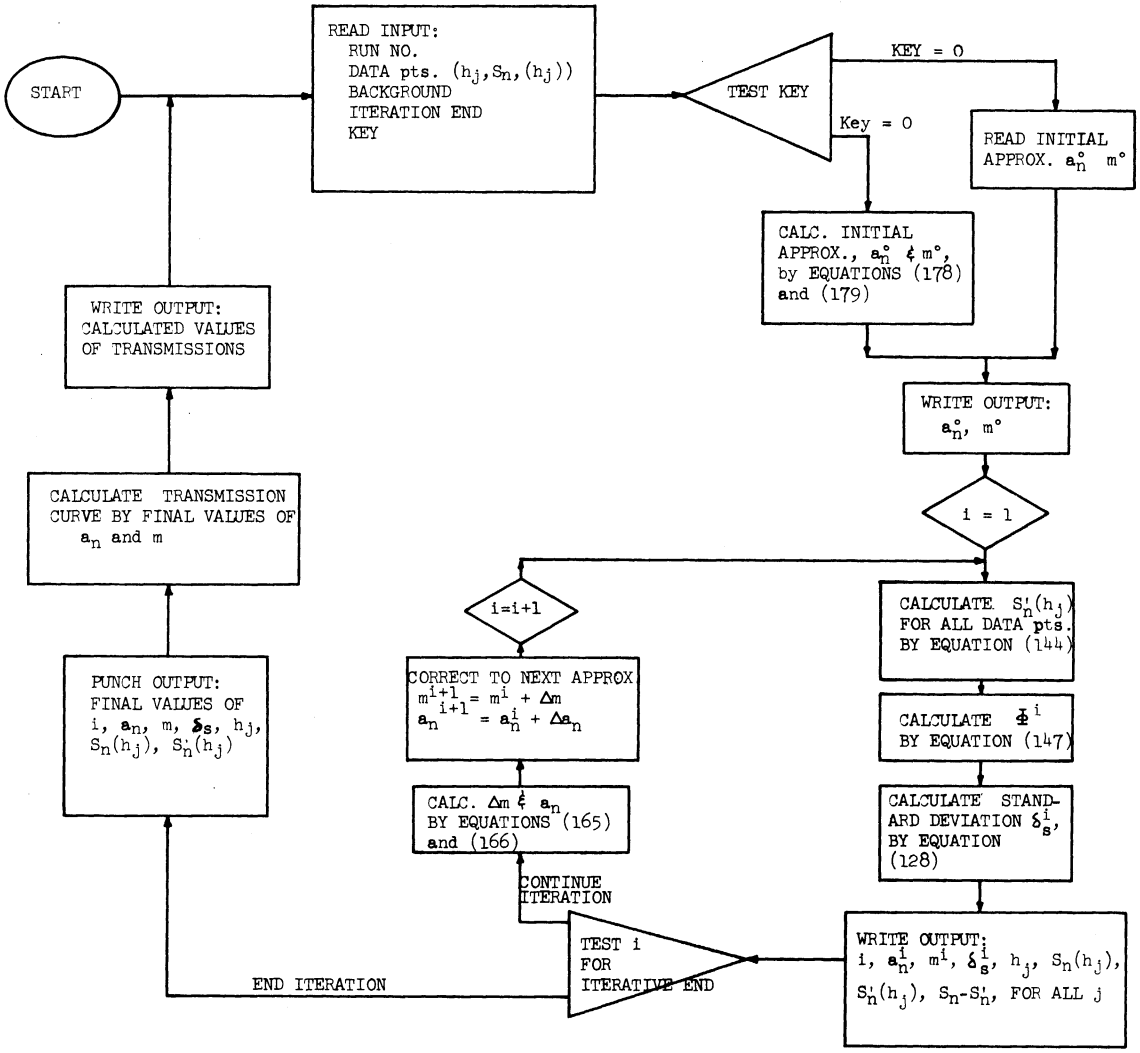

FLOW DIAGRAM FOR CALCULATION OF CROSS SECTIONS:

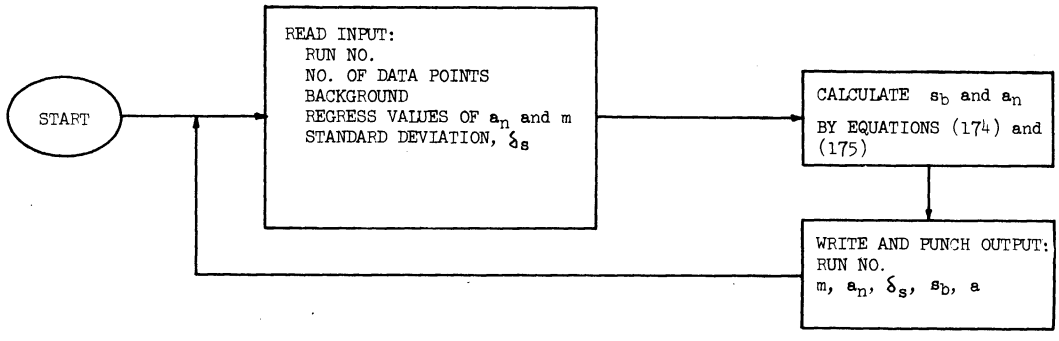

FORTRAN STATEMENTS FOR REGRESSION PROGRAM

```
    DIMENSION H(20),S(20),F(20),CH(20),SH(20),FN(20),DIF(20),R(20),
   X          A(100),B(100),PHE(100)
55  READ INPUT TAPE 7,3,NUR,NH,BG
    READ INPUT TAPE 7,4,(H(J),F(J),J=1,NH)
    READ INPUT TAPE 7,10,KEY,ITF,ITN
    WRITE OUTPUT TAPE 6,5,NUR
    WRITE OUTPUT TAPE 6,6,NH,BG,ITN
    FNH = NH
    DO 99 J=1,NH
99  R(J) = 1.0 /(F(J)*F(J))
    I = 1
    IF (KEY)  57,56,57
56  K = NH
    J = NH - 2
    B(I) = ELOG(F(J)/F(K)) / (H(K)-H(J))
    EP = EXP(B(I)*H(K))
    A(I) = 2.0*B(I) / (EP*F(K)) - B(I)
    GO TO 58
57  READ INPUT TAPE 7,8,A(I),B(I)
58  WRITE OUTPUT TAPE 6,12,KEY,ITF,A(I),B(I)
59  PHE(I) = 0.0
    DO 98 J=1,NH
    EP = EXP(B(I)*H(J))
    EN = 1.0/EP
    CH(J) = 0.5*(EP+EN)
    SH(J) = 0.5*(EP-EN)
    FN(J) = B(I)/(B(I)*CH(J)+A(I)*SH(J))
```

```
      DIF(J) = F(J) - FN(J)
98    PHE(I) = PHE(I) + (DIF(J)*DIF(J)*R(J))
      ARG = PHE(I)/FNH
      SD = 100.0*SQRT(ARG)
      M = ITF + I - 1
      WRITE OUTPUT TAPE 6,11,M,A(I),B(I),SD
      WRITE OUTPUT TAPE 6,13,(H(J),F(J),FN(J),DIF(J),J=1,NH)
      IF (M-ITN) 60,65,65
60    SDB = 0.0
      SDA = 0.0
      SAB = 0.0
      SAA = 0.0
      SBB = 0.0
      DO 97  J=1,NH
      DEN = (B(I)*CH(J)+A(I)*SH(J)) * (B(I)*CH(J)+A(I)*SH(J))
      PA = B(I)*SH(J)/DEN
      PB = (B(I)*A(I)*H(J)*CH(J)+(B(I)*B(I)*H(J)-A(I))*SH(J))/DEN
      DA = -DIF(J)*PA*R(J)
      DB = -DIF(J)*PB*R(J)
      AB = PA*PB*R(J)
      AA = PA*PA*R(J)
      BB = PB*PB*R(J)
      SDA = SDA + DA
      SDB = SDB + DB
      SAB = SAB + AB
      SAA = SAA + AA
97    SBB = SBB + BB
      CA = SBB*SDA - SAB*SDB
      CB = SDB*SAA - SDA*SAB
```

```
      C   = SBB*SAA - SAB*SAB
      DELA = CA/C
      DELB = CB/C
      WRITE OUTPUT TAPE 6,16,SDA,SDB,SAB,SAA,SBB,CA,CB,C,DELA,DELB
      K = I+1
      A(K) = A(I) + DELA
      B(K) = B(I) + DELB
      I = K
      GO TO 59
   65 X = FNH / (FNH-1.0)
      V = SD * SQRT(X)
      WRITE OUTPUT TAPE 6,5,NUR
      WRITE OUTPUT TAPE 6,6,NH,BG,ITN
      WRITE OUTPUT TAPE 6,11,M,A(I),B(I)
      WRITE OUTPUT TAPE 6,11,M,SD,V
      WRITE OUTPUT TAPE 6,13, (H(J),F(J),FN(J),DIF(J),J=1,NH)
      HT = 0.0
      WRITE OUTPUT TAPE 6,5,NUR
      WRITE OUTPUT TAPE 6,11,M,A(I),B(I)
      DO 95 L=1,40
      EP = EXP(B(I)*HT)
      EN = 1.0/EP
      CSH = 0.5*(EP+EN)
      SNH = 0.5*(EP-EN)
      T = B(I) / (B(I)*CSH+A(I)*SNH)
      IF (T-0.000001) 70,71,71
   71 WRITE OUTPUT TAPE 6,9,HT,T
   95 HT = HT + 0.25
   70 PUNCH 3,NUR,NH,BG
```

```
      PUNCH 8,A(I),B(I)
      PUNCH 8,SD,V
      PUNCH 14,(H(J),F(J),FN(J),J=1,NH)
      GO TO 55
    3 FORMAT (2I7,F15.6)
    4 FORMAT (F9.2,F18.6)
    5 FORMAT (1H134H                                        RUN   I7 )
    6 FORMAT (1H0//16H      DATA POINTS I5/15H      BACKGROUND F9.4/
     X          14H      ITERATION I5)
    7 FORMAT (1H 7E17.8)
    8 FORMAT (3E20.8)
    9 FORMAT (1H F20.2,F20.6)
   10 FORMAT (3I7)
   11 FORMAT (1H0 // I7,4E20.8)
   12 FORMAT (1H0 2I7,2E20.8)
   13 FORMAT (1H0 4E17.8/(1H 4E17.8))
   14 FORMAT (3E17.8)
   15 FORMAT (1H F27.2,F47.6)
   16 FORMAT (1H /5E17.8/5E17.8)
```

FORTRAN STATEMENTS FOR CROSS SECTION PROGRAM

```
55   READ INPUT TAPE 7,3,NUR,NH,BG
     READ INPUT TAPE 7,8,A,B
     READ INPUT TAPE 7,8,SD,V
     SB = SQRT (A*A-B*B)
     AA = A-SB
     WRITE OUTPUT TAPE 6,5,NUR
     WRITE OUTPUT TAPE 6,6,B,A,SB,AA,NH,SD,BG
     PUNCH 3,NUR,NH,BG
     PUNCH 8,A,B
     PUNCH 8,SB,AA
     GO TO 55
 3   FORMAT (2I7,F15.6)
 5   FORMAT (1H134H                                        RUN   I7 )
 8   FORMAT (3E20.8)
 6   FORMAT ( 1H0//20H           K CONSTANT F34.5//
    X 35H           ATTENUATION CROSS SECTION F19.5//
    X 39H           BACK SCATTERING CROSS SECTION F15.5//
    X 34H           ABSORPTION CROSS SECTION F20.5//
    X 21H           DATA POINTS I27//
    X 28H           STANDARD DEVIATION F23.2, 11H   PER CENT //
    X 20H           BACKGROUND F35.6 )
```

NOMENCLATURE

A	Absorption cross section per unit volume for black body radiation; ft^2/ft^3.
A	Boundary constant, Equation (81).
A_t	Attenuation ratio on amplifier.
A_λ	Absorption cross section per unit volume for monochromatic radiation; ft^2/ft^3.
a	Bulk absorption cross section per unit volume; ft^2/ft^3.
a_d	Absorptivity of detector.
a_n	Net attenuation cross section per unit volume; $(a + s_b)$; ft^2/ft^3.
B	Boundary constant, Equation (82).
C	Boundary constant, Equation (83).
C_a	Dimensionless absorption parameter, $\frac{aDp}{1 - \delta p}$.
C_B	Bulk heat capacity; $\frac{Btu}{lb. \cdot {}^\circ F}$.
C_s	Dimensionless scattering parameter, $\frac{s_b Dp}{1-\delta p}$.
D	Boundary constant, Equation (84).
D	Determinant in regression solution, Equation (167).
D_a	Determinant in regression solution, Equation (169).
D_m	Determinant in regression solution, Equation (168).
D_p	Nominal particle diameter; ft.
E	Emission cross section per unit volume for black body radiation; ft^2/ft^3.
E_λ	Emission cross section per unit volume for monochromatic radiation; ft^2/ft^3.
F_s	Standard screen factor, $\left(\frac{S_o}{S_o^*}\right)$.
$f(\theta,\theta')$	Angular distribution function for black body radiation.
f_j^i	Calculated S_n for jth data point at ith iteration of data regression, Equation (148).
$f_\lambda(\theta,\theta')$	Angular distribution function for monochromatic radiation.

NOMENCLATURE (cont'd)

h	Packed bed height; ft. or cm.
I	Dimensionless forward flux intensity; Equation (53).
i	Forward flux intensity, Equation (21); $\frac{\text{Btu}}{\text{hr.ft.}^2}$.
i_e	Modulated forward flux intensity for experimental case; $\frac{\text{Btu}}{\text{hr.ft.}^2}$.
i_λ	Specific intensity for monochromatic radiation; $\frac{\text{Btu}}{\text{hr.ft.}^2\text{.steradian}}$.
i_∞	Specific intensity for black body radiation; Btu/hr.ft.^{2}.steradian.
J	Dimensionless backward flux intensity, Equation (53).
j	Backward flux intensity, Equation (22); Btu/hr.ft.^{2}.
j_e	Modulated backward flux intensity for experimental case; Btu/hr.ft.^{2}.
K	Function in Equation (129).
k_c	Bulk conduction-conductivity; Btu/hr.ft.°F.
k_{ir}	Bulk radiation-conductivity at internal points; Btu/hr.ft. °F.
k_r	Bulk radiation-conductivity; Btu/hr.ft.°F.
k_s	Conductivity of solid particles; Btu/hr.ft.°F.
L	Length of bed across packing; ft.
m	Attenuation parameter, $(\sqrt{a_n^2 + s_b^2})$; ft.^{2}/ft.^{3}.
n	Number of data points of a run.
p	Exponential power on temperature, Equation (134).
Q_c	Conduction heat transfer rate; Btu/hr.ft.^{2}.
Q_r	Radiation heat transfer rate; Btu/hr.ft.^{2}.
R	Output meter reading, normalized to unit attenuation.
R_b	Output meter reading for background signal, normalized to unit attenuation.
R_m	Output meter reading, unnormalized.
$\vec{r}$	Position vector, Figure 4.

NOMENCLATURE (cont'd)

S	Scattering cross section per unit volume for black body radiation; $ft.^2/ft.^3$.
$S(h)$	Modulated flux intensity transmitted through bed of height h; $Btu/hr.ft.^2$.
$S_n(h)$	Normalized transmitted flux intensity, $(S(h)/S_o)$, experimental value; $Btu/hr.ft.^2$.
$S'_n(h)$	Correlation value of $S_n(h)$; $Btu/hr.ft.^2$.
S_o	Incident modulated flux intensity; $Btu/hr.ft.^2$.
S_o^*	Value of S_o through standard screen; $Btu/hr.ft.^2$.
S_λ	Scattering cross section per unit volume for monochromatic radiation; $ft.^2/ft.^3$.
s_b	Bulk back scattering cross section per unit volume; $ft.^2/ft.^3$.
t_s, T_s	Source temperature; °F or °R.
t_1, T_1	Hot wall temperature; °F or °R.
t_2, T_2	Cold wall temperature; °F or °R.
V_T	Voltage signal due to modulated flux.
X	Dimensionless position, Equation (53).
x	Position coordinate, ft.
α	Dimensionless absorption coefficient, Equation (54).
β	Dimensionless back scattering coefficient, Equation (54).
γ	Dimensionless radiation-conduction ratio, Equation (54).
δ	Dimensionless temperature ratio, Equation (54).
δ_p	Void fraction of packed media.
δ_s	Standard deviation for transmission curves, Equation (128).
Δ_m	Maximum τ^4 error in Hamaker's approximation.
Δm^i	Correction to m in regression, Equation (145).
Δa_n^i	Correction to a_n in regression, Equation (145).

ΔW	Incremental packing sample weight; lbs. or gms.
ϵ	Emissivity of packing.
ϵ_s	Emissivity of source.
ϵ_w	Emissivity of source walls.
ϵ_1	Emissivity of hot wall (boundary).
ϵ_2	Emissivity of cold wall (boundary).
η	Dimensionless net attenuation parameter, $(\alpha + \beta)$.
Θ	Directional angle, Figure 5.
λ	Wave length of radiation; microns.
ρ_B	Bulk density of packed media; lb./ft.^{3}.
σ	Stephan-Boltzman constant; 1.713×10^{-9} Btu/hr.ft.^{2}°R^4.
τ	Dimensionless temperature, Equation (53).
τ_o	Base temperature for Hamaker's approximation, Equation (76); °F or °R.
Φ	Sum of errors squared, Equation (143).
ϕ	Azimuthal angle, Figure 5.
Ω	Solid angle; steradian.
$\vec{\Omega}$	Vectorial direction of flux propagation, Figure 5.

REFERENCES

1. Argo, W. B. and Smith, J. M. Chem. Eng. Prog., 49, 443 (1953).

2. Bell, J. C. Trans. Am. Foundrymen's Assoc., 56, 365, (1948).

3. Bosworth, R. C. L. Heat Transfer Phenomena. New York: John Wiley and Sons, Inc., (1952).

4. Bunnell, D. G., Irvin, H. B., Olson, R. W., and Smith, J. M. Ind. Eng. Chem., 41, 1977, (1949).

5. Campbell, J. M. and Huntington, R. L. Petroleum Refiner, 31, 123, (Feb., 1952).

6. Damköhler, G. "Der Chemic-Ingenieur." Eucken-Jakob, 3, Part I, 445 Akademische Verlagsgesellschaft M.B.H., Leipzig, (1937).

7. Deissler, R. Trans. ASME, 80, 1417, (1958).

8. Dickson, J. H. Glass. New York: Chemical Publishing Co., Inc., 1951.

9. Eucken, A. Beilage Zu Forschung auf dem Gebiete des Ingenieurwesens, Forshungsheft 353, Ausgabe B, (1932).

10. Glassman, I. and Bonilla, I. CEP Symposium Series No. 5, 49, 153, (1953).

11. Gorring, R. L. and Churchill, S. W. Paper presented at A.I.Ch.E. meeting, Washington, D.C., Dec. 1960.

12. Gouffé, A. Revue D'optique, 24, 1, (Jan.-Mar., 1945).

13. Hamaker, H. C. Philips Research Reports, 2, 55, 103, 112, 420, (1947).

14. Hellums, J. D. and Churchill, S. W. Paper presented at A.I.Ch.E.-A.S.M.E. Heat Transfer Conference, Buffalo, New York, 1960.

15. Hill, F. B. and Wilhelm, R. H. A.I.Ch.E. Journal, 5, 486, (1959).

16. Hodgman, C.D. ed., Handbook of Chem. and Phys., 33rd ed., Cleveland: Chemical-Rubber Publishing Co., 1952.

17. Horton, C. W. and Rogers, F. T. J. Applied Physics, 16, 367, (1945).

18. LaFara, R. L., Miller, E. L., Pearson, W. E., and Peoples, J. F. Tables of Blackbody Radiation and the Transmission Factor for Radiation through Water Vapor. Navord Report 3171, U.S. Naval Ordnance Plant, Indianapolis, 1955.

19. Lapwood, E. R. Proc. Camb. Phil. Soc., 44, 508, (1948).

20. Larkin, B. K. and Churchill, S. W. A.I.Ch.E. Journal, 5, 467, (1959).

21. Laubitz, M. J. Canadian J. of Phys., 37, No. 7, 798, (1959).

22. Lucks, C. F., Linebrink, O. L., and Johnson, K. L. Trans. Am. Foundrymen's Assoc., 55, 62, (1947).

23. Maxwell, J. Electricity and Magnetism, I, 314, Oxford: Oxford University Press, (1873).

24. McAdams, W. H. Heat Transmission. 3rd. ed., New York: McGraw-Hill Book Co., Inc., 1954.

25. Norton, F. H. Refractories. 3rd. ed., New York: McGraw-Hill Book Co., Inc., 1949.

26. "Refractory Grain - Properties and Applications." Norton Co., Worcester, 1959.

27. Nusselt, W. Zeitscher d. bayer Revisionsuer, Nos. 13 and 14, (1913).

28. Perry, J. H., ed., Chemical Engineer's Handbook. 3rd ed., New York: McGraw-Hill Book Co., Inc., 1950.

29. Rayleigh, L. Phil. Mag. V, 34, 481, (1892).

30. Rogers, F. T. and Morrison, H. L. Heat Transfer and Fluid Mechanics Inst., Stanford University Press, 1951.

31. Rosseland, S. Theoretical Astrophysics. Oxford: The Clarendon Press, 1936.

32. Russell, H. W. J. Am. Ceramic Soc., 18, 1, (1935).

33. Schotte, W. "Thermal Conductivity of Insulating Powders." Eng. Res. Lab., E.I.duPont de Nemours and Co., Wilmington, Delaware, 1958.

34. Schumann, T. E. W. and Voss, V. Fuel, 13, 249, (1934).

35. Van der Held, E. F. M. Appl. Sc. Res., A3, 237, (1952), and A4, 77, (1953).

36. Waddams, A. L. Chem. and Ind., 206, (1944).

37. Waddams, A. L. J. Soc. Chem. Ind., 63, 337, (1944).

38. Wilhelm, R. H., Johnson, W. L., Wynkoop, R., and Collier, D. W. Chem. Eng. Prog., 44, 105, (1948).

39. Woodside, W. Canadian J. Phys., 36, 815, (1958).

40. Yagi, S. and Kunii, D. A.I.Ch.E. Journal, 3, 373, (1957).